

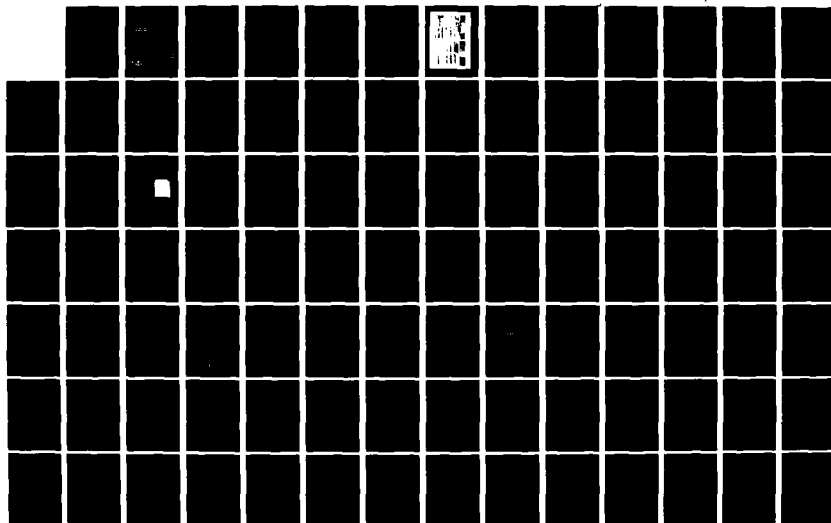
AD-A120 753

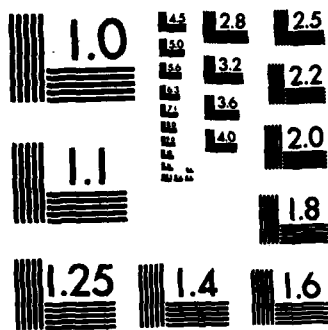
ELECTRONIC SIMULATION OF THE JOSEPHSON EFFECTS (U) NAVY
SURFACE WEAPONS CENTER SILVER SPRING MD D JABLONSKI
01 DEC 81 NSWC/MP-81-519 SBI-AD-F500 077

UNCLASSIFIED

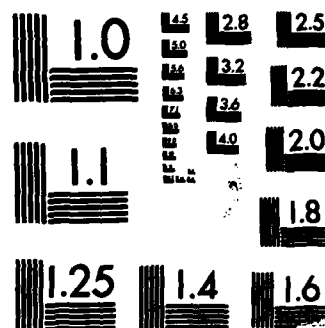
F/G 20/10

NL

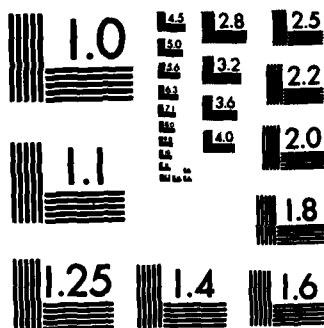




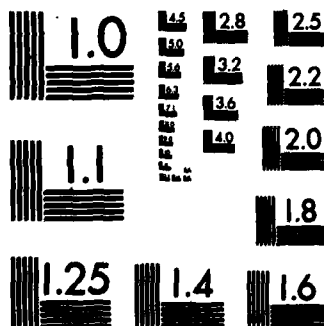
MICROCOPY RESOLUTION TEST CHART
NATIONAL BUREAU OF STANDARDS-1963-A



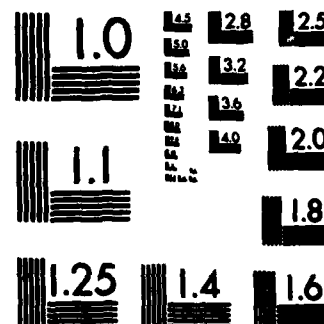
MICROCOPY RESOLUTION TEST CHART
NATIONAL BUREAU OF STANDARDS-1963-A



MICROCOPY RESOLUTION TEST CHART
NATIONAL BUREAU OF STANDARDS-1963-A



MICROCOPY RESOLUTION TEST CHART
NATIONAL BUREAU OF STANDARDS-1963-A



MICROCOPY RESOLUTION TEST CHART
NATIONAL BUREAU OF STANDARDS-1963-A

AD F500077

(12)

NSWC MP 81-519

ADA 120753

ELECTRONIC SIMULATION OF THE JOSEPHSON EFFECTS

BY DANIEL JABLONSKI

RESEARCH AND TECHNOLOGY DEPARTMENT

1 DECEMBER 1981

Approved for public release, distribution unlimited.

DTIC FILE COPY



NAVAL SURFACE WEAPONS CENTER

Dahlgren, Virginia 22448 • Silver Spring, Maryland 20910

DTIC
ELECTE
OCT 20 1982
F

82 10 12 233

UNCLASSIFIED

SECURITY CLASSIFICATION OF THIS PAGE (When Data Entered)

REPORT DOCUMENTATION PAGE		READ INSTRUCTIONS BEFORE COMPLETING FORM
1. REPORT NUMBER NSWC MP 81-519	2. GOVT ACCESSION NO. AD-A120753	3. RECIPIENT'S CATALOG NUMBER
4. TITLE (and Subtitle) ELECTRONIC SIMULATION OF THE JOSEPHSON EFFECTS		5. TYPE OF REPORT & PERIOD COVERED
7. AUTHOR(s) Daniel Jablonski		6. PERFORMING ORG. REPORT NUMBER
9. PERFORMING ORGANIZATION NAME AND ADDRESS Naval Surface Weapons Center White Oak (Code R43) Silver Spring, MD 20910		8. CONTRACT OR GRANT NUMBER(s)
11. CONTROLLING OFFICE NAME AND ADDRESS		10. PROGRAM ELEMENT, PROJECT, TASK AREA & WORK UNIT NUMBERS 61152N; 0; ZR02102; 2R01AA100
14. MONITORING AGENCY NAME & ADDRESS (if different from Controlling Office)		12. REPORT DATE 1 December 1981
		13. NUMBER OF PAGES 312
		15. SECURITY CLASS. (of this report) UNCLASSIFIED
		15a. DECLASSIFICATION/DOWNGRADING SCHEDULE
16. DISTRIBUTION STATEMENT (of this Report) Approved for public release, distribution unlimited.		
17. DISTRIBUTION STATEMENT (of the abstract entered in Block 20, if different from Report)		
18. SUPPLEMENTARY NOTES		
19. KEY WORDS (Continue on reverse side if necessary and identify by block number) Josephson Effects Superconductivity Werthamer Theory Tunnel Junction Electronic Simulator Tunneling Analogue		
20. ABSTRACT (Continue on reverse side if necessary and identify by block number) An electronic simulator of the Josephson effects is described. The device is based on an analogue phase-locked loop design, and includes the effects of voltage, frequency, temperature, and the superconducting energy gap. Results obtained using the simulator are compared with theory and results obtained from actual Josephson tunnel junctions.		

DD FORM 1473
1 JAN 73EDITION OF 1 NOV 68 IS OBSOLETE
S/N 0102-LF-014-6601

UNCLASSIFIED

SECURITY CLASSIFICATION OF THIS PAGE (When Data Entered)

Accession For	
NTIS GRA&I	<input checked="" type="checkbox"/>
DTIC TAB	<input type="checkbox"/>
Unannounced	<input type="checkbox"/>
Justification	
By _____	
Distribution/	
Availability Codes	
Dist	Avail and/or Special
A	

FOREWORD

Electronic analogues have often been used to investigate the properties of Josephson effect devices. However, they have generally been limited to modelling the adiabatic, resistively-shunted junction theory of the Josephson effects. An electronic analogue has been built which models the more sophisticated theory developed by Werthamer for superconducting tunnel junctions. This analogue, based on a phased-lock loop design, includes high frequency and energy gap effects, nonlinear quasiparticle tunnelling, the Riedel peak, the cosine phi term, and the effects of nonzero temperature.

This dissertation starts with summaries of both the resistively-shunted junction (RSJ) theory and the Werthamer theory. A review of existing analogues is presented, and is followed by a discussion of the design and use of an analogue of the RSJ model. Results include current-voltage characteristics measured under a variety of conditions, measurements of the high frequency impedance of the device, and observations of the plasma resonance.

The simulation of the Werthamer theory is discussed in detail. Much attention is given to the synthesis of the electronic filters which model the temperature dependent response functions of a superconductor. There is also a discussion of the accuracy of the analogue. Results obtained with the analogue include measurements similar to those above. Additional results compare the performance of the analogue with digital calculations, and with measurements of actual tunnel junctions.

There is additional discussion of the Werthamer theory, with particular emphasis on the frequency dependence of the cosine phi term. Theoretical results, supported by measurements made with the analogue, suggest that widely accepted interpretations of cosine phi measurements made on tunnel junctions may be in error.

The paper concludes with a comparison of RSJ and Werthamer theories, an assessment of the performance of the analogue, and suggestions for future work.

Two appendices discuss a technique for fabricating superconducting tunnel junctions, and the use of these and other Josephson devices for microwave applications. A third appendix describes various details of the electronic design of the analogue in detail. The remaining appendix is a reprint of a paper by the author which describes the prototype of the analogue.

The work described in this dissertation was performed between October 1977 and November 1981. During that period, extensive financial, technical, and moral support was provided by the United States Naval Surface Weapons Center, Silver Spring, Maryland, and by the Hirst Research Centre of the General Electric Company of England, Wembley, England. Specifically, funds were provided by NSWC during the periods June through September 1978 and from January 1981 to the present. The GEC provided funding for the period from October 1978 through December 1980. In rough terms, the material in chapters 1 through 4 corresponds to the period of GEC support; chapters 5 through 10 the period of NSWC support. However, there is no question that the support of both organizations was essential to the completion of this work, and the author gratefully acknowledges it.

Ira M. Blatstein

IRA M. BLATSTEIN
By direction

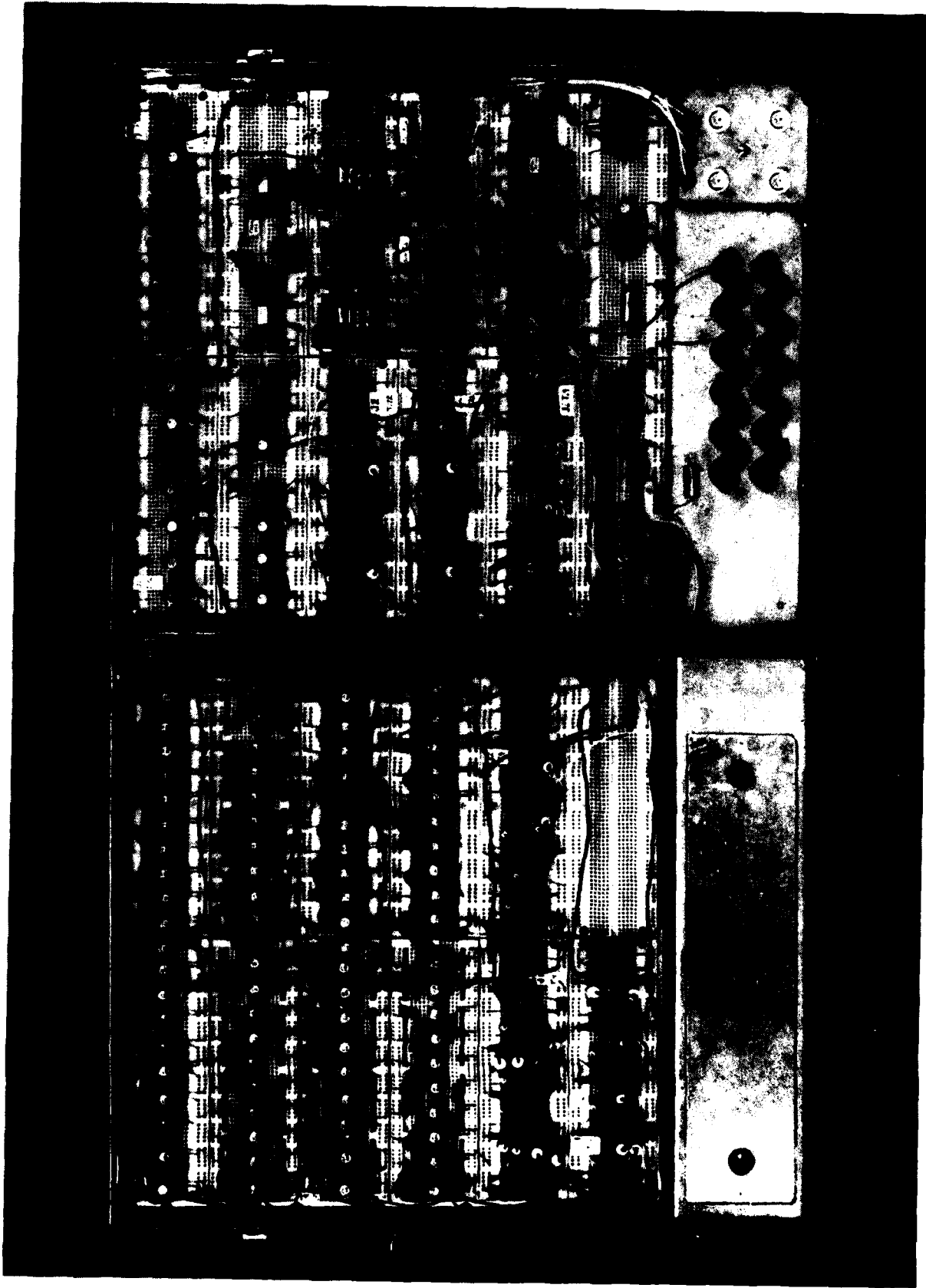
ACKNOWLEDGMENTS

On a personal level, the author would like to acknowledge the technical and personal support of many people. Most of the period between October 1977 and January 1981 was spent at the Cavendish Laboratory, and much assistance was provided by the staff and students of the Low Temperature Physics Section. In particular, the author would like to thank Messrs. Booth and Swainston, S. J. Battersby, and Prof. A. B. Pippard.

At the GEC Hirst Research Centre, considerable assistance was provided by Messrs. C. Brown, G. D. Prichard, and Dr. D. Evans.

At the Naval Surface Weapons Center, the support and assistance of numerous people has been invaluable. To mention only a few of them, A. D. Krall, C. Lufcy, I. Blatstein, and W. Grine were instrumental in obtaining funds, providing technical support, and keeping this project on the tracks.

Finally, the author would like to acknowledge the invaluable assistance of Dr. J. R. Waldram of the Cavendish Laboratory, who provided the supervision and many hours of tuition that are, hopefully, reflected in this dissertation.



AN ELECTRONIC ANALOGUE OF THE JOSEPHSON EFFECTS. THE DEVICE INCLUDES HIGH FREQUENCY AND ENERGY GAP EFFECTS, THE RIEDEL PEAK, AND NONLINEAR QUASIPARTICLE TUNNELLING. THE SYSTEM ALSO MODELS THE TEMPERATURE DEPENDENCE OF THESE EFFECTS.

CONTENTS

<u>Chapter</u>		<u>Page</u>
1	Introduction	1-1
	1.1 Introduction	1-1
	1.2 Summary	1-3
2	Theory of the Josephson Effects	2-1
	2.1 Types of Josephson Devices	2-1
	2.2 Basic Theory of the Josephson Effects	2-3
	2.3 Tunnelling Parameters	2-7
	2.4 The Josephson Effects	2-9
	2.5 Properties of the High Frequency Theory	2-12
	2.6 Calculation of the AC Impedance of a Tunnel Junction ...	2-18
3	Electronic Simulation of the RSJ Model	3-1
	3.1 Introduction	3-1
	3.2 Existing Analogues	3-2
	3.3 Design of an RSJ Analogue	3-9
	3.4 Results Obtained with the RSJ Analogue	3-17
4	Electronic Simulation of the High Frequency Theory	4-1
	4.1 Introduction	4-1
	4.2 Design of the Loop	4-4
	4.3 Design of the Filters	4-5
	4.4 Construction of the Filters	4-12
	4.5 Signs	4-20
	4.6 Results Obtained Using the High Frequency Analogue	4-21
	4.7 Summary	4-51

CONTENTS (Cont.)

<u>Chapter</u>		<u>Page</u>
5	Discussion of the High Frequency Theory	5-1
5.1	Introduction	5-1
5.2	Josephson's Calculation	5-1
5.3	The Werthamer Theory	5-6
5.4	Experimental Corroboration of the Werthamer Theory	5-15
5.5	Electronic Modelling of the Werthamer Theory	5-20
6	The Cosine Phi Problem	6-1
6.1	Introduction	6-1
6.2	Relevance of the Werthamer Theory	6-2
6.3	Experimental Background	6-5
6.4	High Frequency Corrections to the Plasma Resonance Experiment	6-12
6.5	Theoretical Work	6-22
6.6	Suggestions for Future Work	6-24
7	Filter Design	7-1
7.1	Introduction	7-1
7.2	Discussion of J_1 and J_2	7-2
7.3	The Design Problem	7-4
8	Accuracy of the Analogue	8-1
8.1	Introduction	8-1
8.2	Sources of Error in the Analogue	8-1
8.3	Accuracy of the Op Amps and Multipliers	8-3
8.4	VCO Considerations	8-5
8.5	LPF Considerations	8-7

CONTENTS (Cont.)

<u>Chapter</u>		<u>Page</u>
	8.6 Phase Shift Errors	8-13
	8.7 Accuracy of the J_1 and J_2 Filters	8-17
	8.8 Preliminary Results	8-25
9	Further Results	9-1
	9.1 Introduction	9-1
	9.2 Current-Voltage Characteristics at Various Temperatures	9-2
	9.3 Simulation of the Hamilton Experiments	9-9
	9.4 The Plasma Resonance	9-22
	9.5 Anomalous Broadening of the Riedel Peak	9-35
	9.6 SGS in the Capacitively Shunted Analogue	9-40
10	Summary and Conclusions	10-1
	10.1 The Electronic Analogue	10-1
	10.2 The High Frequency Theory	10-2
	10.3 Circuit Considerations	10-4
	10.4 Suggestions for Future Work	10-5
	10.5 Conclusion	10-7
	References	11-1
	Appendix A - Reprint of "An Electronic Analogue of a High Frequency Theory of the Josephson Effect"	A-1
	Appendix B - High Frequency Applications of Josephson Devices	B-1
	Appendix C - Fabrication of Superconducting Tunnel Junctions	C-1
	Appendix D - Low Pass Filter Considerations	D-1

ILLUSTRATIONS

<u>Figure</u>		<u>Page</u>
	Frontispiece: An Electronic Analogue of the Josephson Effects	iii
2-1	Types of Josephson Devices	2-2
2-2	Solutions to the RSJ Equation	2-10
2-3	$J_1(\omega)$ and $J_2(\omega)$ for $T = 0$	2-14
2-4	$J_1(\omega)$ and $J_2(\omega)$ for $T/T_c = 0.7$	2-14
2-5	<u>I-V Characteristic of a Current Biased Junction</u> Calculated from the Werthamer Theory	2-17
2-6	Effect of Shunt Capacitance on the Current Biased Junction ...	2-17
2-7	$\text{Im } J_1(\omega)$ as a Function of Temperature	2-23
3-1	The Bak and Pedersen Analogue	3-3
3-2	A Voltage Controlled Current Source	3-11
3-3	Low Pass Filter Responses	3-14
3-4	A Voltage Source	3-16
3-5	Characteristics of the RSJ Analogue	3-18
3-6	$V(t)$ for Three Values of I_{DC}	3-19
3-7	Effect of Varying Frequency of $I_{RF} \cos \omega t$ for the RSJ Analogue	3-20
3-8	Effect of Varying Amplitude of $I_{RF} \cos \omega t$ for the RSJ Analogue	3-21
3-9	$V(t)$ Within a Current Step	3-22
3-10	Results for the RSJ Analogue vs. Those for a Computer Calculation	3-23
3-11	RF Impedance of the RSJ Analogue Compared with Computer Results	3-25
3-12	RF Impedance of the RSJ Analogue, Continued	3-26

ILLUSTRATIONS (Cont.)

<u>Figure</u>		<u>Page</u>
4-1	Block Diagram of the High Frequency Analogue	4-2
4-2	Sketch of Theoretical $J_1(\omega)$ and $J_2(\omega)$ for $T = 0$	4-8
4-3	A 9 Pole Padé Approximate for $J_1(\omega)$ at $T = 0$	4-10
4-4	Biquadratic Components of the Nine Pole Fit to $J_1(\omega)$ at $T = 0$	4-11
4-5	A 9 Pole Padé Approximate for $J_2(\omega)$ at $T = 0$	4-13
4-6	Biquadratic Components of the Nine Frequency Fit to $J_2(\omega)$ at $T = 0$	4-14
4-7	A Biquadratic Filter	4-15
4-8	Measured Response of the $J_1(\omega)$ Filters	4-17
4-9	Measured Response of the $J_2(\omega)$ Filters	4-18
4-10	Comparison of the Duplicate Filters	4-19
4-11	Voltage and Current Bias	4-23
4-12	The Riedel Peak	4-25
4-13	Effect of Nonzero Source Resistance	4-26
4-14	Effect of Changing the Source Resistance (Voltage Bias Limit)	4-27
4-15	Effect of Changing the Source Resistance (Current Bias Limit)	4-28
4-16	Effect of Series Inductance on Sub-Gap Structure	4-29
4-17	Effect of Series Inductance on Sub-Gap Structure (Continued)	4-30
4-18	Effect of Series Inductance and Parallel Capacitance on Sub-Gap Structure	4-32
4-19	Effect of Shunt Capacitance	4-33
4-20	Anomalous Behavior of the Capacitively Shunted Analogue	4-34
4-21	Effect of Varying the RC Product	4-36

ILLUSTRATIONS (Cont.)

<u>Figure</u>		<u>Page</u>
4-22	Effects of RF Currents at the Gap Frequency	4-38
4-23	Effect of RF Currents at One Half the Gap Frequency	4-39
4-24	Effect of Varying the Frequency	4-40
4-25	Effect of Changing the Source Resistance when RF is Present	4-41
4-26	Effect of Frequencies Above and Below the Gap	4-42
4-27	High Frequency Impedance	4-43
4-28	High Frequency Impedance (Continued)	4-44
4-29	Plasma Resonance vs. RF Amplitude (RSJ Limit)	4-47
4-30	Plasma Resonance vs. $\cos \Phi$ (RSJ Limit)	4-48
4-31	Q of the Plasma Resonance vs. Frequency (RSJ Limit)	4-49
4-32	Plasma Resonance (High Freq Analogue)	4-50
4-33	Plasma Resonance (High Freq Analogue, Continued)	4-52
4-34	Plasma Resonance--Effects of Increasing RF Amplitude (RSJ Limit)	4-53
4-35	Plasma Resonance--Effects of Increasing RF Amplitude (RSJ Limit, Continued)	4-54
5-1	Tunnelling Processes in Josephson Junctions	5-3
5-2	The RSJ and High Frequency Analogues	5-8
5-3	Effect of the Gap Singularity of Quantum Tunnelling	5-9
5-4	Sub-Gap Structure	5-12
5-5	Effect of Shunt Capacitance on the I-V Characteristic	5-17
6-1	Theoretical Calculations of $\text{Im}J_2(\omega)/\text{Im}J_1(\omega)$	6-4
6-2	Plot of f_p/Q vs. f_p for a Tunnel Junction	6-7
6-3	Measured $\cos \phi$ Amplitude as a Function of Temperature for a Tin Tunnel Junction	6-9

ILLUSTRATIONS (Cont.)

<u>Figure</u>		<u>Page</u>
6-4	Measured $\cos\phi$ Amplitude as a Function of Temperature for a Lead Tunnel Junction	6-11
6-5	Im $J_1(\omega)$ as a Function of Frequency and Temperature	6-13
6-6	Plot of f_p/Q vs f_p for a Tunnel Junction, Including Calculations of $f_p/Q = B(1 + \gamma\cos\phi)$	6-17
6-7	f_p/Q vs. f_p for $T/T_c = 0.6$	6-18
6-8	f_p/Q vs. f_p for $T/T_c = 0.7$	6-19
6-9	$1/Q$ vs. I_J for a Tunnel Junction	6-23
7-1	Theoretical $J_2(\omega)$ for $T/T_c = 0.72$	7-8
7-2	Poles and Zeros of Fit to J_2 at $T/T_c = 0.72$	7-10
7-3	Attempt to Fit J_2 at $T/T_c = 0.72$	7-12
7-4	Measured Response of the Electronic Filters for $J_2(\omega)$ at $T = 0.72T_c$	7-13
7-5	Measured Response of Filters for $T = 0.72T_c$	7-15
7-6	Measured Response of Filters for $T = 0.9T_c$	7-16
8-1	Improved Low Pass Filter	8-10
8-2	High Frequency Analogue in RSJ Mode; Comparison of Measured I-V Curve with Theoretical Calculation	8-14
8-3	Measured Voltage Across the High Frequency Analogue (RSJ Limit)	8-15
8-4	Comparison of Measured J_1 Response with Theory	8-19
8-5	Comparison of Measured J_2 Filter with Theory	8-20
8-6	Comparison of Two J_1 Filters	8-21
8-7	Comparison of Two J_2 Filters	8-22
8-8	RF Impedance of RSJ Analogue Compared with Calculations of Auracher and Van Duzer, $f = f_J$	8-27
8-9	RF Impedance of RSJ Analogue Compared with Calculations of Auracher and Van Duzer, $f = 0.4f_J$	8-28

ILLUSTRATIONS (Cont.)

<u>Figure</u>		<u>Page</u>
9-1	I-V Characteristics of Voltage Biased Analogue at Different Temperatures	9-3
9-2	I-V Characteristics of the Current Biased Analogue at Different Temperatures	9-4
9-3	Effect of RF Bias on High Frequency Analogue	9-6
9-4	High Frequency Impedance I	9-8
9-5	High Frequency Impedance II	9-10
9-6	Comparison of Current Bias with a Capacitor with Voltage Bias and No Capacitor	9-12
9-7	Effect of 50 Ohm Source Impedance on Voltage Biased Characteristics	9-15
9-8	Variation of $N = 0$ Josephson Step with RF Voltage	9-17
9-9	Variation of $N = 3$ Josephson and $n = 3$ PAT Steps with RF Power	9-19
9-10	Variation of $N = 0$ Josephson Step with Frequency	9-21
9-11	Photon Assisted Tunnelling Steps: Digital Computer Versus the Electronic Analogue	9-23
9-12	Setup for Plasma Response Experiment	9-24
9-13	Impedance vs. Freq. for the RSJ Analogue Shunted by a Capacitor (Small-Signal Limit)	9-26
9-14	Effect of Low Pass Filter on Q of Plasma Resonance	9-27
9-15	I-V Characteristics for $T = 0.72T_c$	9-30
9-16	Plasma Resonance, J_1 Disconnected, $T = 0.72T_c$	9-31
9-17	Plasma Resonance $T = 0.72T_c$	9-33
9-18	Anomalous Broadening of the Riedel Peak	9-36
9-19	Spectral Analysis of the Riedel Peak Oscillations	9-38
9-20	Effect of Changing the Inductance	9-39
9-21	Effect of Capacitance and Leakage Resistance on Sub-Gap Structure	9-41

TABLES

<u>Table</u>		<u>Page</u>
4-1	Typical Parameters of the Analogue Compared with Those of a Real Superconducting Tunnel Junction	4-6
7-1	Calculation of a Pade Approximate	7-9
7-2	Recalculation of the Pade Approximation After Deletion of Unwanted Poles and Zeros	7-11
8-1	Numerical Interpretation of Figure 8-3	8-16
8-2	Effect of a Mismatch Between the Measured Responses of the J_1 Filters for $T = 0$	8-24
9-1	f_p and $f_{p/0}$ for the RSJ Analogue for Two Different Values of $\cos \Phi_1$ Coefficient	9-29
9-2	Plasma Resonance, $T = .72 T_c$	9-34

CHAPTER 1

INTRODUCTION

1.1 Introduction

The Josephson effects, which arise as a result of the tunnelling of Cooper pairs between weakly-coupled superconductors, are not only an extremely important tool in the investigation of superconductivity, but also find application in such diverse areas as magnetometry, voltage measurement, high-speed digital switching, and low-noise microwave detection.¹ However, the effects are often difficult to observe, and the various theories that describe the effects are highly nonlinear and difficult to use. Even with the help of high-speed digital computers, calculations are formidable.²

The Josephson effects are similar in many respects to the behavior of an electronic phase-lock system. In fact, many of the properties of Josephson devices were discussed in the context of color television, FM radio, and radar long before the Josephson effects were predicted in 1962.³ In 1973, Bak and Perdersen built an analogue of the Josephson effects based on a phase-locked loop.⁴ This widely used analogue provides a relatively simple, fast, and inexpensive way to get results that would be quite elusive in any but the most complicated computer calculations.

The Bak analogue models the widely used resistively-shunted junction, or RSJ model of Josephson tunnelling. In this model, the total current through a Josephson junction is considered to be the sum of a normal current, which is proportional to the junction voltage, and a supercurrent, which is proportional to the sine of the phase difference in the superconducting order parameter across the junction. The RSJ model is a good approximation to the behavior of certain types of Josephson devices, most notably superconducting microbridges. But it neglects many important aspects of the theory of superconducting tunnel

junctions. In particular, it neglects the voltage, temperature, and frequency dependence of the tunnelling parameters, and the effects of the superconducting energy gap. It does not take into account that the resistance associated with the normal current in a tunnel junction is nonlinear, and that there is an additional current which is proportional to the cosine of the phase difference across the junction.

A concise, yet more detailed theory of the superconducting tunnel junction that includes all of these factors has been available for many years.⁵ Several people have performed extensive digital calculations based on this theory, but it seems safe to say that this theory has not been widely used or understood, except in the most academic circles. Given the large amount of scientific interest in superconducting tunnel junctions, along with their many technological applications, there seems to be a clear need for an attempt to make this theory more tractable.

In 1976, Waldram proposed a scheme for an electronic analogue that would model this theory.⁶ The scheme is based on an electronic phase-locked loop, but differs substantially from the system used by Bak and Pedersen. The loop contains sophisticated filters that model the response functions of the superconductors between which tunnelling occurs. These filters are arranged in such a way that both the phase dependent Josephson tunnelling and the nonlinear, but phase independent quasiparticle tunnelling are simultaneously modelled. All of the dynamic effects associated with the junction are implicit in the design.

An analogue based on Waldram's scheme would complement the existing computational tools for investigating the high frequency theory. However, to the author's knowledge, there has been no previous attempt to build one. This thesis describes the theory, design, construction, and use of such a device.

1.2 Summary

Chapter 2 is a brief discussion of the RSJ and high frequency theories of the Josephson effects. This is an overview, and is concerned primarily with the phenomenological aspects of the theories, as opposed to their original derivations.

Chapter 3 introduces the subject of electronic simulation of the RSJ model. A review of previous work done by others is followed by a discussion of the design and use of a simple RSJ analogue. Results are presented which illustrate the basic Josephson effects outlined in Chapter 2.

Chapter 4 describes the first successful attempt to implement Waldram's scheme for modelling the high frequency theory. Much attention is given to the design and construction of the electronic filters which model the superconducting response functions. Although the results are limited to the case where the temperature of the junction is zero, they represent a substantial improvement over results obtainable using the RSJ theory.

Chapter 5 continues the discussion of the high frequency theory. Many aspects of the underlying physics that were neglected in Chapter 2 are presented. In particular, the quantum aspects of the theory are emphasized.

Chapter 6 is concerned solely with a problem concerning what is known as the cosine ϕ term. This is a topic that appears throughout this work, starting in Chapter 2, and which is of considerable academic interest. The chapter contains several calculations which, to the author's knowledge, have not been done before.

Chapter 7 describes the design of electronic filters which enable the analogue to simulate the Josephson effects at finite temperature. This is an important accomplishment, as these filters expand the usefulness of the analogue considerably.

Chapter 8 deals with the accuracy of the analogue. The possible sources of error are presented, and discussed in turn. Various improvements to the analogue are described.

Chapter 9 is a collection of results obtained using the improved analogue. Unlike the results presented in Chapter 4, the data here is often quantitative. Apparent anomalies in the previous results are reinvestigated and discussed in detail. Many of the results are compared with data obtained by others from digital computations and measurements of real tunnel junctions. The agreement is generally good, and illustrates the versatility of the analogue. Results are presented in which the analogue models are tunnelling at finite temperature. These are the first of their kind, and include measurements which support the theory and calculations presented in Chapter 6.

Chapter 10 is a summary of the dissertation, and includes suggestions for work that might be undertaken in the future. This is followed by a series of appendices (Appendices A, B, C, and D) which either elaborate upon the previous chapters or present work related only indirectly to the rest of the paper.

CHAPTER 2

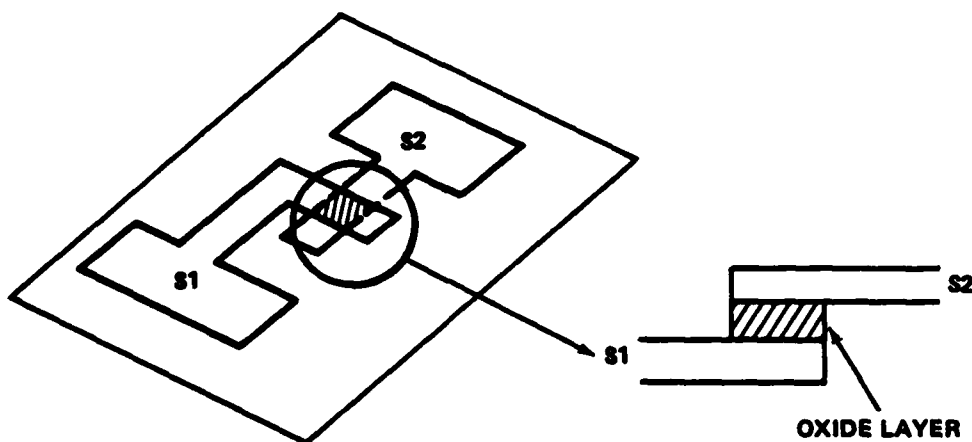
THEORY OF THE JOSEPHSON EFFECTS

2.1 Types of Josephson Devices

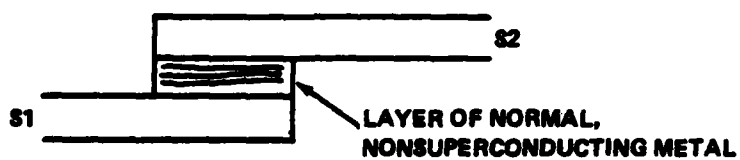
Before discussing the theory of the Josephson effects, it seems worthwhile to discuss briefly the various types of Josephson devices. Figure 2-1 shows a superconducting tunnel junction; a superconductor-normal-superconductor, or SNS junction; a constriction microbridge (also known as a Dayem bridge or just microbridge); and a point-contact junction. Each device is made of two weakly-linked superconductors, such that the behavior of each superconductor influences that of the other, but only as a perturbation.

The superconducting tunnel junction (Figure 2-1a) consists of two superconducting electrodes which overlap over a small cross-sectional area. They are separated by a very thin insulating barrier, which is typically an oxide of one of the metals forming the electrodes, and is only tens of Angstroms thick. The junction is at most only fractions of a millimeter on a side, and often much smaller. The electrodes are usually deposited onto an insulating substrate using conventional thin-film techniques, the base electrode being allowed to oxidize prior to the deposition of the counterelectrode. Provided that the electrodes are large compared to the penetration depth and coherence length of the superconductors forming the junction, they can be of any thickness.

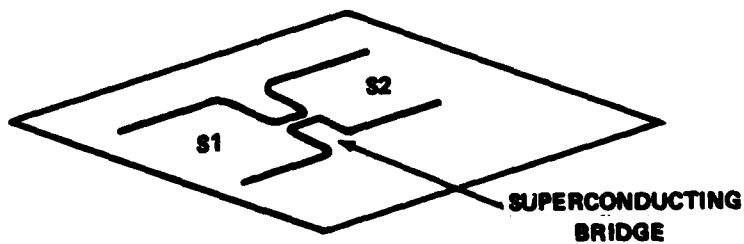
Figure 2-1b shows an SNS junction. This is identical to the tunnel junction, except that in place of the oxide there is approximately 1000 \AA of non-superconducting metal. Needless to say, this is a low resistance device. Aside from investigations of the basic physics of the device, it has few applications.



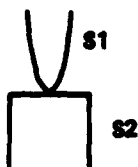
2-1a SUPERCONDUCTING TUNNEL JUNCTION



2-1b SUPERCONDUCTOR-NORMAL-SUPERCONDUCTOR (SNS) JUNCTION



2-1c CONSTRICTION MICROBRIDGE



2-1d POINT CONTACT

FIGURE 2-1. TYPES OF JOSEPHSON DEVICES

Figure 2-1c shows a constriction microbridge. Although this looks like a short circuit, the bridge is sufficiently small (only microns wide) that the junction behaves as two weakly-linked superconductors, and not as one bulk superconductor. Proper tunnelling, as it occurs in a tunnel junction, does not occur in the microbridge. Hence, many aspects of the theory of superconducting tunnel junctions are not applicable.

The last sketch (Figure 2-1d) shows a point-contact junction. This consists of a sharpened point of one superconductor pressed against a polished flat of another. Depending on the shape and size of the point, and the nature of any oxide barriers present, this device can exhibit properties of both a microbridge and a tunnel junction.

2.2 Basic Theory of the Josephson Effects.

When discussing the Josephson effects, one is usually interested in how the current through a Josephson junction is related to the voltage across it. The relationship between the two quantities is usually nonlinear, and either the voltage, current, or both will be functions of time.

The discussion that follows begins with an expression for the current through a superconducting tunnel junction. This equation, derived by Werthamer,⁵ is a generalization of Josephson's original calculation⁷ to the case where both the current and voltage can be rapidly varying functions of time (hence it is often referred to as the "high-frequency theory"). Werthamer's equation is of considerable interest because it contains details essential to the understanding of the physics of a Josephson tunnel junction, and because it describes many aspects of the behavior of real devices that are not accounted for in simpler models. This thesis is largely about the electronic synthesis of this equation.

The current through a superconducting tunnel junction can be written as⁵

$$I(t) = \text{Im} \exp(-i\phi(t)) \int_{-\infty}^t \exp(i\phi(t')) j_1(t - t') dt' + \exp(i\phi(t)) \int_{-\infty}^t \exp(i\phi(t')) j_2(t - t') dt' \quad (2-1)$$

The quantity ϕ is the phase difference between the macroscopic quantum wave functions of the superconductors between which tunnelling occurs. The derivative of ϕ with respect to time is related to the voltage across the junction by

$$\frac{d\phi}{dt} = \frac{2eV}{\hbar} \quad (2-2)$$

where e and \hbar are the electronic charge and Planck's constant.

$j_1(t)$ and $j_2(t)$ are temperature dependent response functions that describe the superconductors in terms of the gap parameter, density of states, Fermi factors, etc. In particular, $j_2(t)$ describes the supercurrent terms first predicted by Josephson,⁷ while $j_1(t)$ describes the nonlinear tunnelling of quasiparticles.* If the junction is at a temperature higher than the transition temperature of either of the superconductors, $j_2(t)$ will be zero. If neither of the electrodes is superconducting, then $j_1(t)$ will reduce to a form consistent with that expected for a metal-insulator-metal tunnel junction.

*Quasiparticles are elementary excitations of the superconducting ground state which obey Fermi statistics.

If the voltage V is held constant, we may write

$$\frac{1}{2} \dot{\phi}(t) = \omega t$$

where

$$\hbar\omega = eV^*$$

Equation 2-1 becomes

$$I(V) = \text{Im } J_1(\omega) + \sin\phi \text{ Re } J_2(\omega) + \cos\phi \text{ Im } J_2(\omega) \quad (2-3)$$

where $J_1(\omega)$ and $J_2(\omega)$ are the Fourier transforms of $j_1(t)$ and $j_2(t)$. The following points should be noted.

1. There is a direct correspondence between ω and V when V is constant.
2. $J_2(\omega)$ describes the Josephson currents.⁷
3. $\text{Im } J_1(\omega)$ describes the ordinary tunnel current. If $\text{Im } J_1(\omega)$ is proportional to ω , then this term is equivalent to an Ohmic resistance where $I \propto V$.
4. $\text{Re } J_1(\omega)$ does not affect the current if V is constant.

Two simplifications of equation 2-3 are worth discussing. If we set $\text{Im } J_1(\omega) \propto \omega$, $\text{Re } J_2(\omega) = \text{Re } J_2(0) = \text{constant}$, and $\text{Im } J_2(\omega) = 0$, we have

$$I(V) = \sigma_0 V + I_J \sin \phi \quad (2-4)$$

where
$$\sigma_0 = \frac{\text{Im } J_1(\omega)}{V} \quad I_J = \text{Re } J_2(0)$$

This is the resistively-shunted junction, or RSJ model. There is no limit in which the RSJ model is theoretically correct, but it is nevertheless a quite useful model. Firstly, it describes most of the Josephson effects by means of

* ω is one half the usual Josephson frequency.

an equation that is far simpler than equation 2-1. Secondly, it is often a reasonable approximation to the behavior of certain types of Josephson devices, notably point-contacts and microbridges.

A compromise between the RSJ and Werthamer equations is obtained by letting $\text{Im } J_1(\omega) = \text{Im } J_2(\omega) \sim \omega$. At nonzero temperature, for small voltages and frequencies, this is a reasonable approximation. The expression for the current becomes

$$I(V) = \sigma_0 V + \sigma_1 V \cos \phi + I_J \sin \phi \quad (2-5)$$

where σ_0 and σ_1 are regarded as being constant.

The basis for this assumption is that the ratio $\text{Im } J_2(\omega)/\text{Im } J_1(\omega)$ is approximately constant at low frequencies,⁸ and that despite their nonlinearity in other regions, $\text{Im } J_1(\omega)$ and $\text{Im } J_2(\omega)$ are approximately linear near $\omega = 0$. However, this is only true at nonzero temperature, as both $\text{Im } J_1(\omega)$ and $\text{Im } J_2(\omega)$ are zero at low frequencies at $T = 0$.

The term $\sigma_1 V \cos \phi$, known as the quasiparticle-pair interference term or simply the $\cos \phi$ term, has been the subject of much attention. Josephson's original calculations shown σ_1/σ_0 to be a positive quantity, approach +1 at low temperatures.⁷ Experiments indicate that the sign is either negative,⁹ or varies with temperature.¹⁰ The prediction that $\sigma_1/\sigma_0 = +1$ is the only one of Josephson's original predictions that is inconsistent with experimental observations.¹¹

2.3 Tunnelling Parameters

For a tunnel junction, the parameters I_J and σ_0 in the RSJ equation are related via the superconducting energy gap.* For a junction comprised of identical superconductors, we have

$$I_J R_N = \frac{\pi \Delta(T)}{2e} \tanh \frac{\Delta(T)}{2KT} \quad (2-6)$$

where $\Delta(T)$ is the temperature dependent energy gap parameter. I_J is known as the critical current, and R_N the normal-state resistance. (This is the resistance that would be measurable at a temperature just above the transition temperature of the junction.) In the RSJ model, σ_0 is usually taken to be $1/R_N$.

At $T = 0$,

$$I_J R_N = \frac{\pi \Delta(0)}{2e} \quad (2-7)$$

For many superconductors, $\Delta(0)$ can be approximated by

$$\Delta(0) = 1.76 K T_c$$

where K is Boltzman's constant and T_c is the transition temperature of the superconductor.¹² For a junction comprised of different superconductors, $\Delta(0)$ is replaced by

$$I_J R_N = \frac{\pi \Delta}{2e} \frac{2\Delta_1 \Delta_2}{\Delta_1 + \Delta_2} \quad (2-8)$$

where the subscripts refer to the different superconductors.

For a typical tunnel junction, Δ/e is a few millivolts, I_J is approximately 1 mA, and R_N is about 1 ohm. These last two parameters can vary

*It is important to note that I_J is dependent on magnetic field. For an applied magnetic field Φ , $I_J \propto (\sin \pi \Phi) / \pi \Phi$ (Reference 6).

by orders of magnitude in either direction, depending on the size of the junction and the thickness of the oxide barrier. The degree to which the measured $I_J R_N$ product agrees with equation 2-7 is often taken as a figure of merit.

The capacitance associated with a tunnel junction is not insignificant. It is typically between 1 pF and 1 nF. The RC time constants are quite short, indicating that a Josephson junction can respond very quickly to changes in voltage or current. However, it is important to realize that R_N does not reflect the strong nonlinearity in junction resistance that exists in tunnel junctions. At voltages less than the gap voltage $\frac{2\Delta}{e}$ the effective resistance of the junction can be orders of magnitude higher than R_N . Consequently, the relevant RC time constant may be orders of magnitude larger than anticipated.

The quantity $2eI_J R_N / h$ can be regarded as a characteristic frequency of a Josephson device. Given that $2e/h$ is 483×10^6 MHz/volt, this Josephson frequency is typically hundreds of GHz. The average power levels associated with Josephson junctions are very small. The quantity $I_J^2 R_N$ might be 10^{-6} watts, but practical considerations limit the useful amount of power that one can put into, or get out of the device, to nanowatts or less.

We can see that a Josephson junction behaves as a low power, high-speed, nonlinear device. As it operates at cryogenic temperatures, it is also expected to be a low-noise device. Consequently, there has been much interest in the use of Josephson junctions for low-noise millimeter wave applications.¹ Because of their high speed and low power consumption, they are also being exploited for digital switching applications.¹³

2.4 The Josephson Effects

We are now in a position to describe the basic Josephson effects in the context of the RSJ model. These are listed briefly:

1. The DC Josephson effect; for $V = 0$, $\frac{d\phi}{dt} = 0$, and ϕ is constant.

The RSJ Equation becomes

$$I = I_J \sin \phi \quad (2-9)$$

This DC supercurrent exists for $|I| < I_J$, the critical current of the junction. This is an unexpected result, particularly in the case of a tunnel junction, where the oxide barrier is clearly an insulator.

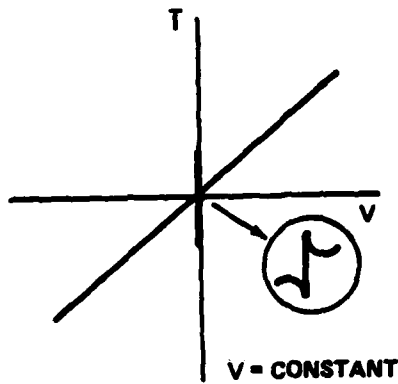
2. The AC Josephson effect; if V is constant, $\phi = \frac{2eVt}{h}$, and

$$I = I_J \sin \frac{2eVt}{h} + \frac{V}{R} \quad (2-10)$$

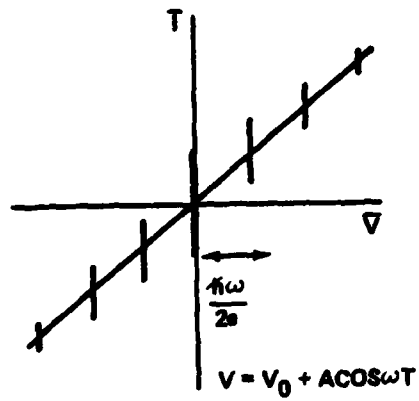
The current oscillates at a frequency $2eV/h$. However, this has no effect on the time average current-voltage characteristic of the junction, which is shown in Figure 2-2a. The DC Josephson effect is represented by a current spike at $V = 0$. In a real experiment, the source impedance is never truly zero, and the spike will appear as the structure shown in the inset.

3. The inverse AC effect; an externally applied AC voltage can phase lock to the internal Josephson oscillations described above. This occurs when the DC voltage is $V = nh\omega/2e$, where ω is the applied frequency. The effect on the time-average current-voltage characteristic is to add supercurrent spikes at these voltages, as shown in Figure 2-2b. The amplitudes of these spikes are proportional to

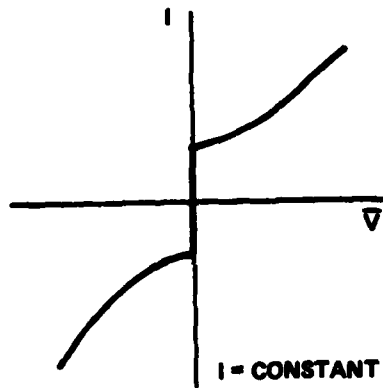
$$J_n \left[\frac{2eV_{rf}}{h\omega} \right] \quad (2-11)$$



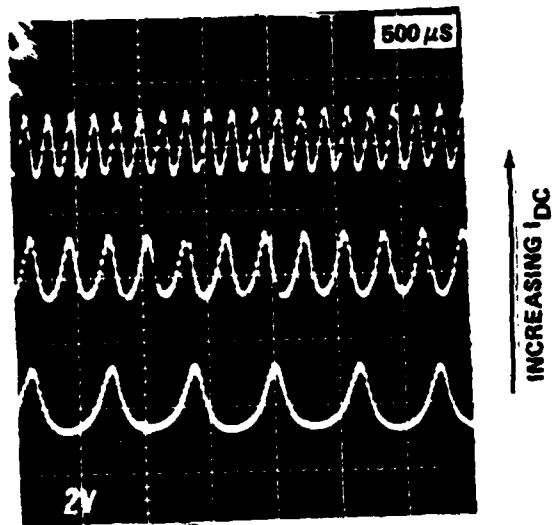
2-2a. VOLTAGE BIAS



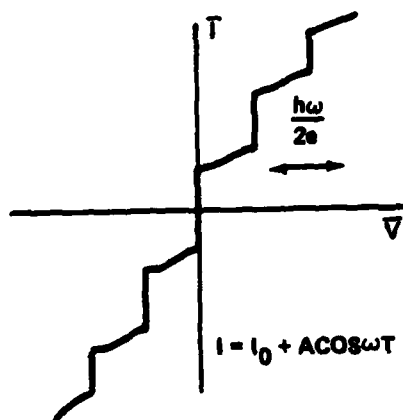
2-2b. VOLTAGE BIAS WITH RF



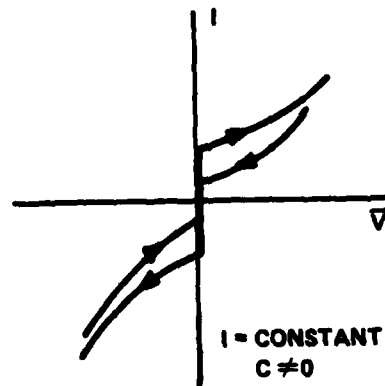
2-2c. CURRENT BIAS



2-2d. VOLTAGE VS. TIME FOR $I = \text{CONSTANT}$



2-2e. CURRENT BIAS WITH RF



2-2f. EFFECT OF SHUNT CAPACITANCE

FIGURE 2-2. SOLUTIONS TO THE RSJ EQUATION

where V_{rf} and ω are the amplitude and frequency of the applied AC voltage.

J_n is a Bessel function of the first kind, and the integer n is given by $\frac{2eV}{\hbar\omega}$.

The effects described above were derived assuming the voltage was the independent variable in the RSJ equation. If we treat I as the independent variable, we must expect the effects to be modified.

4. For $I = \text{constant}$,¹⁴

$$|I| \leq I_J, V = 0 \quad (2-12a)$$

$$|I| > I_J, V = \bar{V} \left[1 + 2 \sum_n \left(\frac{1 - \sqrt{1 - \gamma^2}}{\gamma} \right)^n \cos n\omega_0 t \right] \quad (2-12b)$$

where $\gamma = I_J/I$, $\omega_0 = \frac{2eV}{\hbar}$ (2-12c)

$$\bar{V} = R \sqrt{I^2 - I_J^2} (\text{sgn } I) \quad (2-12d)$$

\bar{V} is the time average voltage. This is plotted against I in Figure 2-2c. $V(t)$ is plotted in Figure 2-2d for three different values of I_{DC}/I_J . Note that for low values of I_{DC} , the Josephson oscillations are non-sinusoidal.

5. If $I = I_{DC} = I_{rf} \cos \omega t$, there will be current steps in the time average I-V curve at the voltages $\bar{V} = n\hbar\omega/2e$. The heights of these steps will vary as a function of I_{rf} in an approximately Bessel function like fashion. These steps are shown in Figure 2-2e.

If there is a capacitance associated with the junction, the RSJ equation becomes

$$I = I_J \sin \phi + \frac{V}{R} + C \frac{dV}{dt} \quad (2-13)$$

The capacitance makes the time average I-V curve appear hysteretic. This is shown in Figure 2-2f. In the above equation, the $\sin\phi$ term can be regarded as a phase dependent inductance

$$L = \frac{\hbar}{2eI_J \cos\phi} \quad (2-14)$$

If the DC voltage is zero, and the AC voltages and currents are small enough that $J_1(2eV_{rf}/\hbar\omega) \approx 2eV_{rf}/\hbar\omega$, then L can be treated as a constant inductance L_0 , given by

$$L_0 = \frac{\hbar}{2eI_J \cos\phi_0} \quad (2-15)$$

where ϕ_0 is determined by the DC current through the junction. Taking the capacitance into account, the junction behaves as a parallel RLC network with resonant frequency and Q given by

$$\omega_p^2 = \frac{2eI_J \cos\phi_0}{\hbar C} \quad (2-16a)$$

$$Q = \omega_p CR \quad (2-16b)$$

This is known as the plasma resonance.

2.5 Properties of the High Frequency Theory

In many respects, the high frequency theory given by equation 2-1 is quite similar to the RSJ model. The DC supercurrents, RF induced steps, and the shapes of the time average I-V curves are qualitatively the same. However, the resistance R is highly nonlinear and has a reactance associated with it, the $\cos\phi$ term is important, and the critical current I_J diverges at a voltage related to the superconducting energy gap. All of these effects are determined by the temperature dependent response functions $j_1(t)$ and $j_2(t)$.

The physical significance of these response functions is evident from an examination of the Fourier transforms $J_1(\omega)$ and $J_2(\omega)$. These are sketched for positive frequency and zero temperature in Figure 2-3. Corresponding analytic expressions are given by Werthamer.⁵ For nonzero temperatures, no analytic expressions exist, and $J_1(\omega)$ and $J_2(\omega)$ must be calculated. This had been done by Harris,^{8,15,16} Shapiro,¹⁷ Schlup,¹⁸ and Poulsen.¹⁹

With reference to equation 2-3, we see that $\text{Im } J_1(\omega)$ is the amplitude of the normal, or quasiparticle current. When the junction voltage is constant, ω is equivalent to eV/\hbar , and $\text{Im } J_1(\omega)$ can be written as $\text{Im } J_1(V)$. Note that the shape of $\text{Im } J_1(\omega)$ corresponds to the shape of the current-voltage characteristic one would expect for a voltage biased tunnel junction, where at $T = 0$, no current flows for voltages less than the gap voltage $2\Delta/e$.

$\text{Re } J_2(\omega)$, which is finite even at zero frequency and voltage, is the amplitude of the Josephson supercurrent. This is related to the quasiparticle current via the $I_J R_N$ product, where

$$I_J R_N = \frac{\text{Re } J_2(0)}{\text{Im } J_1(\omega)} \frac{\hbar \omega}{e} \quad (2-17)$$

This relates the slope of $\text{Im } J_1(\omega)$ at high frequency to the value of $\text{Re } J_2(\omega)$ at zero frequency.

The functions $\text{Re } J_1(\omega)$ and $\text{Im } J_2(\omega)$ are related to $\text{Im } J_1(\omega)$ and $\text{Re } J_2(\omega)$ via the Kramers-Kronig relations. $\text{Re } J_1(\omega)$ is a reactive term associated with the dynamic response of $\text{Im } J_1(\omega)$, and does not affect the current when the voltage is constant. $\text{Im } J_2(\omega)$ is the

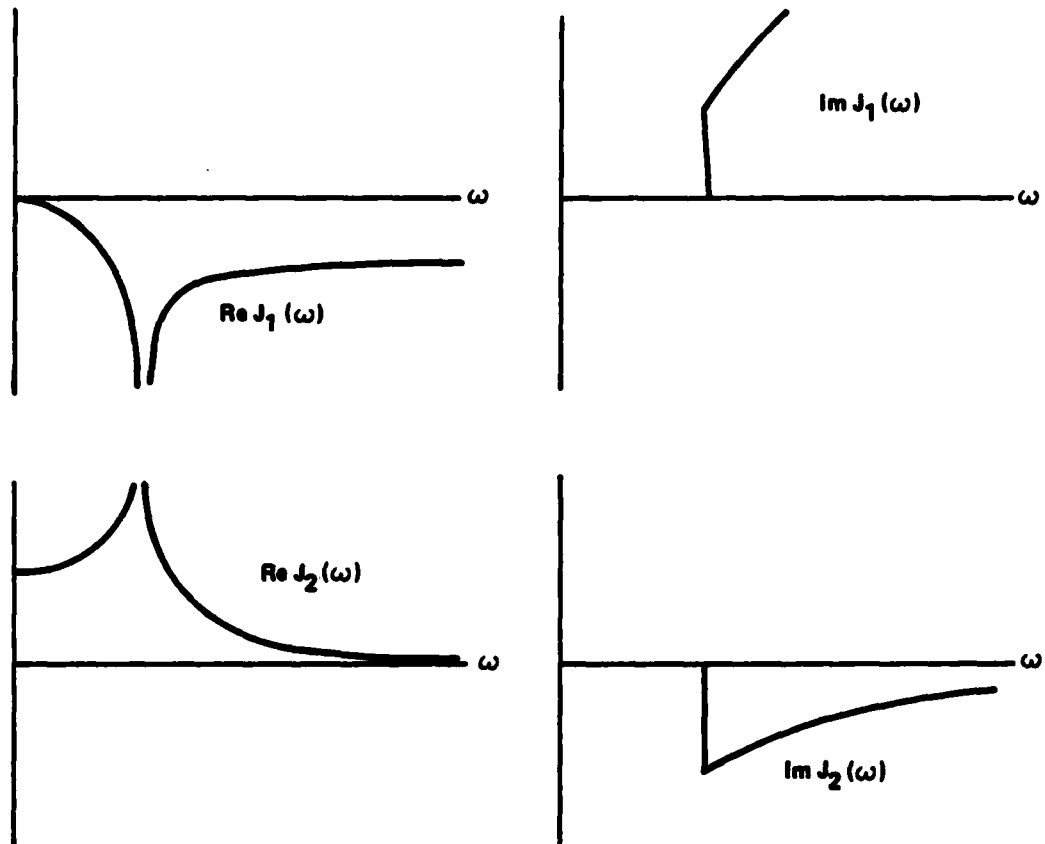


FIGURE 2-3. $J_1(\omega)$ AND $J_2(\omega)$ FOR $T = 0$ (AFTER WERTHAMER⁵)

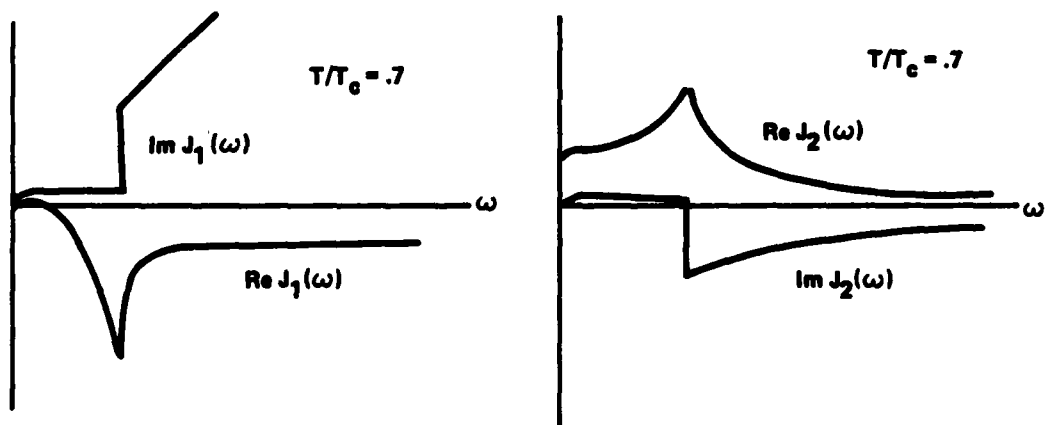


FIGURE 2-4. $J_1(\omega)$ AND $J_2(\omega)$ FOR $T/T_c = .7$ (AFTER HARRIS^{14,15})

amplitude of the cos ϕ current. The divergence of $\text{Re } J_1(\omega)$ and $\text{Re } J_2(\omega)$ at the gap frequency is related to the logarithmic divergence of the density of states in a superconductor on either side of the energy gap.

In the RSJ model, it is assumed that $\text{Re } J_2(\omega) = \text{Re } J_2(0)$. This is a good approximation for voltages $\ll \frac{2\Delta}{e}$, and frequencies $\ll \frac{2\Delta}{\hbar}$. Under these conditions, it is also reasonable to neglect the cos ϕ term, as $\text{Im } J_2(\omega) = 0$. However, the RSJ model also assumes that $\text{Im } J_1(\omega)$ is linear for all frequencies and voltages, which is not true at $T = 0$.

At nonzero temperatures, the functions $J_1(\omega)$ and $J_2(\omega)$ are modified in three respects. First, the gap frequency decreases, causing the divergences and discontinuities in Figure 2-3 to shift to the left. Second, the amplitudes of the functions will decrease. Third, there will be filled states above the energy gap, so that $\text{Im } J_1(\omega)$ and $\text{Im } J_2(\omega)$ will be nonzero below the gap frequency.

Figure 2-4 shows a sketch of Harris' calculations for $J_1(\omega)$ and $J_2(\omega)$ at $T/T_c = .7$, where T_c is the transition temperature of the junction.⁸ Note that $\text{Im } J_1(\omega)$ is approximately linear for small frequencies, which is one of the conditions assumed in the RSJ model. But now $\text{Im } J_2(\omega)$ is nonzero, so even at finite temperatures, there is no limit in which the RSJ model is strictly valid.

If the junction is comprised of two different superconductors, the functions will diverge at a frequency given by $(\Delta_1 + \Delta_2)/\hbar$. There will be additional structure in the functions at a frequency $(\Delta_1 - \Delta_2)/\hbar$.

McDonald, et al. have calculated the DC I-V curves for a current biased junction using the Werthamer model.² Their result is shown in Figure 2-5.

The divergence at $V = 2\Delta/e$ is known as the Riedel peak, and is directly related to the divergence of $\text{Re } J_2(\omega)$ at $\omega = 2\Delta/\hbar$. As in the RSJ model, the voltage varies nonsinusoidally when the current is constant and greater than $\text{Re } J_2(0)$. When an odd harmonic of the Josephson frequency $2eV/\hbar$ is equal to the gap frequency $2\Delta/\hbar$, the divergence in $\text{Re } J_2(\omega)$ causes extra structure in the I-V characteristic. Whether this occurs for even harmonics as well depends on the nature of the source impedance associated with the junction.⁵

Figure 2-6 shows the effect of shunt capacitance. This capacitance causes the I-V curve to be very hysteretic, and the function $\text{Im } J_1(V)$ is traced out as the current is decreased from a high value to $I_{DC} = 0$.

One additional effect which is of importance deals with photon-assisted tunnelling. If a junction is biased with a signal

$$V = V_{DC} + V_{RF} \cos \omega t$$

the DC quasiparticle current will be affected both by the signal V_{RF} and the frequency dependence of $\text{Im } J_1(\omega)$. Specifically, when the voltages $V_{DC} + nhf/e$ (n an integer) coincide with the gap voltage $2\Delta/e$, the discontinuity in $\text{Im } J_1(V)$ will cause a photon-assisted tunnelling step to appear in the DC current-voltage characteristic.²¹ These steps are similar to the RF induced Josephson steps, and have a Bessel function like dependence on V_{RF} . However, they are spaced at voltage intervals hf/e on either side of the gap voltage $2\Delta/e$. The Josephson steps occur at spacings of $hf/2e$ and are centered about zero voltage.*

*Photon-assisted tunnelling is discussed in more detail in Chapters 5 and 9.

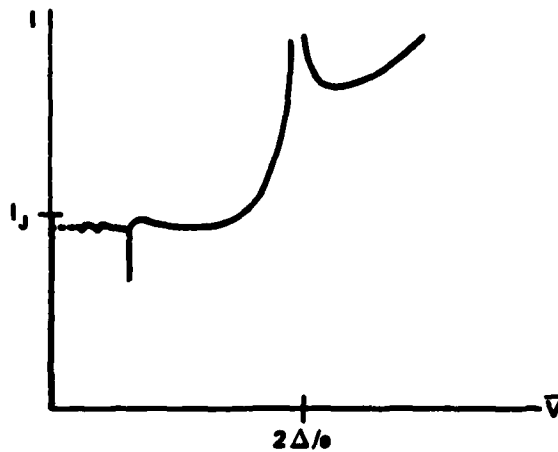


FIGURE 2-5. I-V CHARACTERISTIC OF A CURRENT BIASED JUNCTION CALCULATED FROM THE WERTHAMER THEORY (AFTER MC DONALD, ET AL - REF 2)

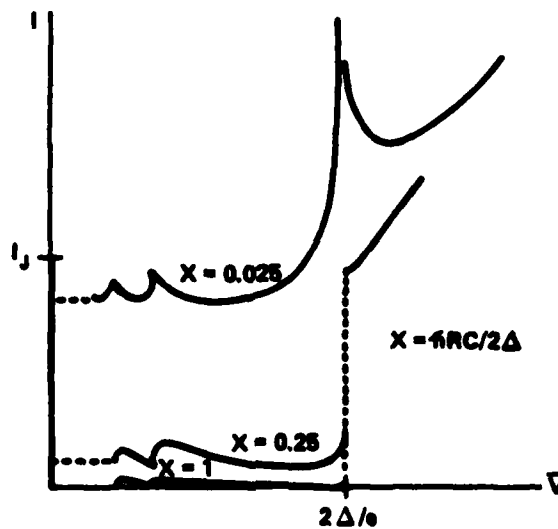


FIGURE 2-6. EFFECT OF SHUNT CAPACITANCE ON THE CURRENT BIASED JUNCTION (AFTER MC DONALD, ET AL - REF 2)

2.6 Calculation of the AC Impedance of a Tunnel Junction

At this stage, it may be helpful to illustrate how one can perform simple calculations using Werthamer's equation. One calculation, which is of considerable interest in connection with high frequency applications, is the derivation of the small signal AC impedance of a tunnel junction. Consider the case where the junction is DC current biased within the zeroth order step, and voltage biased with a small RF signal. We have

$$I = I_{DC} + I_{RF} \cos (\omega t + \theta) \quad (2-18)$$

$$V = A \cos \omega t$$

$$\text{Using } \frac{d\phi}{dt} = 2eV/\hbar, \text{ the phase is } \phi = \phi_0 + \frac{2eA}{\hbar\omega} \sin \omega t \quad (2-19)$$

For the moment, it is convenient to rewrite equation 2-1 in noncomplex notation. Since $j_1(t)$ and $j_2(t)$ can be considered to be real and causal,^{5,8} the integrals in equation 2-1 can be treated as simple convolution integrals. That is

$$\int_{-\infty}^t e^{i\frac{\phi}{2}(t')} j(t-t') dt' = \int_{-\infty}^{\infty} e^{i\frac{\phi}{2}(t')} j(t-t') dt' = e^{i\frac{\phi}{2}(t)} * j(t) \quad (2-20)$$

Equation 2-1 can be rewritten

$$\begin{aligned} I(t) = & \cos \frac{\phi}{2} \left(\sin \frac{\phi}{2} * j_1 \right) - \sin \frac{\phi}{2} \left(\cos \frac{\phi}{2} * j_1 \right) \\ & + \sin \frac{\phi}{2} \left(\cos \frac{\phi}{2} * j_2 \right) + \cos \frac{\phi}{2} \left(\sin \frac{\phi}{2} * j_2 \right) \end{aligned} \quad (2-21)$$

Using equation 2-19, we have

$$\sin \frac{\phi}{2} \approx \sin \frac{\phi_0}{2} \cos \left(\frac{eA}{\hbar\omega} \sin \omega t \right) + \cos \frac{\phi_0}{2} \sin \left(\frac{eA}{\hbar\omega} \sin \omega t \right) \quad (2-22a)$$

$$\cos \frac{\phi}{2} \approx \cos \frac{\phi_0}{2} \cos \left(\frac{eA}{\hbar\omega} \sin \omega t \right) - \sin \frac{\phi_0}{2} \sin \left(\frac{eA}{\hbar\omega} \sin \omega t \right) \quad (2-22b)$$

Rather than struggle with Bessel functions, it is best to limit the calculation to the case where

$$\frac{eA}{\hbar\omega} \ll 1$$

Thus

$$\sin \frac{\phi}{2} \approx \sin \frac{\phi_0}{2} + \cos \frac{\phi_0}{2} \left(\frac{eA}{\hbar\omega} \sin \omega t \right) \quad (2-22c)$$

$$\cos \frac{\phi}{2} \approx \cos \frac{\phi_0}{2} - \sin \frac{\phi_0}{2} \left(\frac{eA}{\hbar\omega} \sin \omega t \right) \quad (2-22d)$$

We can now compute the convolution integrals. The sign conventions used in this thesis are consistent with the definitions

$$\sin \omega t * j(t) = \sin \omega t \operatorname{Re} J(\omega) + \cos \omega t \operatorname{Im} J(\omega) \quad (2-23a)$$

$$\cos \omega t * j(t) = \cos \omega t \operatorname{Re} J(\omega) - \sin \omega t \operatorname{Im} J(\omega) \quad (2-23b)$$

Considering only the terms related to the quasiparticle current in equation 2-21,

$$\begin{aligned} I_{QP} &= \cos \frac{\phi}{2} \left(\sin \frac{\phi}{2} * j_i \right) - \sin \frac{\phi}{2} \left(\cos \frac{\phi}{2} * j_i \right) \\ &= \left[\cos \frac{\phi_0}{2} - \sin \frac{\phi_0}{2} \left(\frac{eA}{\hbar\omega} \sin \omega t \right) \right] \\ &\quad \times \left[\begin{aligned} &\sin \frac{\phi_0}{2} \operatorname{Re} J_1(0) + \cos \frac{\phi_0}{2} \left(\frac{eA}{\hbar\omega} \sin \omega t \right) \operatorname{Re} J_1(\omega) \\ &+ \cos \frac{\phi_0}{2} \left(\frac{eA}{\hbar\omega} \cos \omega t \right) \operatorname{Im} J_1(\omega) \end{aligned} \right] \end{aligned} \quad (2-24)$$

$$\begin{aligned}
& - \left[\sin \frac{\phi_0}{2} + \cos \frac{\phi_0}{2} \left(\frac{eA}{\hbar\omega} \sin\omega t \right) \right] \\
& \times \left[\cos \frac{\phi_0}{2} \operatorname{Re} J_1(0) - \sin \frac{\phi_0}{2} \left(\frac{eA}{\hbar\omega} \sin\omega t \right) \operatorname{Re} J_1(\omega) \right. \\
& \quad \left. - \sin \frac{\phi_0}{2} \left(\frac{eA}{\hbar\omega} \cos\omega t \right) \operatorname{Im} J_1(\omega) \right]
\end{aligned}$$

These expressions are apt to put many people off using the Werthamer theory. But if higher order terms (i.e., anything not at DC or ω) are neglected, the expressions simplify considerably. The quasiparticle current becomes

$$\begin{aligned}
I_{QP} &= \frac{eA}{\hbar\omega} \sin\omega t \left[\operatorname{Re} J_1(\omega) - \operatorname{Re} J_1(0) \right] \\
&+ \frac{eA}{\hbar\omega} \cos\omega t \operatorname{Im} J_1(\omega)
\end{aligned} \tag{2-25}$$

In a similar manner, the supercurrent terms in $j_2(t)$ yield

$$\begin{aligned}
I_{SC} &= \operatorname{Re} J_2(0) \sin\phi_0 \\
&+ \frac{eA}{\hbar\omega} \cos\phi_0 \left[\operatorname{Re} J_2(\omega) + \operatorname{Re} J_2(0) \right] \sin\omega t \\
&+ \frac{eA}{\hbar\omega} \cos\phi_0 \left[\operatorname{Im} J_2(\omega) \right] \cos\omega t
\end{aligned} \tag{2-26}$$

At this point, it is convenient to return to complex notation. Let

$$\begin{aligned}
I &= \operatorname{Re} \left\{ I_{RF} e^{i\omega t} e^{i\phi} \right\} + I_{DC} \\
V &= \operatorname{Re} \left\{ A e^{i\omega t} \right\} \\
\cos\omega t &= \operatorname{Re} e^{i\omega t} \\
\sin\omega t &= \operatorname{Re} \left\{ -i e^{i\omega t} \right\}
\end{aligned}$$

The DC current is

$$I_{DC} = \operatorname{Re} J_2(0) \sin\phi_0 \tag{2-27}$$

and the small signal AC admittance is

$$\begin{aligned}
 y &= \frac{I_{RF} e^{i\theta} e^{i\omega t}}{A e^{i\omega t}} & (2-28) \\
 &= \frac{1}{i\omega} \frac{e}{\hbar} \cos \phi_0 \left[\operatorname{Re} J_2(\omega) + \operatorname{Re} J_2(0) \right] \\
 &\quad + \frac{1}{i\omega} \frac{e}{\hbar} \left[\operatorname{Re} J_1(\omega) - \operatorname{Re} J_1(0) \right] \\
 &\quad + \frac{e}{\hbar} \frac{\operatorname{Im} J_2(\omega)}{\omega} \cos \phi_0 \\
 &\quad + \frac{e}{\hbar} \frac{\operatorname{Im} J_1(\omega)}{\omega}
 \end{aligned}$$

In the RSJ limit,

$$\operatorname{Re} J_2(\omega) = \operatorname{Re} J_2(0) = I_J \quad (2-29)$$

$$\operatorname{Re} J_1(\omega) = \operatorname{Re} J_1(0) = 0$$

$$\frac{e}{\hbar} \frac{\operatorname{Im} J_2(\omega)}{\omega} = 0$$

$$\frac{e}{\hbar} \frac{\operatorname{Im} J_1(\omega)}{\omega} = \frac{1}{R_N}$$

Thus the DC current is just

$$I_{DC} = I_J \sin \phi_0 \quad (2-30a)$$

The AC admittance reduces to

$$\frac{1}{R_J} = \frac{1}{R_N} + \frac{1}{i\omega L_J} \quad (2-30b)$$

where

$$L_J = \frac{\hbar}{2e I_J \cos \phi_0}$$

To include the effect of the $\operatorname{Im} J_2(\omega)$ term (i.e., the $\cos \phi$ term), let

$$\frac{1}{R_N} = \sigma_0$$

$$\frac{e}{\hbar} \times \frac{\operatorname{Im} J_2(\omega)}{\omega} = \sigma_1$$

$$y = \sigma_0 + \sigma_1 \cos \phi_0 + \frac{2eI_J \cos \phi_0}{i\omega\hbar} \quad (2-31)$$

If the junction has a shunt capacitance C , the admittance is

$$y = i\omega C + \frac{2eI_J \cos \phi_0}{i\omega\hbar} + \sigma_0 + \sigma_1 \cos \phi_0 \quad (2-32)$$

This is the admittance of a parallel RCL circuit with resonant frequency

$$\omega_p^2 = \frac{2eI_J \cos \phi_0}{\hbar C} \quad (\text{the plasma frequency}) \quad (2-33a)$$

$$\text{and} \quad Q = \frac{\omega_p C}{\sigma_0 + \sigma_1 \cos \phi_0} \quad (2-33b)$$

Returning to the high frequency limit given by equation 2-28, several points should be noted:

1. I_J is replaced by the average of $\text{Re } J_2(0)$ and $\text{Re } J_2(\omega)$.
2. At the gap frequency, $\text{Re } J_2(\omega)$ diverges and the Josephson inductance goes to zero.
3. As in the DC case, a constant in $\text{Re } J_1(\omega)$ is of no consequence.
4. The term $e \text{Im } J_1(\omega)/\hbar\omega$ is the quasiparticle conductance. At frequencies greater than $2\Delta/\hbar$ (corresponding to voltages greater than $2\Delta/e$), this quantity approaches the constant $1/R_N$. $\text{Im } J_1(\omega)$ is presented for a variety of temperatures in Figure 2-7.⁵² At finite temperatures and for frequencies less than $2\Delta/\hbar$, $\text{Im } J_1(\omega)$ can be regarded as being constant. Thus, over a wide range of frequency, the AC resistance of the junction is proportional to ω . At finite temperatures and extremely low frequencies, $[e\text{Im}J_1(\omega)]/\hbar\omega$ again approaches $1/R_N$. This contradicts calculations reported in the early literature that suggest that the quasiparticle conductance diverges at $V = 0$.⁹

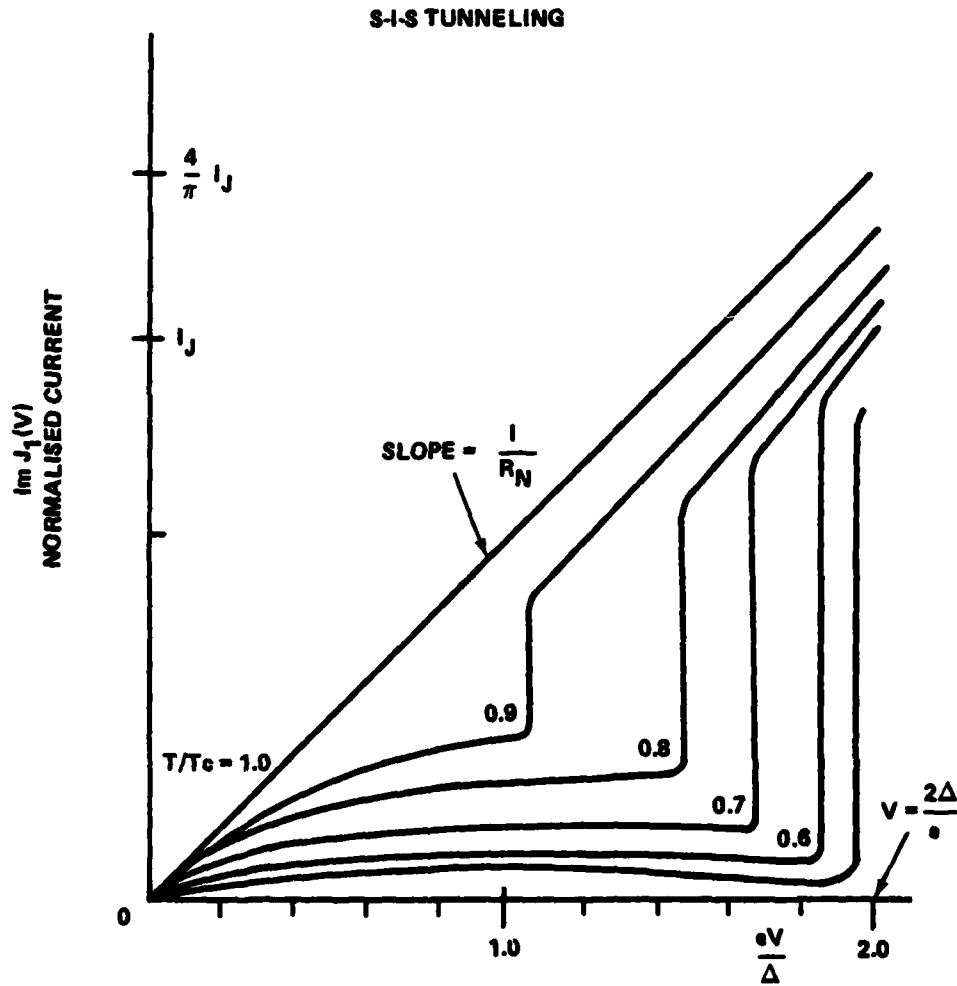


FIGURE 2-7. $\text{Im } J_1(\omega)$ AS A FUNCTION OF TEMPERATURE (AFTER YOUNG⁵²)

NOTE: $\text{Im } J_1(\omega) = \text{Im } J_1\left(\frac{2eV}{h}\right)$ IN THE VOLTAGE BIASED LIMIT

5. In the literature, it is often assumed that $\hbar\omega = 2\text{eV}$, and J_1 and J_2 are written as functions of voltage, not frequency. If the junction voltage is $A\cos\omega_0 t$, this assumption can lead to one's using $J_1(A)$ and $J_2(A)$ in calculations, when $J_1(\omega)$ and $J_2(\omega)$ are the relevant quantities. In the small signal limit, all calculations should be independent of A .

6. At frequencies greater than the gap frequency, $\text{Im } J_2(\omega)$ is negative. The term $[e \times \text{Im } J_2(\omega) \cos\omega t] / \hbar\omega$ will decrease the total AC conductance of the junction. The junction AC resistance, and consequentially the Q of the plasma resonance, will be increased. At frequencies less than $2\Delta/\hbar$, the theory predicts that $\text{Im } J_2(\omega) / \text{Im } J_1(\omega)$ is a positive, temperature dependent constant that approaches +1 at $T = 0$.^{7,8}

Whether this is the case in a real junction is a matter of dispute. Langenberg, Pedersen, and Finnegan suggest that for a lead tunnel junction at 4.2K, $\text{Im } J_2(\omega) / \text{Im } J_1(\omega)$ is approximately -0.7 at 10 GHz.⁹ The above theory suggests that this ratio should be +1 under these conditions.⁸ Langenberg, et al. base their conclusion on measurements of the Q of the plasma resonance. Equation 2-33b says that if $\text{Im } J_2(\omega) / \text{Im } J_1(\omega) = \sigma_1 / \sigma_0$ is negative, then a plot of f_p / Q versus $\cos\phi_0$, where f_p is the plasma frequency, will have negative slope. This is what was observed in the experiment. On the other hand, if the experiment is done at frequencies where $\text{Im } J_1(\omega) / \omega \sim 1/\omega$, then f_p / Q versus $\cos\phi_0$ can have a negative slope independent of the sign of $\text{Im } J_2(\omega) / \text{Im } J_1(\omega)$. This effect is not sufficient to reconcile the results of the Langenberg experiment with the theory. But it suggests that the experimental results are not conclusive. This is discussed further in Chapter 6.

7. The nonlinear quasiparticle resistance can be used for high frequency mixing applications. Because of the reactance associated with $\text{Re } J_1(\omega)$, such a mixer can theoretically show conversion gain.²⁰ If a tunnel junction is connected to a transmission line, the impedance of the transmission line will appear as an additional conductance in equations 2-28 and 2-31. For many applications, it is assumed that one wants to match the transmission line impedance to the normal-state resistance of the junction. In terms of the conductance of equation 2-28, this matching condition will hide the desired nonlinear effect of $\text{Im } J_1(\omega)$. To operate a tunnel junction quasiparticle mixer with gain requires that there be a mismatch between the junction and its microwave surroundings.

CHAPTER 3

ELECTRONIC SIMULATION OF THE RSJ MODEL

3.1 Introduction

Calculations based on either the Werthamer or RSJ models are usually quite intimidating. There are few analytic solutions, and perturbation theories are complicated and tend to diverge.²² Digital calculations are difficult, use much computer time, and occasionally give misleading results. To include the effects of capacitance, source impedance, and time dependent sources in a calculation only makes the problem worse.²

The motivation for using an electronic analogue stems from the extremely close similarity between the RSJ model of a Josephson junction and a phase-locked loop. The correspondence between the two is quite direct in that phase, voltage, and current in one are equivalent to phase, voltage, and current in the other. Mathematically, the only difference between the two is in the sizes of I_J , R_N , and $2e/h$. However, this allows one to make an extremely wide variety of measurements on an analogue that would be difficult to make using a real junction. In terms of speed, simplicity, ease of changing parameters, and ease of interpreting results, an analogue compares favorably with digital methods. The accuracy of measurements obtained using an analogue is often quite good, and there are certain cases where an analogue neatly avoids pitfalls that beset even the most carefully performed digital computations (i.e., calculation of subharmonic step heights).

3.2 Existing Analogues

The original phase-locked loop analogue of the Josephson effects was reported by Bak and Pedersen in 1973.⁴ There have been various other analogues reported in the literature, most of which are also phase-locked loop designs. Before discussing the design and use of a Bak type analogue in detail, we summarize the principles of several analogues.

The Bak and Pedersen Analogue⁴

This is basically a phase-locked loop containing a voltage to current converter. With reference to Figure 3-1, there are five distinct building blocks in the circuit. They are:

VCO Voltage Controlled Oscillator

LO Local Oscillator

X Multiplier

LPF Low Pass Filter

VCCS Voltage Controlled Current Source

The VCO generates a signal

$$V_{VCO} = A_1 \sin(\omega t + K \int V_{in} dt) \quad (3-1)$$

where V_{in} is the voltage at the input to the device. The quantity K is known as the VCO gain constant, and is the analogue of $2e/h$ in a real junction.

The local oscillator produces a signal

$$V_{LO} = A_2 \cos \omega_0 t \quad (3-2)$$

Note that A_1 , A_2 , and K are independent of V_{in} . The outputs of the VCO and LO are multiplied to produce a signal

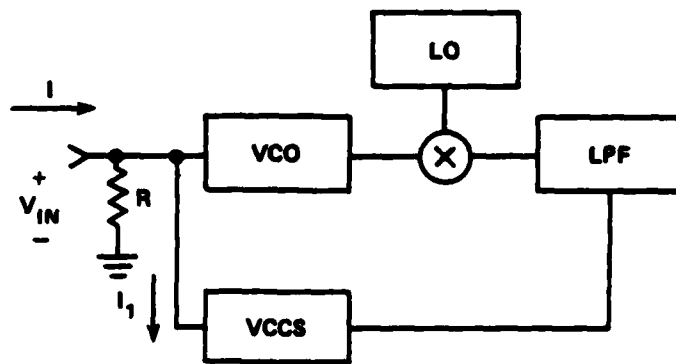


FIGURE 3-1. THE BAK AND PEDERSEN ANALOGUE

$$V_{MULT} = \frac{1}{2} A_1 A_2 A_3 \left[\sin K \int V_{in} dt + \sin (2\omega_0 t + K \int V_{in} dt) \right] \quad (3-3)$$

where A_3 is the conversion gain of the multiplier.

The LPF serves to remove the signal at $2\omega_0$ from the output of the multiplier before the signal reaches the VCCS. We have

$$V_{LPF} = \frac{1}{2} A_1 A_2 A_3 A_4 \sin \phi \quad (3-4)$$

where A_4 is the low frequency gain of the filter, and $d\phi/dt = KV_{in}$.

The VCCS generates a current

$$I = \frac{1}{2} GA_1 A_2 A_3 A_4 \sin \phi \quad (3-5)$$

where G is the transconductance of the current source. If we define

$$I_J = \frac{1}{2} GA_1 A_2 A_3 A_4$$

we have for the current I_1 in Figure 3-1,

$$I_1 = I_J \sin \phi \quad (3-6)$$

At this point, it is stressed that the VCCS can act as both a source and sink of current, and that essentially no current flows into the VCO, it being a high input impedance device.

The output of the VCCS is connected to the input of the VCO. With the addition of a resistor in parallel with the input, the current-voltage relationship of the overall circuit is

$$I = I_J \sin \phi + \frac{V_{in}}{R} \quad \text{where } \frac{d\phi}{dt} = KV_{in} \quad (3-7)$$

Analogue of this form have been widely used.^{23,24} The main advantages of this scheme are its simplicity and the dimensional correspondence between parameters in the analogue and those in a real junction. This makes it easy to

model the effects of shunt capacitance, finite source impedance, etc. An additional advantage is that the $\sin k \int v_{in} dt$ dependence of the analogue is implicit in the operation of the VCO.

There are two major disadvantages to the Bak scheme. First, the LPF introduces a frequency dependent phase shift to the $\sin \phi$ signal. This results in the addition of a voltage dependent $\cos \phi$ term to the overall current-voltage relationship of the device. The amplitude of this term is always negative with respect to the sign of I_J . This amplitude can be made quite small, but not always as small as one might like. The other disadvantage is that the phase of the supercurrent is not directly accessible—that is, there is no signal proportional to ϕ . This prevents the analogue from being used to model double junction SQUIDS or other devices where both ϕ and $\sin \phi$ are of interest.²⁵

The Gallop Analogue*

An analogue based on the Bak principle, but having a nonsinusoidal current-phase relation, was built by Gallop. The device is extremely simple, as the VCO, LO, multiplier, and LPF are incorporated into one phase-locked loop chip. This chip operates in a digital switching mode. That is, it operates using square waves, as opposed to sine waves. This precludes its use for quantitative measurements, but the device will qualitatively model the Josephson effects.

The Taunton and Halse Analogue²⁶

This is basically a quadrature version of the Bak analogue. In addition to the $\sin \phi$ term, there is a second feedback loop that models a $\cos \phi$ term.

*J. Gallop, private communication.

This term is made voltage dependent by the inclusion of a field effect transistor in the cosine loop. This FET gate is connected in such a fashion that it models both the $\sigma_1 V \cos \phi$ term and the $\sigma_0 V$ term in equation 2-5. Since the $\sin \phi$ and $\cos \phi$ terms are independent, and not related via the Kramers-Kronig relations, the amplitude and sign of σ_1 with respect to I_J and σ_0 is arbitrary.

The circuit has been used to investigate the effects of thermal noise and the influence of the $\cos \phi$ term. Good agreement with theory is reported, although the effect of the $\cos \phi$ term is undramatic. The circuit is much more complex than the Bak analogue, and suffers from stability problems.* In addition, the problem of an unwanted phase shift associated with filtering the outputs of the multipliers may result in the introduction of a $\cos \phi$ term in the sine loop, and a $\sin \phi$ term in the cosine loop. However, the circuit seems to have produced useful results.

The Hamilton Analogue ²⁷

This is based on a more traditional style of analogue computation than the Bak analogue is. The equations

$$\frac{dx}{dt} = (kV_{in})y \quad \frac{dy}{dt} = (-kV_{in})x \quad (3-8)$$

are solved subject to the constraint $x^2 + y^2 =$

I_J^2 . This results in the signal y having the form

$$y = I_J \sin \phi, \text{ where } \frac{d\phi}{dt} = kV_{in} \quad (3-9)$$

*M. R. Halse, private communication.

The circuit is built using integrated circuit multipliers, integrators, inverters, and summers. Unlike the Bak analogue, there is no distinct VCO, LO, or LPF. Although the circuit seems reasonable and is relatively simple, it has not been widely used. It may offer advantages over the Bak circuit, as unwanted high frequencies (i.e., $2\omega_0$ in equation 3-3) are not generated. On the other hand, the integrators probably introduce a $\cos\phi$ term similar to that caused by the low pass filter in the Bak analogue. And the use of five multipliers, as opposed to one in the Bak analogue, will increase the noise, harmonic distortion, DC offset error, and cost.

The Magerlein Analogue²⁸

In this analogue, there is no VCO or LPF. Instead, the input voltage to the analogue is integrated explicitly, and the resulting voltage passed through a sine conversion circuit. That is an integrator converts $d\phi/dt$ into ϕ , another circuit takes the sine. The $\sin\phi$ signal is then passed through a voltage to current converter, and fed back to the input. The advantage of this arrangement is that a signal proportional to ϕ is directly available. The disadvantages are that the integrator must be reset whenever ϕ reaches the voltage corresponding to $\pi/2$ (or the device will saturate), and the sine conversion circuit is not necessarily very accurate. The integrator is reset using a flip-flop to drive an electronic switch. This has the unfortunate result of putting a glitch in the Josephson oscillations every time the integrator resets. A copy of the Magerlein circuit has been built and tested by Brady.*

*R. Brady, private communication.

The Tuckerman Analogue²⁵

This is an analogue of a complete DC SQUID. It is essentially two Magerlein analogues connected to form a "superconducting" loop. Gyrator circuits are used to model the inductance of the loop. (A gyrator is a nonreciprocal amplifier circuit that can be used to make a capacitor look like an inductor.) The analogue suffers from the problems described for the Magerlein analogue. However, as the phase is required explicitly, one could not use a Bak type circuit instead.

The Yagi and Kurosawa Analogue²⁹

This is a precision version of the Magerlein analogue. The major difference between the two is the manner in which the sine conversion circuit operates. The Magerlein analogue uses a simple circuit based on the nonlinear behavior of a bipolar transistor. The Yagi simulator uses a series of transistor switches to create a five segment piecewise-linear approximation to a sine wave. The Yagi analogue also incorporates a network for modelling the nonlinear resistance associated with a tunnel junction. This consists of a two step piecewise-linear resistance circuit. There is no reactance associated with this, so it is not a true model of the nonlinear resistance described by the Werthamer theory.

The Prober Analogue

Prober, et al. have developed an analogue of the RSJ model in which the VCO generates short pulses rather than the usual sine or square wave.³² The pulses drive a sample and hold circuit which cleverly fashions a stair step approximation to $\sin\phi$ without the need for a low pass filter. The circuit, which also incorporates a voltage dependent conductance for modelling the nonlinear quasiparticle characteristic, is simple and works well. However,

there is a phase shift associated with the sample and hold technique which introduces a negative $\cos\phi$ amplitude similar to that expected for a low pass filter.

3.3 Design of an RSJ Analogue

In retrospect, the design of an analogue based on the Bak scheme is not very difficult. Of the five components, the VCO, LO, and multiplier require no special design considerations. The VCCS and low pass filter use standard circuit topologies, and computation of component values is not difficult.

The operating parameters of the device were chosen such that simple circuit techniques could be used, and so that the effects of circuit noise and parasitic capacitance are negligible. For the preliminary design:

$$I_J = 1 \text{ mA}$$

$$R_N = 1 \text{ k}\Omega$$

$$2e/h = 1000 \text{ hz/volt}$$

$$f_{LO} = f_{VCO} = 15 \text{ kHz}$$

The half power frequency of the low pass filter is 5 kHz.

The first three parameters are variable. The VCO center frequency can be fine tuned to equal that of the LO. This is to make the DC supercurrent occur at zero DC voltage. If $f_{LO} \neq f_{VCO}$, this "zeroth order step" will occur at finite voltage, and the entire I-V characteristic of the device will be shifted along a load line determined by R_N . This does not affect the shape of the characteristic, or the junction dynamics.

The VCO and LO are built using Intersil 8038 function generator chips. Their frequency of operation is determined by the appropriate choice of a timing

capacitor. The value of $2e/h$ for the VCO is determined by an external amplifier. The harmonic distortion of the 8038 is less than 1 percent at 15 kHz, but there is noticeable drift in the operating frequency due to thermal effects. Fortunately, this has minimal effect on the use of the analogue. The complete design details for the 8038 are described in a manufacturer's applications note.

The multiplier is an Analogue Devices AD530KH. Over its range of operation, its accuracy is quoted as 1 percent. The main disadvantage of the chip is that it requires three external presets.

The VCCS is a standard design, fully described in Motorola Applications Note AN-587. It can act both as a current source and a current sink, and the output impedance is easily made greater than 300 k Ω . With reference to Figure 3-2, we have

$$I_{out} = \frac{-V_{in}}{R_3 + R_L \left(\frac{R_3}{R_4} - \frac{R_2}{R_1} \right)} \quad (3-10)$$

$$Z_{out} = \frac{R_3}{\left[\frac{R_3}{R_4} - \frac{R_2}{R_1} \right]} \quad (3-11)$$

The device is very linear, and can provide several milliamps. However, the circuit will clip if the voltage at the output of the op amp approaches the supply voltage. This, rather than the power rating of the amplifier, is usually the limiting factor in how much current can be provided.

Although the design of the low pass filter is not complicated, its effect on the behavior of the analogue is slightly subtle. The phase shift of the

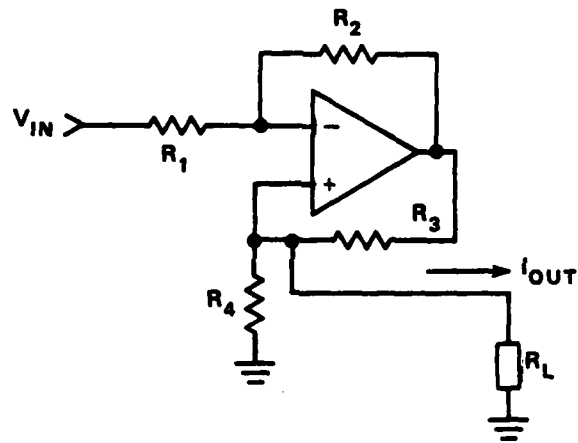


FIGURE 3-2. A VOLTAGE CONTROLLED CURRENT SOURCE

filter introduces a negative $\cos\phi$ term into the analogue. To see this, consider the single pole filter response given by

$$F(j\omega) = \frac{1 - j \omega/\omega_c}{1 + \omega^2/\omega_c^2} \quad (3-12)$$

where ω_c is the half-power frequency.

This response can be realized using a resistor and a capacitor; the resulting filter is referred to simply as an RC filter. When the analogue is biased with a constant voltage, the output of the multiplier will be of the form

$$V = \sin\omega t + \sin(2\omega_o t + \omega t)$$

The filter will eliminate the high frequency component, leaving a voltage

$$V_{LPF} = \sin\omega t \operatorname{Re} F(j\omega) + \cos\omega t \operatorname{Im} F(j\omega)$$

If $\omega \ll \omega_c$

$$\operatorname{Re} F(j\omega) \simeq 1 \quad (3-13)$$

$$\operatorname{Im} F(j\omega) \simeq -\omega/\omega_c$$

and

$$V_{LPF} \simeq \sin\omega t - \omega/\omega_c \cos\omega t$$

This changes the equation for the loop to

$$I = I_J \sin\phi - \frac{V}{R} \frac{\omega J}{\omega_c} + \cos\phi + \frac{V_{IN}}{R_N} \quad (3-14)$$

where $\omega J = 2eI_J R/\hbar$, $\frac{\sigma_1}{\sigma_0} = -\frac{\omega J}{\omega_c}$ (cf. (Eq. 2-31))

The voltage dependent $\cos\phi$ term has the same form as the quasiparticle-pair interference term in equation 2-5. Bak and Pedersen have utilized this similarity to investigate the effect of a negative $\cos\phi$ term on the dynamics of a Josephson junction.^{4,31} For most applications, this term is unimportant.⁸ However, it does affect the high frequency impedance of the device slightly, and can have a noticeable influence on the Q of the plasma resonance.

It was found that the single pole RC filter was not entirely effective in reducing the signal at frequency $2\omega_0 + \omega$. Rather than increase the frequency of the local oscillator, a more sophisticated filter was used. The filter, a three pole Butterworth, has the same half power frequency as the RC filter, but its response falls faster at high frequencies. This is evident in Figure 3-3, which shows the response curves for a one pole RC, three pole RC, and a three pole Butterworth filter. The respective response functions are:

$$F(s) = \frac{1}{1+s} \quad \text{one pole RC} \quad (3-15)$$

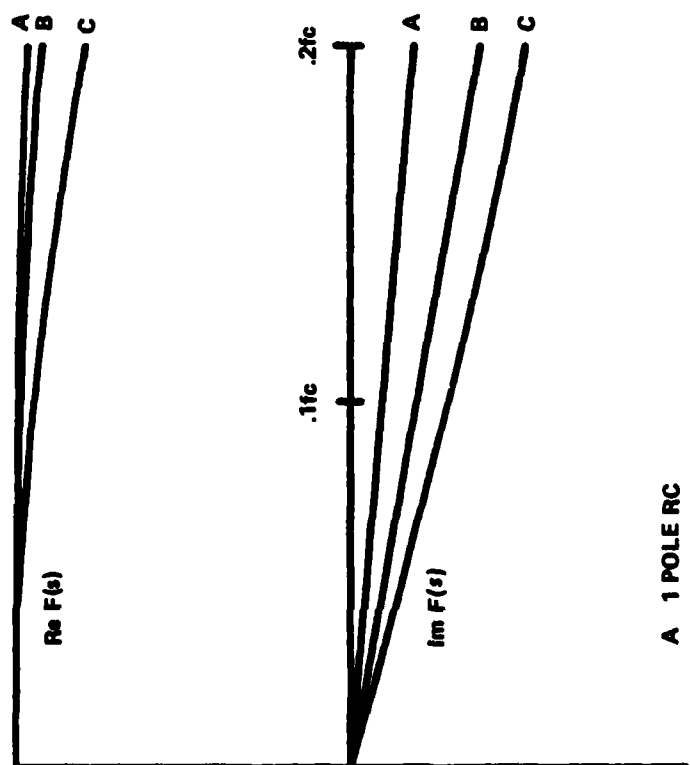
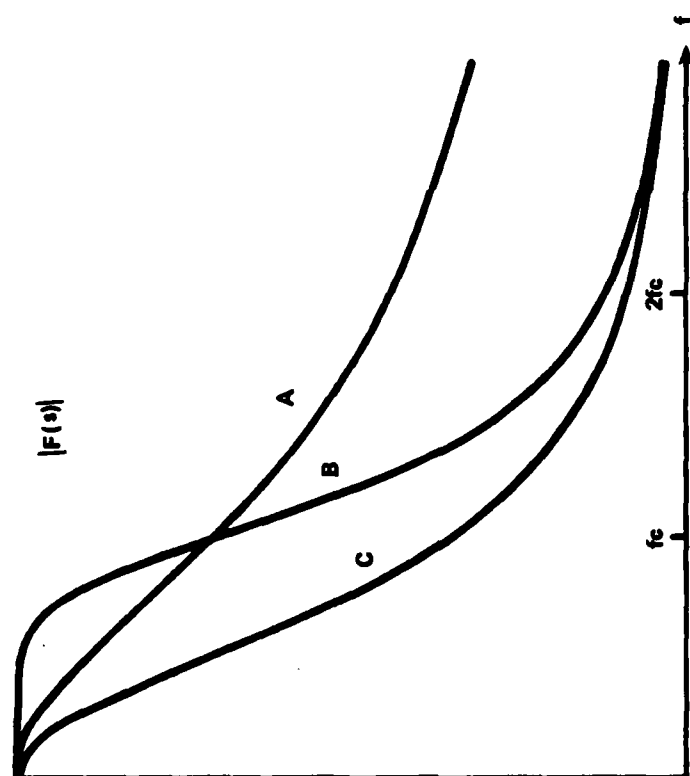
$$F(s) = \frac{1}{(1+s)^3} \quad \text{three pole RC}$$

$$F(s) = \frac{1}{s^3 + 2s^2 + 2s + 1} \quad \text{three pole Butterworth}$$

where $s = j\omega/\omega_c$.

All three filters in the figure have the same value of ω_c . Note that the tradeoff for reduction of high frequency feedthrough is an increase in the amplitude of $\text{Im } F(s)$, and consequently an increase in the $\cos\phi$ amplitude.

For typical parameters of $I_J = 1$ mA, $R_N = 500$ ohm, and $2e/h = 500$ Hz/volt, we have $\omega_J/\omega_c = .05$. Multiplying by 2 (since the Butterworth filter increases the $\cos\phi$ term by about that much), we have $\sigma_1/\sigma_0 = -0.1$.



- A 1 POLE RC
- B 3 POLE BUTTERWORTH
- C 3 POLE RC

FIGURE 3-3. LOW PASS FILTER RESPONSES

For most applications of the RSJ analogue, a $\cos\phi$ term of this magnitude will be unimportant. Provided that one is aware of it, it does not limit the usefulness of the analogue. From a design point of view, the three pole Butterworth is only slightly more complicated than the one pole RC filter.

Using the building blocks described above, the final design of the analogue is straightforward. However, before describing the use of the analogue, there are two more circuits that should be mentioned. The first of these is a multiple input current source for use in driving the analogue. It is similar to the VCCS in Figure 3-2, but allows for mixing of several different input signals. The second circuit, suggested by N. Bett of the Cavendish electronics section, is used to voltage bias the analogue. With reference to Figure 3-4, the voltage V_a is equal to V_{in} , and the signal V_{mon} provides a reference voltage which is proportional to the current through the analogue. The voltage V_{in} is provided by the multiple input current source described above; R_g is a variable source resistance. The voltage and current sources are connected with switches so that the analogue can be changed from voltage to current bias at a moment's notice. By raising R_g to a large value, the voltage source looks like a reasonable current source, but its dynamic range under these conditions is limited.

If proper attention has been given to the selection of part values, operation of the analogue is not complicated. When all of the building blocks are connected, it is necessary to adjust I_J , k , and R to suitable values. This usually means keeping $kI_J R / \omega_c \ll 1$, so that the LPF does not attenuate higher harmonics of the Josephson oscillations. If one wishes to

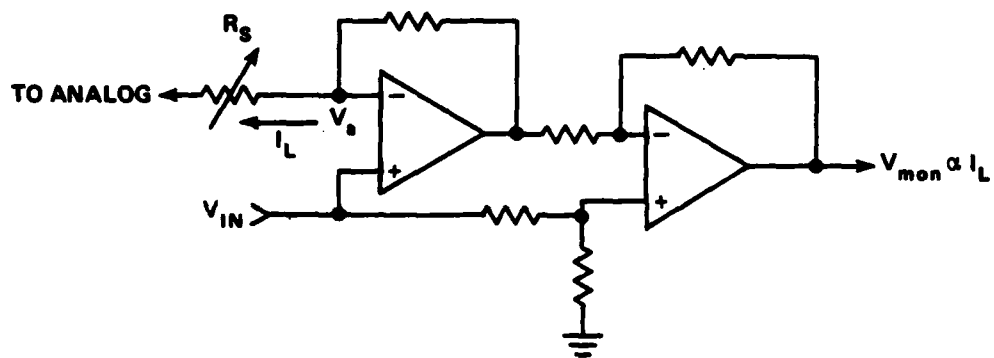


FIGURE 3-4. A VOLTAGE SOURCE

investigate the condition $\sigma_1/\sigma_0 = -1$, which requires that $kI_J R/\omega_c = 1$, the analogue must be operated at frequencies much less than ω_J or the results will be inaccurate.

3.4 Results Obtained with the RSJ Analogue

As the Bak analogue has been widely investigated by others, this section is relatively brief. Figure 3-5a shows the time averaged current-voltage characteristics for the analogue under current bias, voltage bias, and finite source impedance conditions. Figure 3-5b shows the effect of "microwaves" on the I-V characteristics. Figure 3-6 shows the voltage as a function of time for three values of I_{DC} for the current biased case, without microwaves. Figures 3-7 and 3-8 show the effects of varying the frequency and amplitude of the applied RF signal under current bias conditions.

Within a current step, the fundamental frequency of the internal oscillations of the analogue is an exact harmonic of the frequency of the applied RF current. Figure 3-9 shows the voltage as a function of time for the analogue when current biased within each of the first several steps in the I-V characteristic. Note that the signal is periodic, and that the number of pulses per cycle is equal to the "order" of the step. That is, the n^{th} step, which occurs at a DC voltage equal to $\bar{V} = n\hbar\omega/2e$, has n pulses per cycle. McDonald has suggested the use of this phenomenon for pulse generator applications.³⁵

Figure 3-10 compares a result obtained with the analogue with a computer calculation by Waldram, et al.³³ The parameters of the calculation and analogue measurement are similar, but there are no subharmonic steps in the analogue result. The RSJ model predicts that outside of a step, the voltage will be an almost-periodic function of time. It is the author's hypothesis that

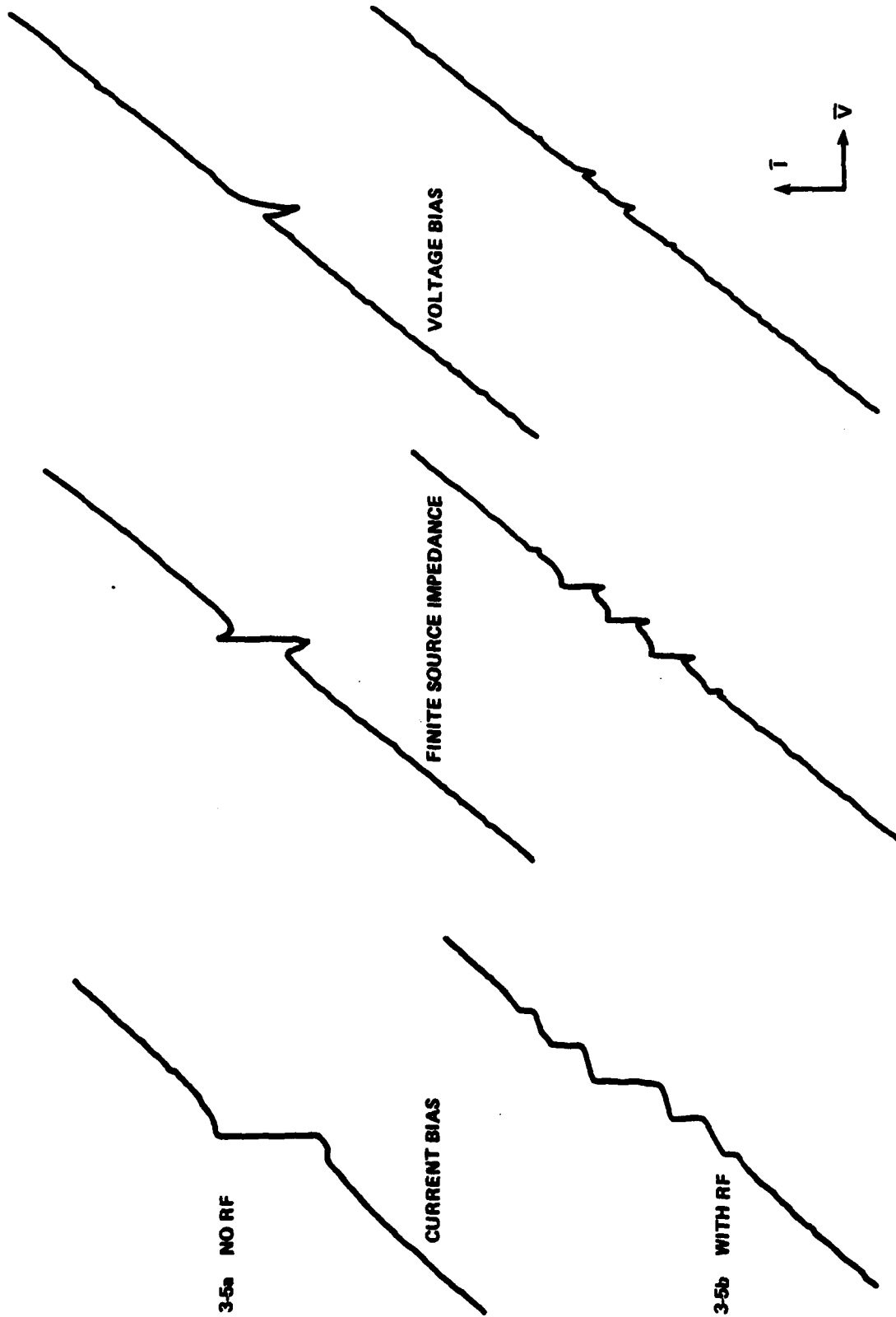
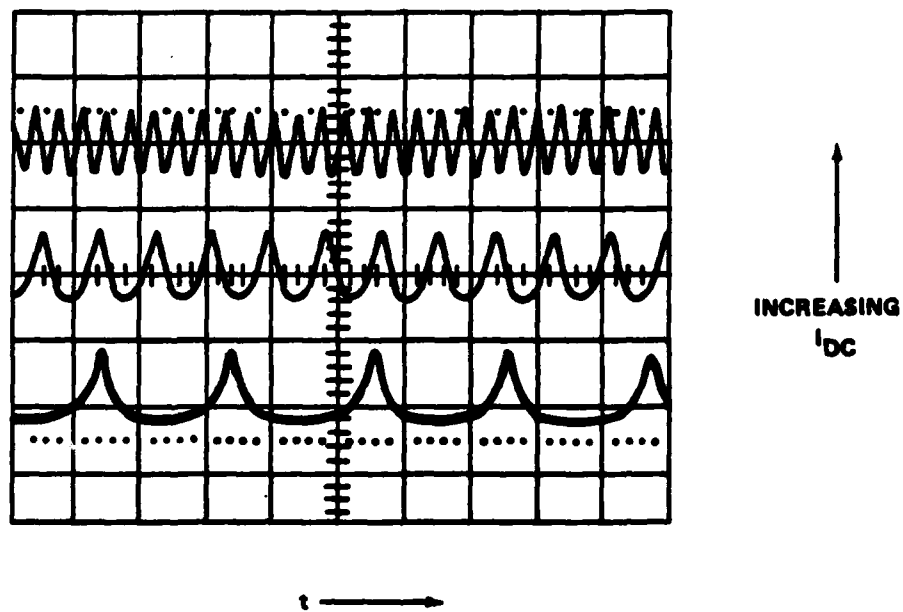


FIGURE 3-5. CHARACTERISTICS OF THE RSJ ANALOGUE



$$I = I_J \sin \phi + \frac{V}{R}$$

$$V(t) = V[1 + 2 \sum_n \left(\frac{1 - \sqrt{1 - \gamma^2}}{\gamma} \right)^n \cos n\omega_0 t]$$

$$\gamma = \frac{I_J}{I_{DC}} \quad \omega_0 = \frac{2eV}{h} \quad V = R \sqrt{I_{DC}^2 - I_J^2}$$

FIGURE 3-6. $V(t)$ FOR THREE VALUES OF I_{DC}

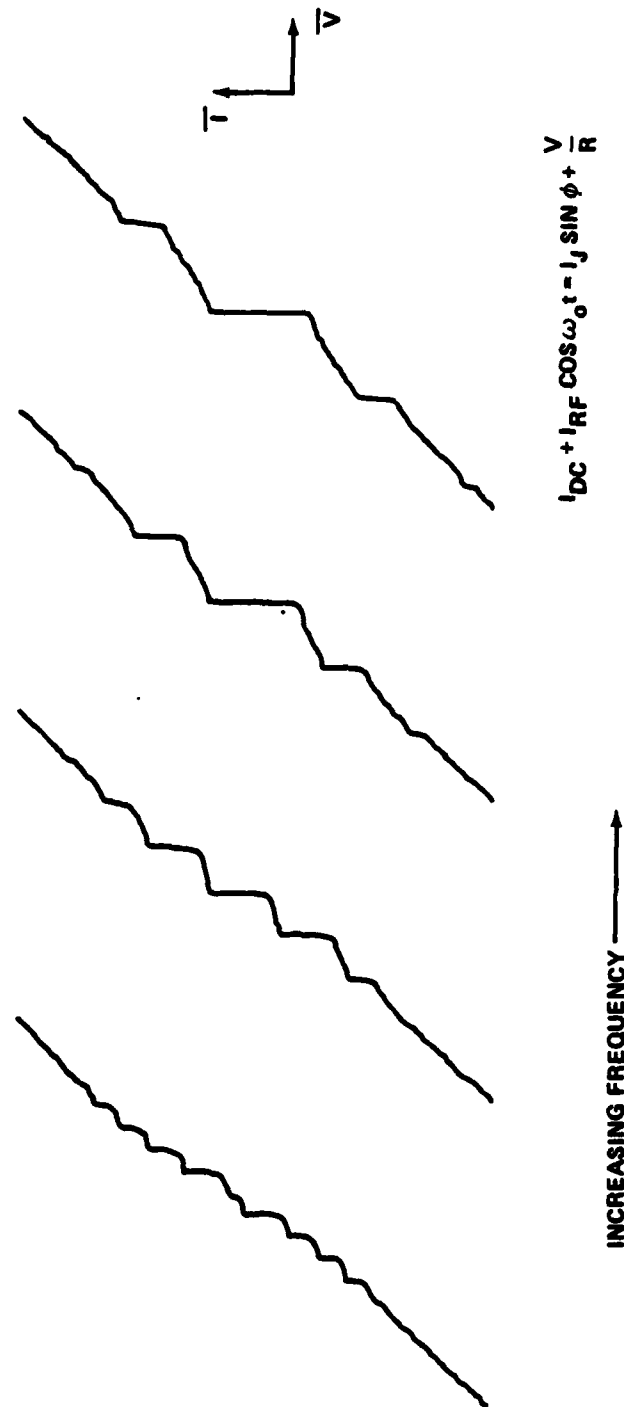


FIGURE 3-7. EFFECT OF VARYING FREQUENCY OF $I_{RF} \cos \omega_o t$ FOR THE RSJ ANALOGUE

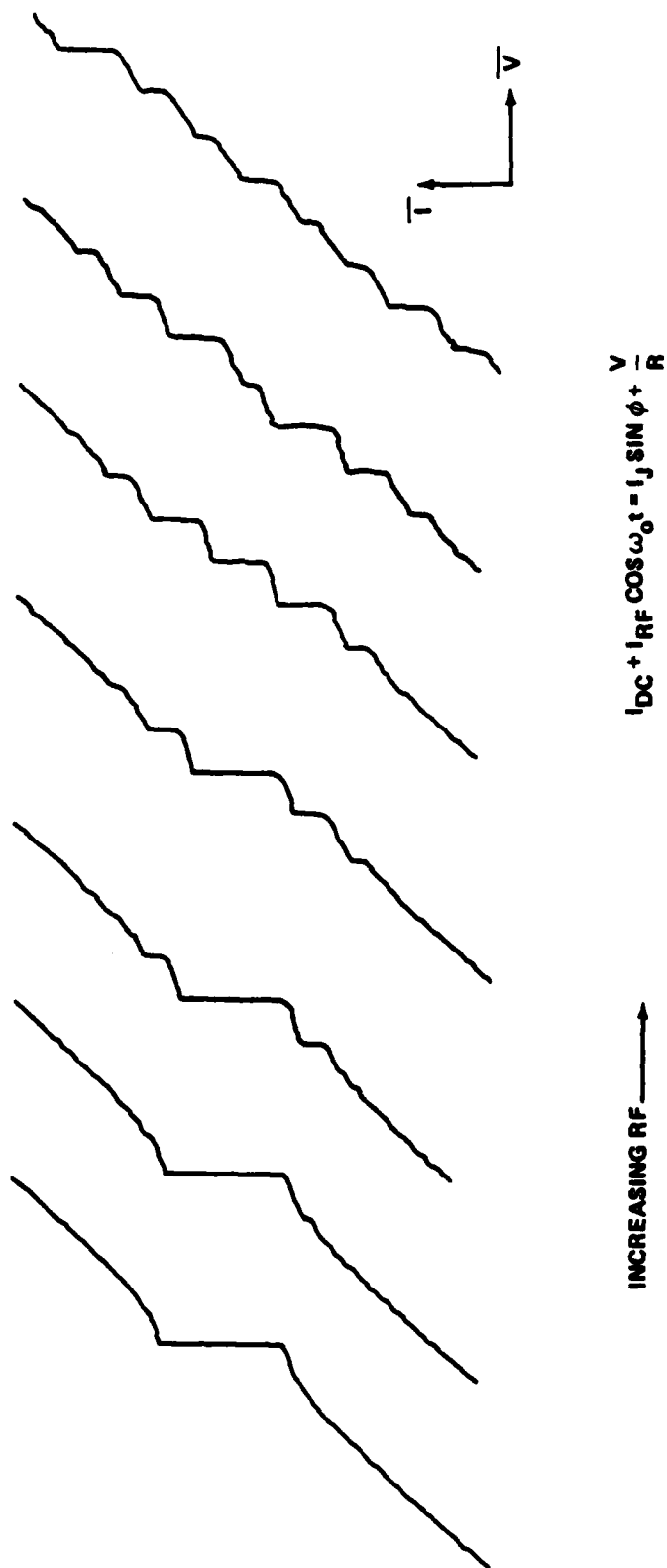


FIGURE 3-8. EFFECT OF VARYING AMPLITUDE OF $I_{RF} \cos \omega_0 t$ FOR THE RSJ ANALOGUE

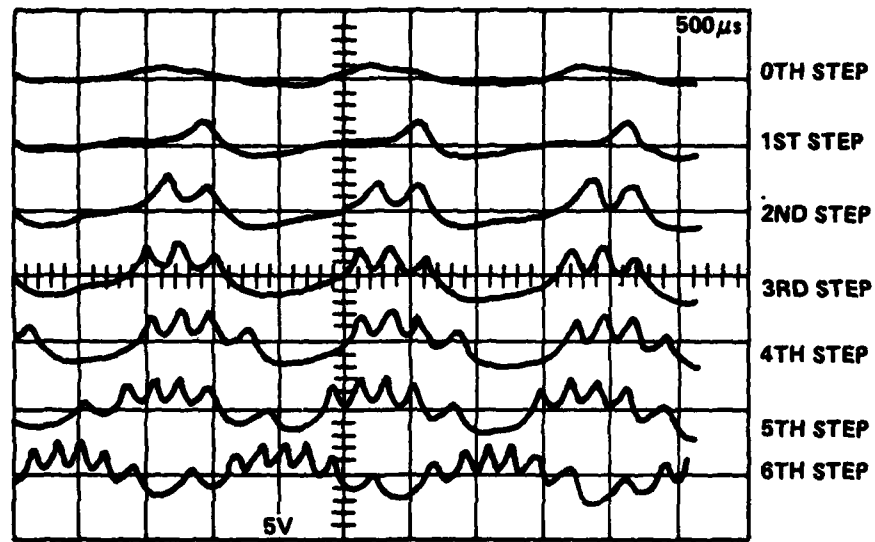


FIGURE 3-9. $V(t)$ WITHIN A CURRENT STEP

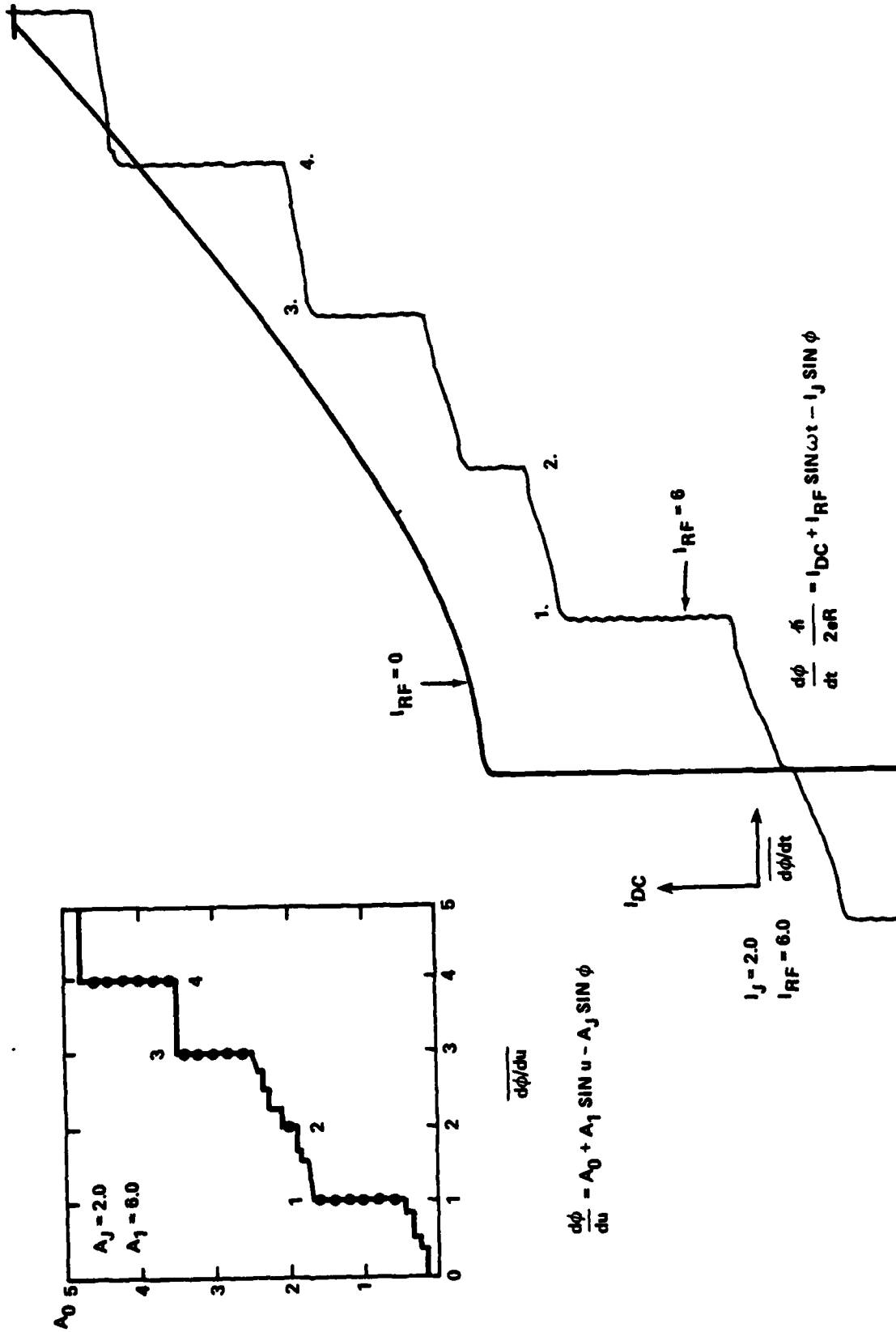


FIGURE 3-10. RESULTS FOR THE RSJ ANALOGUE VS. THOSE FOR A COMPUTER CALCULATION (AFTER WALDRAM, ET.AL. 33)

the computer calculation was not accurate enough to distinguish between periodic and almost periodic behavior in certain regions, and that subharmonic steps appeared as a result. This is an example of a calculation where the analogue avoids pitfalls that can be quite difficult to prevent in a computer calculation.

Figures 3-11 and 3-12 show the AC impedance of the device under conditions where the analogue is current biased by a signal $I = I_{DC} + I_{RF} \cos \omega t$. The impedance is measured by multiplying the voltage across the analogue by a reference signal that is either in phase or 90 degrees out of phase with the applied RF current. The time averaged output of the multiplier is proportional to either the real or imaginary part of the impedance at frequency ω . The results obtained using the analogue are compared with the computer calculations of Auracher and Van Duzer, which are shown as insets in the figures.³⁴ The DC I-V characteristics are plotted to show the relation between the junction impedance and the location of current steps in the characteristic. Note that the reactance between steps is zero. This results from the almost periodic nature of the AC voltage across the junction when it is biased between steps. The instantaneous reactance may be finite, but the time averaged reactance is zero. Within a step, the RSJ analogue works very well, but there is spurious interference between steps. This measurement is a good qualitative indication of the accuracy that one can expect from a simple analogue.

If there is a capacitance in parallel with the analogue, it will add a negative term to the total junction reactance. Within the zeroth order step, this will cause the total reactance to cross through zero at a particular value of DC current. This corresponds to the DC current for which the applied frequency is equal to the plasma frequency.

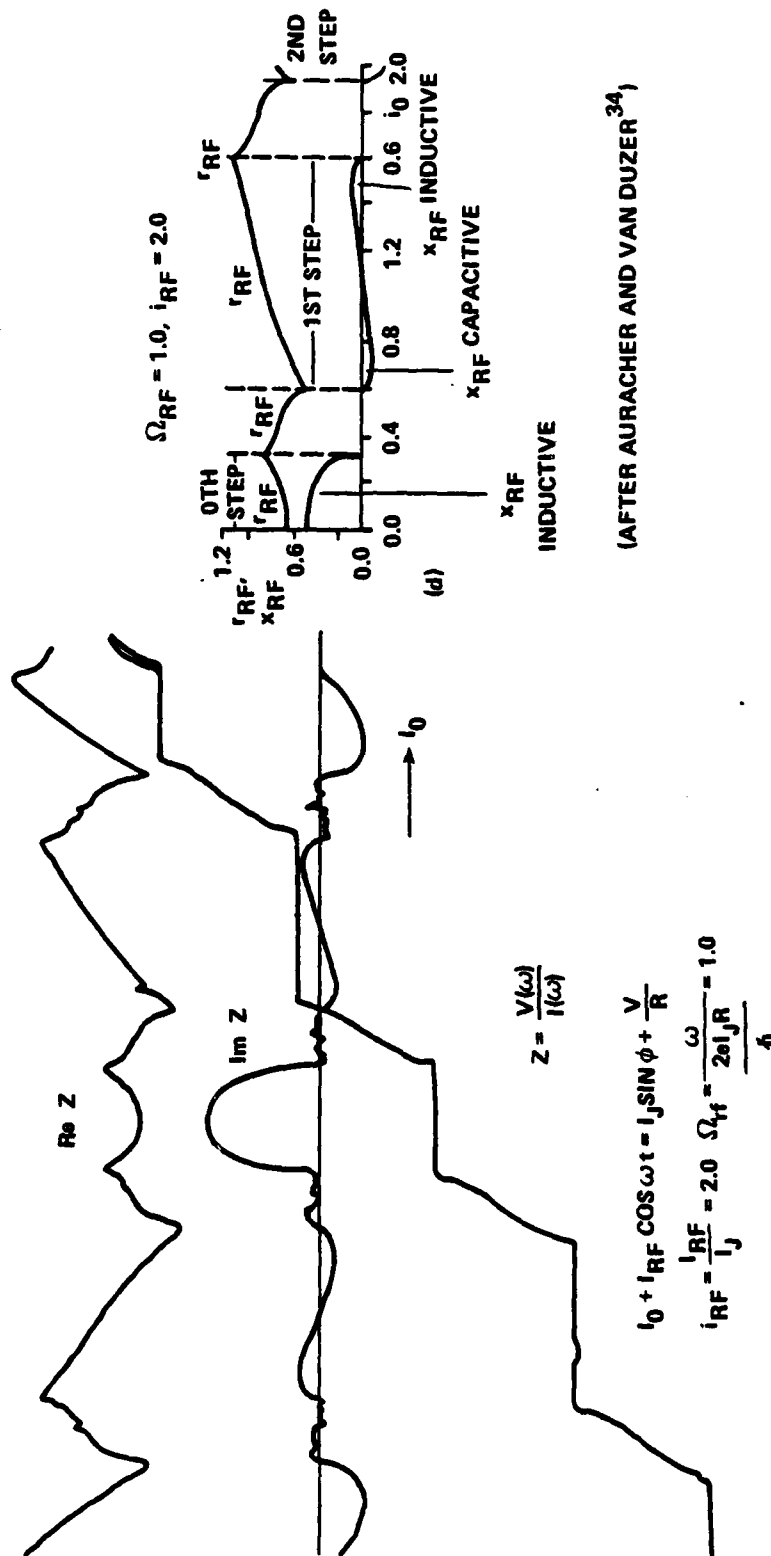
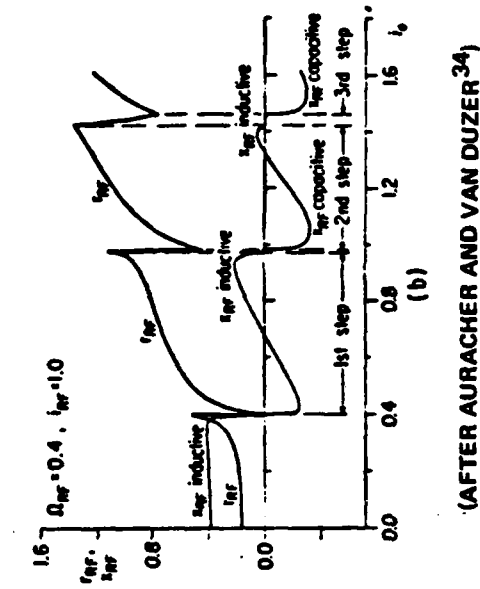


FIGURE 3-11. RF IMPEDANCE OF THE RSJ ANALOGUE COMPARED WITH COMPUTER RESULTS

(AFTER AURACHER AND VAN DUZER³⁴)



$\Omega_{RF} = .4 \quad i_{RF} = 1.0 \quad (\text{cf. FIG. 3-11})$

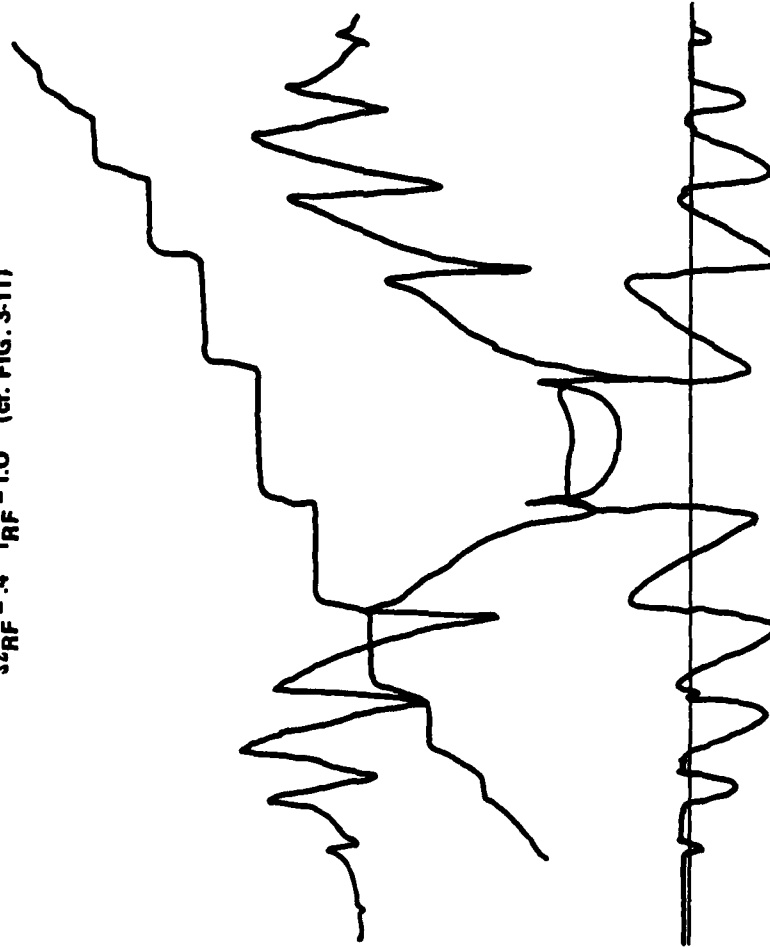


FIGURE 3-12. RF IMPEDANCE OF THE RSJ ANALOGUE, CONTINUED

CHAPTER 4

ELECTRONIC SIMULATION OF THE HIGH FREQUENCY THEORY

4.1 Introduction

The high frequency analogue is based on an idea by Waldram, who suggested that the Werthamer theory could be modelled electronically using a quadrature phase-locked loop and some sophisticated filters.⁶ As shown in section 2.6, equation 2-1 can be written

$$I(t) = \cos \frac{\phi}{2} \left(\sin \frac{\phi}{2} * j_1 \right) - \sin \frac{\phi}{2} \left(\cos \frac{\phi}{2} * j_1 \right) \quad (4-1)$$

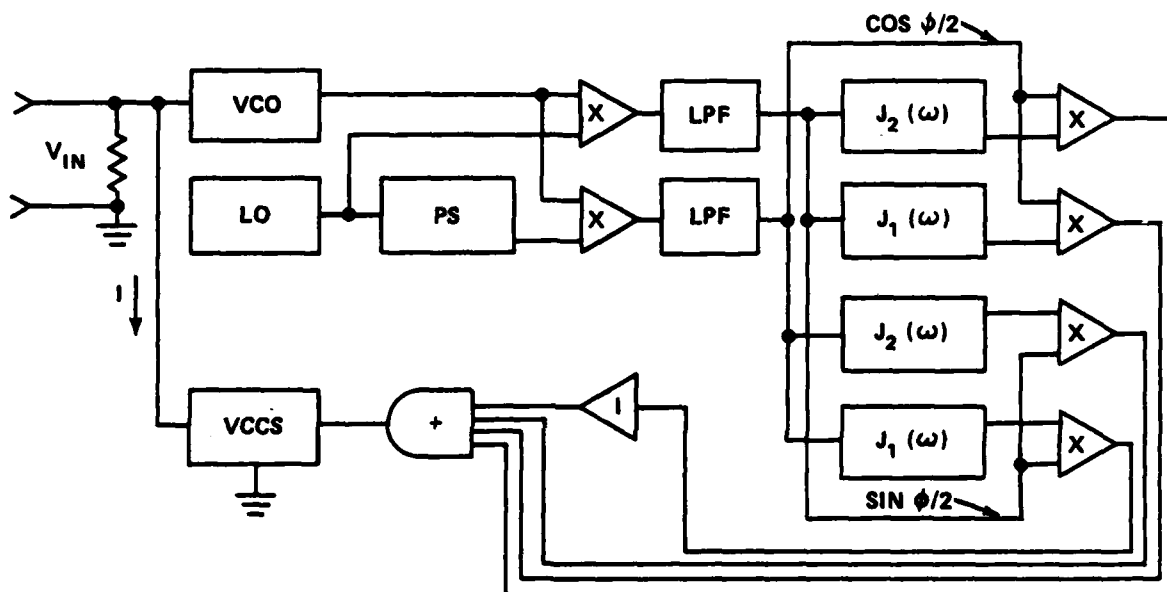
$$+ \sin \frac{\phi}{2} \left(\cos \frac{\phi}{2} * j_2 \right) + \cos \frac{\phi}{2} \left(\sin \frac{\phi}{2} * j_2 \right)$$

where the terms in brackets represent convolution integrals of the form

$$\left(\sin \frac{\phi}{2} * j_1 \right) = \int_{-\infty}^t \sin \frac{\phi(t')}{2} j_1(t-t') dt' \quad (4-2)$$

Electronically, this integral is the equivalent of running a signal $\sin \phi/2$ through a filter with impulse response $j_1(t)$. As $j_1(t)$ and $j_2(t)$ can be regarded as being real and causal, filters with suitable pulse responses can, in principle, be constructed.

The complete simulation of equation 4-1, including the generation of the $\sin \phi/2$ and $\cos \phi/2$ signals, is done using an elaboration of the Bak scheme described in the previous chapter. The essential differences are the inclusion of the filters and the use of two local oscillator signals instead of one. The scheme used is shown in Figure 4-1.



VCO	VOLTAGE CONTROLLED OSCILLATOR
LO	LOCAL OSCILLATOR
PS	PHASE SHIFTER
VCCS	VOLTAGE CONTROLLED CURRENT SOURCE
LPF	LOW PASS FILTER
I	INVERTER
+	ADDER

FIGURE 4-1. BLOCK DIAGRAM OF THE HIGH FREQUENCY ANALOGUE

The operation of the building blocks is identical to that in the Bak analogue. The only new component, apart from the filters, is the 90 degree, unity-gain phase shifter. This provides a quadrature reference to the local oscillator, which in turn allows the generation of both $\sin \phi/2$ and $\cos \phi/2$ signals. The VCO gain constant k now represents e/h instead of $2e/h$. If the J_1 filters are omitted, and the J_2 filters bypassed (i.e., $-J_2(\omega) = 1$), the circuit in Figure 4-1 reduces to a complicated version of the Bak analogue.

The prototype of the high frequency analogue is reported in a paper by Jablonski and Waldram,³⁵ a copy of which is attached as Appendix A. The paper is a self-contained description of how simple filters were used to model $j_1(t)$ and $j_2(t)$, and what results were obtained when these filters were incorporated into a quadrature phase-locked loop. The loop was built using the circuits described in Chapter 3, with additional filters based on calculations by Waldram, who matched the response curves of simple three and four pole RLC networks to sketches of Werthamer's expressions for $J_1(\omega)$ and $J_2(\omega)$ at $T = 0$. Although the prototype demonstrated the feasibility of the high frequency analogue, the filters were not accurate enough for the analogue to be very useful.

Attempts at improving the filters were made by P. Sinclair as part of a final year undergraduate physics project.* This effort was based on constructing several sets of electronic filters having adjustable parameters. Using what were essentially trial and error techniques, the parameters were varied to model $J_1(\omega)$ and $J_2(\omega)$ at a variety of temperatures. Unfortunately, this was not very successful.

*P. L. Sinclair, private communication

Simple numerical methods used by the author, however, proved quite successful for modelling $J_1(\omega)$ and $J_2(\omega)$ at $T = 0$. The increased accuracy of the resulting filters made it necessary to improve the performance of the quadrature phase-locked loop circuit. This chapter describes the design of the loop, the design and construction of the improved filters, and the results obtained with this second version of the high frequency analogue.

4.2 Design of the Loop

The prototype analogue had problems with harmonic distortion and temperature drift in the LO and VCO circuits. To cure this, these circuits were replaced by two commercial signal generators. One, with quadrature outputs, was used in place of the LO and phase shifter. The other was used as a VCO. The LO frequency of the analogue was set to 60 kHz, the maximum frequency of the quadrature generator.* The previous problems of harmonic distortion and drift essentially disappeared.

The six multipliers and the VCCS are the same circuits used in the Bak analogue. The low pass filters are four pole Butterworth's with a half power frequency of 50 kHz. The equivalent $\cos\phi$ amplitude (cf. Eq. 3-14) is $-.04$. The effect of this term on the current-voltage relationship of the analogue is not as simple as before, as the unwanted phase shift of the low pass filters affects both the $\sin\phi/2$ and $\cos\phi/2$ signals. However, provided that this phase shift is small, it can usually be neglected. The only measurement where this proved to be important was the investigation of the Q of the plasma resonance.

*In later versions of the analogue, the LO frequency was increased to 100 kHz, then subsequently reduced to 30 kHz (cf. Chapter 8).

Typical operating parameters of the analogue, along with the equivalent values for a real junction, are shown in Table 4-1.

4.3 Design of the Filters

All of the information concerning temperature, high frequency effects, and energy gap effects is contained in the expressions for $j_1(t)$ and $j_2(t)$. Consequently, the accuracy of the analogue is largely a question of the accuracy of the filters.

As was shown by Sinclair's work, the extension of Waldram's curve fitting techniques to more complicated filters is not very practical. Efforts were made by the author to match Werthamer's analytic expressions for $J_1(\omega)$ and $J_2(\omega)$ at $T = 0$ to the generalized expansion of a multipole RLC response, but it proved impossible to systematically match the Lorentzian behavior of the RLC networks to the logarithmic behavior of the Werthamer expressions.

A numerical approach was tried next. This was based on matching the response of a multipole RLC network to the numerical values of $J_1(\omega)$ and $J_2(\omega)$ at an arbitrary number of frequencies. This method was surprisingly successful, and has the advantage of being useful for designing filters to model tunnelling at $T = 0$, where analytic expressions for $J_1(\omega)$ and $J_2(\omega)$ do not exist. This numerical method is described below.

The response of an RLC network can be expressed as

$$F(\omega) = \frac{a_0 + a_1 s + a_2 s^2 + \dots + a_{n-1} s^{n-1}}{1 + A_1 s + A_2 s^2 + \dots + A_n s^n} \quad (4-3)$$

where $s = j\omega$

Table 4-1 Typical Parameters of the Analogue Compared With Those
of a Real Superconducting Tunnel Junction

	<u>The Analogue</u>	<u>A Tunnel Junction</u>
I_J	.7 mA	1 mA
R_N	1500 ohm	2.5 ohm
$2e/h$	1500 hz/volt	483 MHz/ μ volt
$f_{\text{gap}} = 2 \Delta/h$	1000 hz	725 GHz
$V_{\text{gap}} = 2\Delta/e$	1.33 volts	3 mV

$F(s)$ contains $2n$ unknowns, and can be matched to an expression for $J_1(\omega)$ or $J_2(\omega)$ at n different frequencies. (The real and imaginary parts of $F(s)$ and $J(\omega)$ are simultaneously matched; as $J_1(\omega)$ and $J_2(\omega)$ are 0 for $\omega = \infty$, a_n has been set to zero.) The choice of the n frequencies is completely arbitrary. However, the quality of the fit of $F(s)$ to $J(\omega)$ at other frequencies can be made very good by suitable choice of the n frequencies.

As an example, consider a nine point fit to $J_1(\omega)$ at $T = 0$. Figure 4-2 shows a sketch of the function. Rather than design a filter having a divergent response as $\omega \rightarrow \infty$, a linear term has been subtracted from $\text{Im } J_1(\omega)$. This term is added back by means of a resistor placed in parallel with the input to the analogue (cf. Figure 4-1). Removal of the linear term in $\text{Im } J_1(\omega)$ causes $\text{Re } J_1(\omega)$ to be shifted by a constant, which has no effect on the behavior of the analogue (cf. section 2.6).

Numerical values for the resulting expressions at nine different frequencies are entered into a Hewlett-Packard desk top computer.

By expressing $\text{Re } J_1(\omega)$, $\text{Im } J_1(\omega)$, and ω as numbers, the equation

$$F(s) = J(\omega)$$

becomes a linear equation whose unknowns are the a_n and A_n of equation 4-3. Separating this equation into real and imaginary parts for nine choices of ω yields a system of 18 linear equations in 18 unknowns. A simple program, stored on magnetic tape, is used by the computer to calculate the $18 \times 19 = 342$ coefficients of these equations. Another program, supplied by Hewlett-Packard, solves these equations, and the a_n and A_n are printed out. The resulting expression for $F(s)$ is known as a Padé approximate.

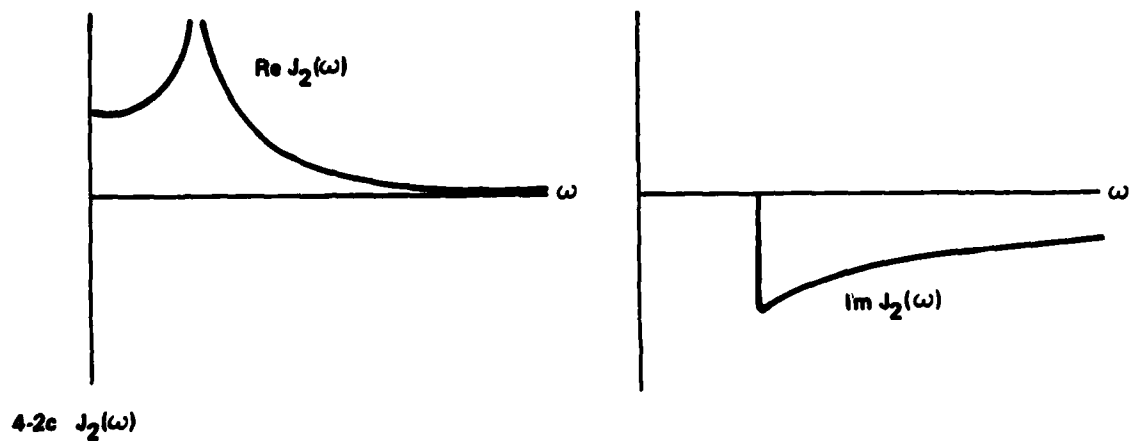
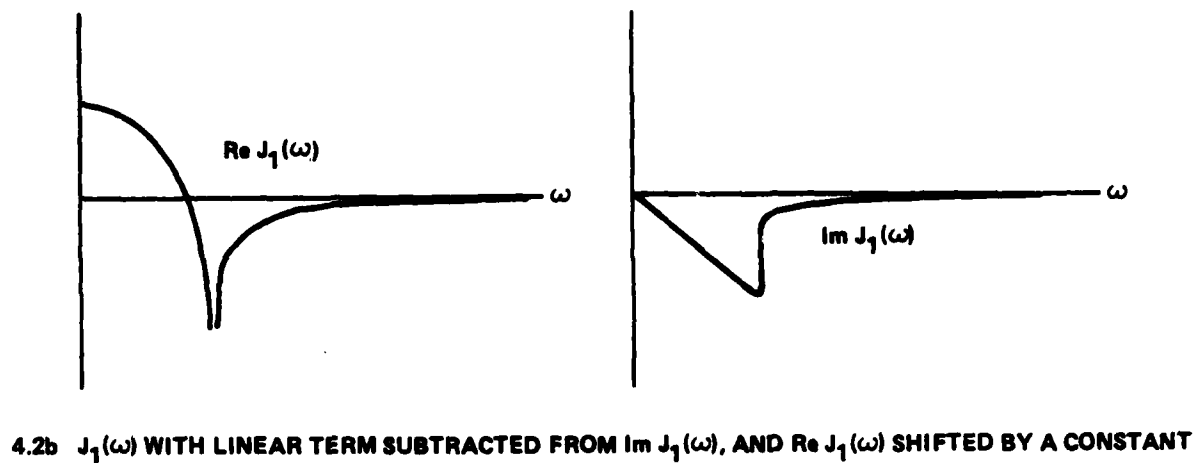
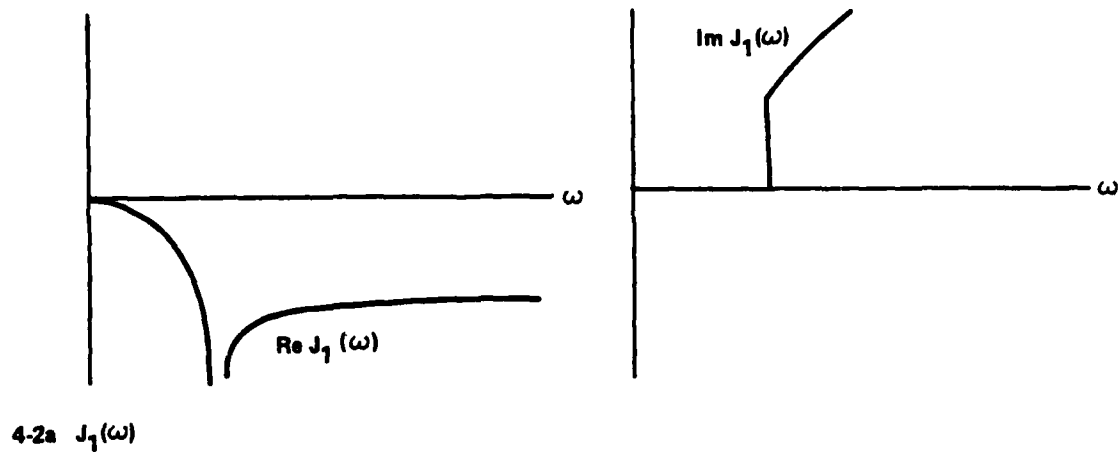


FIGURE 4-2. SKETCH OF THEORETICAL $J_1(\omega)$ AND $J_2(\omega)$ FOR $T = 0$

To verify that the Padé approximate can be implemented using electronic filters, it is necessary to factor the denominator and check that all of the poles of $F(s)$ lie in the left half of the complex frequency plane. This is done using a modified version of another Hewlett-Packard program. If the Padé approximate proves to be causal, a fourth program is used to plot $F(s)$. If the expression for $F(s)$ is not causal, or the plot does not look like $J(\omega)$, the whole process is started again using a new set of trial frequencies.

If $F(s)$ is a good match to $J(\omega)$, a program is used to calculate a biquadratic partial fractions expansion of $F(s)$. That is, $F(s)$ is written as

$$F(s) = \sum_n \frac{m_n s^2 + c_n s + d_n}{s^2 + a_n s + b_n} \quad (4-4)$$

By using the ratio of two quadratics, the coefficients a , b , c , d , and m will always be real. As will be seen, this form of $F(s)$ is particularly amenable to synthesis using active electronic filters.

Figure 4-3 shows a plot of the calculated nine pole Padé approximate to $J_1(\omega)$ at $T = 0$.^{*} The x's show the points at which the Padé approximate is equal to the theoretical expression for $J_1(\omega)$. The overshoot at the gap frequency is similar to the Gibbs phenomena associated with the use of Fourier techniques to model a discontinuity. Figure 4-4 shows the individual biquadratic components of the Padé approximate. Each curve corresponds to the response of a one or two pole RLC network, and can be viewed as being the combination of low pass and bandpass filter responses. Note that the parameter m for each filter is zero (i.e., the high frequency response of each filter goes

^{*}The linear term in $\text{Im } J_1(\omega)$, which was subtracted prior to the calculation, has been added to the result plotted in Figure 4-3. The corresponding constant in $\text{Re } J_1(\omega)$, however, has not.

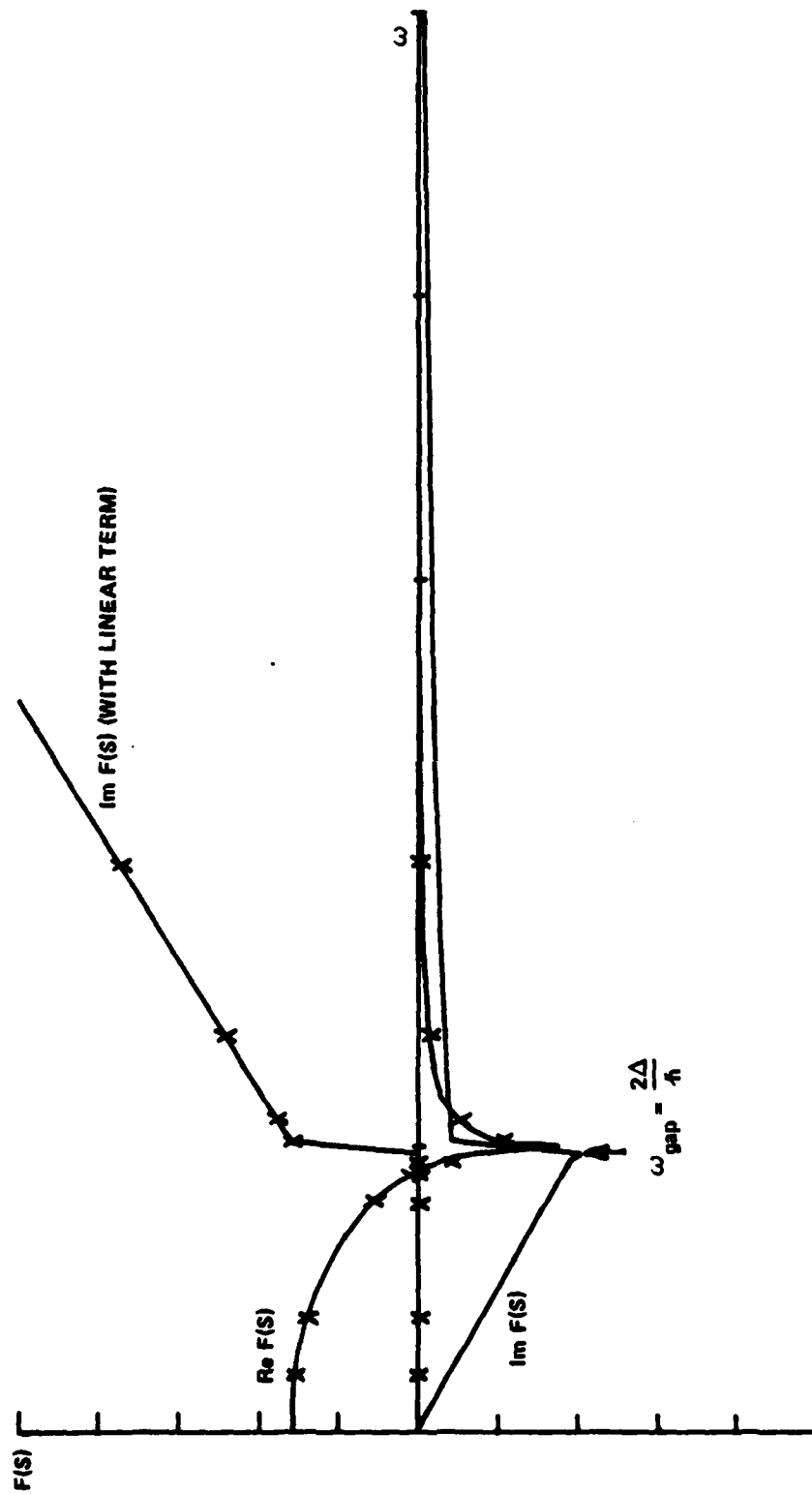


FIGURE 4-3. A 9 POLE PADÉ APPROXIMATE FOR $J_1(\omega)$ AT $T=0$

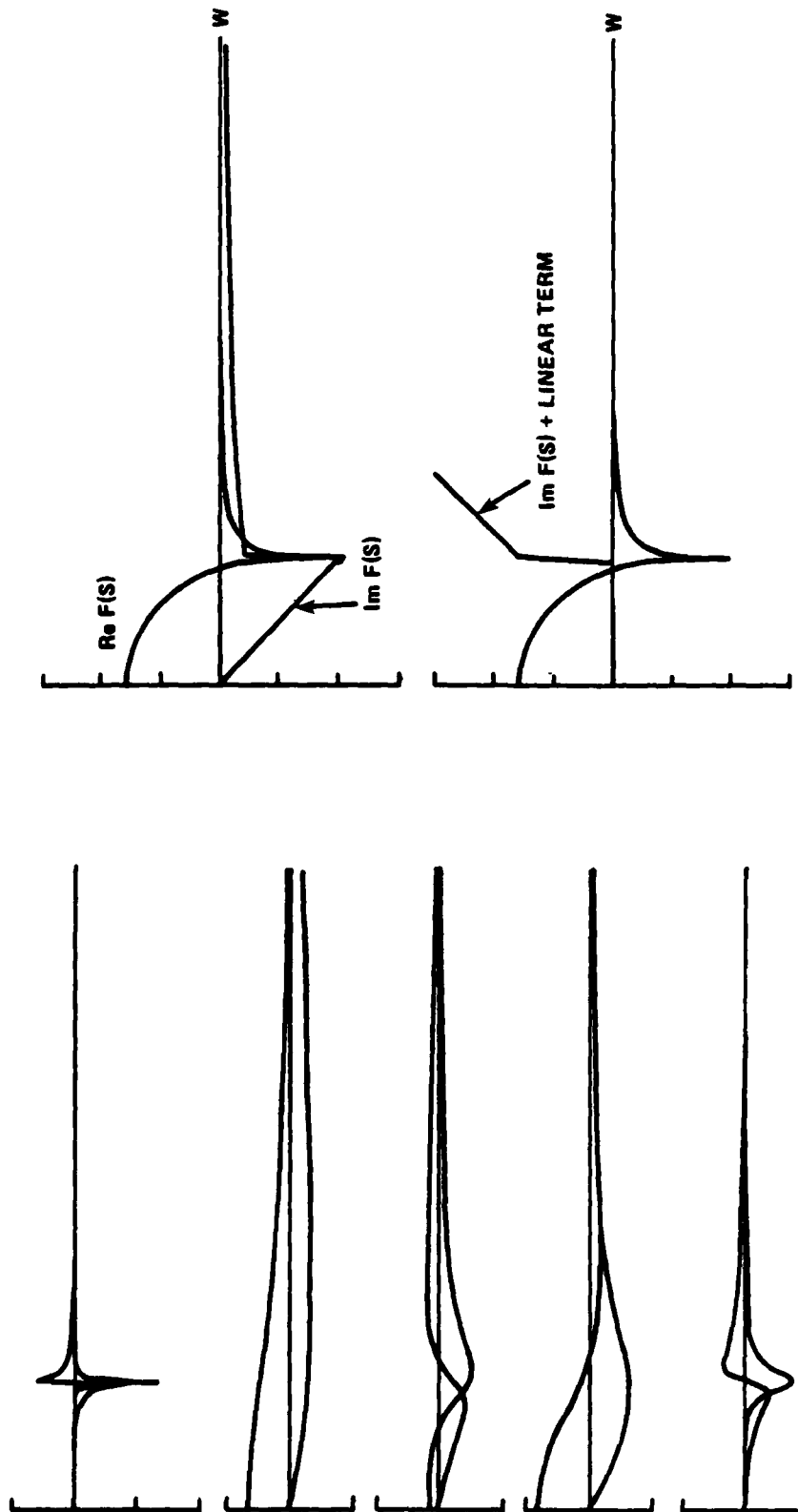


FIGURE 4-4. BIQUADRATIC COMPONENTS OF NINE POLE FIT TO $J_1(\omega)$ AT $T = 0$

to zero). Inspection of the individual curves suggests that trial and error techniques to determine the filter parameters would have been very difficult.

Figure 4-5 and 4-6 show the corresponding nine point fit to $J_2(\omega)$, along with its biquadratic components.

4.4 Construction of the Filters

The filters were built using an active op amp circuit known as the "biquad".³⁶ The circuit, shown in Figure 4-7, has a transfer function

$$\frac{V_{out}}{V_{in}} = \frac{ms^2 + cs + d}{s^2 + as + b} \quad (4-5)$$

where $s = j\omega$

The parameters a , b , c , d , and m are determined by appropriate choice of component values. The relative signs of c and d are determined by whether the point X in the circuit is connected to Y or Y' . Setting $m = 0$ is accomplished by removing R_7 from the circuit.

The performance of the biquad is comparable with, if not better than, its passive RLC equivalent.³⁷ As it contains no inductors, and has no special interface requirements, it is actually more convenient to design and use. An entire biquad costs about the same as the ferrite core needed for a single large inductor.

The choice of component values is very flexible. The main limitation is that R_1C_1 should equal R_3C_2 . This minimizes the sensitivity of the Q to variation in component values. For an arbitrary choice of a , b , c , and d (m is assumed to be zero), subject to the constraint $R_1C_1 = R_3C_2$, five component values must be computed. In the actual filters used in the analogue,

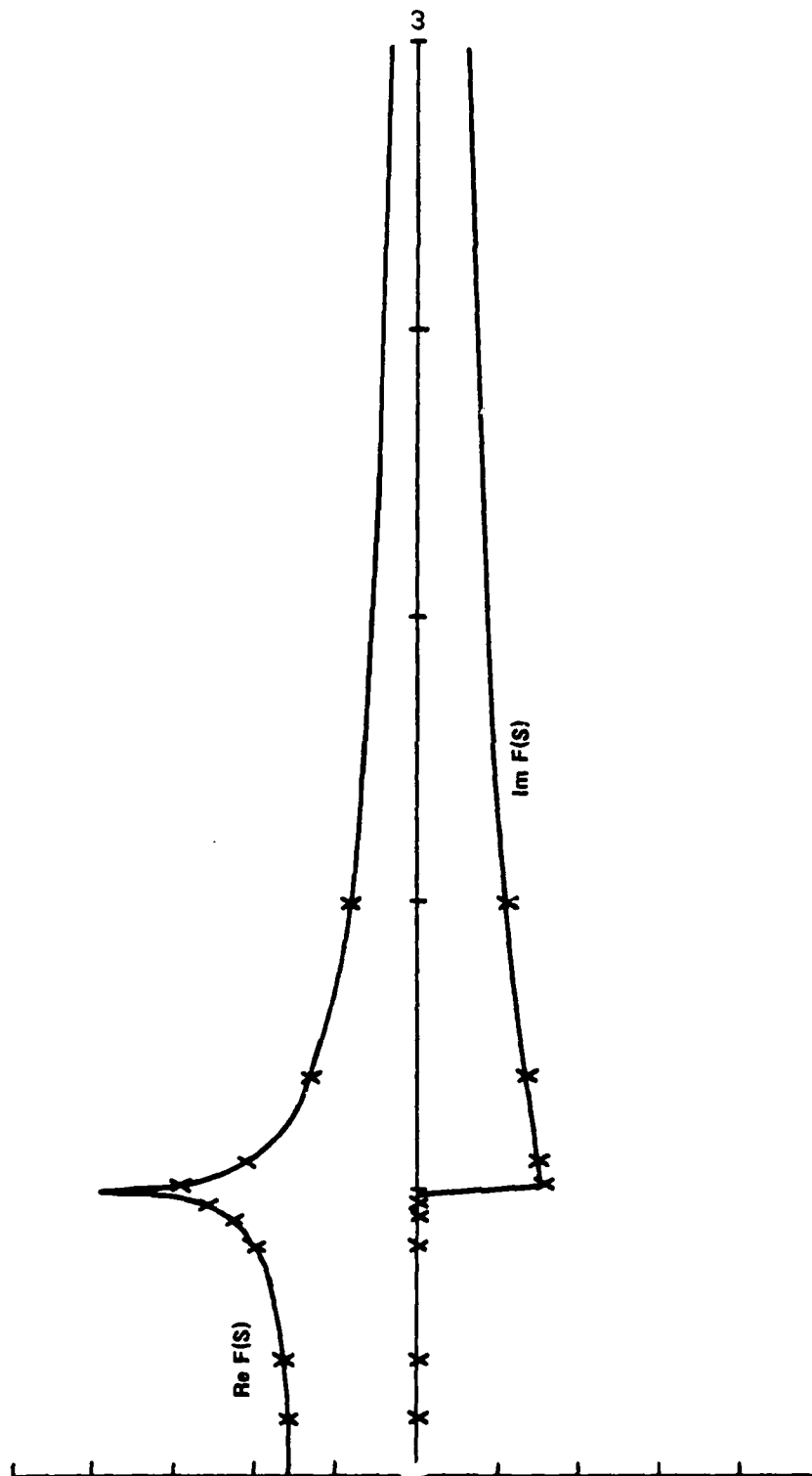


FIGURE 4-5. A 9 POLE PADE APPROXIMATE FOR $J_2(\omega)$ AT $T = 0$

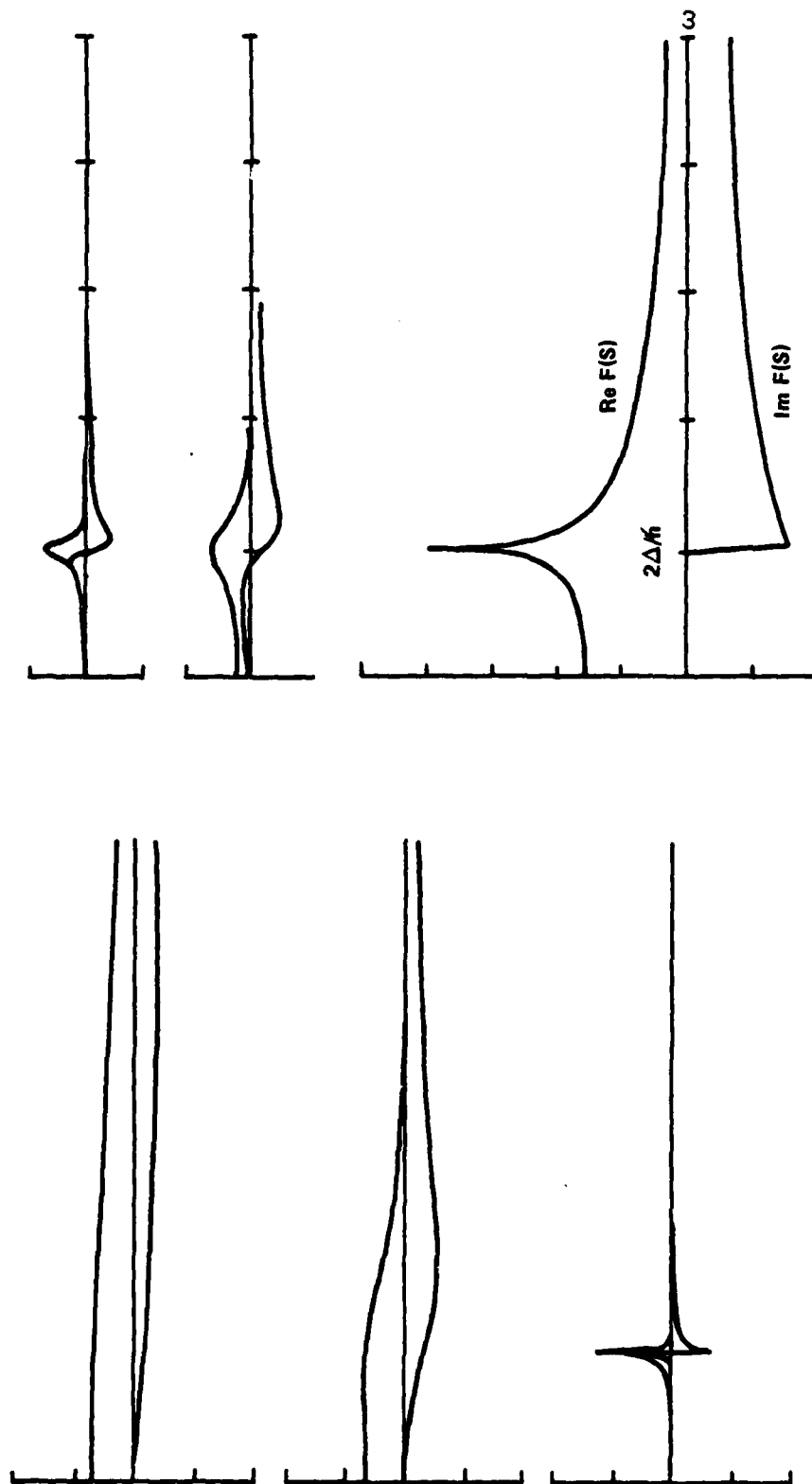


FIGURE 4-6. BIQUADRATIC COMPONENTS OF THE NINE FREQUENCY FIT TO $J_2(\omega)$ AT $T=0$

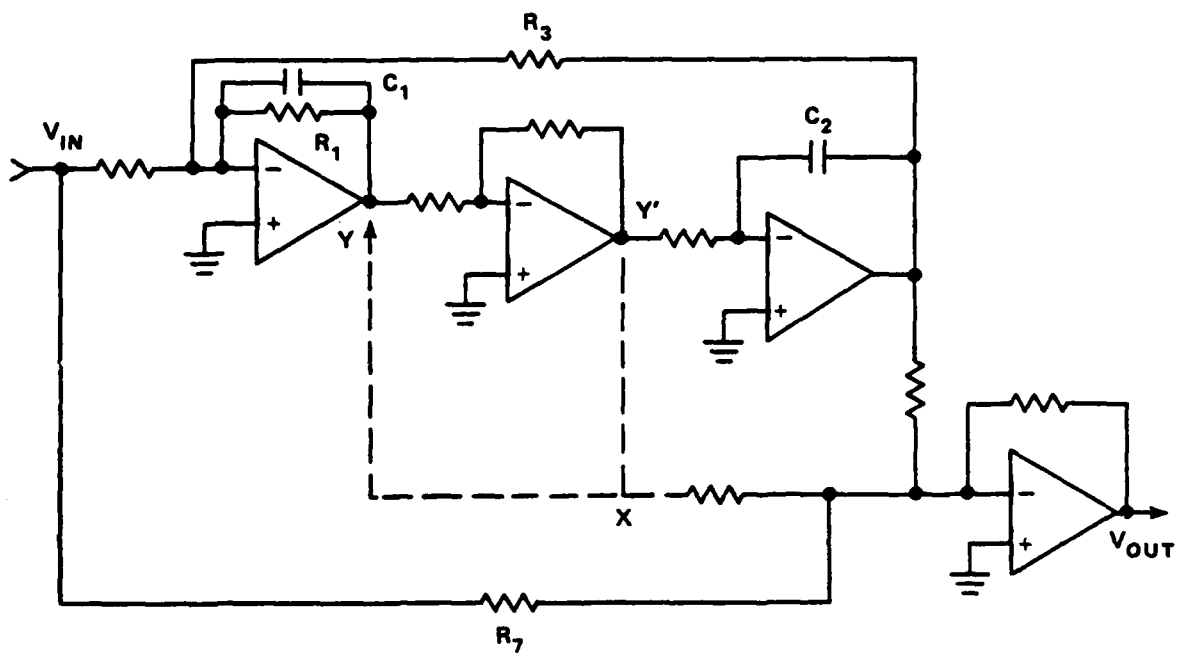


FIGURE 4-7. A BIQUADRATIC FILTER

each calculated value is implemented using two components. For example, if the calculated value for R_6 was 49,260, R_6 would be wired in the circuit as a 47k resistor in series with a 2.2k resistor.

To model the nine point fit to either $J_1(\omega)$ or $J_2(\omega)$ requires four biquads with two poles each, and a low pass filter having one pole. The filters are wired in parallel. That is, they all have the same input signal, and their outputs are summed.

Figures 4-8 and 4-9 show the measured response of the filters built to model the nine point fits to $J_1(\omega)$ and $J_2(\omega)$ at $T = 0$.

With reference to Figure 4-1, two $J_1(\omega)$ and two $J_2(\omega)$ filters are used in the analogue. By using filters having response functions $(J_1 + J_2)$ and $(J_1 - J_2)$, this redundancy could have been avoided. However, the use of duplicate J_1 and J_2 filters permits separate control of the pair and quasiparticle currents, which is a useful feature of the analogue. Figure 4-10 shows the response curves of the duplicate filters used in the analogue plotted together. Note that the resonance peaks occur at slightly different frequencies. Although undesirable, this inaccuracy does not appear to be a major shortcoming of the analogue. This problem is discussed in greater detail in Chapter 8.

To adjust the "temperature" of the analogue, it is necessary to modify $J_1(\omega)$ and $J_2(\omega)$. Unfortunately, preliminary attempts to do this by designing additional filters failed consistently. For the $T \neq 0$ case, the Pade approximate technique kept resulting in nonrealizable filter responses, where one or more of the poles of $F(s)$ were in the positive half of the complex frequency plane. This problem was overcome eventually (cf. Chapter 7). However, results presented in this chapter are limited to the case where the analogue models Josephson tunnelling at $T = 0$.

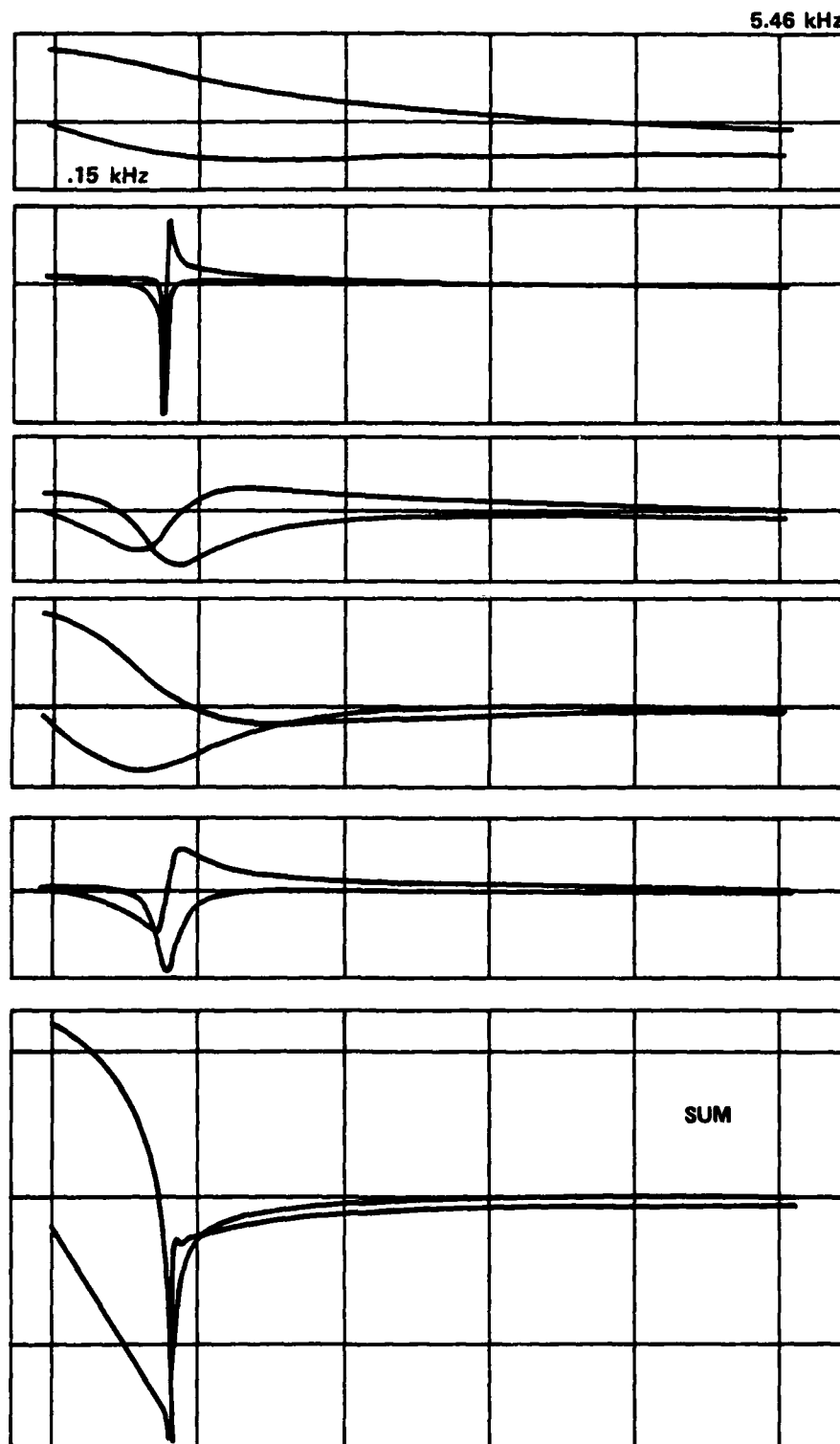


FIGURE 4-8. MEASURED RESPONSE OF THE $J_1(\omega)$ FILTERS

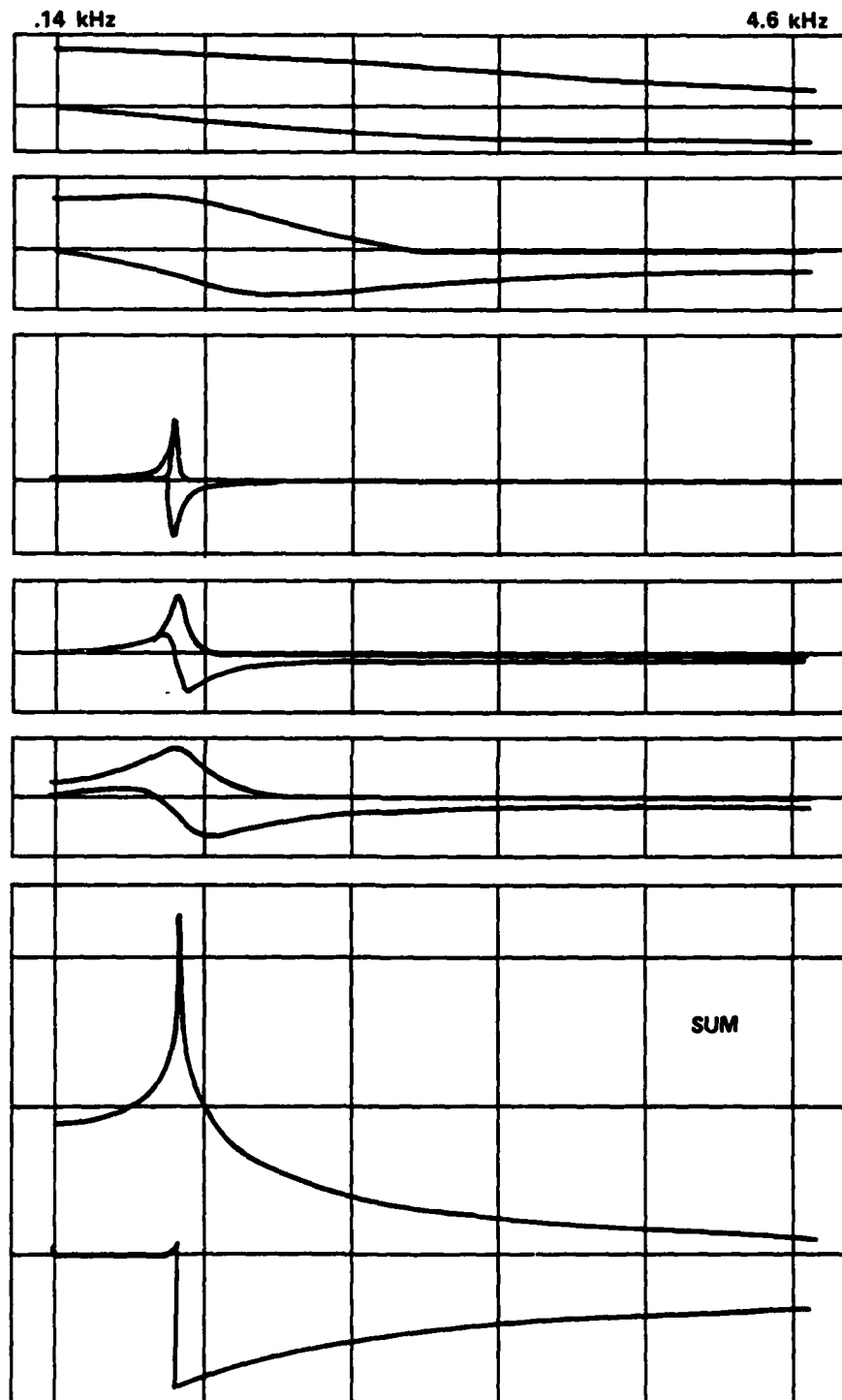


FIGURE 4-5. MEASURED RESPONSE OF THE $J_2(\omega)$ FILTERS

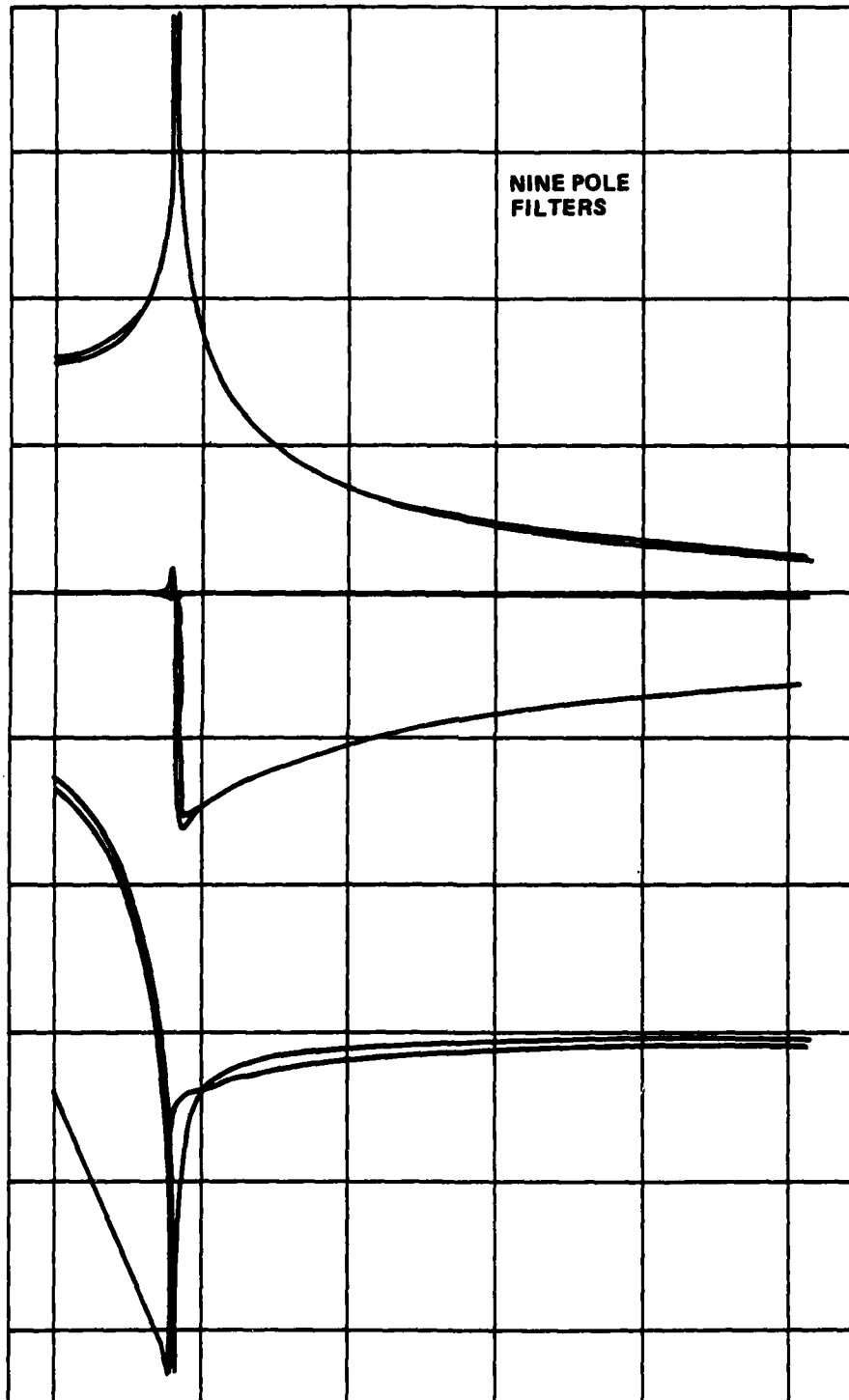


FIGURE 4-10. COMPARISON OF THE DUPLICATE FILTERS

4.5 Signs

Before discussing the results obtained using the analogue, a brief word about signs is in order. The literature is full of discrepancies concerning the sign conventions for $J_1(\omega)$ and $J_2(\omega)$. Harris has discussed this in detail.⁸ In the analogue, the signs largely take care of themselves. The filters in the analogue will always satisfy causality requirements, and the signs adjust themselves accordingly. It is not possible for the designer to influence the sign relation between the real and imaginary part of $J_1(\omega)$ and $J_2(\omega)$. What signs one uses in describing these functions depends largely on convention. However, the designer can add an overall sign change to either or both $J_1(\omega)$ and $J_2(\omega)$. This will affect both the real and imaginary parts of each function. Changing the sign of $J_1(\omega)$ will make the quasiparticle resistance look negative instead of positive, an obviously unphysical situation. The overall sign of $J_2(\omega)$, however, has no effect on the input/output characteristics of the analogue. It only affects whether the VCO phase-locks at 0 degrees or 180 degrees with respect to the LO when the analogue is biased within the zeroth order step.

The sign of $\text{Im } J_1(\omega)$ is usually taken to be positive. This is consistent with the association of positive current with positive voltage. Relative to this, and for the sign conventions implied by equation 2-1, the sign of $\text{Im } J_2(\omega)$ is negative at frequencies greater than the gap frequency $2\Delta/h$. At frequencies less than this, the theoretical expression for $\text{Im } J_2(\omega)$ is either zero or positive, depending on temperature.

4.6 Results Obtained Using the High Frequency Analogue

Once the prototype was working, results followed quickly. These are summarized in the figures that follow. Most of the data is in the form of time averaged current-voltage characteristics, which can be compared directly with characteristics of real junctions. The presented data were chosen to illustrate the aspects of the Josephson effects that are not included in the RSJ model. These include the Riedel peak, sub-gap structure, the nonlinear quasiparticle resistance and its associated reactance, and the cosine ϕ term.

The results begin with graphs of the time averaged I-V characteristics measured under current and voltage bias conditions. Certain parts of the characteristic are not accessible under current bias conditions. The next figures show how this difficulty can be avoided through the use of a voltage source and a large series inductance. The shape of the Riedel peak and the related sub-gap structure are clearly evident. Later figures show the effect of nonzero source resistance, leakage currents, and shunt capacitance.

There is a brief digression to illustrate a subtle problem connected with the use of the nine point $T = 0$ filters. This is followed by a series of I-V characteristics showing the effects of RF currents and voltages.

Some measurements of the AC impedance of the junction are shown for both the RSJ and high frequency limits of the analogue (i.e., with and without the filters connected). After this are some measurements of the impedance associated with the plasma resonance. These illustrate the effects of $\text{Re } J_1(\omega)$ and $\text{Im } J_1(\omega)$ on the resonant response.

The behavior of the analogue can be summarized in a few paragraphs. First, the analogue seems to do a good job of modelling gap effects. The appearance of sub-gap structure is consistent with predicted behavior, in that it appears only

at odd submultiples of the gap voltage for a current biased junction.^{2,5} For a suitable choice of source impedance, structure is observed at even submultiples as well.

The qualitative performance of the analogue in modelling nonlinear quasiparticle tunnelling is good. But there is a problem associated with fine structure in the imaginary part of the response of the $J_1(\omega)$ filter. Under certain conditions, this causes the quasiparticle resistance to appear negative. The problem can be avoided at a cost of decreasing the resistance at voltages below the gap. (This is discussed further in section 8.7.)

The accuracy of this version of the analogue was not sufficient to permit good quantitative measurements of small signal effects, such as the plasma resonance. Although qualitative results were good, the numbers did not come out as they should. Part of this can be blamed on the unwanted cosine ϕ term introduced by the low pass filters. A combination of noise problems, particularly in the VCO, and calculation errors by the six multiplier chips is responsible for much of the additional error. These faults were subsequently improved in a later version of the analogue. (This is discussed in Chapter 8.) However, the results presented on the following pages are the first of their kind, and represent a significant step in the development of the improved analogue discussed in subsequent chapters. Furthermore, these results do provide some insight into the complexities of the high frequency theory of Josephson tunnelling.

Figure 4-11 shows I-V characteristics for the analogue under current and voltage bias conditions (cf. Fig. 2-6). Under current bias conditions, negative resistance regions in the characteristic are inaccessible, and hysteresis is evident. Note the similarity between the voltage biased characteristic and the filter response $\text{Im } J_1(\omega)$.

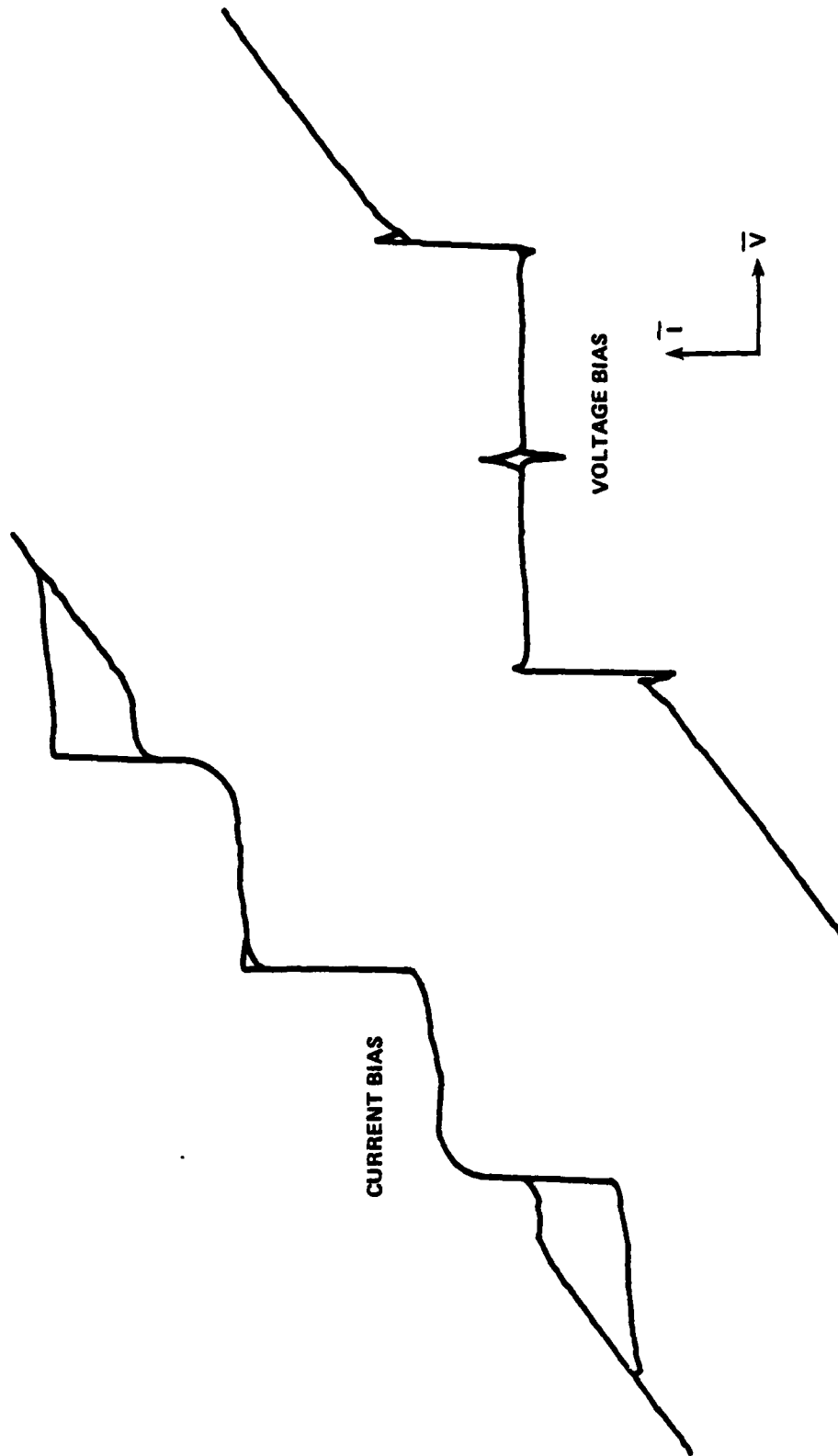


FIGURE 4-11. VOLTAGE AND CURRENT BIAS

To investigate the nature of the Riedel peak, the analogue was connected to a voltage source via a large inductance. This serves to make the analogue look voltage biased at DC, and current biased at AC. Figure 4-12 shows the results for two values of L . Note that the back of the Riedel peak is now accessible and that sub-gap structure is evident. The Riedel peak in Figure 4-12a is surprisingly broad. This effect was later traced to the existence of negative resistance oscillations, which result from the presence of the large source inductance. This is discussed in section 9.5.

In Figure 4-12b, sub-gap structure appears only at odd submultiples of the gap voltage $2\Delta/e$. This is consistent with theoretical predictions.^{2,5}

Figure 4-13a shows the effect of adding a resistance in series with the voltage source and inductor. The gap hysteresis is still there, but the finite source resistance causes the hysteretic segments to have negative slope. Figure 4-13b shows the effect of reducing the shunt resistance from that predicted by the $I_J R_N$ product. This reduces the effective AC source impedance, thus eliminating much of the gap hysteresis. (There is no resistance in series with the voltage source in Figure 4-13b.)

The inductor is removed for the measurement shown in Figure 4-14, in which the analogue is connected to the voltage source through different values of series resistance. Note the transition from voltage bias to current bias. Figure 4-15 shows the opposite effect. The analogue is connected to a current source, and the shunt resistance is varied. In 4-15a, the shunt resistance is that given by the $I_J R_N$ product. As this resistance is decreased, the hysteresis diminishes, and the junction begins to look RSJ like.

Figures 4-16 and 4-17 are a closer examination of the effects of voltage biasing the analogue through a series inductance. As the inductance is

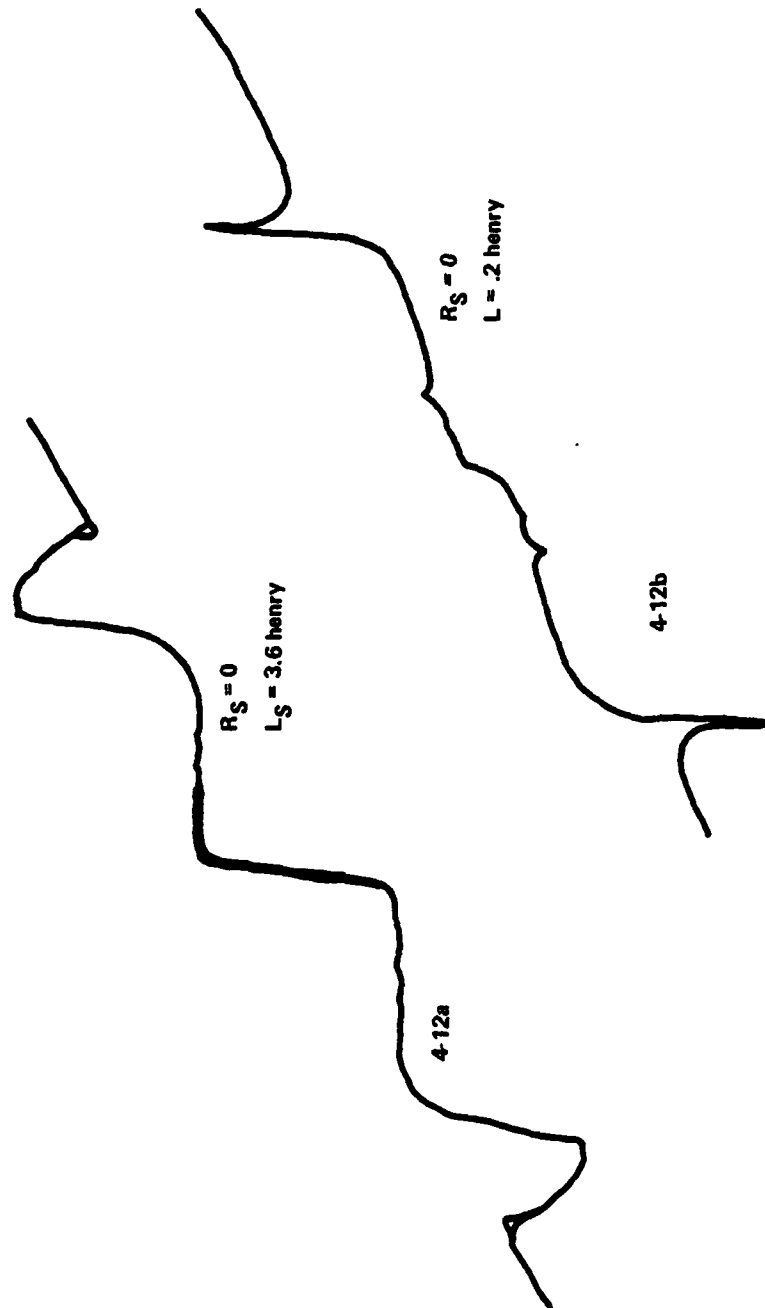


FIGURE 4-12. THE RIEDEL PEAK

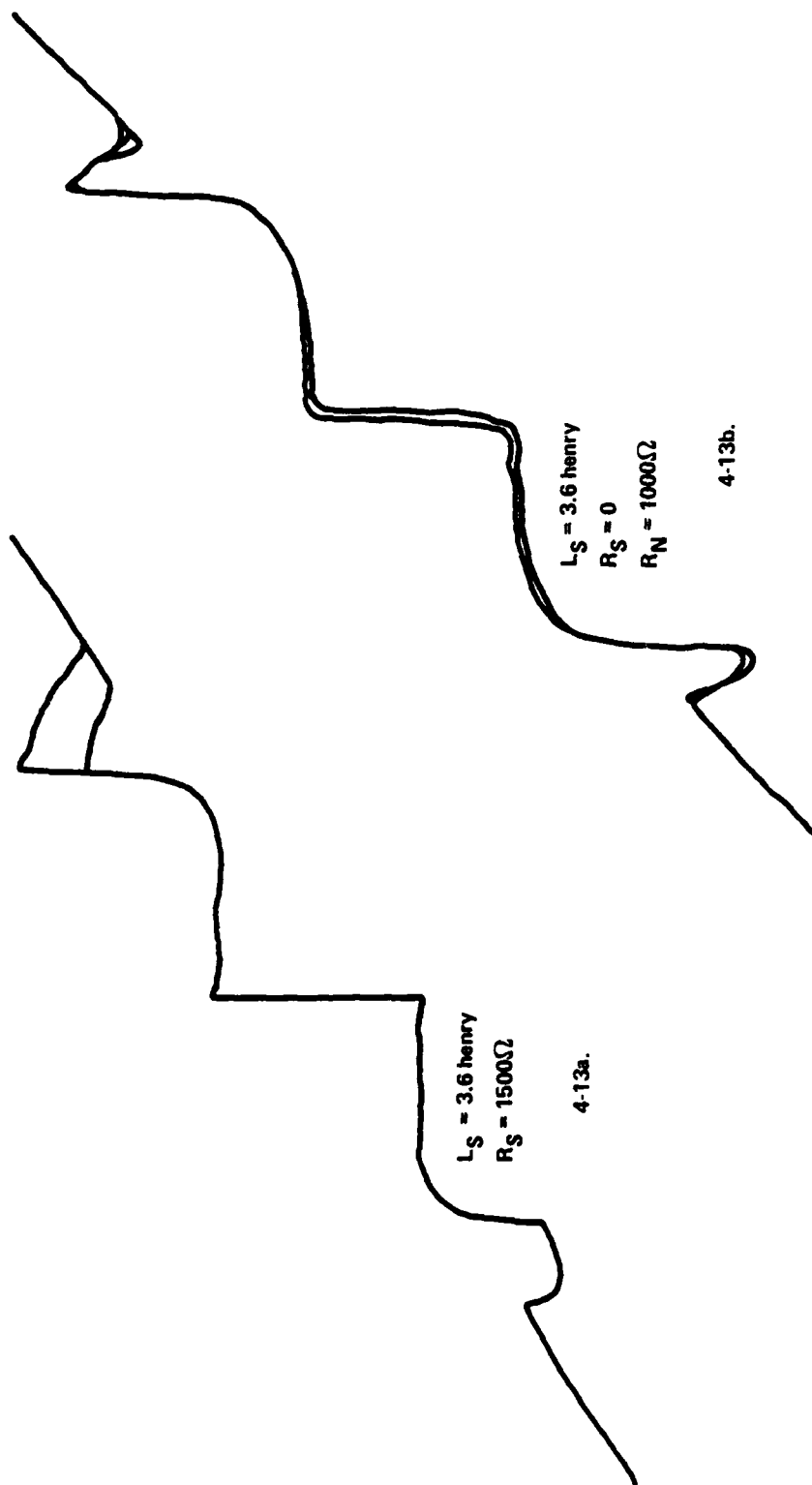


FIGURE 4-13. EFFECT OF NONZERO SOURCE RESISTANCE

AD-A120 753

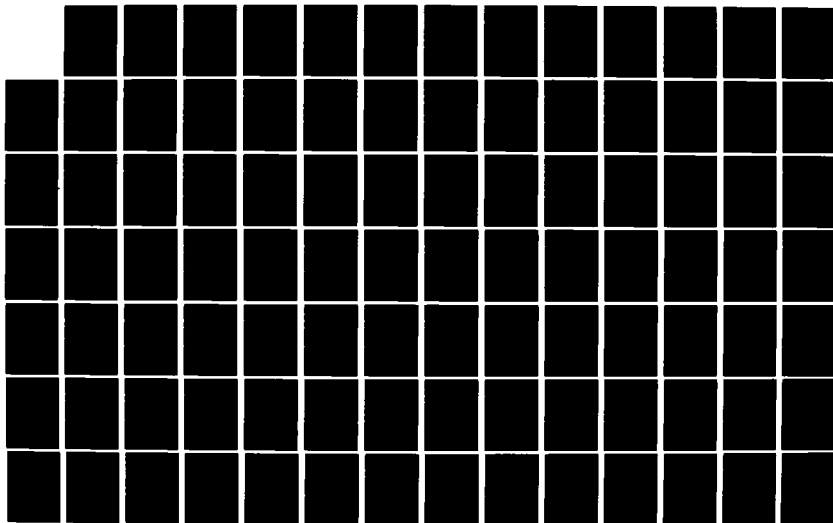
ELECTRONIC SIMULATION OF THE JOSEPHSON EFFECTS(U) NAVAL
SURFACE WEAPONS CENTER SILVER SPRING MD D JABLONSKI
01 DEC 81 NSWC/MP-81-519 SBI-AD-F500 077

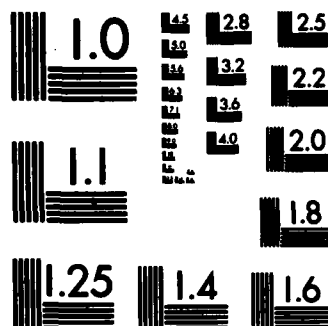
2/4

UNCLASSIFIED

F/G 20/10

NL

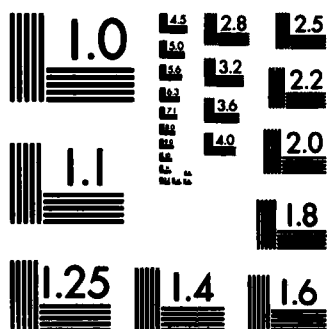




MICROCOPY RESOLUTION TEST CHART
NATIONAL BUREAU OF STANDARDS-1963-A



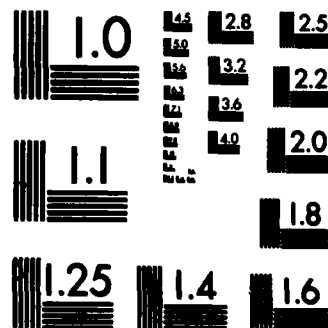
MICROCOPY RESOLUTION TEST CHART
NATIONAL BUREAU OF STANDARDS-1963-A



MICROCOPY RESOLUTION TEST CHART
NATIONAL BUREAU OF STANDARDS-1963-A



MICROCOPY RESOLUTION TEST CHART
NATIONAL BUREAU OF STANDARDS-1963-A



MICROCOPY RESOLUTION TEST CHART
NATIONAL BUREAU OF STANDARDS-1963-A

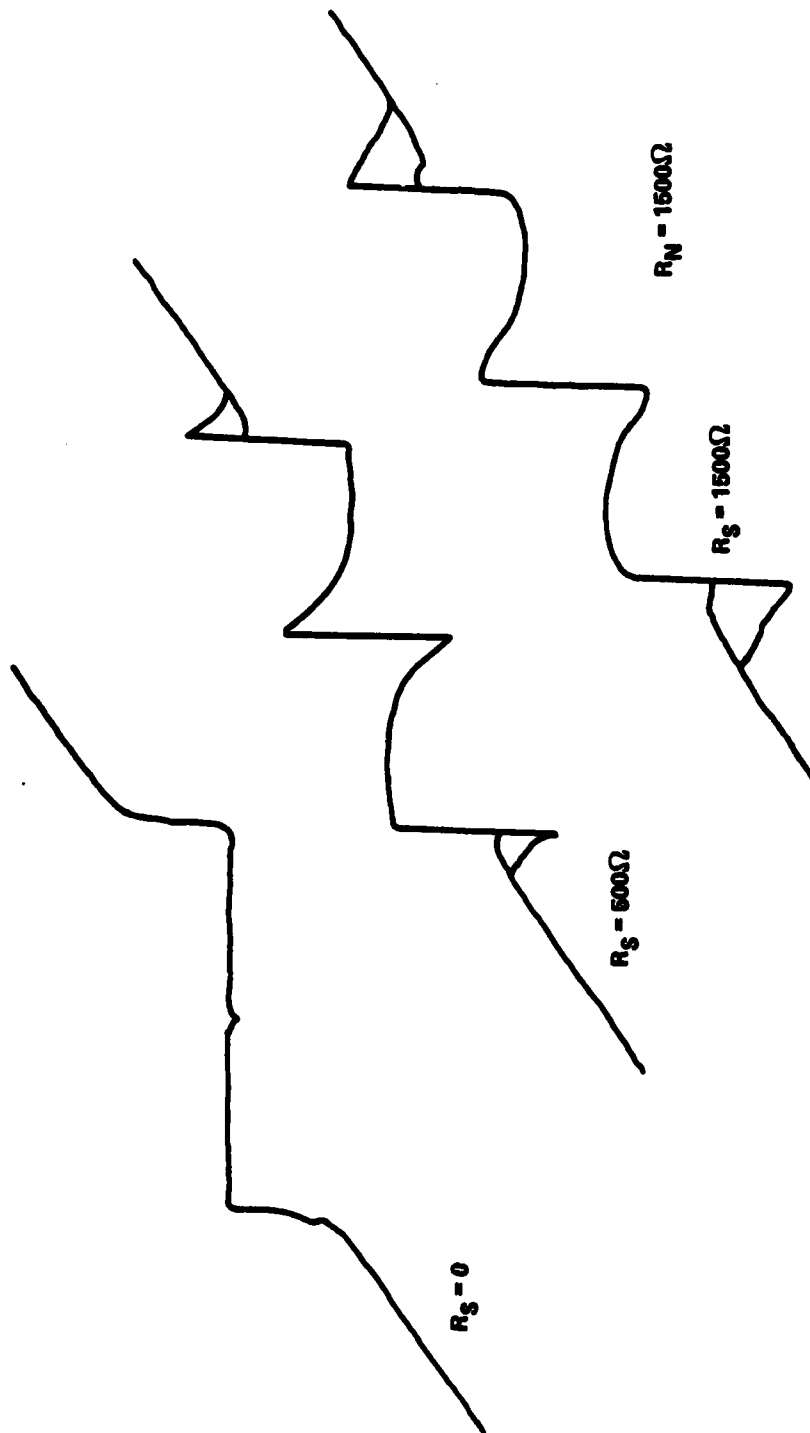


FIGURE 4-14. EFFECT OF CHANGING THE SOURCE RESISTANCE (VOLTAGE BIAS LIMIT)

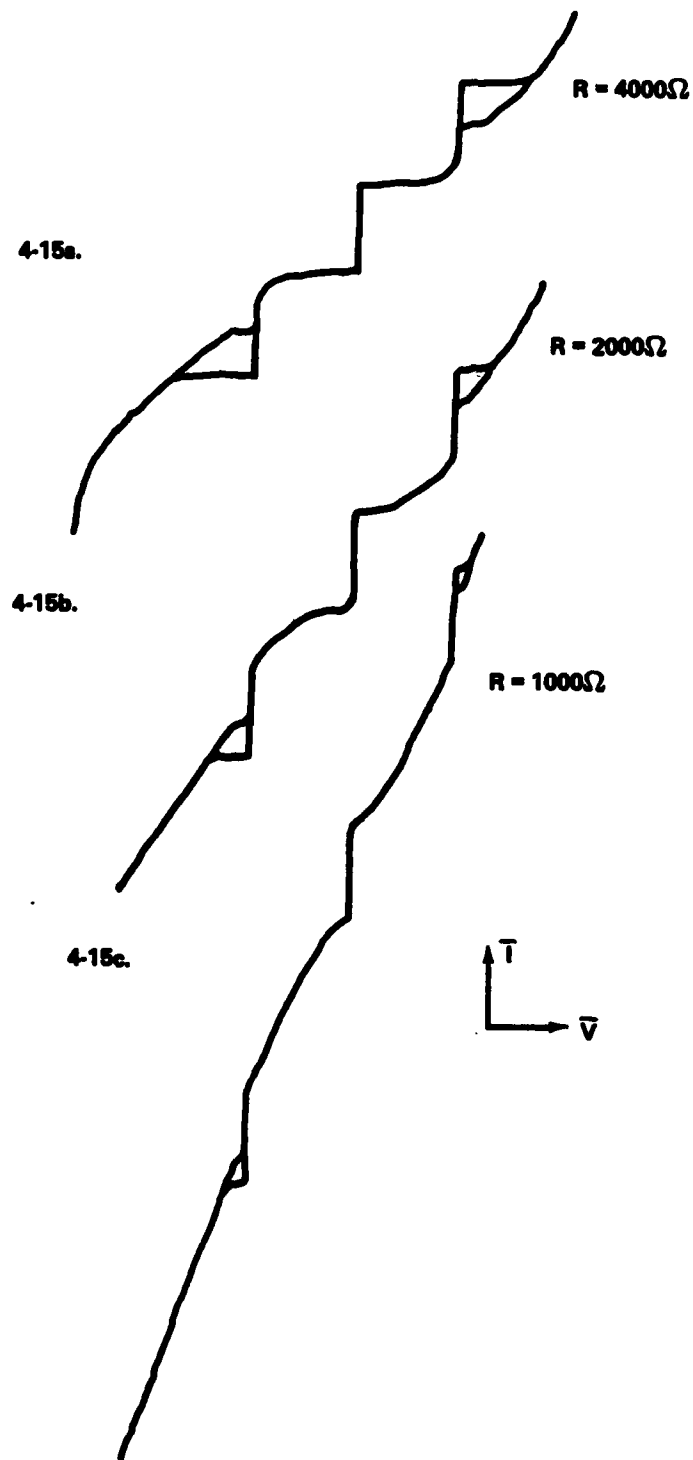


FIGURE 4-15. EFFECT OF CHANGING THE SOURCE RESISTANCE (CURRENT BIAS LIMIT)

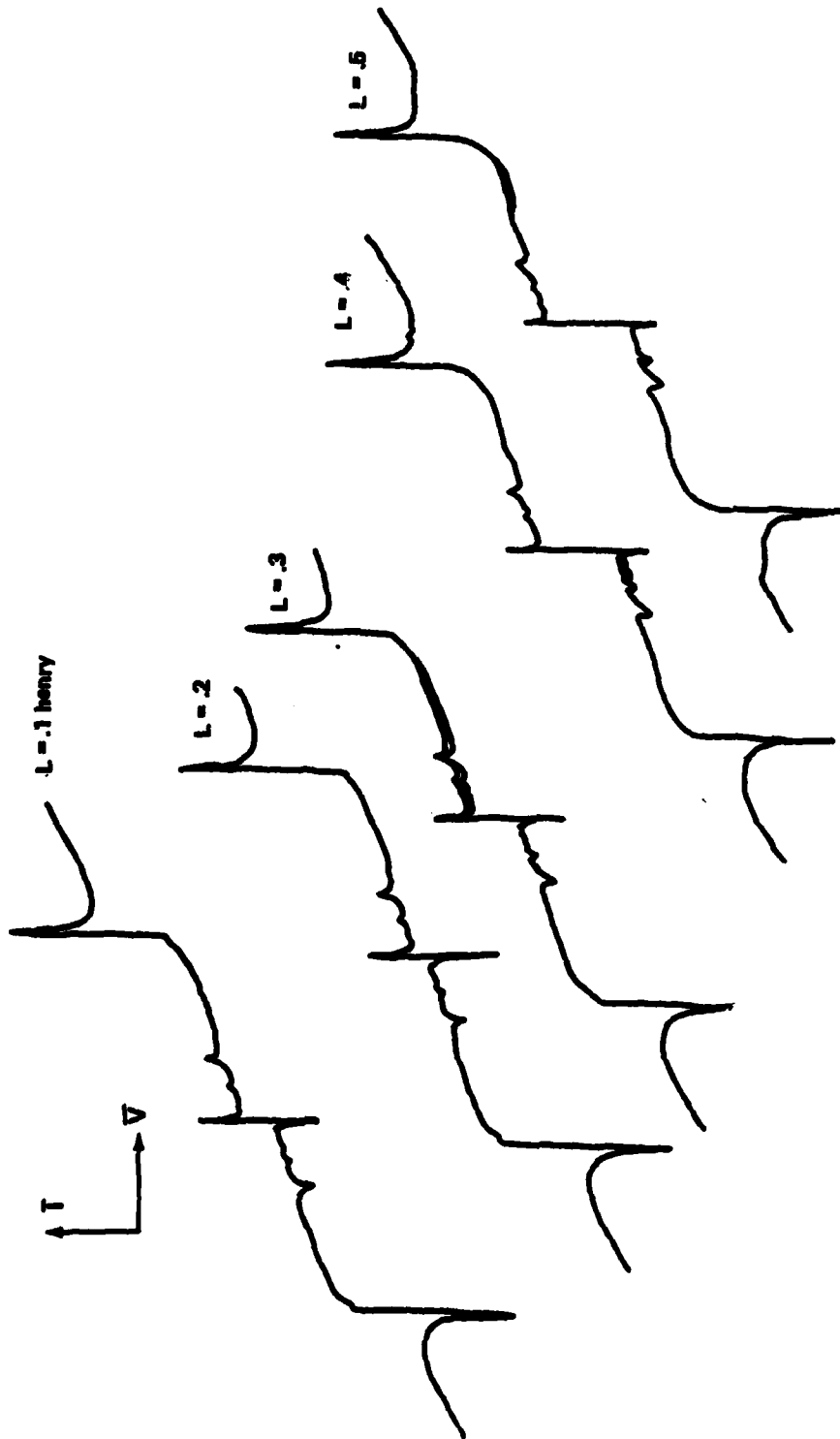


FIGURE 4-16. EFFECT OF SERIES INDUCTANCE ON SUB GAP STRUCTURE

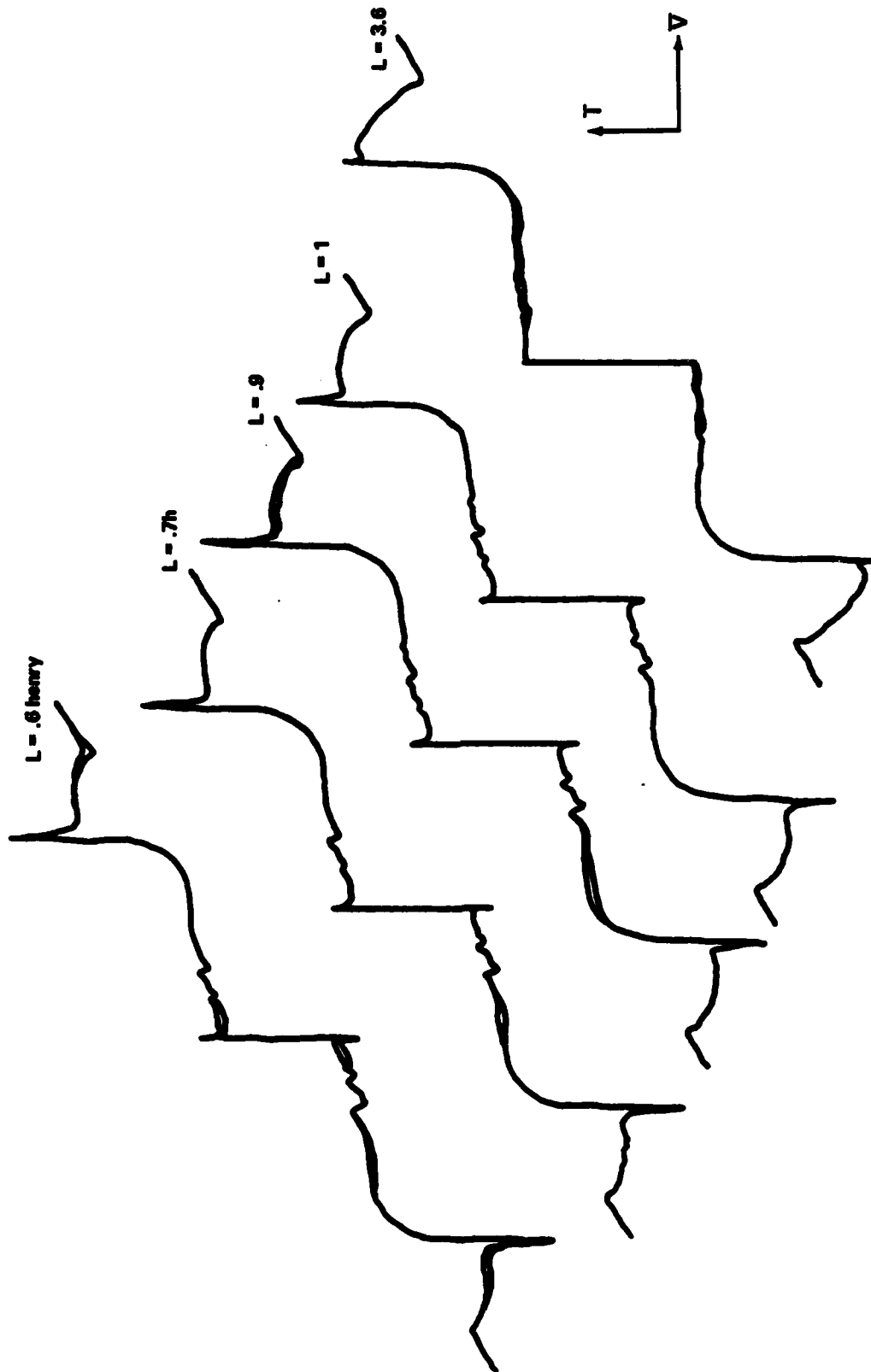


FIGURE 4-17. EFFECT OF SERIES INDUCTANCE ON SUB GAP STRUCTURE (CONTINUED)

increased, the characteristic approaches that of the current biased case. Note that the sub-gap structure occurs only at odd submultiples of the gap voltage, and that the Riedel peak gradually broadens (cf. section 9.5).

Figure 4-18 shows the effect of adding a shunt capacitance to the analogue, which is still voltage biased through an inductor. The AC equivalent circuit is an LC network in parallel with the analogue. This cavity apparently causes structure to appear at even submultiples of the gap voltage. This is consistent with the predictions of Werthamer and Harris.^{2,5}

Figure 4-19 illustrates the effects of shunt capacitance on the DC I-V characteristics of a current biased analogue. Results are shown for the analogue operating in both the RSJ and high frequency modes. The amount of hysteresis depends on the RC product. In the high frequency case, the value of R to be used is that of the differential resistance at $V = 0$. In the figure, this is approximately ten times as large as R_N . Thus, for a given amount of hysteresis, only one tenth the capacitance is needed as in the RSJ case. The large amount of hysteresis is typical of that observed in a real superconducting tunnel junction.

When using the analogue with the nine pole $T = 0$ filters, unrealistic behavior was observed when there was a shunt capacitance and a high source impedance. This is shown in Figure 4-20. The characteristics of the current biased and voltage biased analogue are superimposed. Under current bias conditions, the I-V curve enters a negative resistance region. That is, the curve enters the second and fourth quadrants of the I-V plane, and the I-V product is negative. This unrealistic effect was traced to the overshoot in the $\text{Im } J_1(\omega)$ filter response at the gap frequency. The overshoot is apparent in

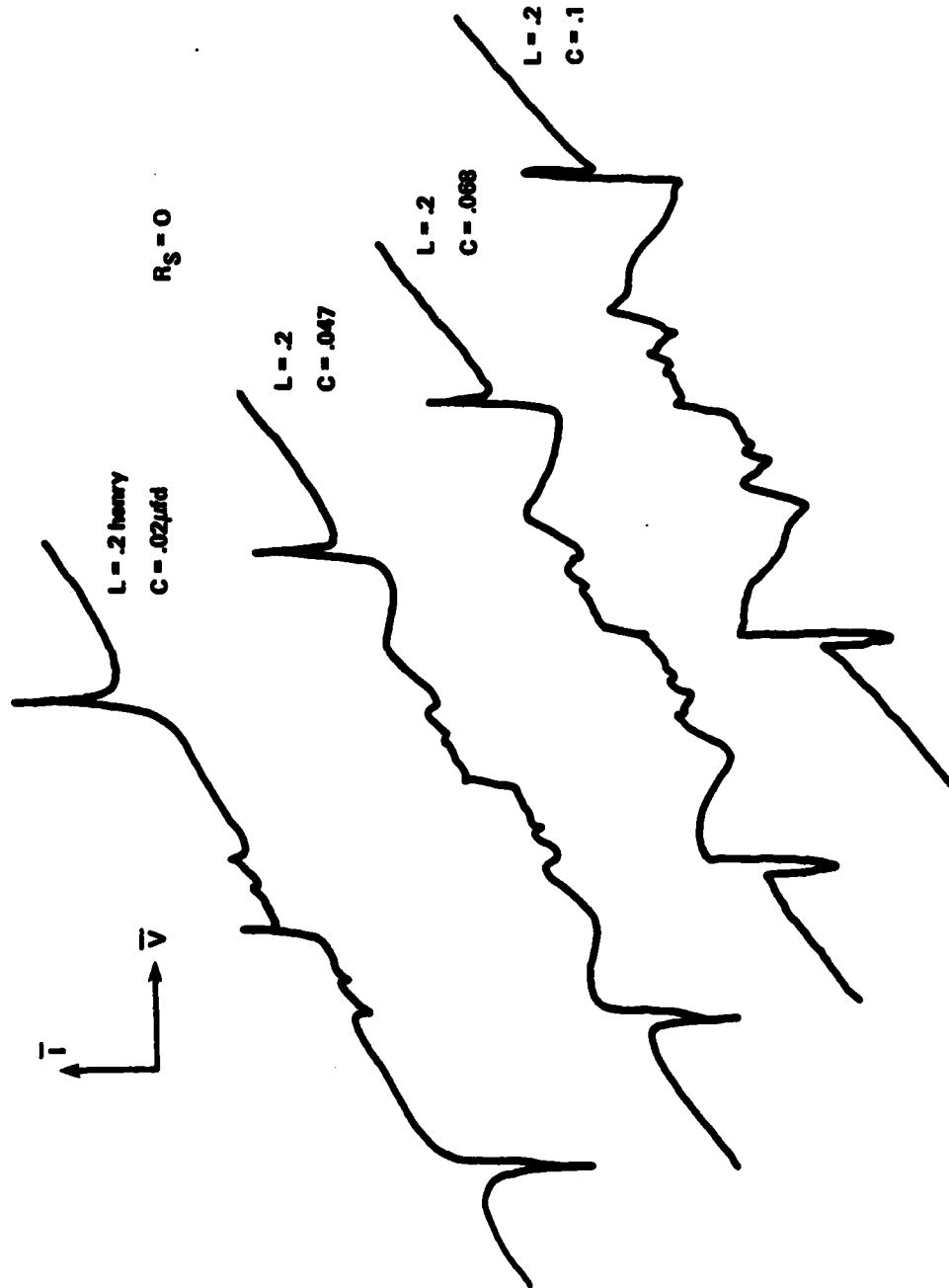


FIGURE 4-18. EFFECT OF SERIES INDUCTANCE AND PARALLEL CAPACITANCE ON SUB GAP STRUCTURE

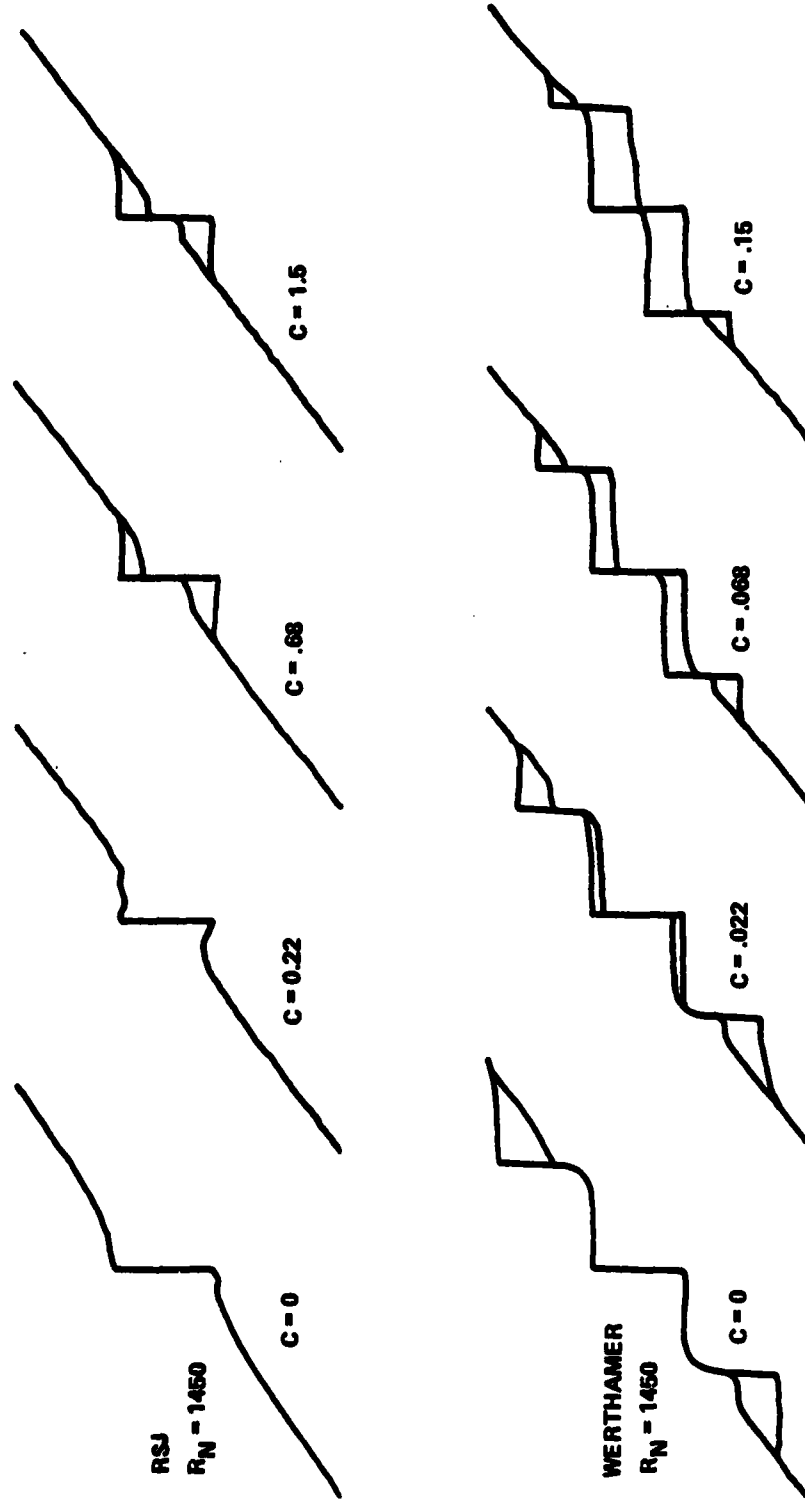


FIGURE 4-19. EFFECT OF SHUNT CAPACITANCE

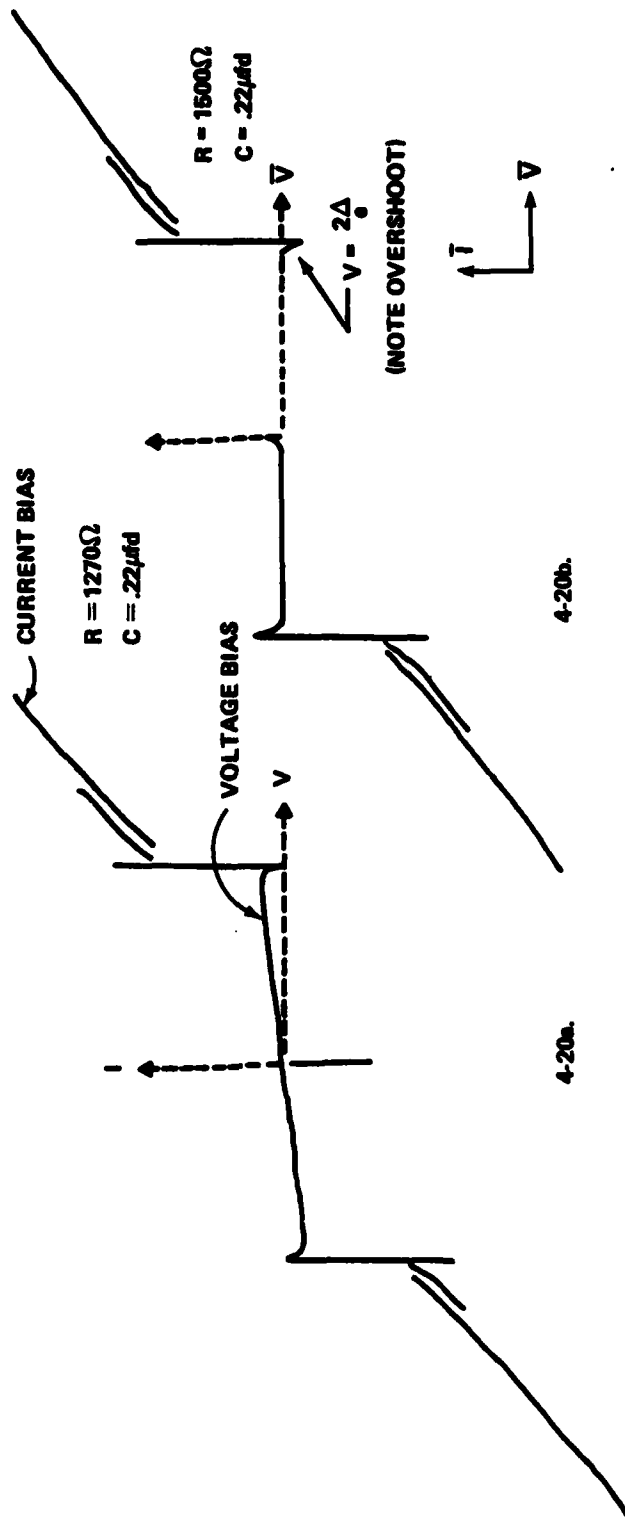


FIGURE 4-20. ANOMALOUS BEHAVIOR OF THE CAPACITIVELY SHUNTED ANALOGUE

the voltage bias curve of 4-20b at the gap voltage $2\Delta/e$. Before making measurements with the capacitively shunted analogue, the shunt resistance was decreased until the I-V characteristic looked realistic from an energy conservation point of view. This is illustrated in Figure 4-20a. Note that the current biased curve starts behaving properly when R_N is adjusted to lift the overshoot in the voltage biased curve to just above the axis. In the time domain, this overshoot shows up as a voltage source at the gap frequency. If the shunt capacitance is sufficient to make the plasma frequency approach the gap frequency, the analogue will oscillate. The oscillations disappear when the shunt resistance is decreased, or the capacitance is removed. For most measurements not involving capacitance, the shunt resistance was set to satisfy the $I_J R_N$ product. For measurements using a capacitor, R_N was decreased sufficiently to get rid of the problem. This usually meant lowering R_N from 1500 to 1200 ohms. It may be that the overshoot in $\text{Im } J_1(\omega)$ is responsible for the apparent structure at half the gap voltage in Figure 4-12a. A negative resistance at the gap frequency might generate oscillations at half that frequency, resulting in the observed structure. As the source impedance is decreased, the structure goes away.

Figure 4-21 shows the I-V characteristics for an assortment of RC products. The $I_J R_N$ product is less than $\pi\Delta/2e$ for all four curves, so the problem described above is avoided. Note the structure in the excess currents below the gap voltage in Figure 4-21b. This is the sort of behavior seen in a real junction. There has been some controversy as to whether it is caused by multiparticle tunnelling, which is not modeled by the analogue, or self-coupling effects, which are.³⁸

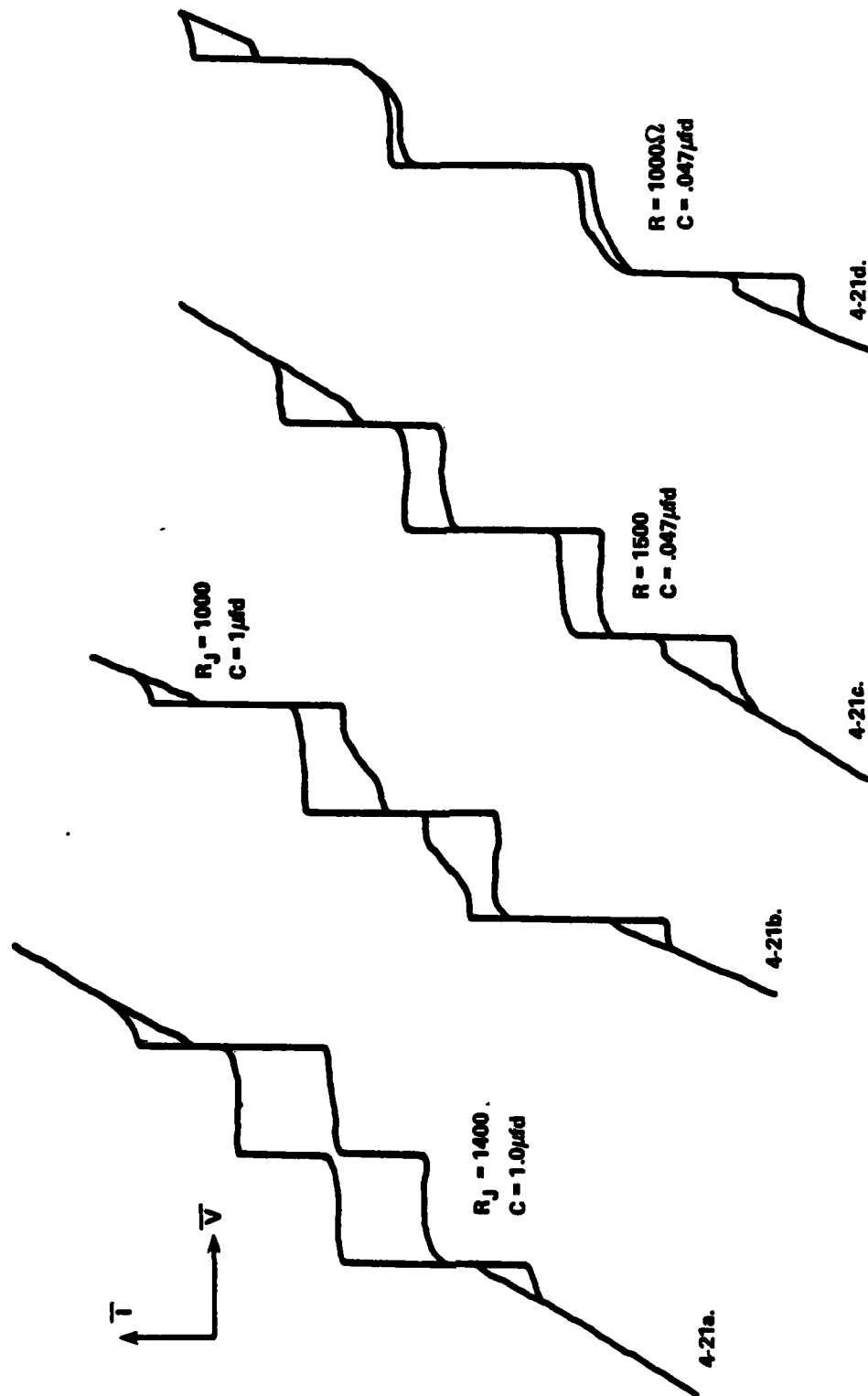


FIGURE 4-21. EFFECT OF VARYING THE RC PRODUCT

The next few figures show the effects of microwaves. Figures 4-22 and 4-23 show characteristics for the current biased analogue with the drive frequency at the gap frequency and half the gap frequency, respectively. As the RF amplitude is increased, the characteristics get washed out. Much of this effect can be attributed to the existence of the photon-assisted tunnelling (PAT) steps, which interfere with the Josephson steps and smear the characteristic. A discussion of this, along with quantitative measurements, is included in Chapter 9.

Figure 4-24 shows the effect of varying the drive frequency while holding the amplitude of the drive current constant. There seem to be some spurious effects in curve a, but the spacing between steps is correct.

Figure 4-25 was obtained by varying the source resistance. The gradual change from current spikes to current steps, and the disappearance of gap hysteresis, is well illustrated.

Figure 4-26 shows the effect of driving the analogue at frequencies just above and below the gap frequency. There appears to be some spurious behavior.

The next several pages deal with the AC impedance of the analogue. The measurements are similar to those described in Chapter 3 for the RSJ model. Figures 4-27 and 4-28 show results obtained using the analogue in both the RSJ and high frequency modes (i.e., with and without the filters connected). Note that the impedance curves for the high frequency case are not symmetric with respect to positive and negative current, because of the hysteresis (apparently RF induced) in the I-V characteristic. The current is swept in only one direction for the impedance measurement, which would otherwise appear hysteretic. In the RSJ limit, the reactance of the analogue should be zero between steps. This is not quite the case when the analogue is operated in the RSJ mode, and is probably due to cumulative multiplier error. However, in the

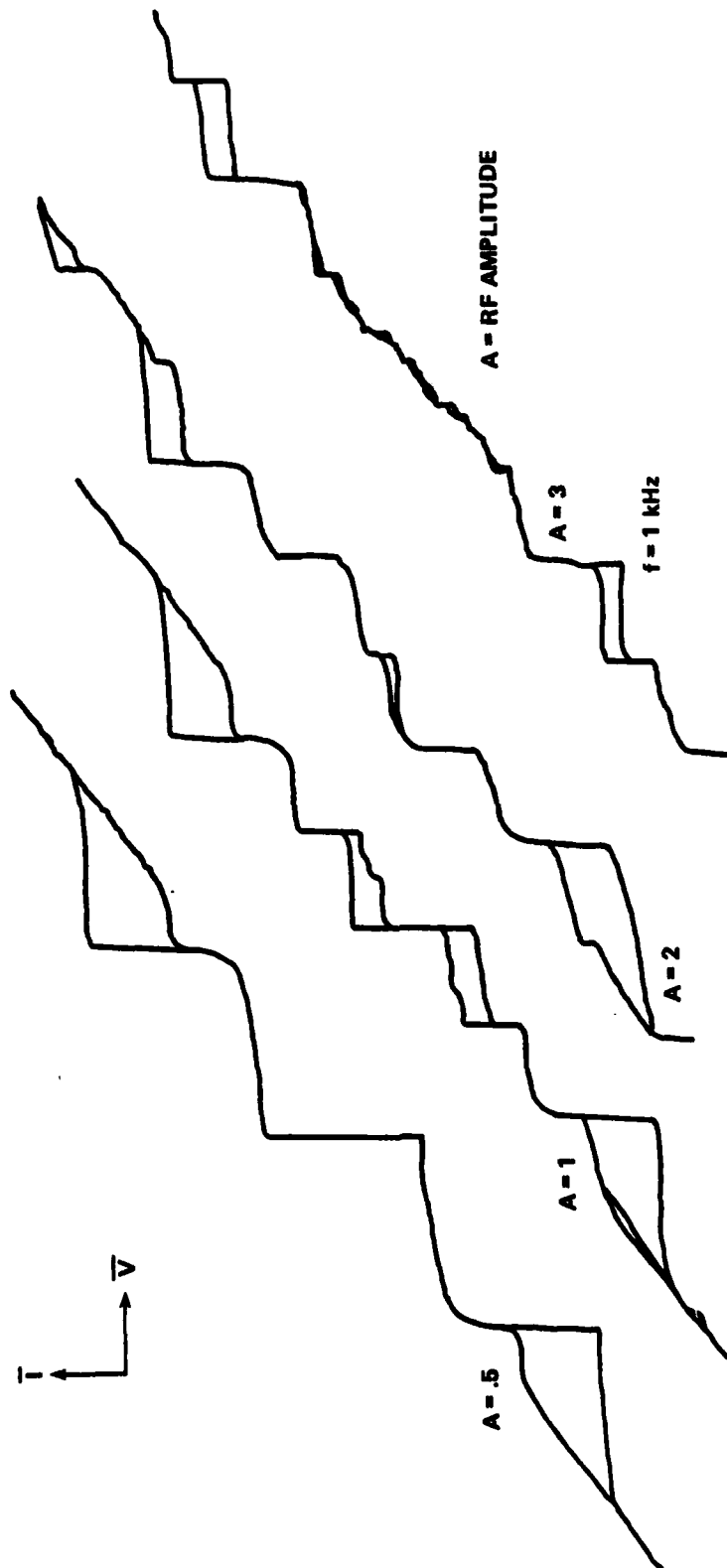


FIGURE 4-22. EFFECTS OF RF CURRENTS AT THE GAP FREQUENCY

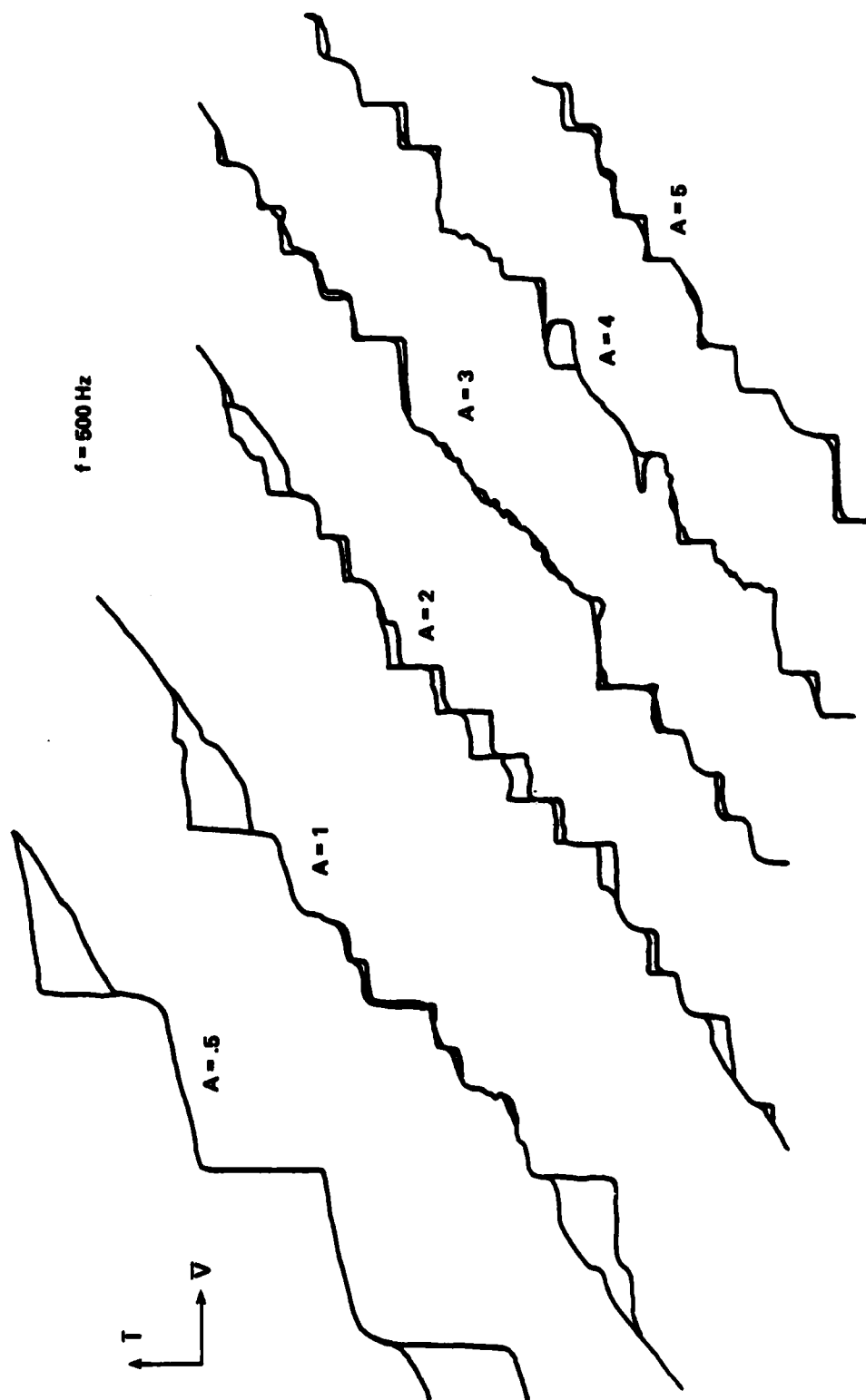


FIGURE 4-23. EFFECTS OF RF CURRENTS AT ONE HALF THE GAP FREQUENCY

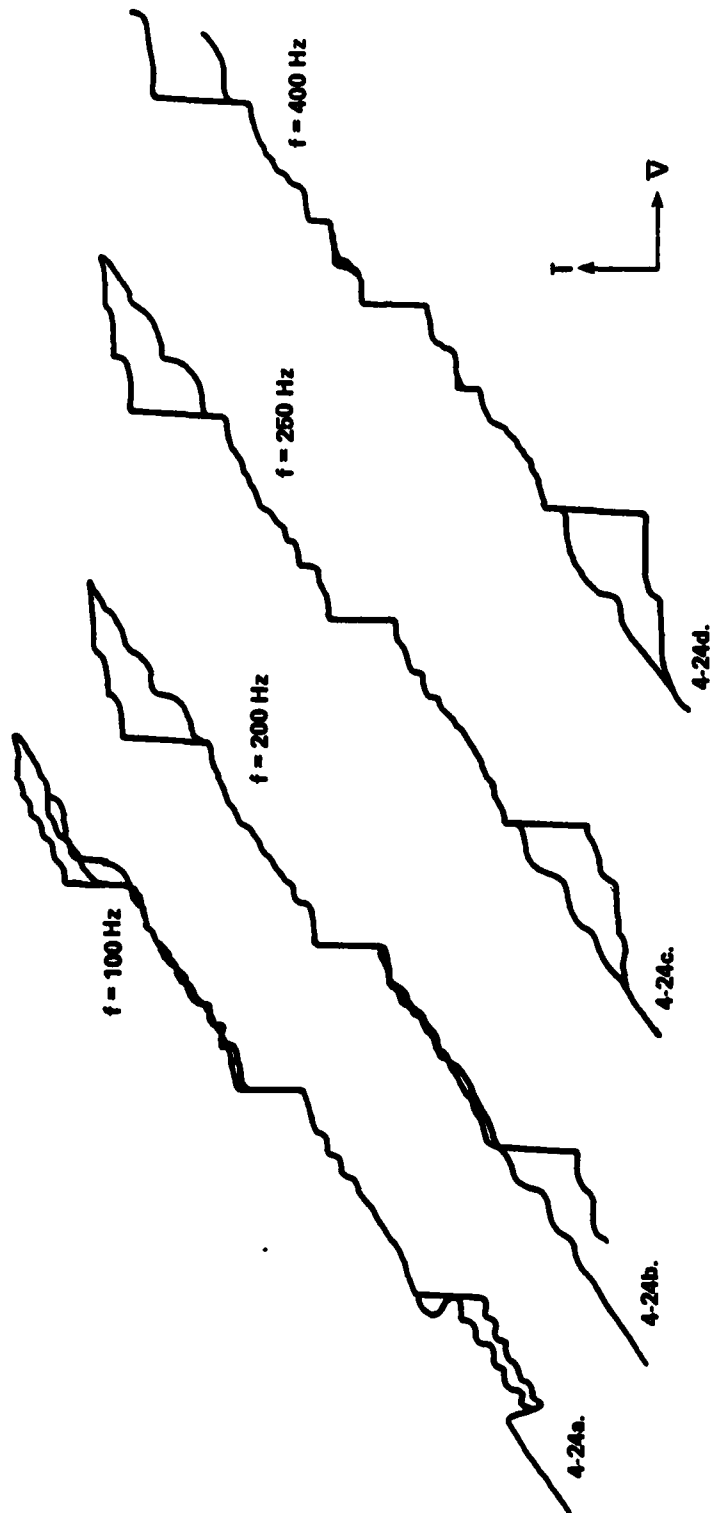


FIGURE 4-24. EFFECT OF VARYING THE FREQUENCY

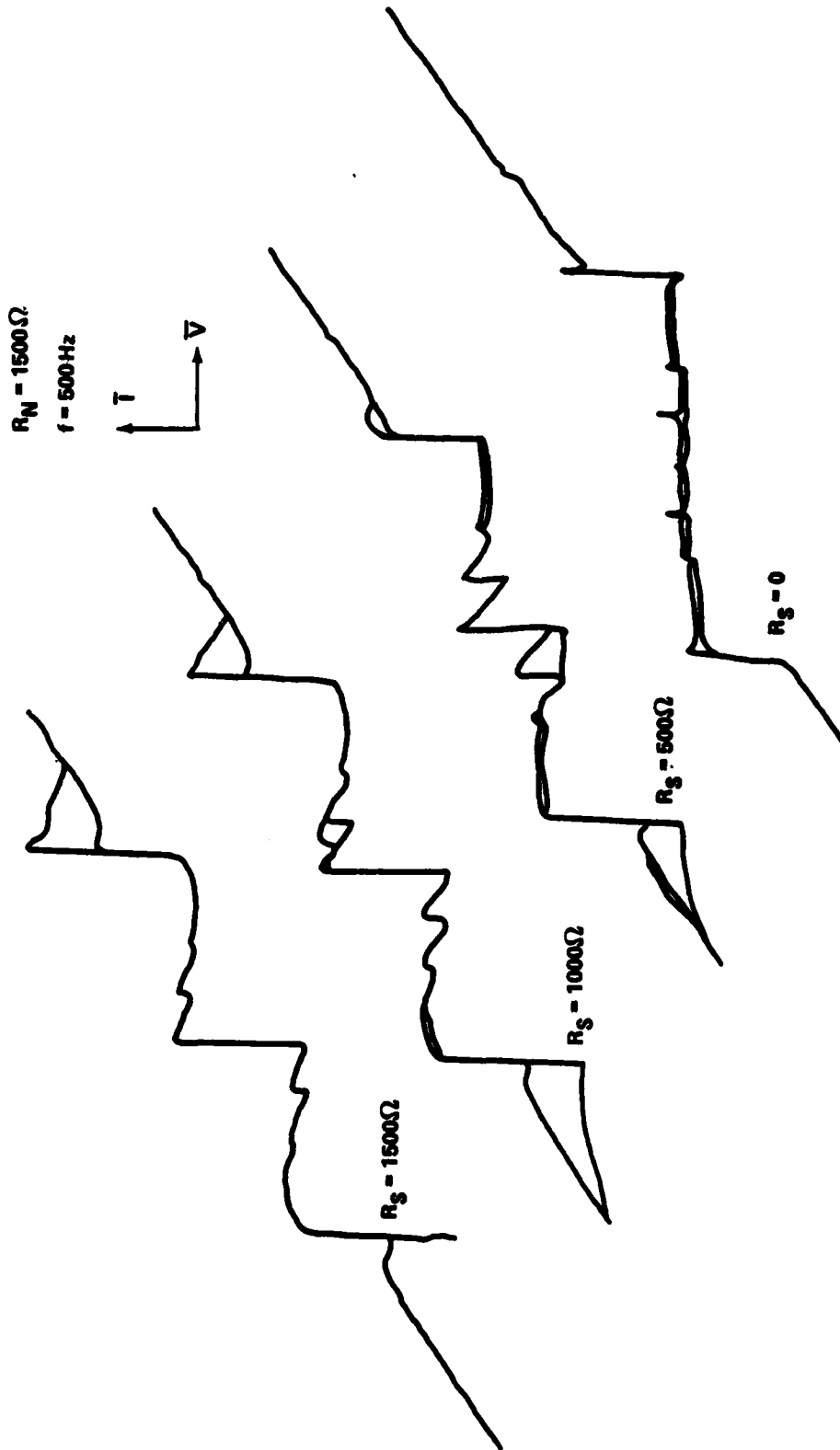


FIGURE 4-25. EFFECT OF CHANGING THE SOURCE RESISTANCE WHEN RF IS PRESENT

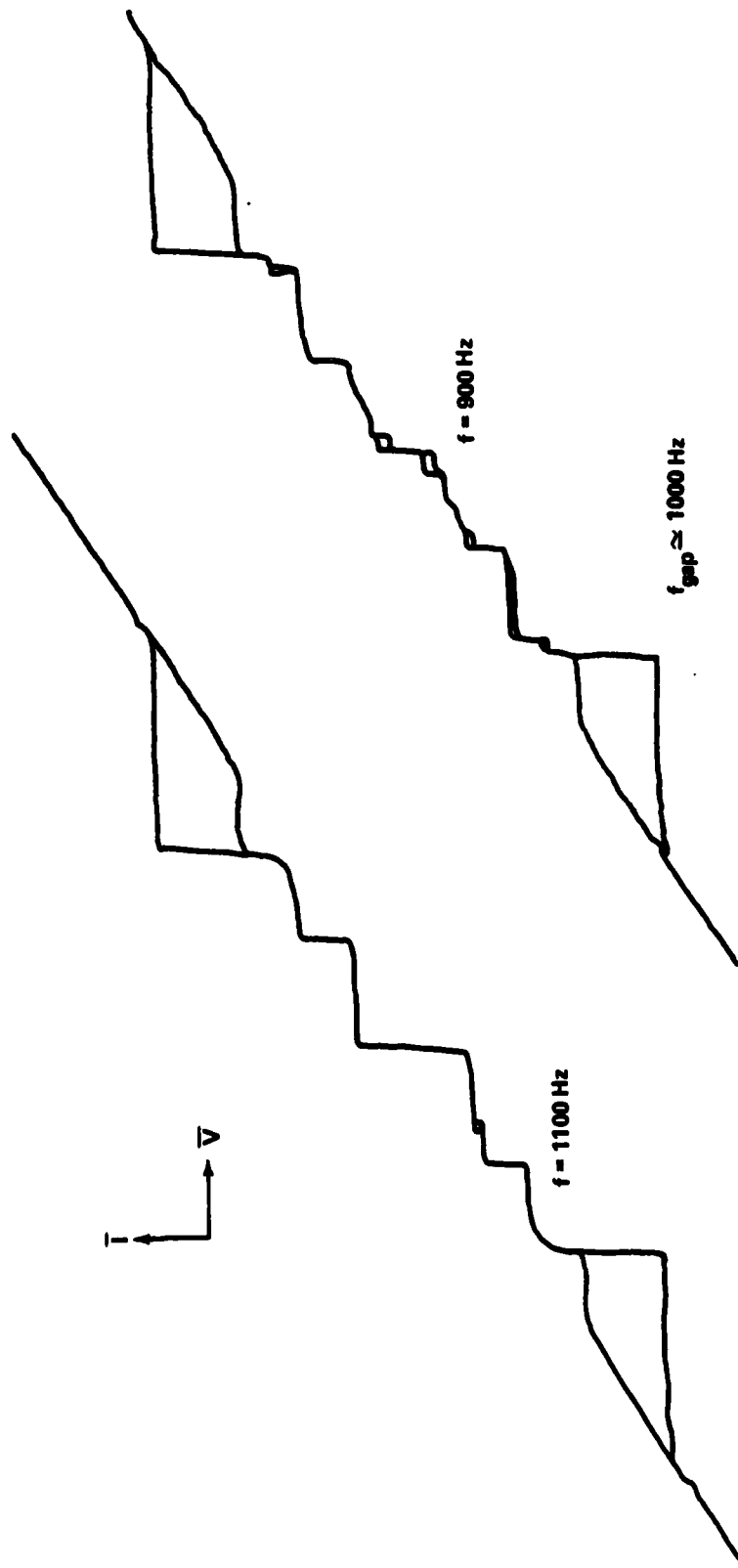


FIGURE 4-26. EFFECT OF FREQUENCIES ABOVE AND BELOW THE GAP

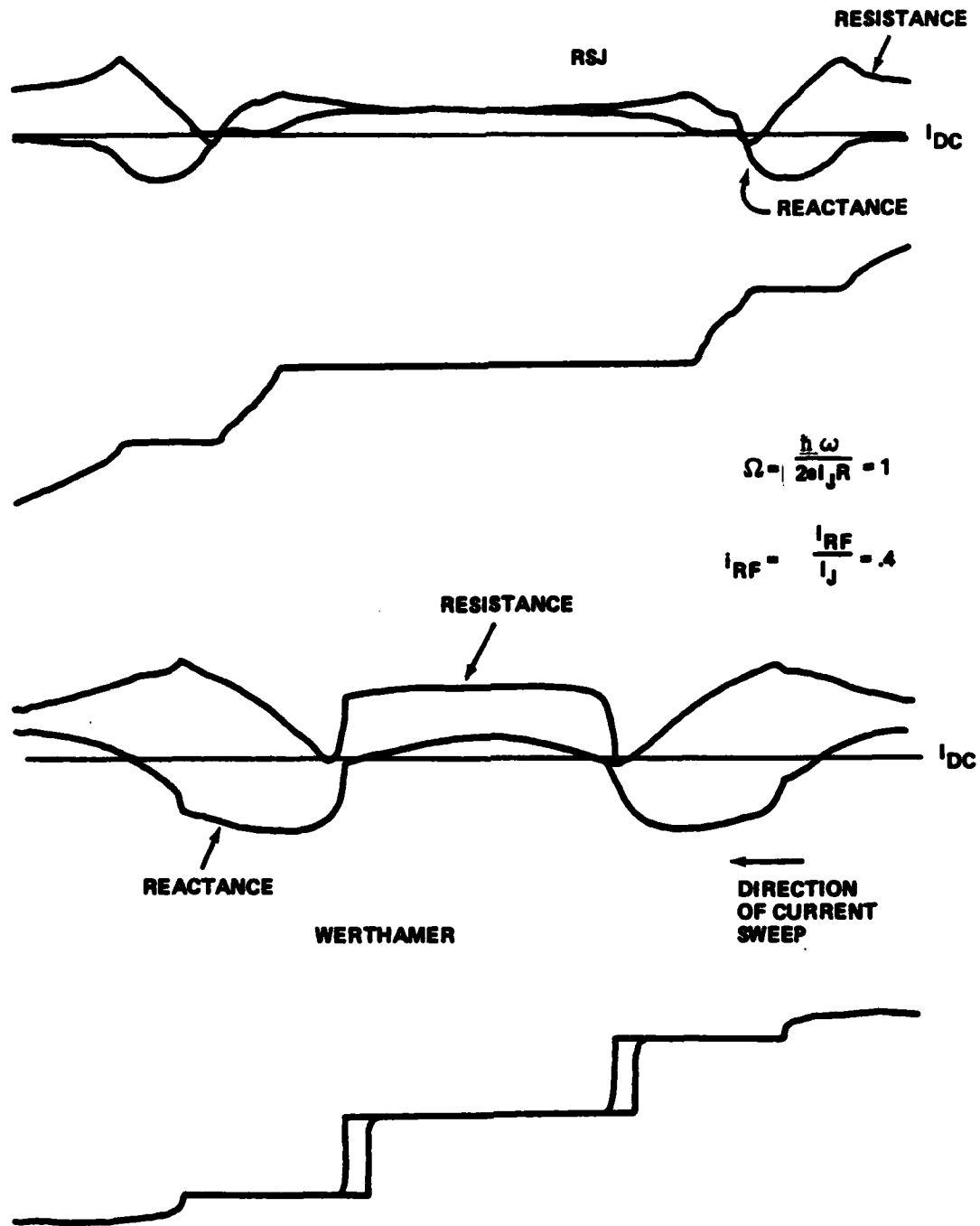


FIGURE 4-27. HIGH FREQUENCY IMPEDANCE

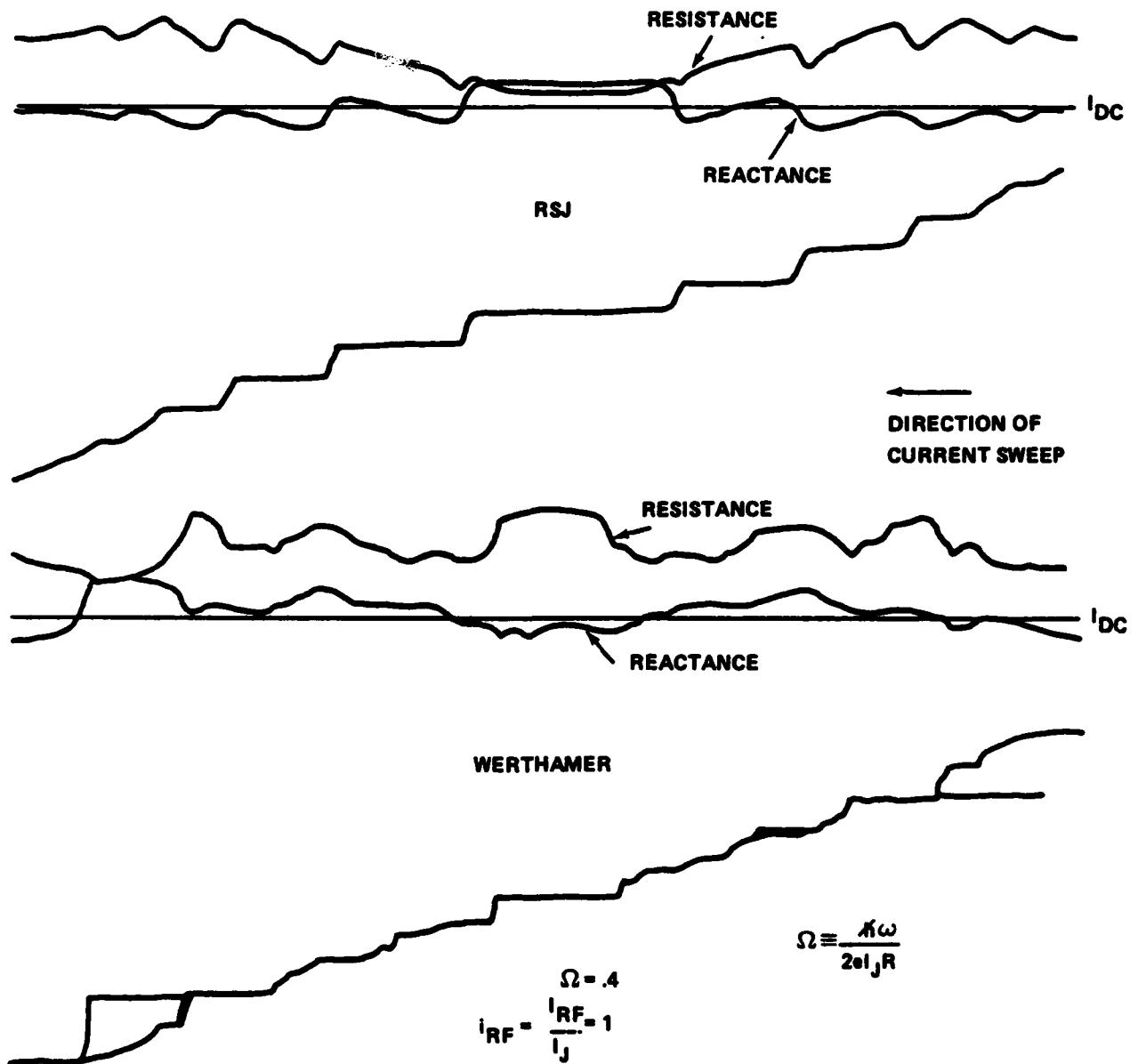


FIGURE 4-28. HIGH FREQUENCY IMPEDANCE (CONTINUED)

high frequency mode, one would expect $\text{Re } J_1(\omega)$ to contribute a reactive term between steps. It is interesting to note that in Figure 4-28b, the reactance is negative in the zeroth order step. This is a consequence of the large difference in the quasiparticle resistance between the RSJ and Werthamer limits when $\Omega = .4$. This is discussed in section 9.2.

The last few figures deal with the plasma resonance. The capacitively shunted analogue is current biased within the zeroth order step. For small RF currents, the analogue will look like a parallel RCL network, with resonant frequency given by equation 2-32. The Q of this resonance is affected by the sign and magnitude of the $\cos\phi$ term. To investigate this, efforts were made to measure the Q under a variety of conditions. However, the quantitative interpretation is complicated since, in the region of interest, the extraneous $\cos\phi$ term introduced by the low pass filters can be significant. As a result, the measured Q was often larger than it should have been, as the negative $\cos\phi$ term increased the effective resistance of the analogue. However, the dependence of the plasma frequency on $\cos\phi$ (cf. Eq. 2-32), was quite well followed. And for small input signals, the resonance was clearly Lorentzian.

For the first five figures, the analogue was operated in the RSJ mode. The figures show the real and imaginary parts of the impedance of the capacitively shunted analogue as a function of frequency. The measurement technique is

identical with that used for previous impedance measurements, except that the DC bias current is held constant, and the frequency varied. Figure 4-29 shows a typical resonance for several values of RF input current. The resonant peaks, as well as the half power points, are at approximately the same frequencies independent of current amplitude. The amplitude of the resonance varies linearly with the amplitude of the input current.

Figure 4-30 shows the impedance for several values of DC bias current. The plasma frequency changes in the appropriate manner, and the Q follows the expected behavior to a reasonable degree. Figure 4-31 is a plot of f_p/Q versus f_p for a series of measurements. If the $\cos\phi$ term is zero, f_p/Q should be constant, and all of the points should fall on the line given by $(2\pi RC)^{-1}$. The scatter in the data points is reproducible, which indicates a frequency dependent source of error in the analogue. Investigation suggests that multiplier inaccuracy is partly to blame. Other measurements similar to those of Figure 4-31 were made, but they were considerably less consistent with theory. Attempts to make quantitative measurements using the analogue in the high frequency mode were abandoned until the necessary improvements were made to the circuitry. The resulting quantitative data are presented in Chapter 9. However, the simple qualitative results presented here illustrate the effects of $J_1(\omega)$ and $J_2(\omega)$. Figure 4-32 shows the plasma resonance for a frequency less than the gap frequency. The top curves are for the RSJ limit. The second set of curves are with the $J_2(\omega)$ filters connected. This causes some structure at the gap frequency, but the Q is not greatly affected. The third set of curves are for the analogue with both $J_1(\omega)$ and $J_2(\omega)$ connected. The dramatic increase in Q is a result of the high quasiparticle resistance at voltages below the gap. The decrease in resonant frequency is due to the inductance of $\text{Re } J_1(\omega)$ (cf. Section 2.6).

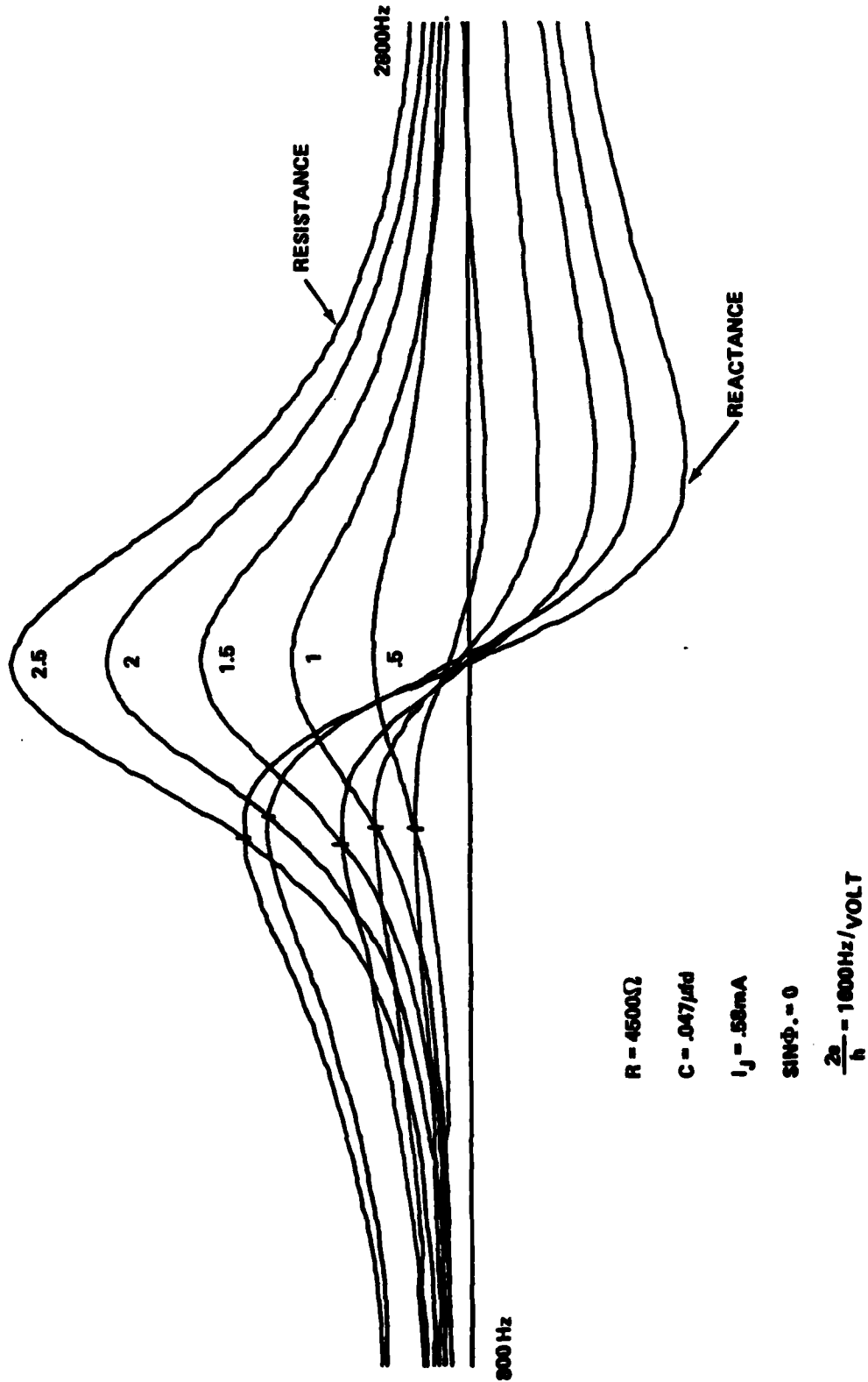


FIGURE 4-29. PLASMA RESONANCE VS RF AMPLITUDE (RSJ LIMIT)

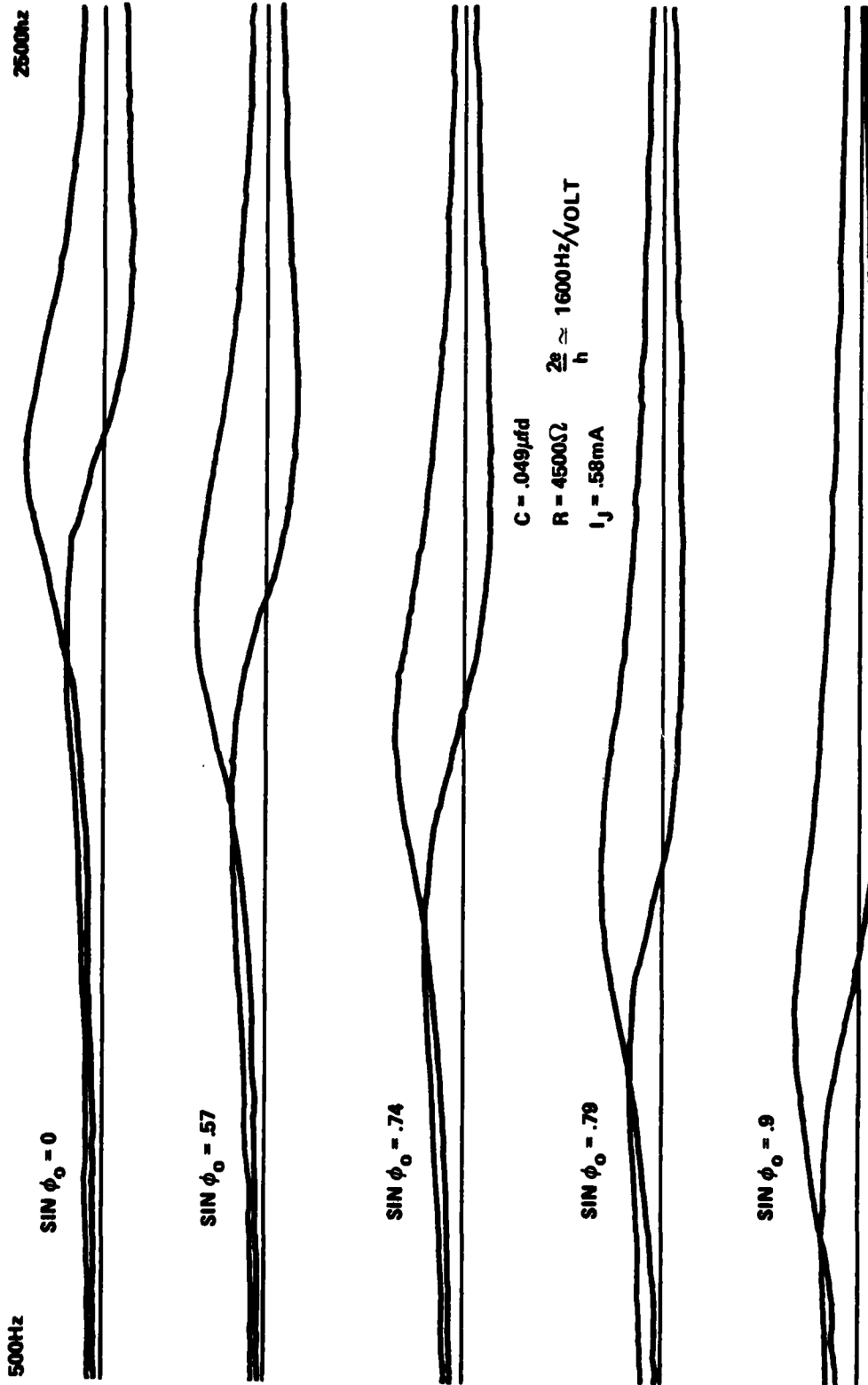


FIGURE 4-30. PLASMA RESONANCE VS COS PHI (RSJ LIMIT)

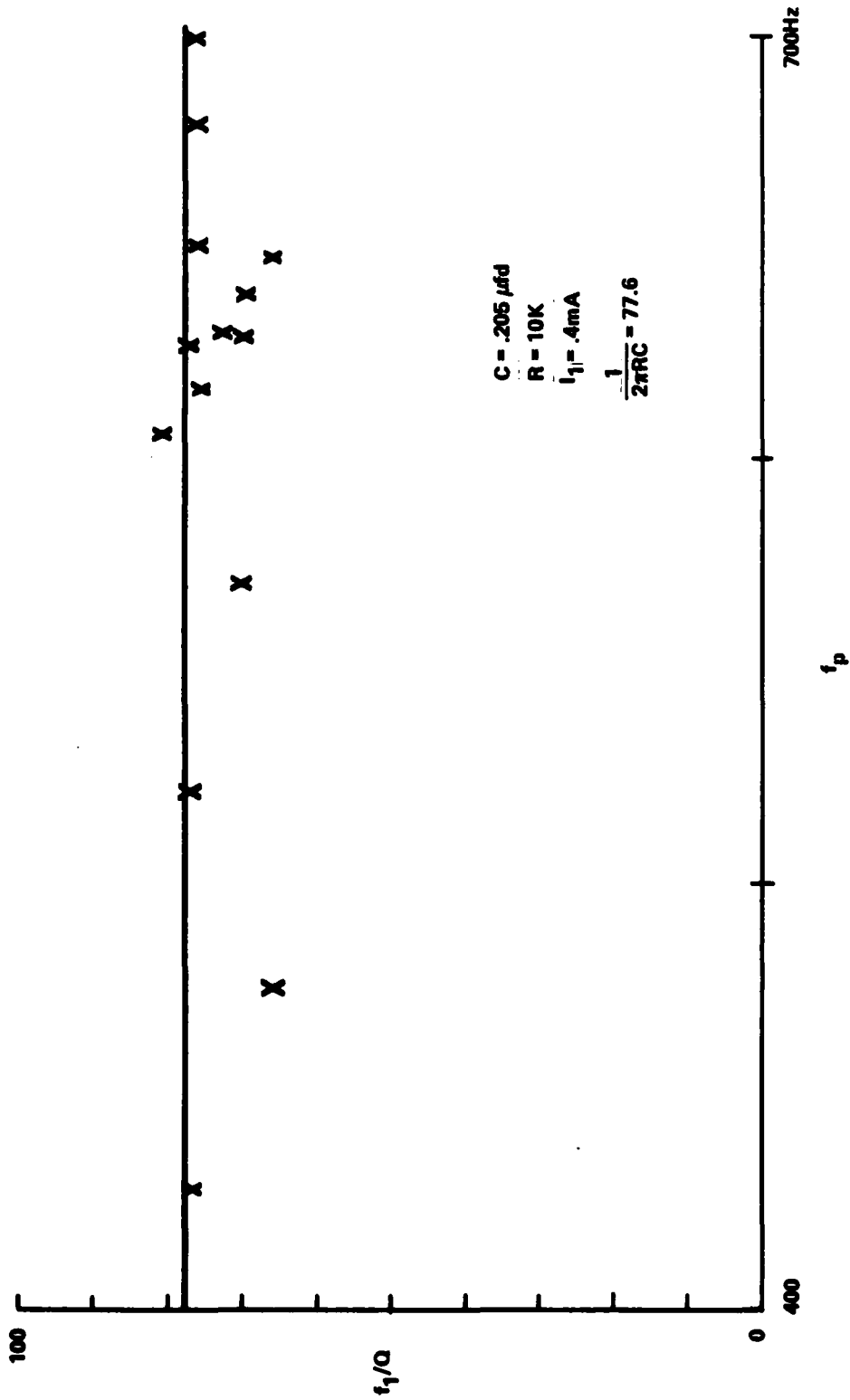


FIGURE 4-31. Q OF THE PLASMA RESONANCE VS FREQUENCY (RSJ LIMIT)

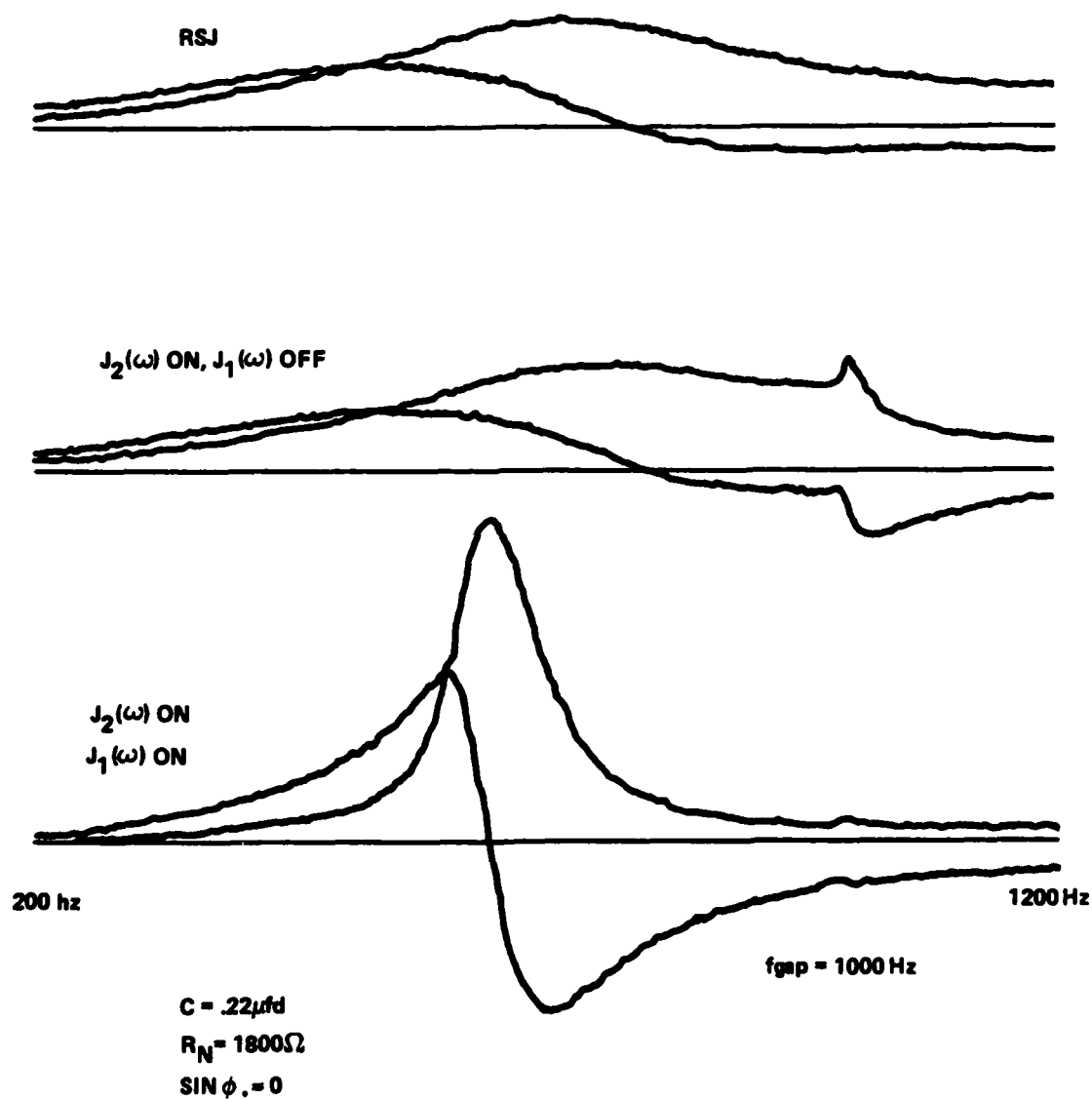


FIGURE 4-32. PLASMA RESONANCE (HIGH FREQ ANALOGUE)

The measurements illustrated in Figure 4-33 are identical to those of Figure 4-32, except that the plasma frequency is greater than the gap frequency. The top curves, for the RSJ limit, are reasonably Lorentzian. As in Figure 4-32, the effect of connecting the $J_1(\omega)$ filters is to lower the resonant frequency. However, the Q is not raised dramatically, as the $J_1(\omega)$ filter has little influence on the resistance of the analogue above the gap frequency. In Figure 4-33b, the large negative amplitude of $\text{Im } J_2(\omega)$ above the gap frequency seems to increase the Q slightly.

Figures 4-34 and 4-35 show the effect of increasing the amplitude of the RF input to the analogue when operated in the RSJ mode. As expected, the curves begin to look very non-Lorentzian.

4.7 Summary

The discussion and results presented in this and the previous chapters represent an overview of the design of the original versions of the high frequency analogue. The results have demonstrated that Waldram's scheme for modelling the high frequency theory is not only feasible, but practical as well. Inspired by this, further improvements were made to the analogue, and experiments were repeated in a quantitative, as opposed to qualitative, manner.

The next several chapters describe this work, beginning with additional discussion of the high frequency theory. This is followed by a description of how the analogue has been improved, and a summary of the numerous additional results that have been obtained.

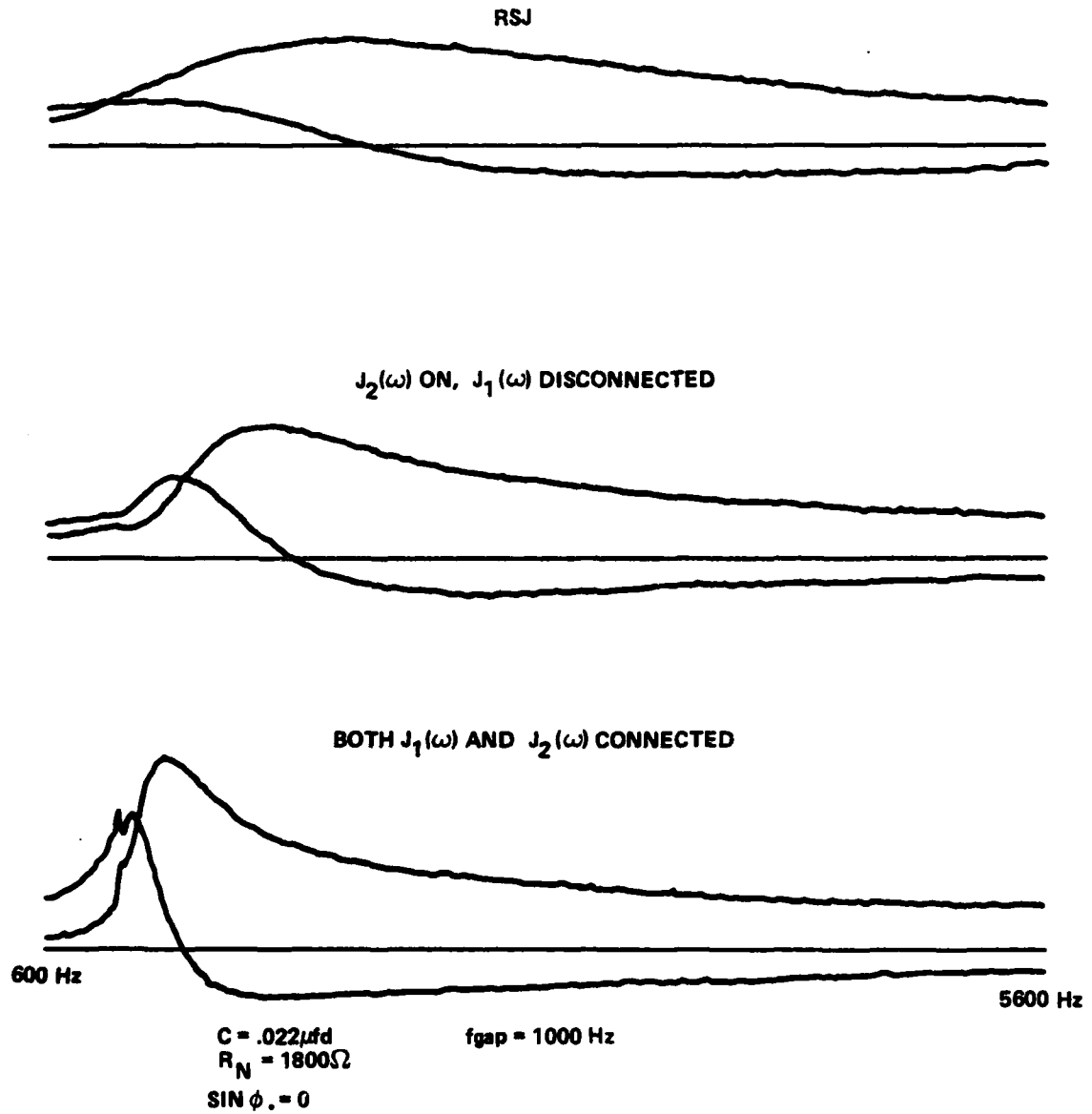


FIGURE 4-33. PLASMA RESONANCE (HIGH FREQ ANALOGUE, CONTINUED)

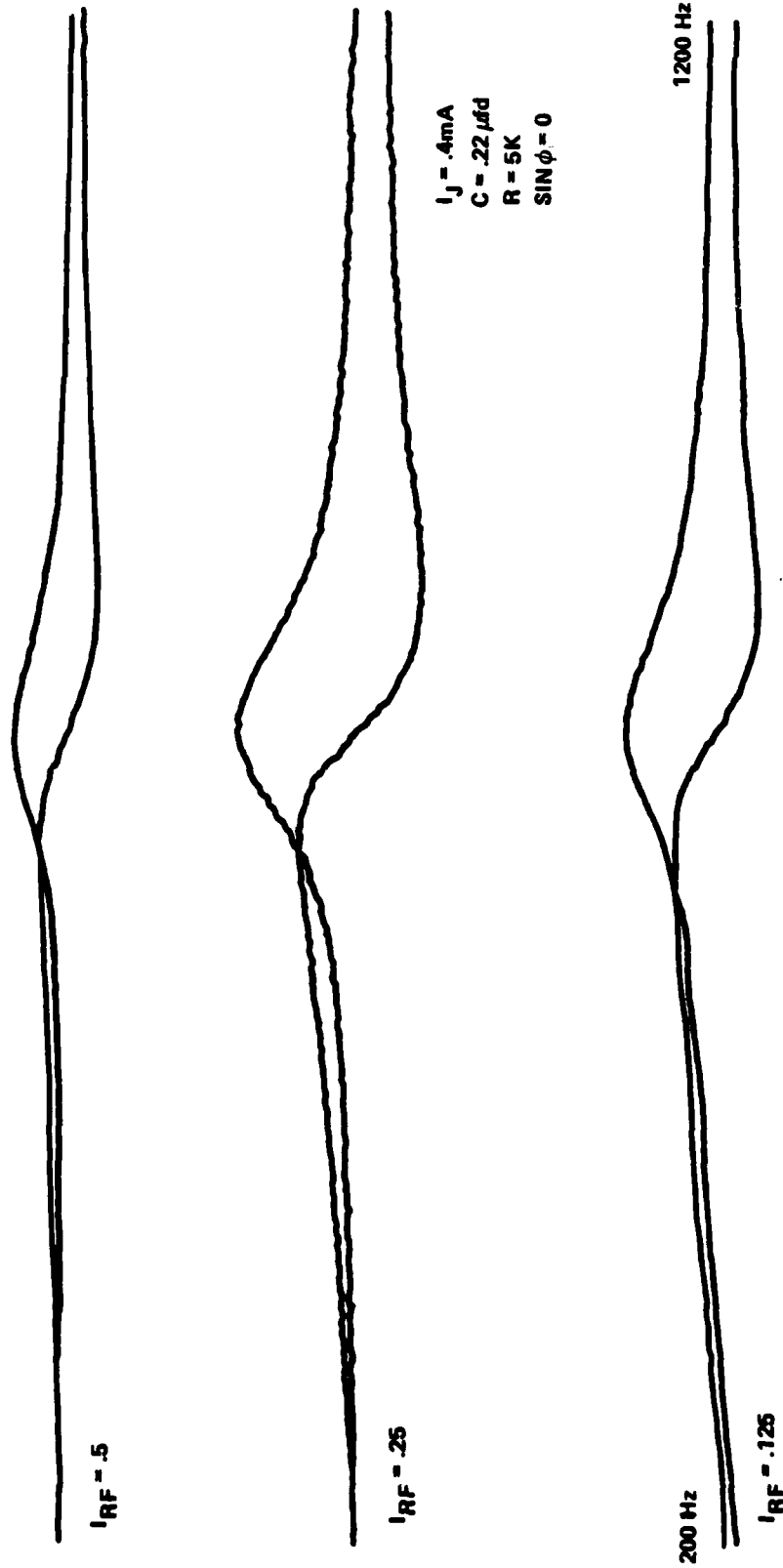


FIGURE 4-34. PLASMA RESONANCE-EFFECTS OF INCREASING RF AMPLITUDE (RSJ LIMIT)

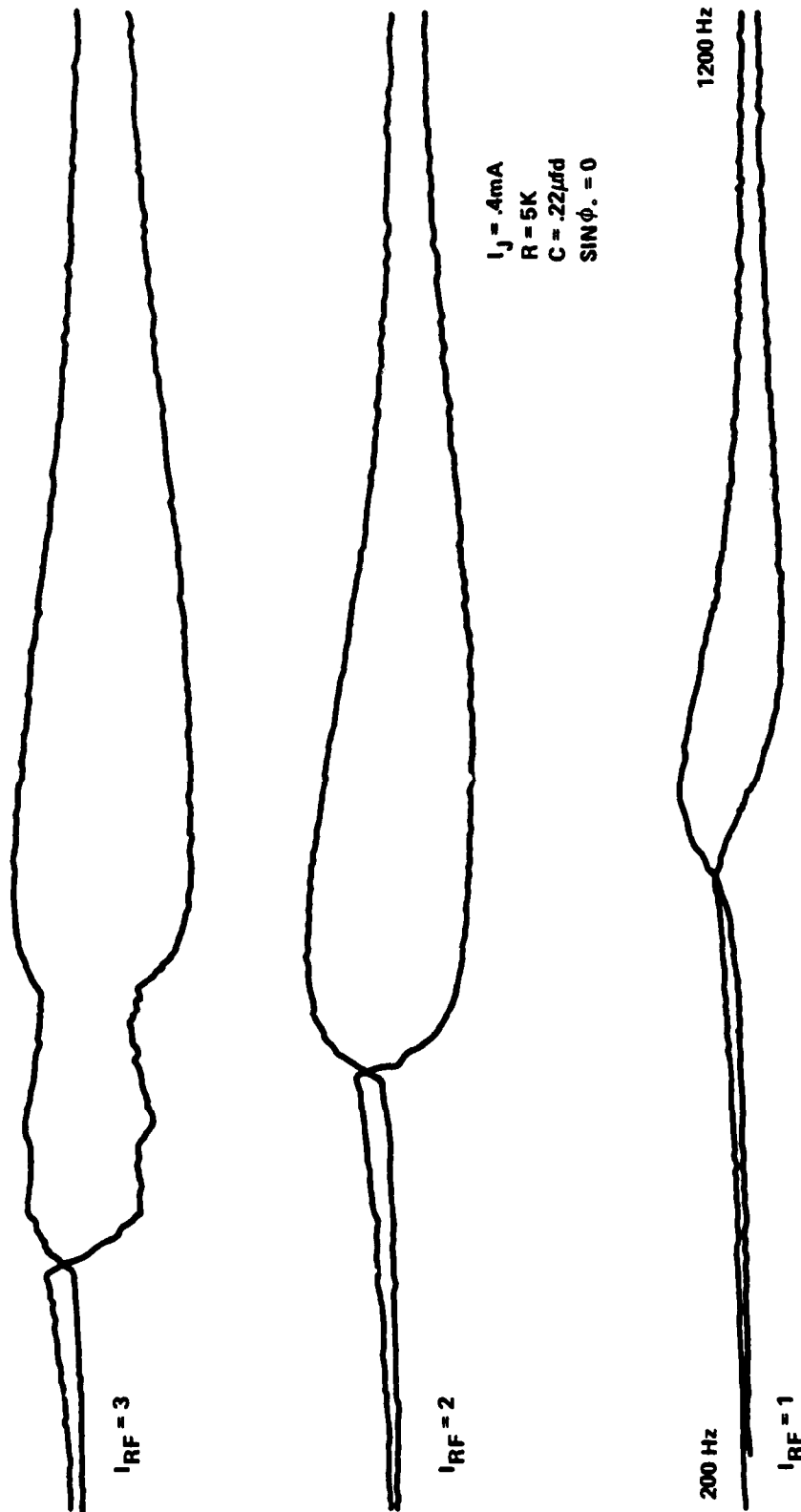


FIGURE 4-35. PLASMA RESONANCE—EFFECTS OF INCREASING RF AMPLITUDE (RSJ LIMIT)
(CONTINUED)

CHAPTER 5

DISCUSSION OF THE HIGH FREQUENCY THEORY

5.1 Introduction

In Chapter 2, the high frequency theory developed by Werthamer was discussed in very pragmatic terms, with little attention given to the underlying physics. In this section we elaborate on the earlier discussion by calling attention to the various assumptions implicit in the theory, and also to the strengths and weaknesses of the theory. As the basics of the RSJ and Werthamer models have already been discussed, this section is relatively informal. It is designed to stress points that have not been discussed earlier, and is not a complete, self-contained discussion of the theory.

5.2 Josephson's Calculation

Prior to Josephson's work, it was believed that multiparticle tunnelling between two superconducting electrodes could occur. However, it was assumed that such tunnelling would be highly improbable, and thus unobservable, compared to single particle tunnelling. For example, if the current due to single particle tunnelling is proportional to the square of a matrix element, T^2 , the current due to events in which two electrons tunnel simultaneously would be expected to be proportional to T^4 . This was based on the assumption that the simultaneous transfer of two electrons was an incoherent process, and that its probability was proportional to the product of the probabilities of the separate one electron transfers.¹¹

Josephson demonstrated the existence of a coherent process in which two electrons tunnel simultaneously. This process has an effective matrix element proportional to T^2 , but since it is coherent, the tunnel current

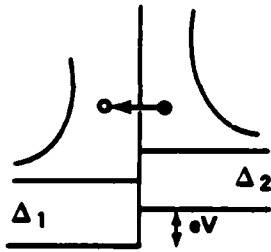
is proportional to the effective matrix element, and not to its square. The current is thus proportional to T^2 , as in single particle tunnelling. This process is illustrated in Figure 5-1. (In the various sketches, the possible contributions to the tunnel current are shown with respect to the Bose condensate of paired electrons at the Fermi energy, and the bands of excited quasiparticle states above the Fermi energy.) Figure 5-1a shows the transfer of a single excitation across the barrier. This particular process will occur only at finite temperature, as it relies on the existence of occupied states above the Fermi level. This process is proportional to T^2 .

Figure 5-1b illustrates a multiparticle tunnelling event in which two excitations cross the barrier simultaneously. This is shown in terms of a virtual state, which is a convenient way of illustrating the intermediate state that arises in the perturbation theory used to describe the event. The tunnel current for the process in Figure 5-1b is proportional to T^4 , as the two electrons tunnel incoherently. This process also occurs only at finite temperature.

Figure 5-1c shows the pair tunnelling process predicted by Josephson.⁷ In this case, two electrons from the condensate cross the barrier coherently, resulting in a contribution to the current proportional to T^2 , not T^4 . Note that this process occurs at zero voltage. This is the DC Josephson effect. (As before, the virtual state is a means of illustrating certain aspects of the perturbation theory used to describe the transition.) The DC Josephson effect can occur at zero temperature.

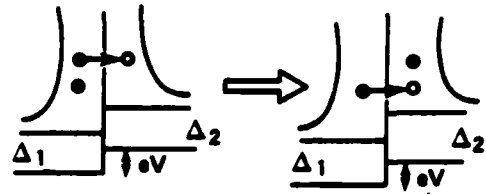
The next few sketches show other tunnelling events that are of interest. Figure 5-1d shows how breaking a Cooper pair can result in the transfer

5-1(a)



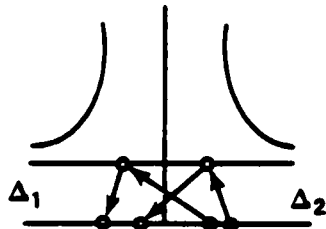
QUASIPARTICLE TUNNELING
AT FINITE TEMPERATURE

5-1(b)



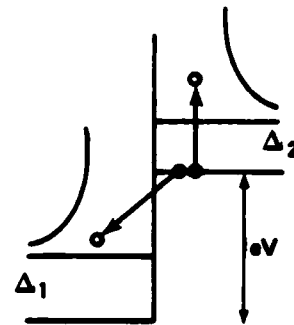
MULTIPARTICLE TUNNELING

5-1(c)



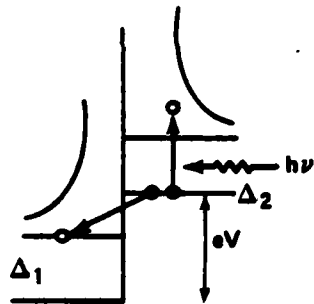
DC JOSEPHSON EFFECT ($V = 0$)

5-1(d)



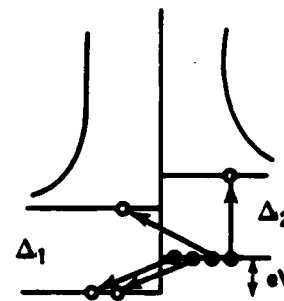
QUASIPARTICLE TUNNELING AS A
RESULT OF PAIR BREAKING

5-1(e)



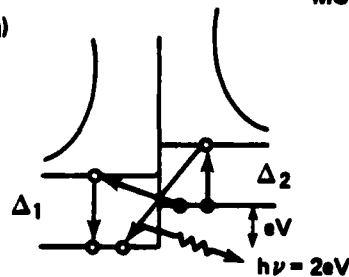
PHOTON-ASSISTED TUNNELING

5-1(f)



MULTIPARTICLE TUNNELING

5-1(g)



AC JOSEPHSON EFFECT

FIGURE 5-1 TUNNELING PROCESSES IN JOSEPHSON JUNCTIONS

of a single electron across the barrier. Note that for voltages $eV < \Delta_1 + \Delta_2$, this process will not occur, as sufficient energy is not available. However, with the addition of a photon (or phonon), this process can happen, as shown in 5-1e. Figure 5-1f shows an example of an energy conserving multiparticle tunnelling event. The energy gained by the transfer of a pair across the barrier is sufficient to break another pair and form two quasiparticle excitations, one on either side of the barrier. This process is of much higher order than T^2 . As processes such as these are highly improbable, Josephson neglected them in his calculation. The last sketch, Figure 5-1g, shows the transfer of a Cooper pair as in Figure 5-1c, but for nonzero voltage. Note that a photon of energy $hf = 2eV$ is emitted. This is the AC Josephson effect.

Various aspects of the Josephson effects will be discussed in more detail in connection with the Werthamer theory. At this point, it is worth discussing more completely some of the assumptions implicit in Josephson's original work.

First, in his original calculation,⁷ Josephson required that the voltage across the tunnel junction be constant, or at most slowly varying. This meant that the phase difference could be defined very simply by $\phi = 2\pi ft$, where f is the Josephson frequency $2eV/h$. This greatly simplified his calculation, but eliminated many interesting aspects of the problem.

Second, Josephson chose a situation in which higher order processes, such as the multiparticle tunnelling in Figures 5-1b and 5-1f, would be negligible with respect to the single electron and coherent pair processes. On the other hand, these latter events were assumed to be highly probable, yet

describable in terms of simple perturbation theory. In a real situation, this corresponds to a tunnel junction where the barrier is neither too wide (no tunnelling probable) nor too narrow (higher order processes probable). That this situation is reasonable can be seen from the following argument.

Simple quantum tunnelling through a barrier can be described by an expression $I = A \exp(-x/B)$, where x is the barrier thickness and B is related to the barrier height. For a typical situation, this transmission coefficient can be approximated by $\exp(-x/\text{Angstrom})$, or $\exp(-x)$, where x is in Angstroms. A higher order, multiparticle tunnelling current would be proportional to $\exp(-2x)$. For x on the order of an Angstrom, $\exp(-x)$ and $\exp(-2x)$ are comparable in magnitude. However, for $x = 10$, the transmission coefficient is large enough that $\exp(-x)$ describes an observable current, is small enough that this current can be described as a small perturbation, and is such that terms proportional to $\exp(-2x)$ can be completely neglected. Barrier thicknesses of this size are what one achieves if the barrier is formed by natural means, such as letting a thin film of superconductor oxidize in a room atmosphere until reaching equilibrium.

In an actual tunnel junction, one can be reasonably confident that multiparticle effects are small, if not negligible. If multiparticle effects were a major contribution to the tunnel current, the total current would be in significant disagreement with the current predicted by the $I_J R_N$ product deduced by Josephson, and this turns out not to be the case. On the other hand, it is sometimes likely that a tunnel junction will have spots where the tunnel barrier is locally much thinner than for the rest of the junction. This permits some multiparticle tunnelling to occur, but in

amounts small enough not to make the total current behave in an un-Josephsonlike manner. Such locally thin regions are found in junctions made using simple evaporation and oxidation techniques, where pinholes in the barrier are common. However, state-of-the-art techniques permit fabrication of junctions that show no sign of multiparticle effects,¹³ and Josephson's original assumptions are well established as to their validity.

In making the assumption that the junction voltage was constant, Josephson greatly simplified his calculations. By making the further assumption that the voltage was small compared to the gap voltage of the superconductor (which in the voltage bias limit corresponds to saying the current, as well as the voltage, is slowly varying), Josephson was able to treat quantities such as the critical current and junction voltage as being constant. This assumption allows one to ignore much of the BCS theory once the calculation is complete. For example, the RSJ model contains no direct reference to temperature or the superconducting energy gap.

Lastly, Josephson worked completely within the framework of the BCS theory. With respect to the RSJ model, any corrections to BCS (to take into account strong coupling effects, for instance) would be reflected primarily in an adjustment of the $I_J R_N$ product.

5.3 The Werthamer Theory

Simply put, the Werthamer theory is a repeat of Josephson's calculation, but with no simplifying assumptions made about the magnitudes or frequencies of the junction voltage and current.⁵ The assumptions about higher order effects and validity of perturbation theory are the same, and the calculation is done within the confines of the BCS theory. The

differences between Josephson's first calculation and the Werthamer theory are well seen by examining the differences between the block diagram of the RSJ analogue (Figure 5-2a) and that of the high frequency analogue (Figure 5-2b). Note that the RSJ analogue contains only a sine term (no cosine term, except for the extraneous contribution caused by the unwanted phase shift of the low pass filter), and that the temperature and frequency dependent response functions J_1 and J_2 are either ignored or treated as being constant.

It might be well to note that J_1 and J_2 represent spectral response functions, which contain all of the information about the quantum response of a tunnel junction to an applied current or voltage. The use of the functions J_1 and J_2 allows for a classical model of a quantum phenomenon (e.g., the filters in the electronic analogue model quantum behavior in a classical way).

Figure 5-3 illustrates some of the important aspects of the Werthamer theory in more detail. Figure 5-3a shows the transfer of a single excitation via a pair splitting process at $eV = \Delta_1 + \Delta_2$. As mentioned before, this process will not occur for voltages less than $eV = \Delta_1 + \Delta_2$. However, due to the singularities in the densities of states at the gap edge, the onset of this current at $eV = \Delta_1 + \Delta_2$ will be extremely rapid. This accounts for the sharp knee observed in the quasiparticle current of a tunnel junction at the gap voltage (cf. Figure 5-3b). For $T > 0$, there will also be excitations of the form diagrammed in Figure 5-1a, resulting in quasiparticle current at voltages less than the gap voltage.

The singularity in the density of states is also reflected in the Riedel peak in the supercurrent at the gap voltage for a current biased

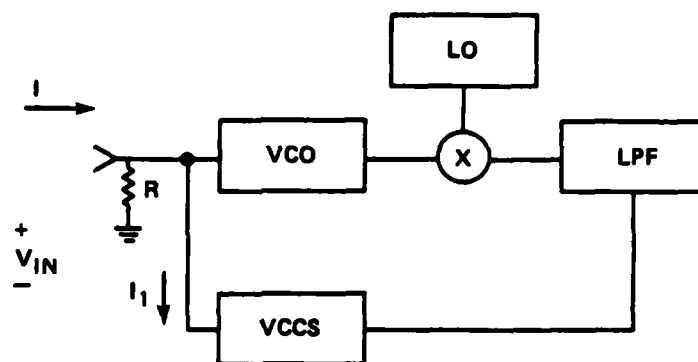
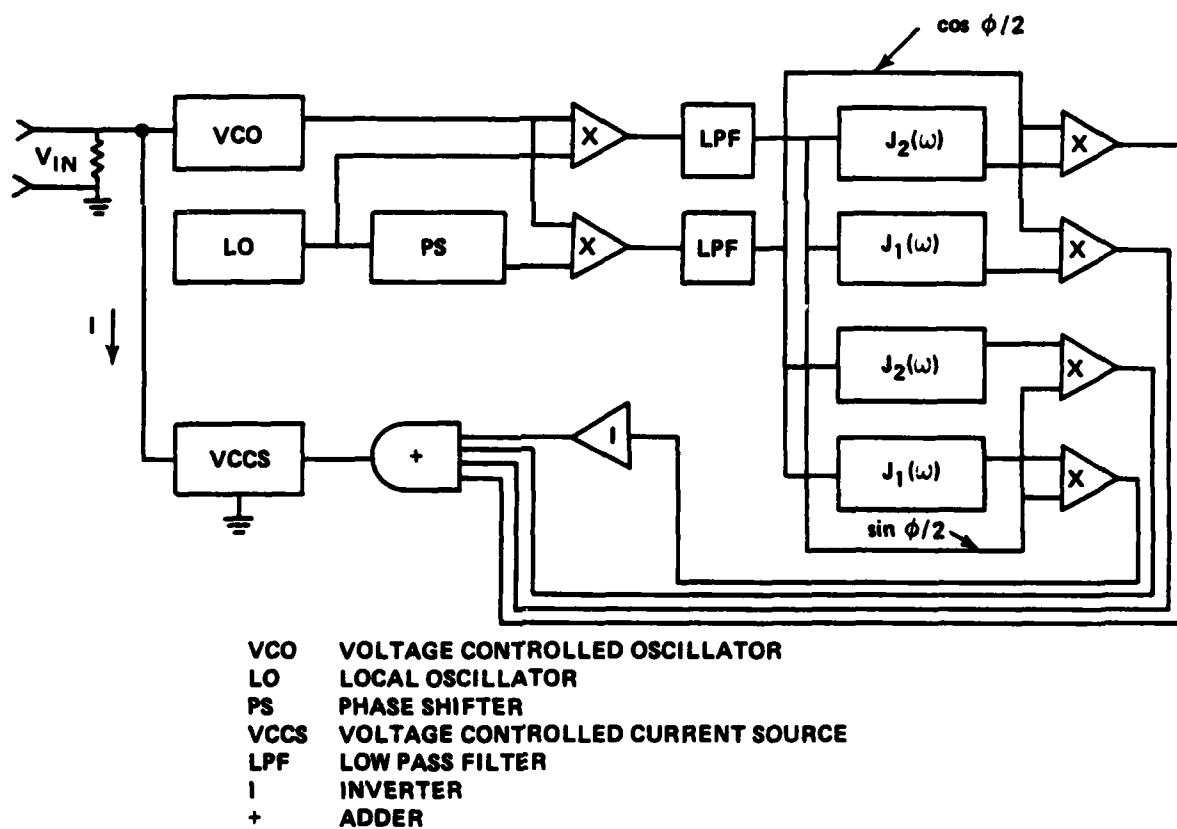
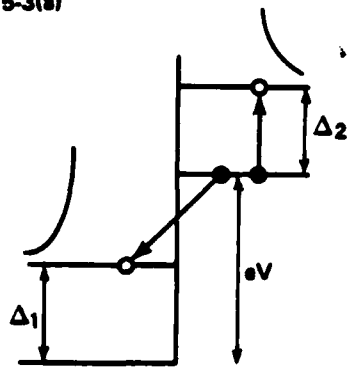
5-2a THE RSJ ANALOGUE (AFTER BAK AND PEDERSEN)⁴

FIGURE 5-2b BLOCK DIAGRAM OF THE HIGH FREQUENCY ANALOGUE

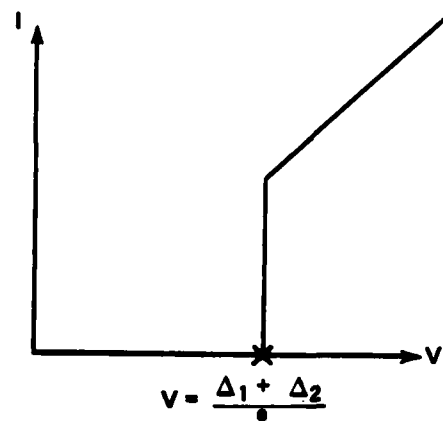
FIGURE 5-2. THE RSJ AND HIGH-FREQUENCY ANALOGUES

5-3(a)



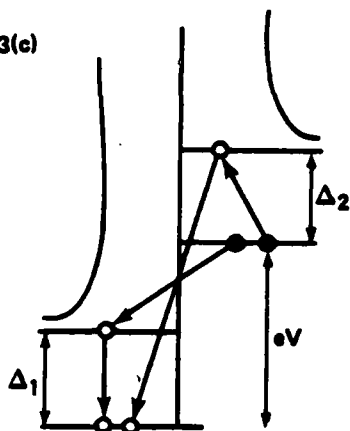
PAIR SPLITTING
AT $eV = \Delta_1 + \Delta_2$

5-3(b)



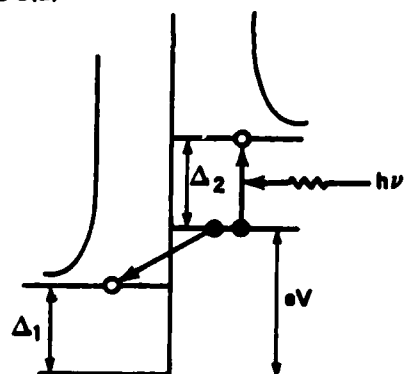
QUASIPARTICLE CURRENT
VS VOLTAGE AT $T = 0$

5-3(c)



THE RIEDEL PEAK-PAIR
TUNNELLING AT $eV = \Delta_1 + \Delta_2$

5-3(d)



PHOTON-ASSISTED
TUNNELLING

FIGURE 5-3 EFFECT OF THE GAP SINGULARITY
ON QUANTUM TUNNELLING

tunnel junction. This is sketched in Figure 5-3c. The supercurrent is represented by the transfer of a pair across the barrier via an intermediate state. In second order perturbation theory, the probability of this transfer is proportional to the inverse of the difference between the energy of the original state and that of the intermediate state. For a given bias level, the probability is dominated by the intermediate state contributions in which the difference between these two energies is at or near zero. When $eV = \Delta_1 + \Delta_2$, the intermediate state for which the energy difference is zero can coincide with the singularity in the density of states at the gap edge. The Riedel peak in the supercurrent at $eV = \Delta_1 + \Delta_2$ arises from this coincidence.

Figure 5-3d shows a single excitation crossing the barrier for a voltage eV less than $\Delta_1 + \Delta_2$. The extra energy required to break a pair is provided by a photon. In the sketch, the photon has just enough energy to create excitations at the edge of the excitation spectrum, where the density of states is singular. In this case the photon must provide energy

$$h\nu = (\Delta_1 - eV) + \Delta_2 \quad (5-1)$$

This photon-assisted tunnelling causes steps to appear in the time-averaged I-V characteristic of the junction at the voltages

$$eV = \Delta_1 + \Delta_2 \pm nh\nu \quad (5-2)$$

where n is an integer.

At this point we can discuss the existence of structure at submultiples of the energy gap voltage $(\Delta_1 + \Delta_2)/e$. If the photon assisted

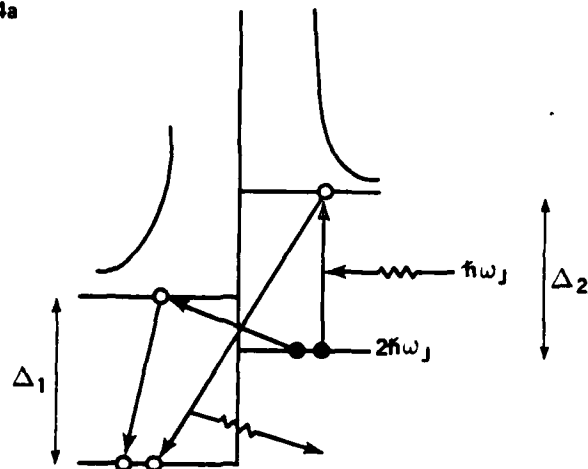
tunnelling described above is caused by the feedback of current at multiples of the Josephson frequency from the source impedance, as opposed to being provided externally by photons of arbitrary frequency, then there will be a relationship between the energy of the photons and the bias voltage. This results in the presence of various structure in the time-averaged current-voltage characteristic of the junction.⁵ For example, if the junction is biased through a finite source impedance at an average value eV , then photons will be available at all multiples of the Josephson frequency $hf_J = 2eV$. (Strictly speaking, DC supercurrent can only exist when the source impedance is nonzero. In the constant voltage limit, there is no time average supercurrent, and the effects we are discussing will not be apparent in the DC I-V characteristic.) These photons can contribute to additional pair splitting, and at certain bias levels this effect is enhanced by the singularity in the density of states at the gap edge.

For example, Figure 5-4a shows a photon of energy hf_J (generated by the transfer of a pair across the barrier as in Figure 5-1g) being fed back to the junction via a complex interaction with the source impedance. If the bias voltage is such that the energy hf_J is just enough to split a pair and create excitations at the gap edge, then this feedback effect will be enhanced by the singularity at the gap edge. That is, when

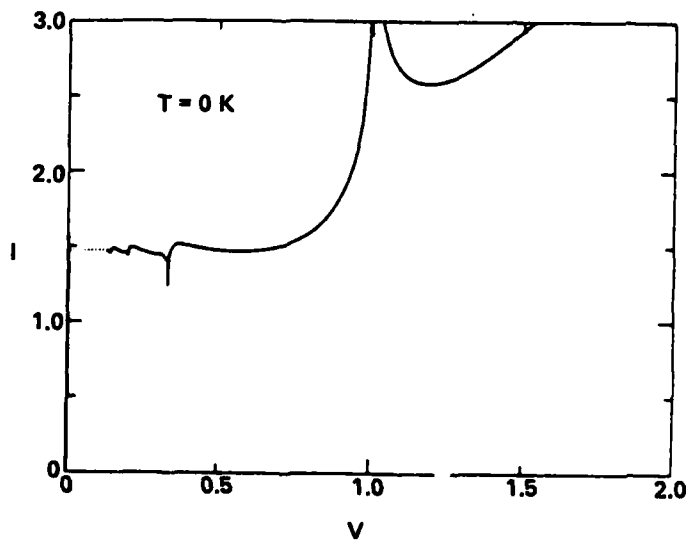
$$hf_J = \Delta_1 - eV + \Delta_2 \quad (5-3)$$

When the pair recombines, a photon must be emitted with energy mhf_J (m is an integer) such that

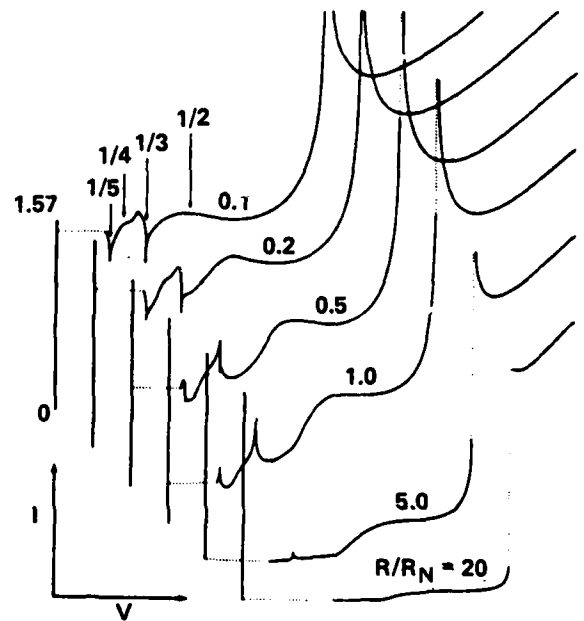
5-4a



GENERATION OF
SUB-GAP STRUCTURE AT $eV = \frac{\Delta_1 + \Delta_2}{3}$



5-4b ODD SUB-GAP STRUCTURE
IN A CURRENT-BIASED
TUNNEL JUNCTION
(AFTER MCDONALD, ET.AL.)²



5-4c EXAMPLE OF EVEN
SUB-GAP STRUCTURE
DUE TO THE PRESENCE
OF A MATTIS-BARDEEN
SUPERCONDUCTING LOAD
(AFTER MCDONALD, ET.AL.)²

FIGURE 5-4 SUB-GAP STRUCTURE

$$mhf_J = hf_J + 2eV \quad (5-4)$$

Since $hf_J = 2eV$, we have $m = 2$. In the general case, the splitting of a pair with a photon of energy hf_J is enhanced by the gap singularity whenever

$$nhf_J = \Delta_1 + \Delta_2 - eV \quad (5-5a)$$

or

$$eV = (\Delta_1 + \Delta_2)/(2n + 1) \quad (5-5b)$$

The emitted photon has an energy

$$mhf_J = nhf_J + 2eV \quad (5-5c)$$

or

$$m = n + 1 \quad (5-5d)$$

For the case where $n = 0$, we have the Riedel peak at $eV = \Delta_1 + \Delta_2$. For $n > 0$, we see "images" of the Riedel peak at sub-gap voltages given by

$$eV = (\Delta_1 + \Delta_2)/(2n + 1) \quad (5-5e)$$

For a current biased junction, this odd series shows up as extra structure in the time-averaged I-V characteristic (cf. Fig. 5-4b). This feedback of Josephson photons back to the junction via the source impedance is sometimes referred to as "frequency dependent self-coupling".³⁹

An additional effect which is of interest occurs at even submultiples of the gap voltage $2\Delta/h$. In this case, currents at multiples of the Josephson frequency are affected by the sharp rise in the surface impedance of the junction electrodes at the gap frequency.⁵ This rise, which is

relatively broad compared to the sharp structure associated with the Riedel peak, shows up in the time-averaged I-V characteristic as broad structure at the voltages $eV = 2\Delta/2n$, where n is an integer. In the case of a junction comprised of different superconductors, structure appears at voltages $eV = 2\Delta_1/2n$ and $2\Delta_2/2n$. This broad structure is shown in Figure 5-4c as calculated for a junction comprised of identical superconductors having a surface impedance of the type described by Mattis and Bardeen.²

Another process which will yield an odd series of sub-gap structure can result from higher order, multiparticle tunnelling as shown in Figure 5-1f. The energy required to split a pair and create two quasi-particles (one of which crosses the barrier) is generated by the simultaneous direct transfer of one or more pairs across the barrier.^{2,5} This is enhanced by the gap singularity when

$$2neV = \Delta_1 - eV + \Delta_2 \quad (5-6a)$$

or

$$eV = (\Delta_1 + \Delta_2)/(2n + 1) \quad (5-6b)$$

As discussed earlier, this process is not included in either Josephson's or Werthamer's treatment of the tunnelling problem.

One of the shortcomings of the Werthamer theory is that it ignores non-BCS effects in, for example, lead tunnel junctions, where strong-coupling effects are present. Some of these effects can be incorporated into the Werthamer theory by modifying the functions J_1 and J_2 . In the simplest case, this would mean adjusting these functions so that the $I_J R_N$ product and gap frequency agree with experimental observation.⁴⁰ Kulik, et al.⁴¹ have carried this a step further by modifying the individual

response curves to account for anisotropy and relaxation effects, and the influence of electrode inhomogeneity.

Another effect which is not included in the Werthamer theory is phonon-assisted tunnelling. However, this is of little consequence in junctions comprised of weak-coupling superconductors (e.g., tin), and disappears in all types of junctions as T approaches zero.⁴²

In any event, deviations from BCS are not expected to change the basic nature of the frequency, temperature, and voltage dependences described by Werthamer. Furthermore, in junctions comprised of weak-coupling superconductors, which are well described by the BCS theory, one would expect the Werthamer description to be quite good. As for multiparticle and any anomalous effects, the current experimental situation seems to be that people are striving to fabricate junctions that conform with the theory, as opposed to developing more complex theories that describe nonideal junctions. The conclusion is that for tunnel junctions which are currently of interest, the theoretical model used by Werthamer is sound, and represents a substantial improvement over the RSJ model. (As pointed out in an earlier chapter, other types of weak links, such as microbridges, are more adequately described by the RSJ model. One would expect that the theories of microbridges and tunnel junctions might differ substantially, so this is not necessarily a criticism of the Werthamer formulation.¹¹)

5.4 Experimental Corroboration of the Werthamer Theory

Surprisingly, there is not a great deal of experimental evidence to support the finer details of the Werthamer theory. There is also experimental evidence that is in direct disagreement with it. Most of the difficulty

arises from the presence of the shunt capacitance in a tunnel junction. This causes the time-averaged current-voltage characteristic to be highly hysteretic, with the result that most of the structure predicted by the theory is hidden. For example, the Riedel peak and corresponding sub-gap structure are completely wiped out for even relatively small values of shunt capacitance. This is shown in Figure 5-5.²

On the other hand, the presence of the highly nonlinear quasiparticle curve is clearly demonstrated in the high capacitance limit. In a tunnel junction, this current is often in good agreement with the prediction that I approaches $Im J_1$ as the source impedance is lowered.¹⁷

The most significant disagreement between theory and experiment seems to be the question of whether the cosine ϕ term is positive or negative with respect to the quasiparticle term in the low frequency, low voltage limit.¹¹ Most experimental evidence suggests that the sign of the $\cos \phi$ term is negative, whereas the Werthamer theory clearly predicts it will be positive.^{8,9,43,44} The interpretation of the experimental evidence has been done on the basis of the RSJ model with modification to include the cosine ϕ term, however. As discussed in the next chapter, this can lead to important errors in both the qualitative and quantitative evaluation of the data. However, taking this into account does not resolve the discrepancy.

There are two popular explanations for the discrepancy. First of these is the suggestion that "relaxation effects" introduce a negative $\cos \phi$ term in much the same way the low pass filter in the Bak analogue does. This argument is generally put forth with little or no theoretical justification or discussion.^{43,45} Although relaxation processes having a negative $\cos \phi$

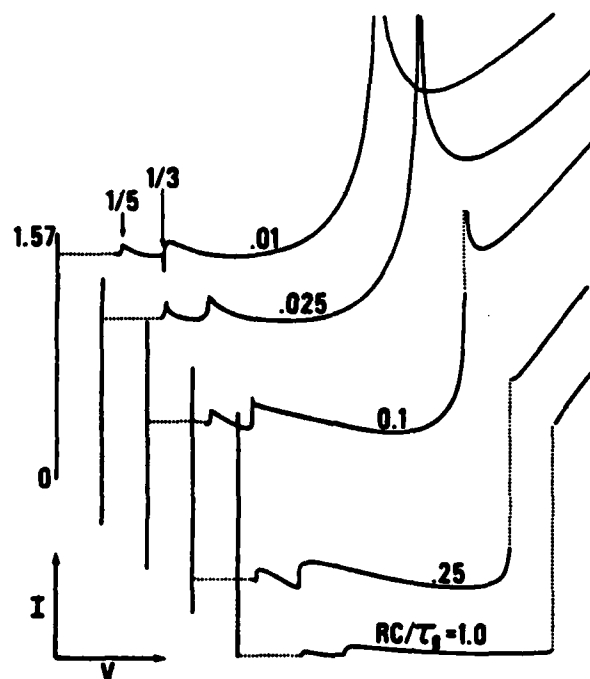


FIGURE 5-5 EFFECT OF SHUNT CAPACITANCE ON THE I-V CHARACTERISTIC.

$\tau_g = h/2e\Delta$. (AFTER McDONALD, ET. AL.)²

term may well exist in other types of weak links (e.g.- microbridges),⁴⁶ relaxation effects are already built into the Werthamer theory in the first place by including the time dependence of the superconducting response functions throughout the entire derivation. There may be other relaxation effects that have not been considered properly, but the ad hoc addition of a negative cosine ϕ term due to relaxation seems unjustified at this time.

The second explanation, put forth by theorists,⁴¹ suggests that one or more factors (such as gap anisotropy or electrode inhomogeneity) cause a smearing of the Riedel peak. This in turn affects the response function $\text{Im } J_2$ via the Kramers-Kronig relationship. This argument seems plausible, and it leads to the conclusion that the $\cos \phi$ term will be positive near the transition temperature of the junction, and then go negative as the temperature is reduced. This is in qualitative agreement with many experimental results, but the predicted temperature at which the transition from positive to negative occurs is substantially different from that measured experimentally.^{43, *} As it stands now, the problem with the sign of the $\cos \phi$ term is still an unresolved controversy.

The support for the Werthamer theory comes from three major observations: the strong nonlinearity in the quasiparticle current as described by the function $\text{Im } J_1$, observation of sub-gap structure in the measured current-voltage relationships of a tunnel junction, and measurement of step heights.^{17,38,21} In a sense, the first observation predates the Werthamer theory, as one need not derive the Josephson effects to derive the quasiparticle current. However, one of the key points in the Werthamer theory is that the response function $\text{Im } J_1$ is intimately connected to the

*N. F. Pedersen personal communication

other response functions (i.e., the earlier theoretical and experimental work by Giaever and others is really a limiting case of the Werthamer theory). Anyway, there is good agreement between the observed quasiparticle characteristics of tunnel junctions and those predicted by theory.¹⁷ (When there are strong quantitative disagreements, they can often be explained by well understood processes such as gap anisotropy, phonon-assisted tunnelling, and strong-coupling effects. In addition, changing the conditions under which the junction is oxidized will often improve the agreement.)

With respect to the second of the three lines of support mentioned above, the observation of sub-gap structure has generally been consistent with the Werthamer theory. The difficulty arises from the fact that it is also in agreement with the behavior predicted for multiparticle tunnelling as described in the previous section. The most important work on the subject is that of Giaever and Zeller, who used a tunnel junction having a light sensitive barrier to vary the tunnelling probability for the electrons.⁴⁷ Using arguments similar to the discussion of multiparticle tunnelling in section 5.2, they demonstrated that Werthamer's explanation of sub-gap structure based on frequency dependent self-coupling is a better argument than that of multiparticle tunnelling.

In his investigation of the high frequency theory, Hamilton measured the power and frequency dependence of both the microwave induced Josephson steps and the photon-assisted quasiparticle steps in a junction's DC characteristic.²¹ He was able to show the existence of the Riedel peak, as well as good agreement between theory and experiment for the dependence of step heights on both frequency and RF power. His measurements, made using

tin tunnel junctions, indicated some smearing of the Riedel peak. This offers support to the theoretical efforts to explain the cosine ϕ problem in these terms.

With the exception of the cosine ϕ controversy, the Werthamer theory seems to be on relatively firm ground, even though there is not an overpowering amount of experimental evidence either to deny or support it. As the state-of-the-art in junction fabrication progresses, the size and capacitance of tunnel junctions will decrease substantially, and there will be more direct experimental evidence to either support or refute the Werthamer theory. There is a strong case to be made that some of the earlier experiments done to verify the theory should be repeated using the smaller, improved junctions that can be fabricated today. This will eliminate much of the controversy concerning self-field limiting effects, poor tunnelling barriers, and unknown junction parameters.

5.5 Electronic Modelling of the Werthamer Theory

The basic premise of this thesis is that it is possible to accurately model the Werthamer theory. There has been some skepticism that a non-quantum device such as the analogue can successfully model quantum phenomena such as photon-assisted tunnelling. It is safe to say that anything that is in Werthamer's equation for the current through a tunnel junction will be modelled by the analogue. The accuracy with which this is done will depend on the linearity and dynamic range of the electronic circuitry, the accuracy with which the functions J_1 and J_2 are modelled, and noise pickup. The "classical" nature of the analogue is not a limitation, as we are dealing with average macroscopic quantities, and not

with individual quantum fluctuations. For example, the analogue cannot model the response of a junction to a single photon, which has an element of uncertainty to it. But the same is true of the Werthamer theory itself, and of all quantum theory. The analogue is an accurate model for the predictions of the Werthamer theory, but the theory can only predict how a junction behaves on average. Fortunately, we are in practice concerned only with large currents and photon densities, and the quantum statistical fluctuations can be safely ignored.

As an example of what goes on inside the analogue when it is modelling what are essentially quantum phenomena, consider the generation of photon-assisted tunnelling steps. If the analogue is biased with a constant voltage, the output of the voltage controlled oscillator will be sinusoidal. The outputs of the J_1 and J_2 filters will also be sinusoidal, and the only DC current will be that drawn by the quasiparticle resistance. If photons are added (by biasing the analogue with an RF signal generator as well as a DC voltage source), then the VCO output will no longer be purely sinusoidal. The sine ϕ and cosine ϕ signals will contain harmonics of all of the sum and difference frequencies of the Josephson frequency and the applied RF. At particular combinations of DC bias (which controls the Josephson frequency) and applied RF, the sine $\phi/2$ and cosine $\phi/2$ signals will contain harmonics which coincide with the gap frequency. When this happens, the outputs of the J_1 filters will be enhanced by the discontinuity in $\text{Im } J_1$. The J_1 outputs will also be phase shifted in such a way that the time average of the products of their outputs at the gap frequency with the original sine $\phi/2$ and cosine $\phi/2$

signals will be nonzero. This causes additional DC current to be drawn from the source, resulting in a photon-assisted tunnelling step.

Josephson steps also arise from the non-sinusoidal output of the VCO. However, Josephson steps do not depend on the shape of the J_1 or J_2 filter responses for their existence (although the filters affect their heights), but are a result of phase-locking between the Josephson frequency and the applied RF signal.

CHAPTER 6

THE COSINE PHI PROBLEM

6.1 Introduction

In section 2.2 it was noted that the Josephson effects are often described by the equation

$$I(V) = \sigma_0 V + \sigma_1 V \cos \phi + I_J \sin \phi \quad (6-1)$$

where there is significant controversy concerning the amplitude and sign of σ_1 with respect to σ_0 .^{41,43,44} In this section we review this problem from the point of view of the Werthamer formulation of the Josephson effects, as opposed to the more commonly used RSJ model. The following points will be brought out:

1. Adding the cos phi term to the RSJ model on an ad hoc basis is often incorrect and misleading.
2. The use of the Werthamer theory instead of the RSJ model can lead to a substantial change in the interpretation of existing experimental data. This casts doubt on the conclusions published in at least one important paper on the subject.
3. If one takes the high frequency effects into account, there is still a discrepancy between theory and experiment. To date, this cannot be explained by modifying the theory to include non-BCS phenomena such as broadening of the Riedel peak.

The discussion that follows begins with a section on the nature of the cos phi problem, followed by a brief review of the various experimental results relevant to the issue. One of the experiments is then discussed in detail in terms of the Werthamer theory. This is followed

by a very brief description of some recent theoretical work. The chapter concludes with a short summary of the current $\cos \phi$ situation, and a suggestion for future work.

6.2 Relevance of the Werthamer Theory

As shown in equation 2-3, under voltage bias conditions (source impedance = 0 and $V = \text{constant}$), the current through a tunnel junction is given by

$$I(V) = \text{Im } J_1 + \text{Re } J_2 \sin \phi + \text{Im } J_2 \cos \phi \quad (6-2)$$

where J_1 and J_2 can be written as either functions of voltage or frequency (because $f = 2eV/h$).

In the RSJ limit,

$$\begin{aligned} \text{Im } J_1(V) &= \sigma_0 V \\ \text{Im } J_2(V) &= 0 \end{aligned} \quad (6-3)$$

$$\text{Re } J_2(V) = I_J$$

$$\text{and we have} \quad I = I_J \sin \phi + V/R \quad (6-4)$$

where $\sigma_0 = 1/R_N$, and R_N is the normal state resistance given by $I_J R_N = \pi \Delta / (2e)$, where both I_J and Δ are evaluated at zero frequency and zero temperature.

As pointed out in Chapter 2, this model leaves out many important details concerning temperature and frequency. However, this is the model most often used in interpreting microwave experiments done using tunnel junctions.

The cosine ϕ term is usually written as

$$I(V) = I_J \sin \phi + \sigma_0 V + \sigma_1 V \cos \phi \quad (6-5a)$$

$$\text{or} \quad I(V) = I_J \sin \phi + \sigma_0 V(1 + \gamma \cos \phi) \quad (6-5b)$$

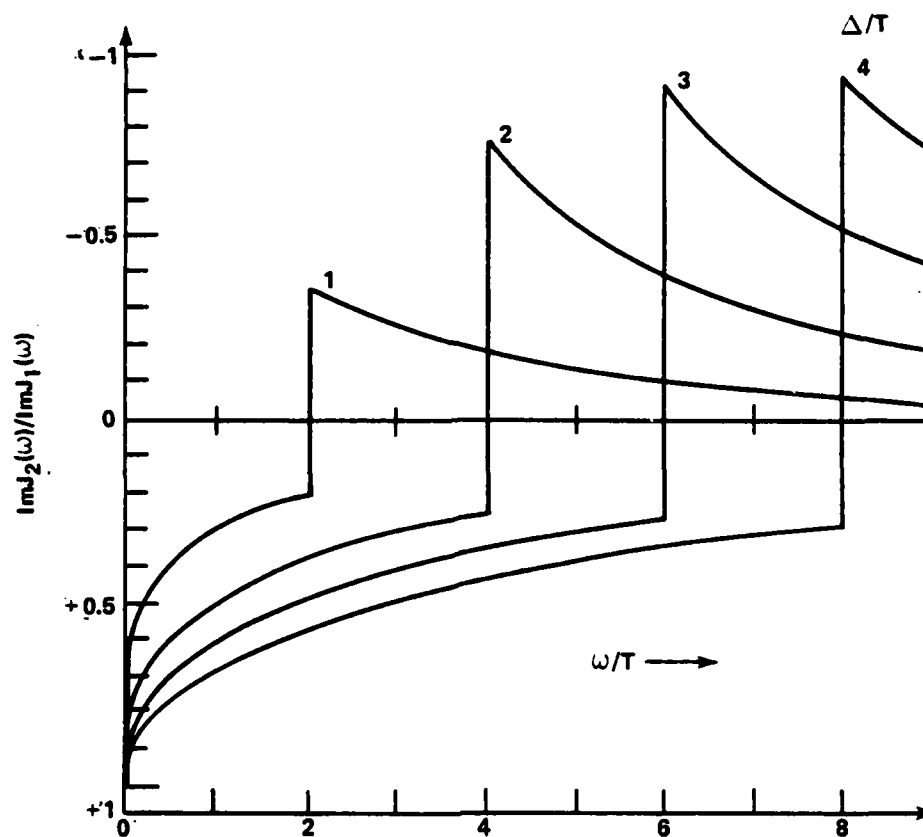
In the RSJ limit, γ is taken to be the limit as V , f , and T go to zero of the ratio

$$\gamma = \text{Im } J_2 / \text{Im } J_1 \quad (6-6)$$

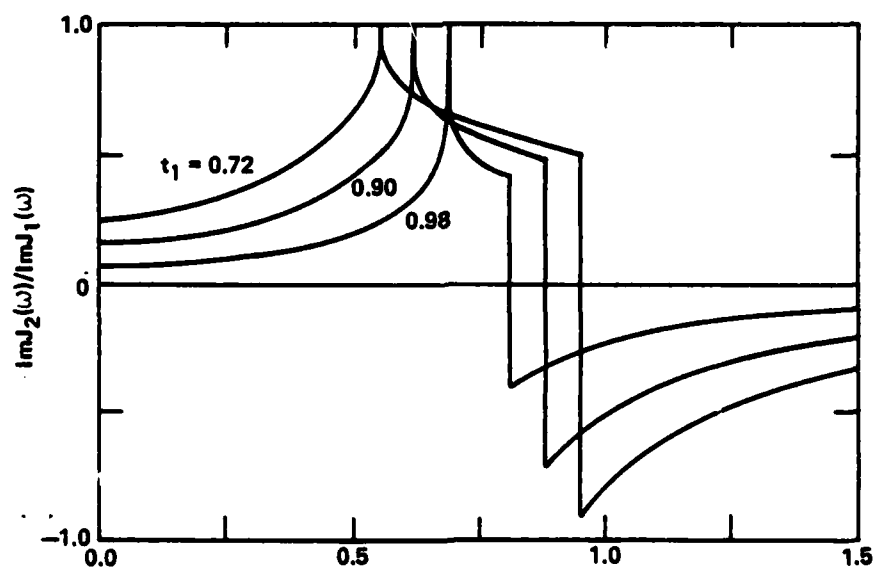
The quantity $\text{Im } J_2(f) / \text{Im } J_1(f)$ is shown in Figure 6-1a for a tunnel junction comprised of identical superconductors, and in Figure 6-1b for a junction made of different superconductors. (The apparent sign difference is a result of different sign conventions used in calculating each figure. Figure 6-1a has been annotated so as to agree with Figure 6-1b, and with the sign conventions used throughout this thesis). Several points should be noted:

1. At the frequency (or voltage) corresponding to $\Delta_1 - \Delta_2$, there is noticeable structure in the curves. When $\Delta_1 = \Delta_2$, this happens at $f = V = 0$.
2. Although related to the logarithmic singularity in the density of states at the edge of the energy gap, this structure is finite.
3. When $\Delta_1 = \Delta_2$, the $V = f = 0$ limit yields a value of $\gamma = +1$, independent of temperature.
4. γ is both temperature and frequency dependent.
5. For frequencies and voltages below the gap (i.e., $V < 2\Delta(T)/e$ and $f < 2\Delta(T)/h$), γ is always positive.

Item number 5 above is at the crux of the problem. Experiments done at a variety of temperatures at frequencies of the order 10 GHz consistently indicate that γ is negative.^{9,41,43,44} This has been the



6-1a γ FOR A JUNCTION COMPRISED
OF IDENTICAL SUPERCONDUCTORS
(AFTER SCHLUP)¹⁸



6-1b γ FOR A JUNCTION COMPRISED
OF DIFFERENT SUPERCONDUCTORS
(AFTER HARRIS)⁸

FIGURE 6-1 THEORETICAL CALCULATIONS OF $\text{Im}J_2(\omega)/\text{Im}J_1(\omega)$

case for both lead and tin junctions of varying sizes measured using a variety of techniques. These experiments are reviewed below.

6.3 Experimental Background

The major experimental efforts to measure gamma for a tunnel junction involve measuring the microwave response of a junction in the small signal limit at frequencies well below the gap frequency $2\Delta/h$. The junction is DC current biased within the zeroth order step, with an RF signal applied such that the phase ϕ makes small excursions about the equilibrium phase ϕ_0 . In this case, the $\cos \phi$ amplitude gamma contributes in a simple way to the RF impedance of the junction. As cosine ϕ can be varied by changing the DC current bias, it is possible to systematically vary the effect of gamma and hence separate its effect on junction performance from that of other parameters.

Since tunnel junctions have an intrinsic shunt capacitance, it is extremely useful to exploit the plasma resonance, whose frequency depends on both C and cosine ϕ as

$$\omega_p^2 = (2eI_J \cos \phi_0) / \hbar C \quad (6-7)$$

The first experiment, done by Pedersen, Finnegan, and Langenberg, involved measuring the Q of the plasma resonance at several values of cosine ϕ (and hence f_p).⁹ The Q of the resonance is simply $Q = 2\pi f_p CR$, where R is given by

$$\frac{1}{R} = \sigma_0 (1 + \gamma \cos \phi_0) = (1 + \gamma \cos \phi_0) / R_N \quad (6-8)$$

The slope of a plot of f_p/Q versus cosine ϕ for several values of cosine ϕ should yield a value for gamma from the formula

$$f_p/Q = (1 + \gamma \cos \phi_0) / (2\pi R_N C) \quad (6-9)$$

Pedersen, et al. measured gamma from plots of the type shown in Figure 6-2. The resistance R_N was derived from a measurement of I_J via the $I_J R_N$ product (with no corrections made for nonzero temperature), and the capacitance was calculated from a measurement of f_p for a particular value of I_J and cosine phi. The value of $\gamma = -.8$ was then inferred from Figure 6-2. The peak in the curve was attributed to a geometrical resonance within the junction. The experimental details will be discussed at length in the next section, but it should be pointed out that the junctions were large compared to the Josephson penetration depth λ_J , and one would expect geometrical and self-field limiting effects to be important. (For the junctions used in the experiment, $.5 < L/\lambda_J < 4$, where L is the length of the junction; the junction width was approximately $1/2 L$.) In a junction with dimensions comparable to or larger than the penetration depth, the critical current will be smaller than that predicted by the $I_J R_N$ product. In addition, cosine phi will not be constant over the area of the junction, and at the edge of the junction the $I-\phi$ relationship will begin to deviate from its ideal sinusoidal behavior. As the junctions used in the experiment were made of lead, strong-coupling effects may also be relevant. Finally, as the measurement frequency was varied between 8 and 12 GHz, it is necessary to include the frequency dependence of the junction quasiparticle resistance, which the authors failed to do.

The next experiment was done by Pedersen, Mygind, and Soerensen using tin junctions.⁴³ The plasma oscillations at 9 GHz were observed

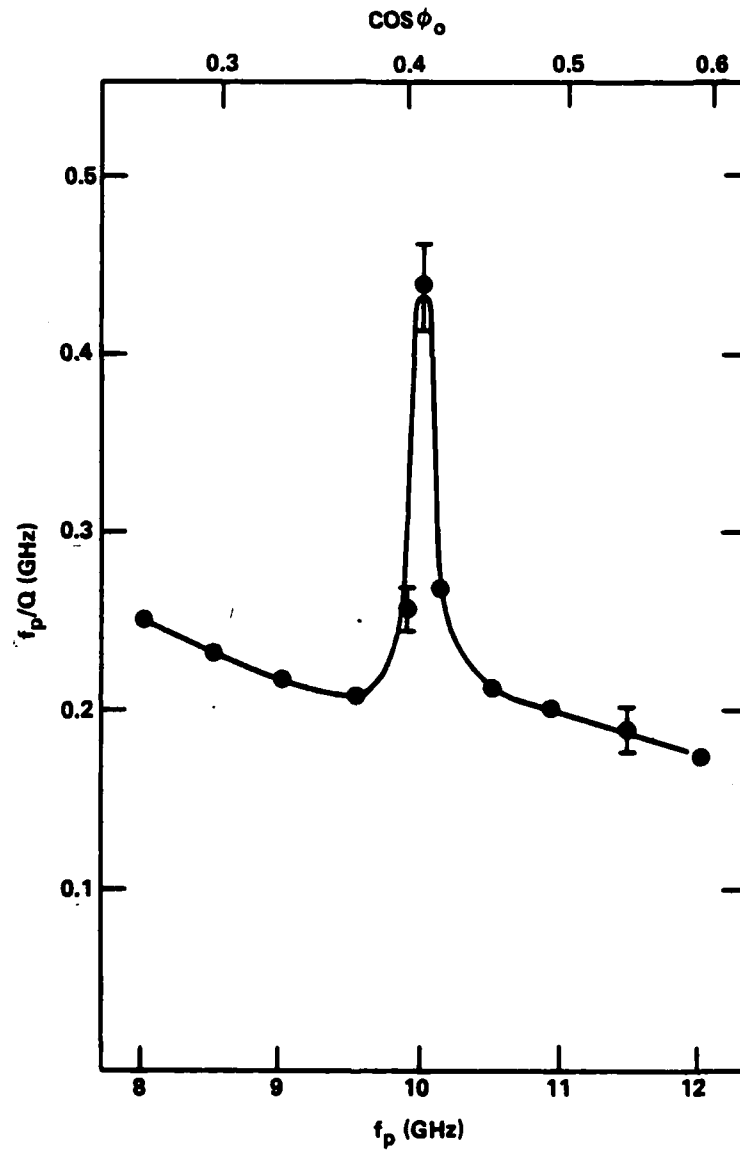


FIGURE 6-2 PLOT OF f_p/Q VS f_p FOR A TUNNEL JUNCTION
(AFTER PEDERSEN, FINNEGAN, AND LANGENBERG)⁹

over a small range of temperatures near $T = T_c$. Measurements included:

1. Exciting the junctions at 4.5 GHz and measuring their response at 9.0 GHz.
2. Observing the mixing between signals at 9 and 18 GHz.
3. Measuring the threshold conditions for half-harmonic oscillations at an applied frequency of 18 GHz.

This last measurement was complicated by the onset of "noise rise" due to complicated instability effects associated with the Josephson sine phi term.⁴⁹ However, using results from the first two measurements, Pedersen, et al. were able to infer a temperature dependent value for gamma. This is shown in Figure 6-3a. The figure indicates that gamma is positive near $T = T_c$, changes sign near $T = .96T_c$, and approaches -1 as T is decreased further. At 4.2K, this is in qualitative agreement with the work by Pedersen, Finnegan, and Langenberg for lead junctions.⁹ Figure 6-3b shows the corresponding RF resistance of the junction.

The results in Figures 6-3a and 6-3b were arrived at via a complex series of curve fits of measured junction response (e.g., mixing efficiency, RF impedance, etc.) to equations such as 6-5, 6-6, and 6-8. Although high frequency modifications to the RSJ model were not considered directly, the junction parameters R and C, as well as gamma, were treated as variables in the fitting process. This indirectly allowed any difference between the high and low frequency values of R and gamma to be taken into consideration. However, the many degrees of freedom when fitting the curves allowed for excellent fits to the observed data for more than one set of values of gamma, R, and C, as shown in Figure 6-3c. The choice of solutions was determined by a

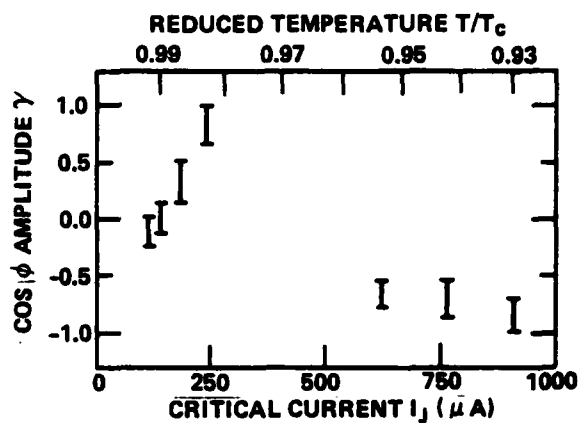


FIGURE 6-3a

"Measured $\cos \phi$ amplitude vs junction critical current and normalized temperature." (after Pedersen, et al.)⁴³

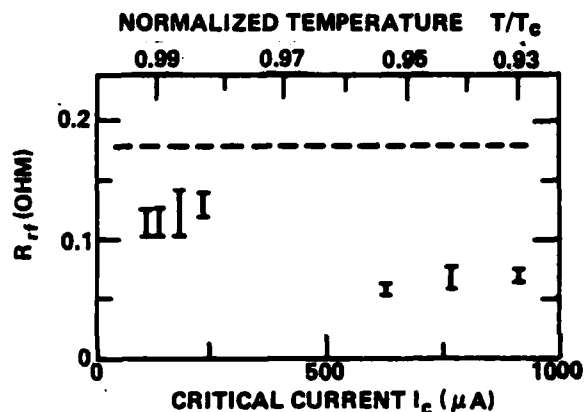


FIGURE 6-3b

"Measured rf resistance R_{rf} as a function of junction critical current and normalized temperature. The dashed line is the normal-state dc resistance $R = 0.18 \Omega$." (after Pedersen, et al.)⁴³

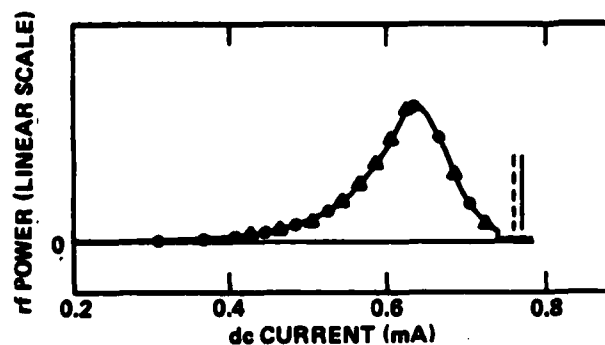


FIGURE 6-3c

"Lower sideband mixing component as a function of the dc-bias current. The vertical lines show the critical currents with no applied microwave signal and with the two signals applied simultaneously (full and dashed lines, respectively). $f_2 = 17.268$ GHz, $f_1 = 8.669$ GHz, and $T/T_c = 0.942$. The circles are calculated with $\omega_0/2\pi = 13.104$ GHz, $Q_0 = 1.832$, and $\epsilon = -0.8$. The triangles: $\omega_0/2\pi = 12.091$ GHz, $Q_0 = 3.496$, and $\epsilon = 0$." (after Pedersen, et al.)⁴³

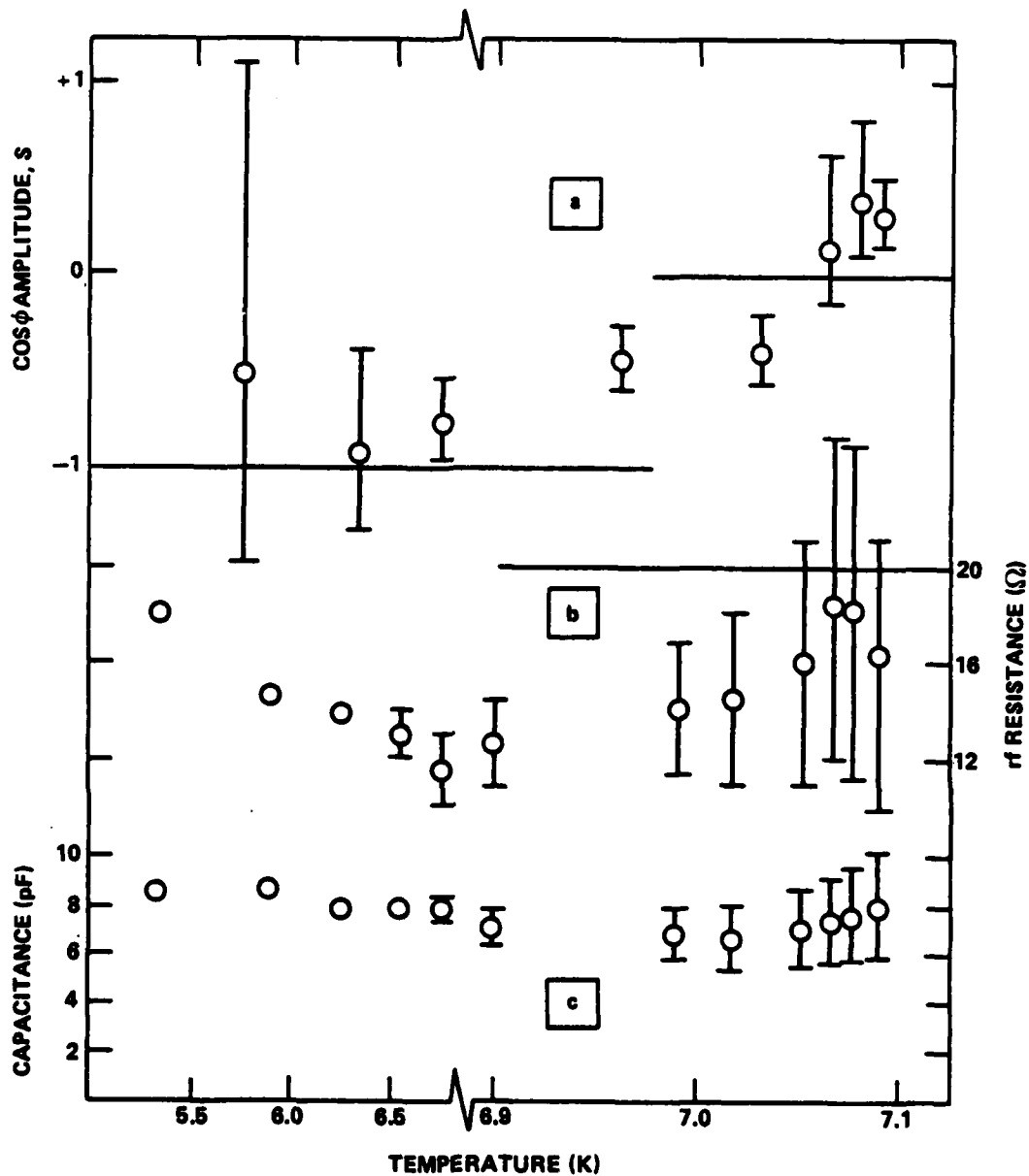
FIGURE 6-3 MEASURED $\cos \phi$ AMPLITUDE AS A FUNCTION OF TEMPERATURE FOR A TIN TUNNEL JUNCTION (AFTER PEDERSEN, ET. AL.)⁴³

complicated process of reconciling the calculations with the theoretical temperature dependences of the plasma frequency and critical current. (Although the junction capacitance was a variable in the curve fitting program, it was assumed to be independent of temperature.) The RF resistance shown in Figure 6-3b is in disagreement with the prediction that the RF resistance should be greater than the DC normal state resistance and should increase with decreasing temperature (cf. Sections 2.6 and 6.4). In addition, there seems room for skepticism for an experimental analysis that contains so many degrees of freedom. An independent measurement of the junction capacitance would be an obvious first improvement to the experiment. It should be noted that Pedersen has a good deal of faith in the results of this particular experiment, whereas he agrees that there are problems with the interpretation of the results in the Pedersen, Finnegan, and Langenberg paper. *

The last important experiments were done by Rudner and Claeson, who measured the response of small lead junctions (18 micron by 18 micron) over a wide range of temperature.⁴⁴ Their primary measurement was the microwave reflection from a single junction connected to a microwave stripline. The frequency (approximately 10 GHz) was fixed while the temperature and magnetic field were varied. (The temperature was changed between 4.2K and 7.2K.)

As in the previous experiments, γ , R, and C were used as parameters in a sophisticated curve fitting routine. The results are presented in Figure 6-4. It should be noted that Figure 6-4 supersedes the authors' original interpretation of their microwave data.

*N. F. Pedersen, private communication



"(a) $\cos\phi$ amplitude, (b) rf resistance, and (c) capacitance, all measured at zero bias, are given as functions of temperature for a junction with normal state resistance 20Ω . Note the change in temperature scale."

FIGURE 6-4 MEASURED $\cos\phi$ AMPLITUDE AS A FUNCTION OF TEMPERATURE FOR A LEAD TUNNEL JUNCTION (AFTER RUDNER AND CLAESON)⁴⁴

As in the Pedersen, Mygind, and Soerensen experiment, there seems good reason to be skeptical of an experimental technique that relies on the accurate fit of so many variables to a theory that is at best an approximation. For one thing, the curve fit depends on an extremely accurate assessment of the VSWR and insertion loss of the microwave circuitry external to the cryostat. In addition, there might be unrecognized problems associated with the use of an external magnetic field as the independent parameter (e.g., problems with screening and trapped flux).

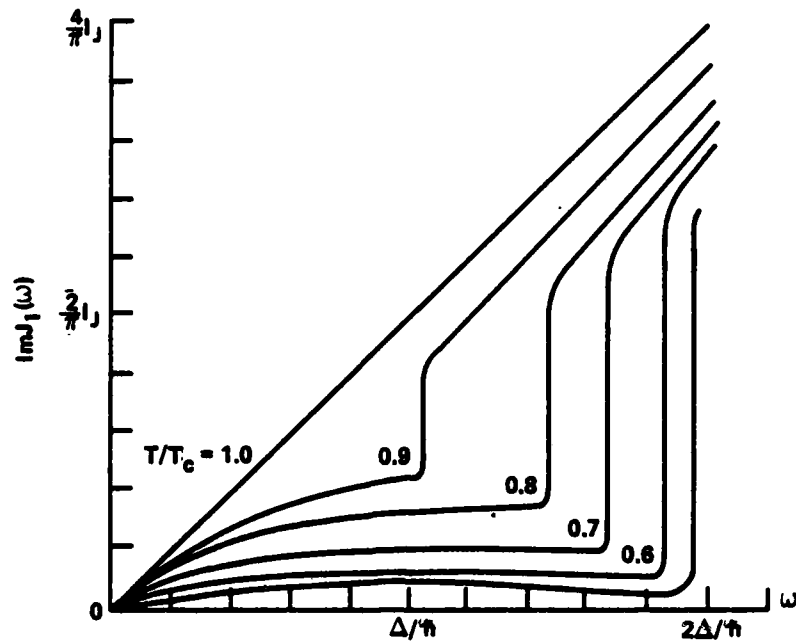
The plot of capacitance versus temperature in Figure 6-4 seems reasonable, as C is expected to be independent of T . However, one would expect the RF resistance to increase dramatically as T is reduced (cf. Figure 6-5, equation 6-12). This is not the case, and the peculiar fluctuation of R_N with T in Figure 6-4 suggests that there are some problems with the experiment.

However, the results of Rudner and Claeson are qualitatively consistent with those of Pedersen, Mygind, and Soerensen and Pedersen, Finnegan, and Langenberg. Given that the experiments were done by measuring different quantities on different sized junctions made of both lead and tin, there seems little doubt that there is a genuine discrepancy between the actual and theoretical values of the cosine ϕ amplitude.

6.4 High Frequency Corrections to the Plasma Resonance Experiment

At this stage it is worth investigating the Pedersen, Finnegan, and Langenberg experiment in detail. Unlike the other two experiments, the microwave frequencies at which the junction response was measured varied over a wide range. However, the frequency dependences of the

6-5(a)



6-5(b)

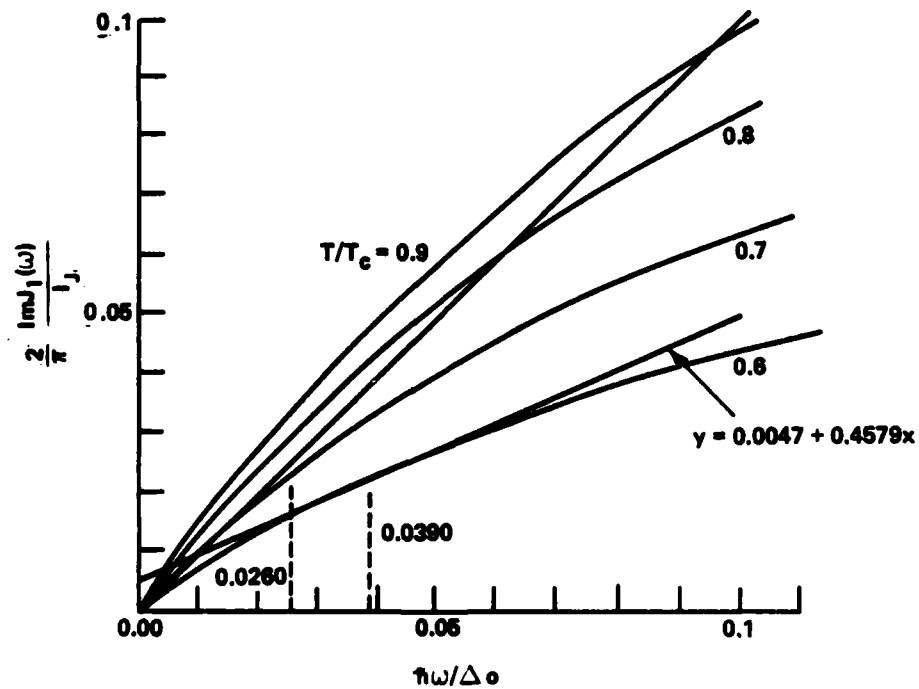


FIGURE 6-5 $\text{Im}J_1(\omega)$ AS A FUNCTION OF FREQUENCY AND TEMPERATURE (AFTER YOUNG)⁵²

quasiparticle resistance and the cosine phi term were not taken into account. This can be done using the Werthamer theory, and is shown below. As the Pedersen experiment was done using lead tunnel junctions at liquid helium temperatures, the following discussion has been specifically directed to lead junctions at 4.2K.

The Pedersen experiment was done at frequencies between 8 and 12 GHz. Normalized to the measured gap frequency $2\Delta/h$ of 616 GHz for lead, we have a reduced frequency that varies between .0260 and .0390 on the graph of $\text{Im } J_1$ versus frequency in Figure 6-5 (after M. Young⁵²). The transition temperature of lead is given by Rickayzen as 7.2K, which yields a reduced temperature of .58.⁴⁸ The line for T/T_c in Figure 6-5 for $T = .6$ was digitized for the interval $.026 < f < .039$ to yield $y = .0047 + .4579x$. Scaled to the gap parameter and critical current, this gives an expression for $\text{Im } J_1(f)$ of:

$$\text{Im } J_1(f) = \frac{2}{\pi} I_J(0) \{ .0047 + .4579hf/\Delta \} \quad (6-10)$$

(If the graph had slope = 1 and y intercept = 0, as in the RSJ limit, then we would have $\text{Im } J_1(f) = (2/\pi) I_J(0) (hf/\Delta)$. At $f = 2\Delta/h$, $\text{Im } J_1(f) = (4/\pi) I_J(0)$, which is consistent with an $I_J R_N$ product of $\frac{\pi\Delta(0)}{2e}$.)

For the plasma resonance experiment,

$$f_p/Q = 1/(2\pi RC) , \text{ where } 1/R = (1/R_f) (1 + \gamma \cos \phi_0) \quad (6-11)$$

where R_f is the quasiparticle resistance at a particular frequency.

It is important to remember that the ratio gamma, as well as σ_0 , depends on frequency. In the argument that follows, gamma will be treated as a constant, and we will be concerned with the frequency dependence

of σ_0 . The frequency dependence of gamma will then be added in a qualitative manner. Werthamer and Harris give a derivation of the high frequency quasiparticle resistance which leads to the following expression^{5,15} (cf. section 2.2):

$$\frac{1}{R_N} = \frac{e}{hf} \operatorname{Im} J_1(f) \quad (6-12)$$

So,

$$\frac{f_p}{Q} = \frac{1}{2\pi C} \times \frac{e}{hf} \times \frac{2}{\pi} I_J(0) (.0047 + .4579 \frac{hf}{\Delta}) (1 + \gamma \cos \phi_0) \quad (6-12)$$

where $I_J(0)$ is related to R_N by $I_J(0) = \pi\Delta/(2eR_N)$.

Thus:

$$\frac{f_p}{Q} = \frac{1}{2\pi R_N C} \left[\frac{.0047\Delta(0)}{hf} + .4579 \right] (1 + \gamma \cos \phi_0) \quad (6-15)$$

NOTE THAT FOR $\gamma = 0$, f_p/Q WILL DECREASE WITH FREQUENCY.

Cosine phi can be written as

$$\cos \phi = \frac{\pi h C f_p^2}{e I_J(T)} \quad (6-16)$$

Note that I_J is the measured value of I_J at a particular temperature. This will be different from $I_J(0)$. (As Young's calculations were scaled with respect to $\Delta(0)$, R_N , and $I_J(0)$, it is correct to use $\pi\Delta(0)/(2eR_N) = I_J(0)$ for calculating $\operatorname{Im} J_1(f)$ at T not equal to zero.) For the time being, let $I_J(T = .6T_C) = I_J(0)$. Any inaccuracy this causes can be subsequently corrected by modifying gamma slightly, as $\gamma \cos \phi = \gamma \pi h C f_p^2 / e I_J$.

We now have

$$\frac{f_p}{Q} = \frac{1}{2\pi R_N C} \left\{ \frac{.0047\Delta(0)}{hf_p} + .4579 \right\} \left(1 + \frac{\gamma \pi h C}{e I_J} f_p^2 \right) \quad (6-17)$$

Pedersen, et al. give $R_N = .46$ ohm, and $C = 1.5nFd$ (8). $\Delta(0)/h$ is 308 GHz. Rewriting $\pi h C / e I_J$ as $(2R_N C) / [\Delta(0)/h]$ we have

$$\frac{f_p}{Q} = .2307 \left[\frac{1.49}{f_p} + .46 \right] [1 + \gamma \times 4.48 \times 10^{-3} f_p^2] \quad (6-18)$$

where f_p is in Gigahertz. This is plotted against Pedersen's results for several values of gamma in Figure 6-6. (Pedersen's graph is not very accurate, as evidenced by the disagreement between his line for $1/(2\pi R_N C)$ and a replotted $1/(2\pi R_N C) = .2307$. Presumably, the inaccuracy is a result of artistic license when the graph was prepared for publication.)

Figure 6-6 is based on the assumption that gamma is constant. With reference to Figure 6-1, it can be seen that gamma decreases with increasing frequency. In terms of f_p/Q versus f_p , this means that one should draw a "load line" on Figure 6-6 reflecting this decrease. This will have the effect of shifting the line for f_p/Q versus f_p downwards with increasing f_p for positive values of gamma, and upwards with increasing f_p for negative values of gamma.

Figures 6-7 and 6-8 show f_p/Q versus f_p repeated for $T = .6T_c$ and for $T = .7T_c$ (also based on Young's calculations). Note that the line for gamma = -1 is by no means the obvious choice for explaining the data of Pedersen, et al. It is also interesting that f_p/Q is so sensitive to the reduced temperature. (The frequency dependence of gamma has not been included in Figure 6-7 or 6-8.)

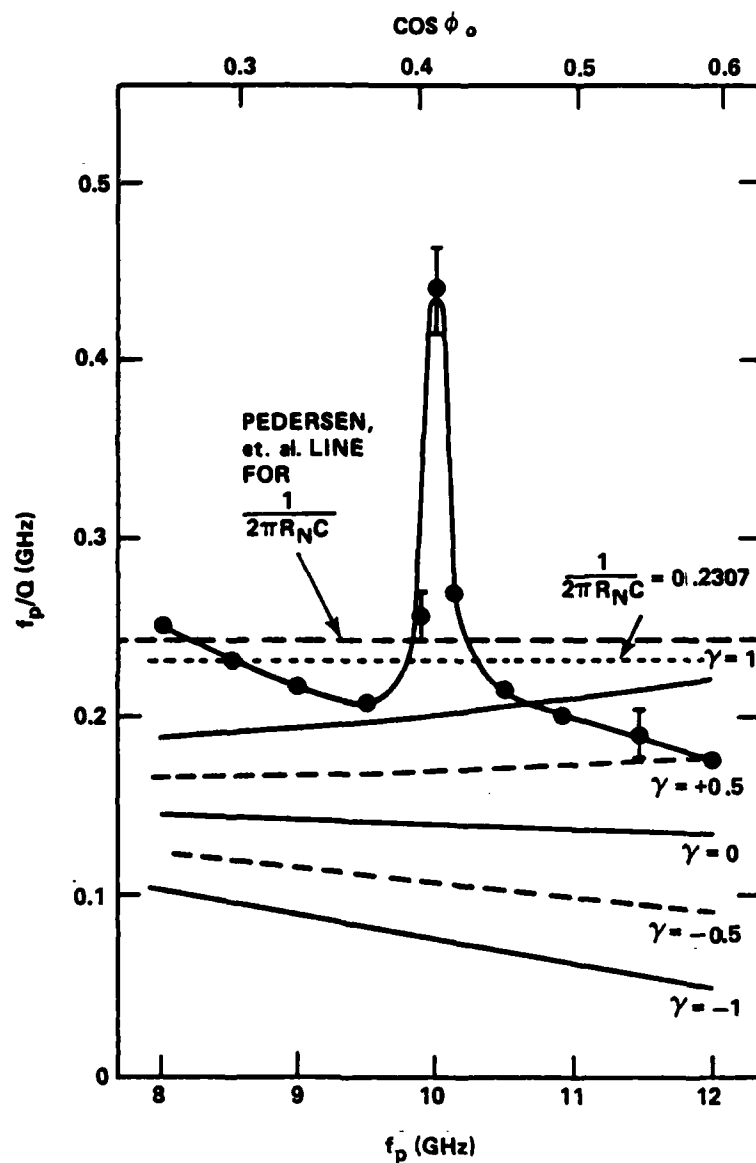


FIGURE 6-6 PLOT OF f_p/Q VS f_p FOR A TUNNEL JUNCTION, INCLUDING CALCULATIONS OF $f_p/Q = \beta(1 + \gamma \cos \phi)$ (AFTER PEDERSEN, FINNEGAN, AND LANGENBERG)⁹

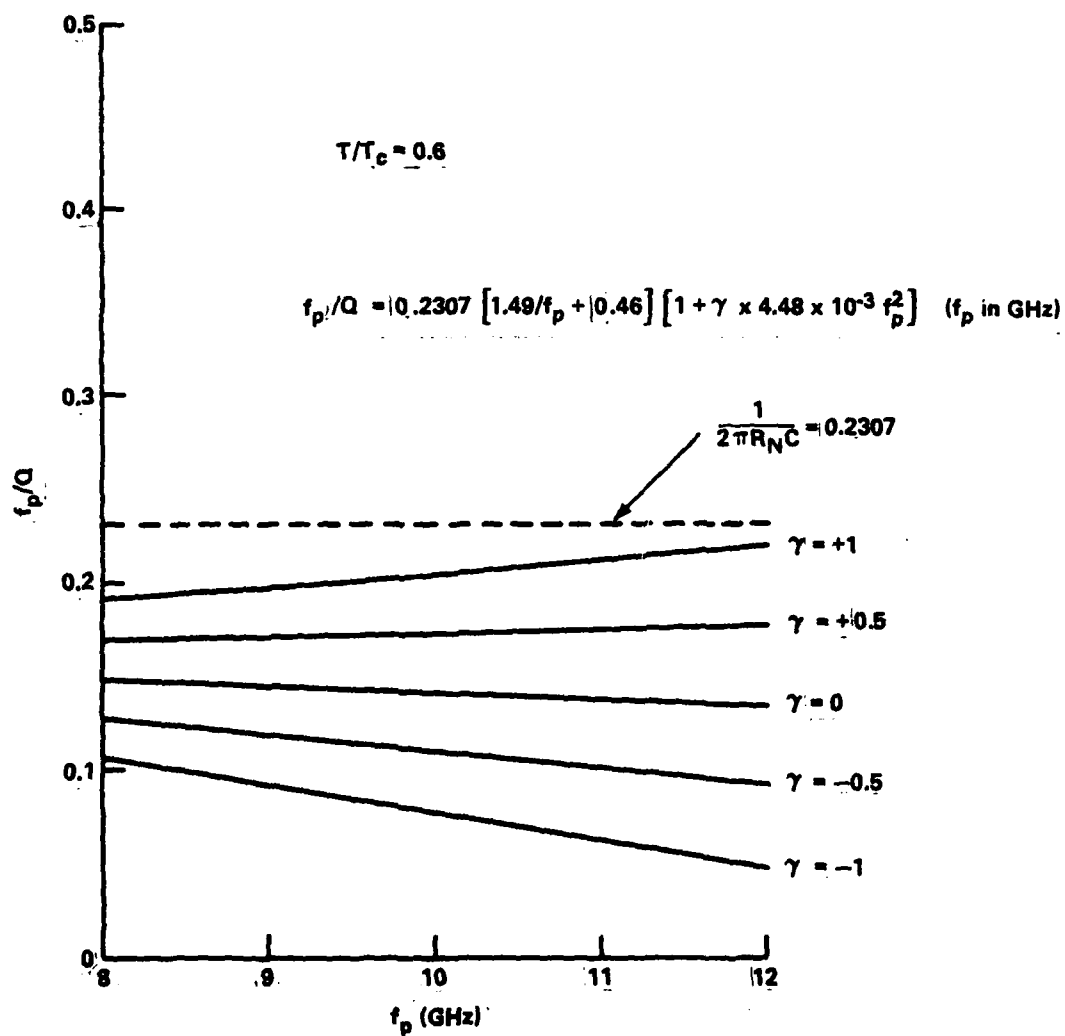
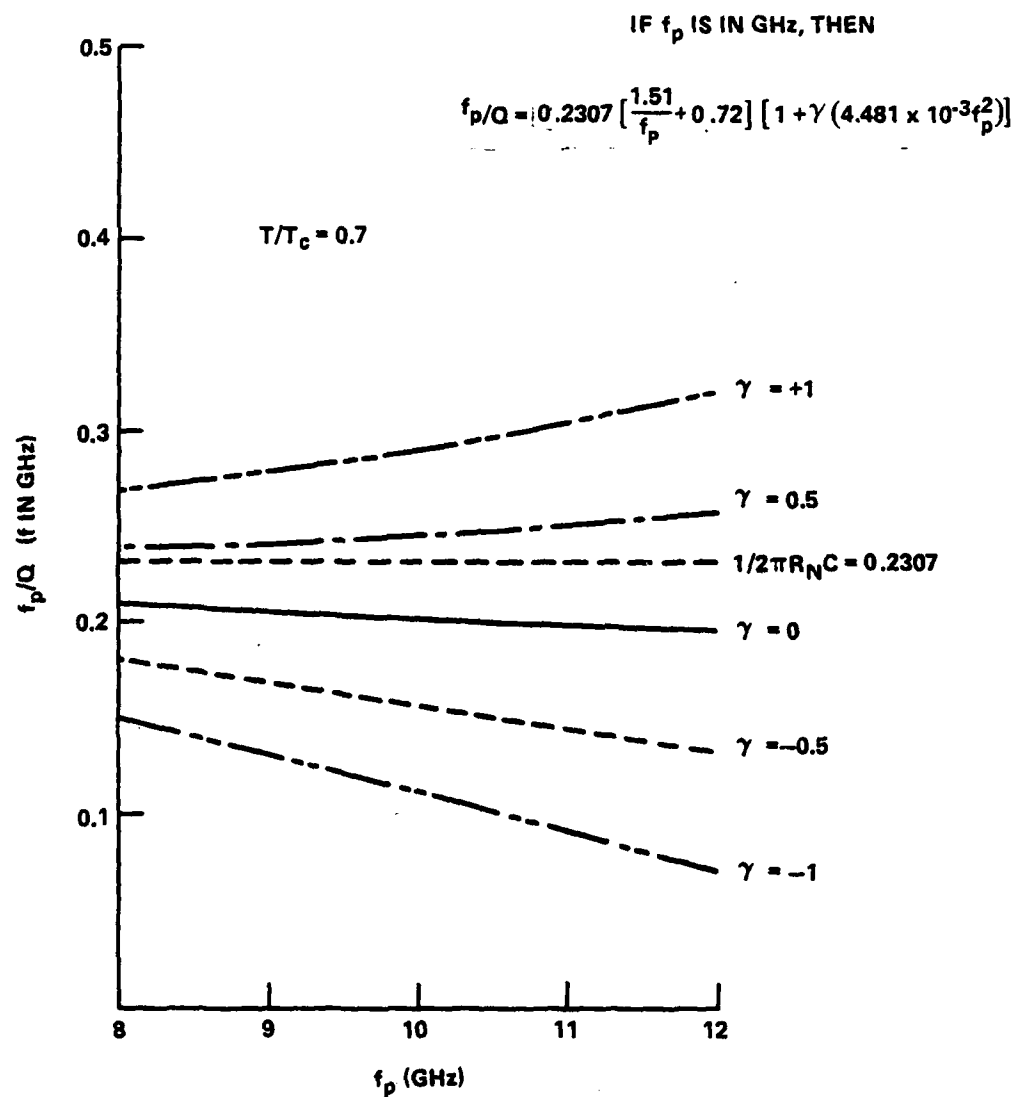


FIGURE 6-7 f_p/Q VS f_p FOR $T/T_c = 0.6$

FIGURE 6-8 f_p/Q VS f_p FOR $T/T_c = 0.7$

It is difficult to draw any definite conclusions from the above analysis without knowing more details for the experiment. However, the foregoing discussion suggests that the RSJ model is inadequate for analysis of the cosine phi problem. Several other points concerning the data merit discussion.

First, Pedersen, et al. computed R_N from the $I_J R_N$ product using the value for I_J measured at $T = 4.2K$. They did not take into account that

$$I_J(T) = \frac{\pi \Delta(T)}{2eR_N} \times \tanh \left[\frac{\Delta(T)}{2kT} \right] \quad (6-19)$$

If we assume that $\Delta(4.2K) = .9\Delta(0)$, and $2\Delta(0)/kT_c = 4.1$ (after Rickayzen⁴⁸), then

$$I_J(4.2k) = .82 I_J(0) \quad (6-20)$$

This change in I_J would cause a corresponding change in the calculated value of R_N such that $R_N = .38 \text{ ohm}$ instead of $.46 \text{ ohm}$. This would have the effect of shifting $1/(2\pi R_N C)$ upwards in Figure 6-6.

On the other hand, lead is a strong-coupling superconductor, and a lead junction is expected to have a critical current that is approximately 15% lower than that predicted by BCS (see Ginsberg and Harris⁴⁰). This would mean using a value of $I_J(0)$ that is 15% lower than the BCS value when computing the $I_J R_N$ product. In other words, the temperature correction of I_J is offset by the strong-coupling correction, and the value of $.46 \text{ ohm}$ for R_N is probably reasonable. (According to Pedersen, neither of these corrections was taken into account.*)

Second, the normal-state resistance was not measured independently during the course of the experiment. Nor were the DC I-V characteristics

*N. F. Pedersen, private communication

recorded. The quality of the junctions was ascertained by comparing the height of the zero voltage supercurrent with the height of the current "knee" at $V = 2\Delta/e$. (This agreed with theory, including the strong-coupling correction for lead.)

Third, there is an inconsistency between two sets of measurements reported in the Pedersen paper. The authors present a plot of the inverse Q of the plasma resonance versus the critical current at fixed frequency. The data was obtained from several junctions having different values of I_J . The RSJ theory predicts that the inverse Q should vary with critical current as

$$\frac{1}{Q} = (1 + \gamma \cos \phi_0) / (2\pi f_p R_f C) \quad (6-21)$$

where R_f is the resistance of the junction at the plasma frequency and is given by

$$R_f = hf / [e \text{Im} J_1(f)] \text{ evaluated at } f = f_p \quad (6-22)$$

Substituting

$$\cos \phi = \hbar C \omega_p^2 / [2e I_J(T)] \text{ and } R_N = \frac{\pi \Delta(0)}{2e I_J(0)}$$

we have

$$\frac{1}{Q} = [2e I_J(0) / (2\pi^2 f_p C \Delta(0))] \frac{R_N}{R_f} \left[1 + \frac{\gamma \hbar C f_p^2}{2e I_J(T)} \right] \quad (6-23)$$

Note that as I_J approaches zero, $1/Q$ approaches

$$\frac{1}{Q} = \gamma \frac{R_N}{R_f} [2\pi \hbar f_p I_J(0)] / [\pi \Delta(0) I_J(T)] \quad (6-24)$$

The published graph (cf. Figure 6-9) suggests that at $I_J = 0$, $1/Q$ is approximately .001. If we assume that $I_J(T) = I_J(0)$ and $R_f = R_N$, then $1/Q$ should approach

$$\frac{1}{Q} = \frac{\gamma h f_p}{\pi \Delta(0)} \quad (6-25)$$

For lead, $\Delta(0)/h = 308$ GHz. In the experiment, $f_p = 9$ GHz. If $1/Q = .001$ when I_J is zero, then Figure 6-9 suggests that $\gamma = .11$.

On the other hand, if γ is -1 , then $1/Q$ for $I_J = 0$ should be approximately $-.01$. Figure 6-9 suggests that this is clearly not the case.

Finally, the lead tunnel junctions used in the experiment were quite large with respect to the Josephson penetration depth:

$$.5\lambda_J < L < 4\lambda_J$$

This suggests that geometrical and self-field effects could have a major effect on the experiment (cf. section 6.3). This is supported by the observation of the resonant peak observed in f_p/Q versus f_p measurements.

6.5 Theoretical Work

In the previous sections we have discussed the various cosine ϕ measurements. They have obvious shortcomings, but the conclusion that γ is negative when theory predicts it to be positive is difficult to refute. In an effort to provide a theoretical basis for the experimental observations Kulik, Schrieffer, Likharev, et al. have reanalyzed the Werthamer theory in terms of the derivations of the response functions $J_1(\omega)$ and $J_2(\omega)$ ⁴¹. As $\text{Im } J_2(\omega)$ is related to $\text{Re } J_2(\omega)$ via the Kramers-Kronig relations, Kulik, et al. surmise that a broadening of the Riedel peak in $\text{Re } J_2(\omega)$ can lead to regions where $\text{Im } J_2(\omega)$, and

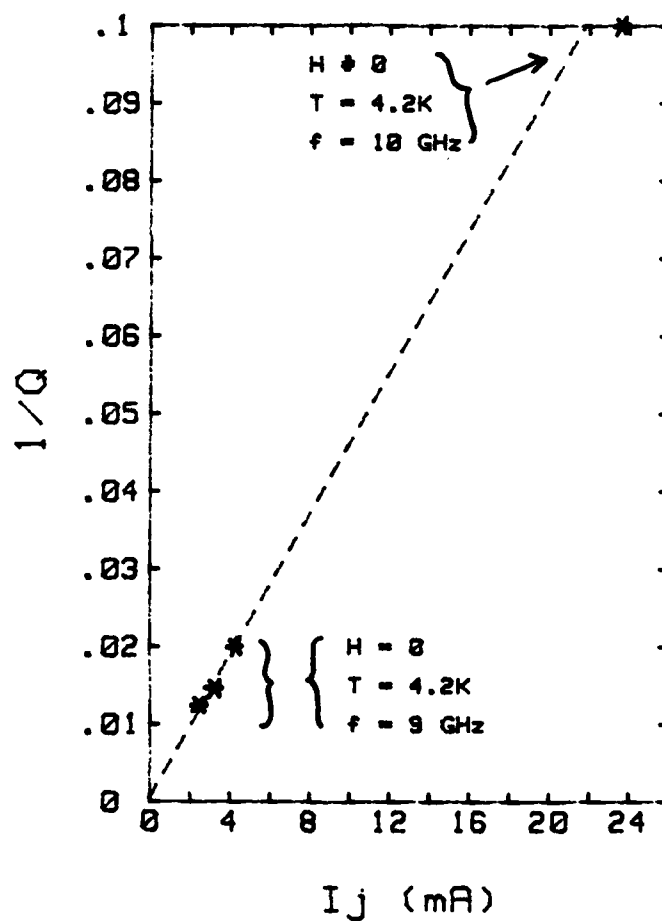


FIGURE 6-9. $1/Q$ VS I_j FOR A TUNNEL JUNCTION (AFTER PEDERSEN, ET AL, REF 9)

consequently γ , are negative below the gap frequency. Of the various causes of smearing of the Riedel peak, they conclude that inhomogeneity of the materials comprising the junction electrodes leads to the cosine ϕ behavior most consistent with experimental results.

Pedersen and Rudner do not believe that the Kulik explanation fits the cosine ϕ behavior they have observed in their different experiments.* Kulik, et al. conclude that smearing of the Riedel peak will cause γ to be positive at high temperatures, but negative as T approaches zero. However, the temperature at which γ switches sign is near $T = T_c$ in the experiments. The Kulik theory apparently cannot explain the occurrence of the sign change at a temperature so close to T_c .

Another explanation as to why γ might be negative is the popular relaxation effect which arises from time-dependent Ginzburg-Landau theory in connection with microbridges.^{45,46} This theory seems to have no basis for a tunnel junction (cf. Chapter 5).

6.6 Suggestions for Future Work

The final conclusion of this chapter is that there is still a major discrepancy between theory and experiment concerning the amplitude of the cosine ϕ term. Of the three experiments, the original Pedersen, Finnegan, and Langeberg experiment seems to be the most amenable to theoretical interpretation, as opposed to complex numerical analysis. However, the original experiment was done using large junctions made of a strong-coupling superconductor. Unfortunately, many of the quantities necessary for an accurate interpretation of the data were not measured (e.g., the DC I-V characteristics measured under current and voltage bias conditions), and the high frequency corrections to the RSJ model

*Private communications with N. F. Pedersen and S. Rudner

were not taken into account. Furthermore, to account properly for geometric and large junction effects could be extremely difficult.

It seems likely that if the Pedersen, Finnegan, and Langenberg experiment was repeated more carefully, over a wider range of frequencies, and with smaller junctions, it would yield much useful information. The use of lead, tin, and lead/tin combination junctions in the same geometry would allow one to identify any anomalous effects that might occur due to geometry or peculiarities of the material. Finally, the direct measurement of R_N and $\text{Im } J_1(V)$ from the I-V characteristics, as well as an independent assessment of the junction capacitance, should remove some of the doubts about existing experimental results. In conclusion, there seems to be a good case for repeating the original plasma resonance experiment.

CHAPTER 7

FILTER DESIGN

7.1 Introduction

The numerical technique that was used to design the filters for $T = 0$ failed consistently when attempts were made to design filters that model $J_1(\omega)$ and $J_2(\omega)$ for finite temperature. The numerical calculations yielded Pade approximates for J_1 and J_2 that were neither accurate nor causal. It is not difficult to show that the expressions for J_1 and J_2 are causal, so one can be confident that an accurate approximation to J_1 and J_2 will also be causal, or can be made to be causal with only slight modification. However, there was the distressing possibility that J_1 and J_2 for finite temperature could not be modelled accurately without an inordinate number of poles. This turned out not to be the case, and the synthesis problem was finally solved by using the existing numerical design technique with a new twist. The resulting Pade approximates for J_1 and J_2 at finite temperature are quite good, and have since been transformed into electronic filters. The improved version of the electronic analogue can model the Josephson effects at $T = 0$, $T = .72T_c$ and $T = .9T_c$.

In this chapter, we discuss the design and evaluation of the new filters. However, before describing the actual methods involved, there is a brief section on some of the basic properties of the functions $J_1(\omega)$ and $J_2(\omega)$.

It should be remembered that although the design of these filters is engineering, and not physics, this subject is crucial to the development of the analogue. The synthesis techniques described herein are, to the best of the author's knowledge, completely new and are not

based on standard electrical engineering techniques. The idea for this method was not suggested to the author by anyone, although in retrospect it seems like an obvious route to pursue.

7.2 Discussion of J_1 and J_2

The Werthamer paper presents a derivation of the functions J_1 and J_2 in terms of the BCS theory and the assumptions about tunnelling presented in Chapters 2 and 5. However, Werthamer and subsequent authors say little about two properties of these functions that are central to the design of the electronic analogue.^{5,8,18,19} First, it has tacitly been assumed that as functions of time, $j_1(t)$ and $j_2(t)$ are causal. Second, it has been assumed that the functions are real.

If the functions $j_1(t)$ and $j_2(t)$ were not causal, it would be impossible to build filters which could be connected in such a way as to model the current through the junction. However, as the values for $j_1(t)$ and $j_2(t)$ for $t < 0$ have no effect on the current through a tunnel junction (cf. eq. 7-1), these functions can always be modified so as to be causal. Fortunately, the expressions for $J_1(\omega)$ and $J_2(\omega)$ as derived by Werthamer and others already satisfy the Kramers-Kronig relations, and need no modification.

$$I(t) = \left\{ e^{-i\frac{\phi}{2}t} \int_{-\infty}^{i\frac{\phi}{2}} j_1(t-t') dt' + e^{+i\frac{\phi}{2}t} \int_{-\infty}^{i\frac{\phi}{2}} j_2(t-t') dt' \right\} \quad (7-1)$$

If the functions were causal, but not real, it would still be possible to build the analogue. Substitution of a complex function for $j_1(t)$ or $j_2(t)$ would complicate matters, but one could still model Equation 7-1 electronically. This would require construction of

separate filters for the real and imaginary parts of each function, which would then be connected to the proper combination of $\sin \phi$ and $\cos \phi$ signals.

As it turns out, $j_1(t)$ and $j_2(t)$ can be regarded as being real. In the case of tunnel junction comprised of identical superconductors, this can be demonstrated for $j_2(t)$ using the condition that the junction must be insensitive to the polarity of the bias voltage, and the current must, therefore, be an odd function of voltage. In the voltage bias limit, we have

$$f = 2eV/h \quad (7-2a)$$

and

$$I(V) = \text{Im}J_1(V) + \text{Re}J_2(V)\sin\phi + \text{Im}J_2(V)\cos\phi \quad (7-2b)$$

By inspection, we see that $\text{Re} J_2(V)$ must be an even function of voltage, as ϕ changes sign when V does, and $\sin\phi$ is, therefore, odd. Likewise, $\text{Im} J_2(V)$ must be odd, because $\cos\phi$ is even. The inverse Fourier transform of a function whose imaginary part is odd and real part is even is a real function of time.

Although $\text{Re} J_1(V)$ does not show up explicitly in equation 7-2b, one is tempted to believe that a similar macroscopic argument also holds for $j_1(t)$.

In the microscopic limit, the derivation of $j_1(t)$ and $j_2(t)$ involves the sum over states of both hole and electron like excitations. Completely unrelated to the argument concerning bias polarity, one can show that the existence of symmetry between these hole and electron states will result in $j_1(t)$ and $j_2(t)$ being real in the general case, regardless of whether the junction is comprised of identical super-

conductors.* This hole-electron symmetry allows a one-for-one pairing between hole states at a particular energy below the Fermi energy, and electron states at the corresponding energy above the Fermi energy. This correspondence results in the sum over states, and hence, $j_1(t)$ and $j_2(t)$, being real.

Strictly speaking, the hole-electron symmetry is not exact. However, because the Fermi energy of a superconductor is so large compared to the range of energies that contributes to the summation described above, it is a very good approximation (e.g., good to one part in ten thousand), and it is sufficient to say that hole-electron symmetry, as well as the parity requirements placed on the bias voltage, make it valid to treat $j_1(t)$ and $j_2(t)$ as real functions of time.

7.3 The Design Problem

The previous failure of the Pade approximate technique was a result of two things. First, the choice of data points was not always consistent with the frequency resolution attainable by a Pade approximate having a given number of poles. Second, accuracy limitations of the data used for the calculations were not taken into account.

The first problem is related to the fact that there are no analytic pole/zero expansions for J_1 and J_2 , even for $T = 0$. In all likelihood, this means that it is impossible to model the functions exactly with a Pade approximate having a finite number of poles. The limitation that this places on the choice of data points can be understood from the following properties of Pade approximates.

*J. R. Waldram, personal communication

1. The number of poles in the Pade approximate is equal to the number of frequencies at which the approximate is set equal to the original function (e.g., the number of data points used in the calculation).
2. If the Pade approximate has less poles than the function being modelled, the approximate need not be causal.
3. If one uses a sufficient number of data points, it is possible for the Pade approximate to have more poles than the function being modelled. For example, if data at ten frequencies are used to calculate an approximation to a function having six poles, the Pade will contain four pairs of poles and zeros having the same location in the complex frequency plane. These extra poles and zeros need not lie in the left half of the complex frequency plane (i.e., the causal half-plane). The Pade approximate will remain causal, as the excess poles are cancelled by the zeros at the same locations, and have no effect on the Pade approximate.

If we are interested in modelling J_1 or J_2 with a Pade approximate having a finite number of poles, the data points must be chosen so as to represent a function having no more than this number of poles. Roughly speaking, this suggests that to model accurately a function over a bandwidth f using n data points, no details requiring frequency resolution better than f/n should be included in the calculation. In the case of J_1 and J_2 , this means that there is some limitation on the accuracy with which the gap singularity can be modelled simultaneously with the broad structure away from the gap for a given number of data points. If one tries to model too much of the curve with too few data points, the resulting Pade approximate will be neither accurate nor

causal, even though it will fit the original function at all of the data points. (Nevertheless, practical experience indicates that more data points should be taken from near the Riedel peak than from regions containing no fine structure.)

The second problem is more subtle. Assuming that the Pade approximate has more than enough poles to model the original function with the desired resolution, there will be extra pole/zero pairs lying in both the left and right half-planes. These will be in addition to the poles and zeros, which are not paired, which represent the original functions. If the real and imaginary parts of the input data are subject to small, uncorrelated error, the poles and zeros will move from their original positions. In the case of the unpaired poles and zeros, the shift in position will equate to random noise in the Pade approximate. However, all of the unpaired poles should remain in the left half-plane. At the same time, the paired poles and zeros will move slightly, such that they are still approximately paired, but no longer identical. This will also appear as random noise. However, as the right half-plane poles are no longer matched by zeros, the Pade approximate will become noncausal. From a slightly different point of view, the uncanceled poles in the right half-plane result from the essentially non causal error to the original data.

An increase in the number of data points used in the calculation will result in two benefits. First, the amount of detail that can be modelled will increase. Second, the effect of inaccurate data will decrease. Using simple statistical arguments, one would expect the accuracy of the overall fit to improve as the square root of the number of data points.

The new filter design technique is based on using 15 judiciously chosen data points to calculate a Pade approximate, and then removing any noncausal poles and their closest zeros. In addition, there will usually be a comparable number of causal poles which, along with their closest zeros, can be removed with little effect on the Pade approximate. The resulting seven or eight pole function is then used as the basis for an electronic filter.

An example of such a calculation is shown on the next few pages. Data for $J_2(\omega)$ at 15 frequencies is obtained by digitizing published graphs.^{8,15} The data, plotted in Figure 7-1 with the graph from which it was obtained, is used to calculate a 15 pole Pade approximate (cf. Table 7-1). This is factored to yield its poles and zeros, which are plotted in Figure 7-2. After deletion of the paired poles and zeros (circled in the figure), the Pade is reconstructed (cf. Table 7-2). Figure 7-3 compares a plot of the original 15 pole padé approximate, which is noncausal, with the new seven pole approximate, which is causal.

Figure 7-4 shows a comparison of the original function with the measured response of an electronic filter designed using the results in Table 7-2. (The gap frequency of the filter is 1 kHz; the plot was obtained using a computer controlled frequency response analyzer, and the difference between the computed and measured filter response is negligible.) The overall fit of the filter response to the original function could be improved by using additional data points near the gap singularity. However, this would have resulted in a more complex filter, and it was felt that the design of filters containing more than

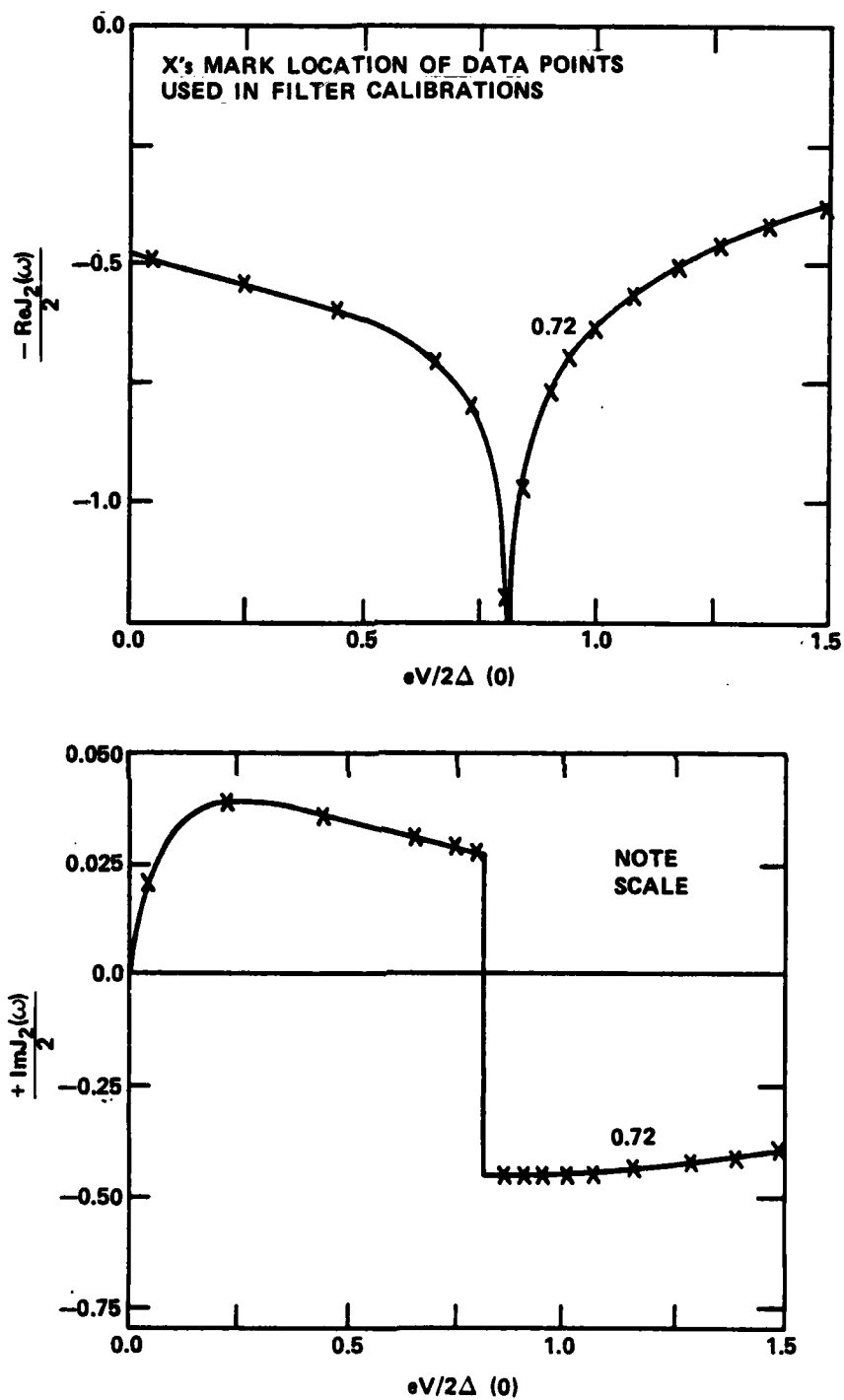
FIGURE 7-1 THEORETICAL $J_2(\omega)$ FOR $T/T_c = 0.72$ (AFTER HARRIS) ⁸

TABLE 7-1 CALCULATION OF A PADE APPROXIMATE

FIFTEEN POLE FIT TO j_2 AT $T = .72T_c$

THE NUMBER OF DATA POINTS IS 15			THE ZEROS ARE	
FREQ	REAL	IMAG		
.050	.491000	.023000	-.076	-1.402
.250	.546000	.039000	.033	-1.007
.450	.600000	.036000	-.315	-.723
.650	.708000	.031000	-.005	-.825
.750	.835000	.028000	-.076	1.402
.810	1.060000	.027000	-.083	-1.177
.850	.891000	-.459000	-.075	-.798
.910	.759000	-.461000	-.005	.723
.950	.695000	-.461000	-.083	1.177
1.000	.634000	-.455000	-.347	-.000
1.110	.544000	-.448000	-.075	.798
1.200	.488000	-.440000	-.005	.825
1.310	.441000	-.424000	.033	1.007
1.410	.404000	-.416000		
1.510	.375000	-.403000		
COEFFICIENTS OF NUMERATOR			THE POLES ARE	
.481232	7.823959	30.074568	-.075	-1.402
478.199937	615.893597	424.248797	-1.711	-.000
32.277055	21.954916	184.162426	-.082	-1.176
		435.348653	.033	-1.007
		187.268190	-.232	-.772
		155.948633	-.002	-.824
			-.090	-.000
			-.082	1.176
			-.431	-.000
			-.061	-.809
			-.075	1.402
			-.232	.772
			-.061	.809
			-.002	.824
			.033	1.007

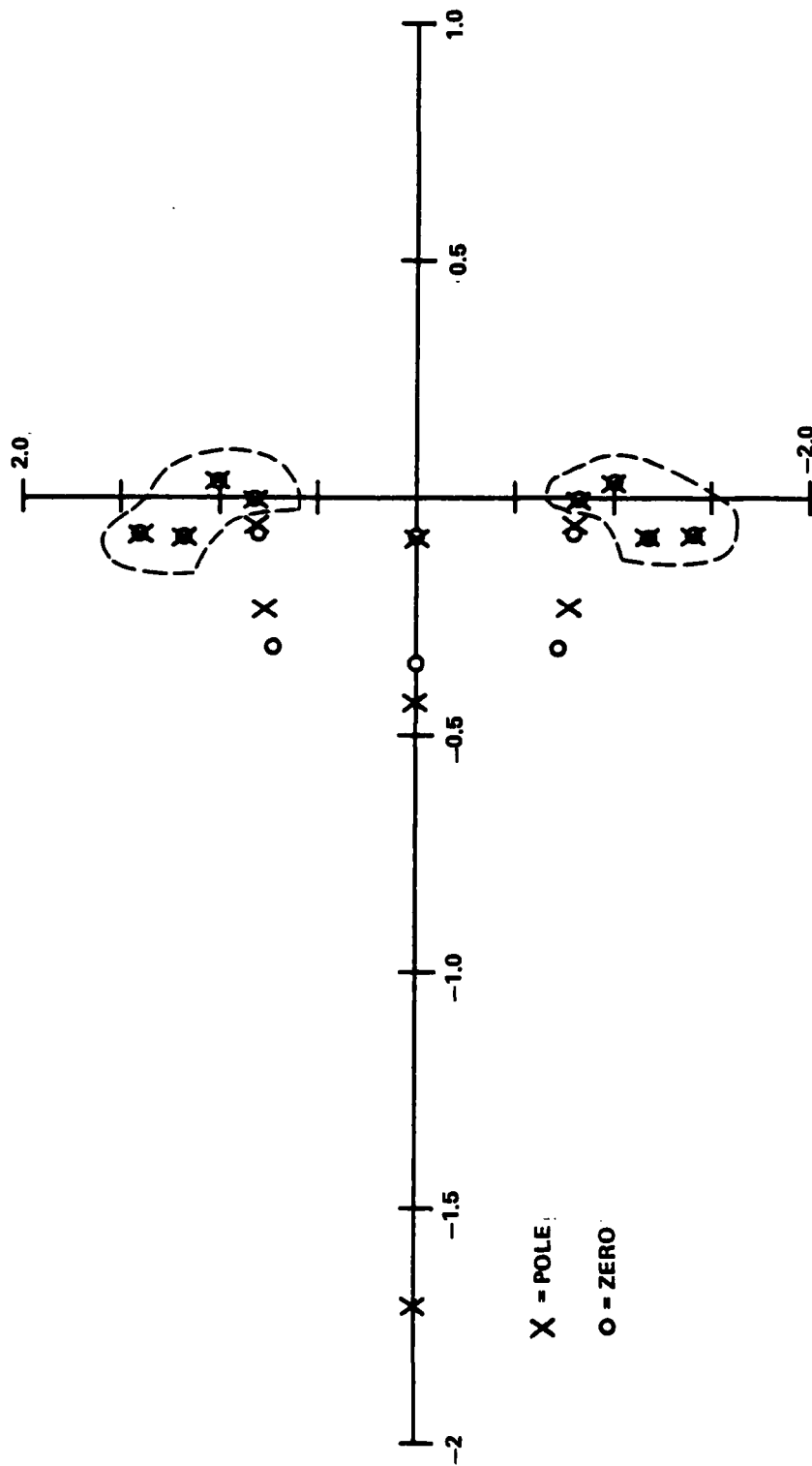


FIGURE 7-2 POLES AND ZEROS OF FIT TO J_2 AT $T/T_c = 0.72$

TABLE 7-2 RECALCULATION OF THE PADE APPROXIMATION AFTER DELETION OF UNWANTED POLES AND ZEROS

THE SCALE FACTOR IS Fact = .481

THE NEW ZEROS ARE

-.347000	0.000000
-.315000	-.723000
-.315000	.723000
-.075000	-.798000
-.075000	.798000
-.083000	0.000000

THE NUMERATOR IS

.012	0.000
.186	0.000
.653	0.000
1.105	0.000
1.723	0.000
1.210	0.000
1.000	0.000

THE SCALED NUMERATOR IS

.481	7.785
72.056	50.600

THE NEW POLES ARE

-1.711000	0.000000
-.232000	-.772000
-.232000	.772000
-.090000	0.000000
-.431000	0.000000
-.061000	-.809000
-.061000	.809000

THE DENOMINATOR IS

.028	0.000
.423	0.000
1.403	-.000
2.595	.000
4.042	0.000
3.603	0.000
2.010	0.000
1.000	0.000

THE SCALED DENOMINATOR IS

1.000	14.915
142.391	126.919

49.426
99.272

91.402
35.228

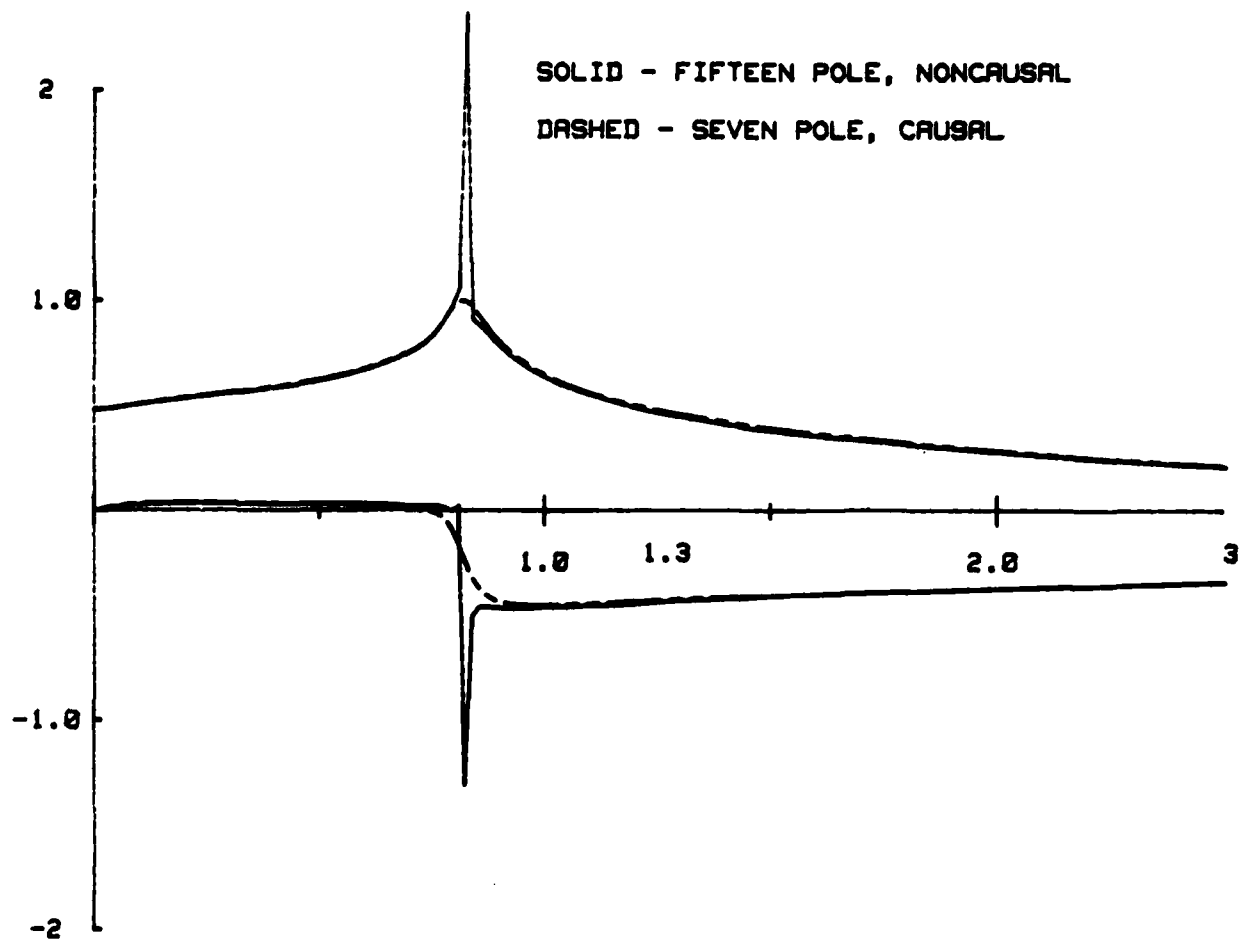


FIGURE 7-3 ATTEMPT TO FIT J_2 AT $T/T_c = 0.72$

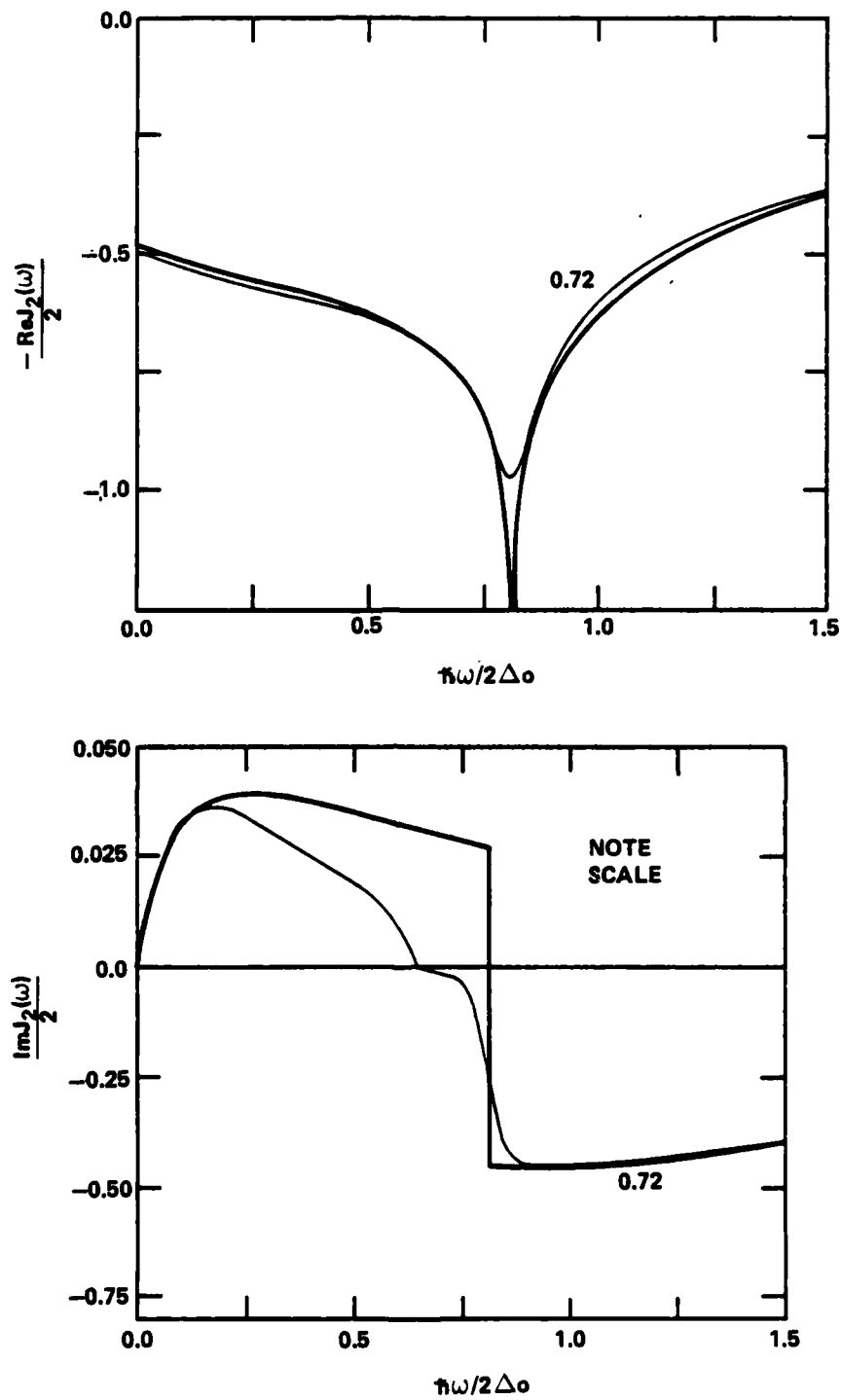
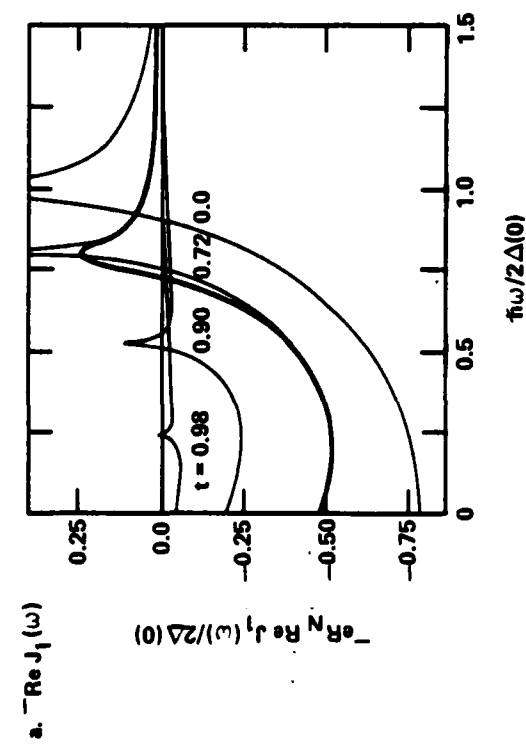
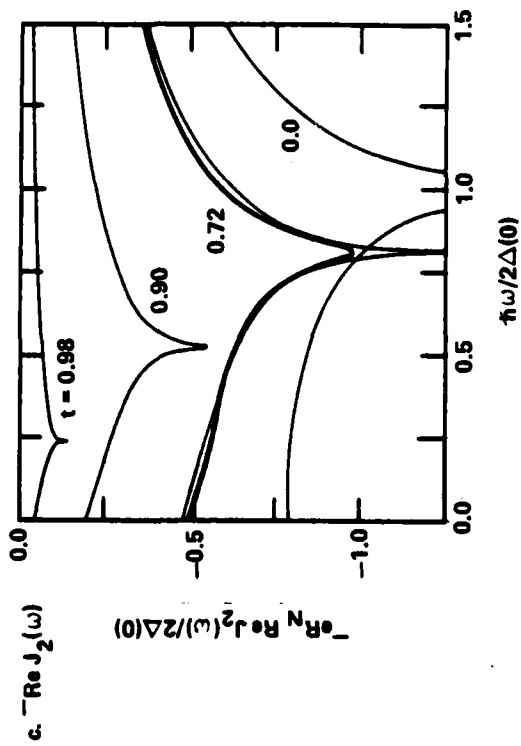


FIGURE 7-4 MEASURED RESPONSE OF THE ELECTRONIC FILTERS FOR $J_2(\omega)$ AT $T = 0.72 T_c$ (THEORETICAL CURVES AFTER HARRIS) ⁸

seven or eight poles would not be practical. Figures 7-5 and 7-6 show measured responses of the filters that model tunnelling at $T = .72T_c$ and $T = .9T_c$. A photograph of the most recent version of the analogue, which contains these filters, is shown as the frontispiece of this dissertation. Results obtained using the analogue with these filters are presented in Chapter 9.



d. $\text{Im } J_2(\omega)$

b. $\text{Im } J_1(\omega)$ (LINEAR TERM ADDED)

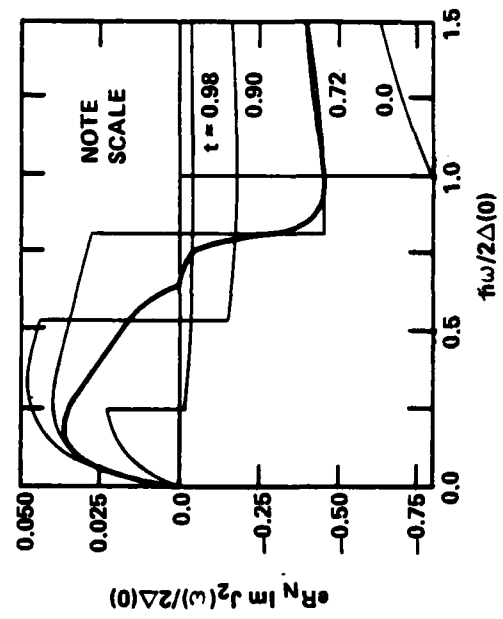
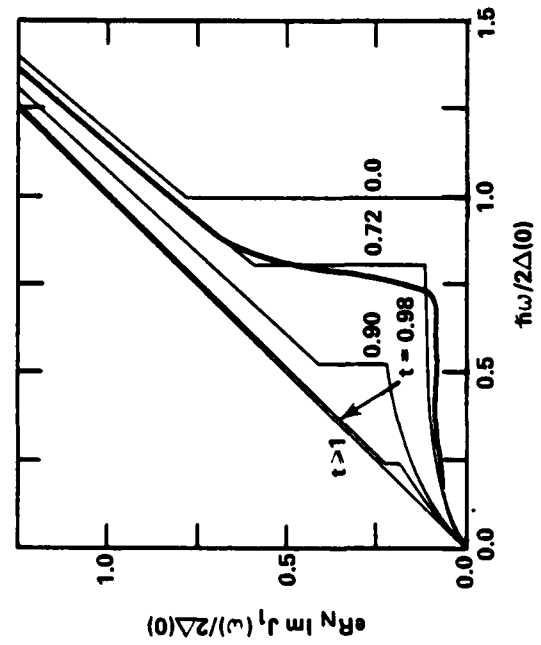
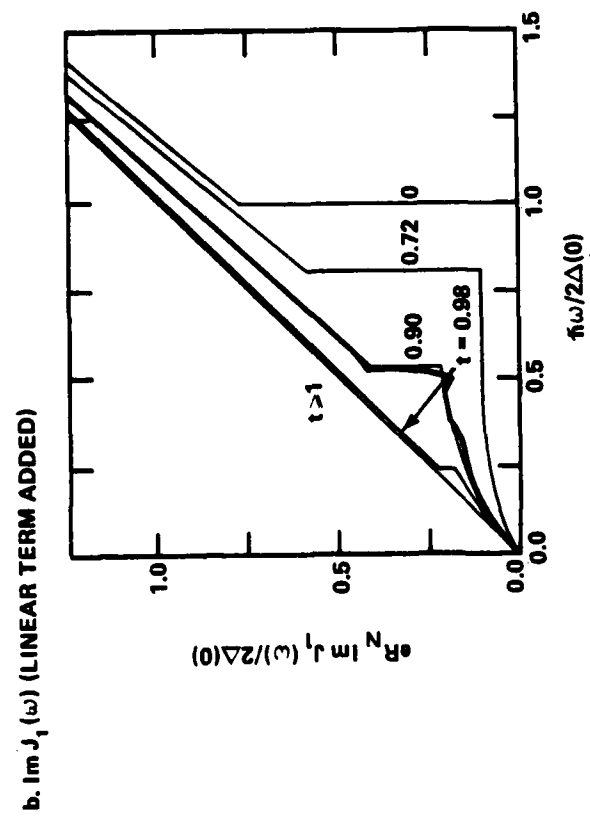
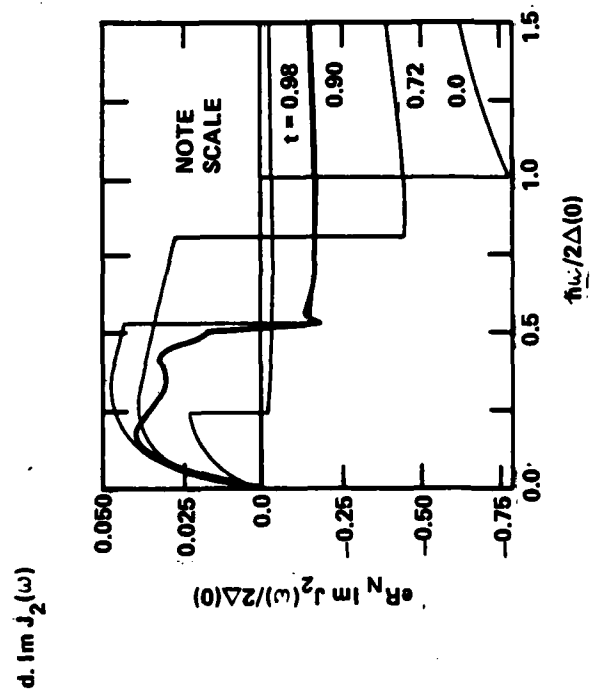
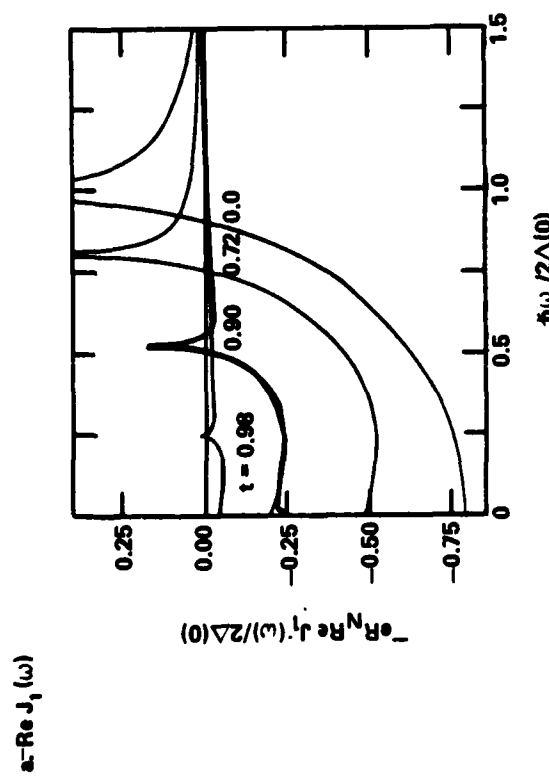
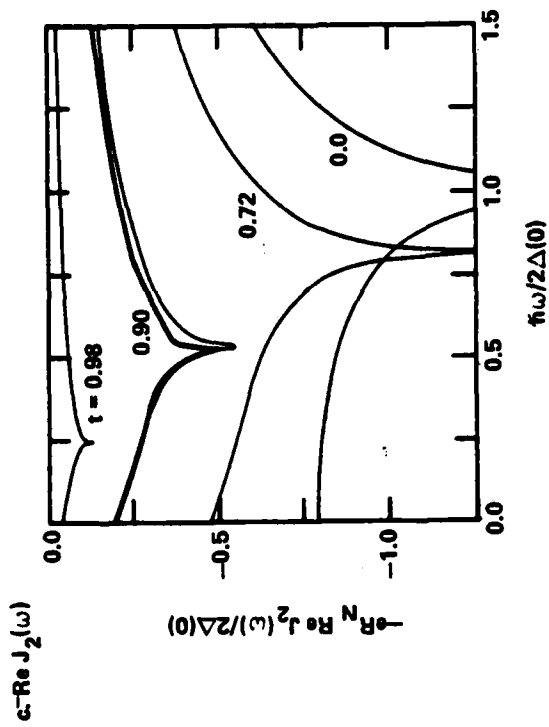


FIGURE 7-5 MEASURED RESPONSE OF FILTERS FOR $T = 0.72T_c$ ($2\Delta(0)/\hbar\omega = 1\text{KHz}$) (THEORETICAL CURVES AFTER HARRIS 8,15)


FIGURE 7-6 MEASURED RESPONSE OF FILTERS FOR $T = 0.9 T_c$ (THEORETICAL CURVES AFTER HARRIS ^{8,15}) ($2\Delta(0)\hbar\omega = 1\text{KHz}$)

CHAPTER 8

ACCURACY OF THE ANALOGUE

8.1 Introduction

The results presented in previous chapters indicate that the electronic analogue is capable of providing a good qualitative fit to the Werthamer theory. However, efforts to obtain good quantitative data were complicated by several problems, such as noise within the VCO, the unwanted $\cos \phi$ term introduced by the phase shift of the low pass filters, errors resulting from difficulties in adjusting the DC offsets of the multiplier chips, and an assortment of measurement problems. After additional study, these problems were overcome, and it became possible to compare the performance of the analogue with other calculations and data in a quantitative, as opposed to a qualitative, manner.

In this and the next chapter, we describe how these problems were overcome, and discuss the results that have since been obtained. The discussion begins in this chapter with a summary of the various improvements to the circuit design, and an assessment of the accuracy of the analogue. This is followed in Chapter 9 with a comparison of results obtained using the analogue with an assortment of theoretical and experimental results.

8.2 Sources of Error in the Analogue

The accuracy of both the RSJ and Werthamer analogues is affected by several factors, which are listed briefly below:

1. Component Accuracy
2. Multiplier Accuracy
3. VCO Harmonic Distortion

4. LO Harmonic Distortion
5. VCO Gain Linearity
6. Transconductance linearity of the voltage controlled current source (VCCS)
7. Output impedance of the VCCS
8. Temperature drift of the LO and VCO center frequencies
9. Op Amp accuracy
10. Phase shift introduced by the low pass filter (LPF)
11. High-frequency rejection of the LPF
12. Noise pickup
13. VCO phase jitter
14. Accuracy of the phase shift between the sin phi and cos phi signals
15. Accuracy of the J_1 and J_2 filters

Many of the above quantities can immediately be characterized in terms of percent accuracy. For example, the resistors and capacitors used in the analogue are rated at 2%. The multipliers have an accuracy of .25% over the bandwidth used in the circuit. The harmonic distortion of both the VCO and LO is less than 1%, and the VCO gain is linear to approximately 1%. The transconductance of the voltage controlled current source is also constant to within 1% over the operating range of the analogue.

Other items from the above list must be described in terms of the operating parameters of the analogue. For example, the output impedance of the VCCS appears in parallel with the shunt resistance of the analogue, and can be considered as an error to the value of the shunt resistance. The VCCS output impedance is easily adjusted to be greater than 200 kilohm, which has less than a one percent effect on the apparent value of the

Josephson shunt resistance, which is typically 1500 ohms or less. (However, at voltages less than the gap voltage, the resistance is considerably higher than R_J , and the output resistance of the VCCS could be important. This turns out not to be the case, and in any event, one can always measure the effective resistance directly from an I-V curve.)

Another important factor which can be a source of error concerns the temperature stability of the VCO and LO. This determines whether the operating point of the analogue will drift with time. For example, a change in either the VCO or LO center frequencies will have the same effect on the junction current as a change in input voltage. The VCO and LO used in the analogue are commercial units and have extremely low temperature drift. Over the course of several minutes, there is no observable change in the bias point; even over a period of several hours, drift is almost negligible.

The remaining sources of error are more complicated, and will be discussed individually in the next sections.

8.3 Accuracy of the Op Amps and Multipliers

Inaccuracies due to op amps generally result from two things. First, most circuits that use op amps are designed on the assumption that the gain of the op amp is infinite. This is not a good assumption at high frequencies, but is quite reasonable at the frequencies at which the analogue operates. The second problem is the effect of the phase shift introduced by the compensation capacitor inside the op amp. This capacitor, which prevents parasitic oscillations, causes the op amp to behave as a single-pole low pass filter, and introduces a slight cosine ϕ term having negative amplitude. This term can be made negligible by

using an op amp having a very high cutoff frequency. However, the higher the cutoff frequency of the op amp, the more susceptible it is to noise pickup and instability.

Fortunately, the phase shift due to the accumulation of op amps, each contributing a slight phase shift, has a negligible effect on most measurements done using the analogue. For one thing, many of the circuits used in the analogue have a considerable amount of capacitative feedback anyway, as in the case of a biquadratic filter. Second, many of the op amps in the analogue are nested in multiple feedback loops, which reduces the influence of the compensation capacitors very dramatically.

The influence of op amp phase shift was noticed in the evaluation of an improved low pass filter circuit, and in some of the plasma resonance experiments. These effects could have been reduced almost totally by using op amps having a cutoff frequency higher than that of the ubiquitous 741 type amplifier. However, the op amps are not the major source of $\cos \phi$ error (the LPF is), and in the interests of minimizing noise pickup and instability, it was decided not to change to a different op amp. (Quantitative details about these effects are included in the discussion of the low pass filter design in Appendix D, and in the presentation of plasma resonance data in the next chapter.)

Related to the discussion of op amp accuracy is the question of multiplier accuracy. As mentioned above, the multipliers used in the most recent versions of the high frequency and RSJ analogues are specified as being accurate to .25%. This is a considerable improvement over the multipliers used in the previous version of the analogue, which were quoted at 2%. However, the more important practical consideration is that the new

multipliers are internally trimmed, and do not require external potentiometers. This results in an elimination of 18 adjustments which, in the earlier analogue, were difficult and time consuming. The new multipliers (Analog Devices Model AD534) were considerably more expensive (\$50 as opposed to \$14 each), but were well worth it, and their accuracy seems to be more than adequate. Hopefully, the results presented later will present a convincing argument for this.

8.4 VCO Considerations

The next four items from the list of possible sources of error are interrelated in a complex manner. The LPF, which determines how well the unwanted VCO center frequency is removed from the sine and cos phi signals, and what the unwanted cosine phi amplitude will be, is designed in accordance with the choice of the center frequency of the VCO. In turn, the choice of VCO center frequency is related to the problems of noise pickup and VCO phase jitter. In this section, we consider the operating parameters of the VCO.

Generally speaking, there was no difficulty in arranging the signal levels in the VCO circuitry so that the signal to noise ratio was acceptable. However, noise at the input to the VCO is of special interest, as it causes errors in the phase phi. With the VCO as originally set up, it was difficult to keep the noise pickup at the input at a sufficiently low level. The problem was solved by deliberately reducing the VCO gain constant, while increasing the level of the input signal.

Related to the noise pickup is the problem of phase jitter within the VCO. This results from the internal operation of the VCO, which in the case of the analogue is not really an oscillator, but a voltage controlled

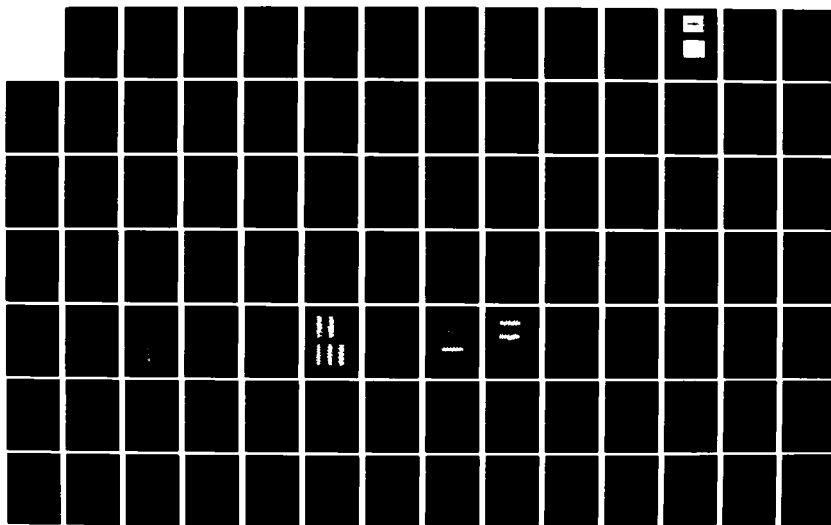
AD-A120 753

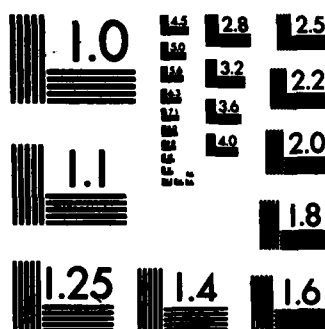
ELECTRONIC SIMULATION OF THE JOSEPHSON EFFECTS(U) NAVAL 3/4
SURFACE WEAPONS CENTER SILVER SPRING MD D JABLONSKI
01 DEC 81 NSWC/MP-81-519 SBI-AD-F500 077

UNCLASSIFIED

F/G 20/10

NL





MICROCOPY RESOLUTION TEST CHART
NATIONAL BUREAU OF STANDARDS-1963-A



MICROCOPY RESOLUTION TEST CHART
NATIONAL BUREAU OF STANDARDS-1963-A



MICROCOPY RESOLUTION TEST CHART
NATIONAL BUREAU OF STANDARDS-1963-A



MICROCOPY RESOLUTION TEST CHART
NATIONAL BUREAU OF STANDARDS-1963-A



MICROCOPY RESOLUTION TEST CHART
NATIONAL BUREAU OF STANDARDS-1963-A

function generator. Instead of modulating a tuned LC network with a varactor diode, the function generator relies on a complicated network of threshold detectors and trigger circuits to determine the output frequency. Unlike varactor diode oscillators, which are primarily radio frequency devices, the voltage controlled function generators operate very well at the frequencies at which op amp techniques are useful. Unfortunately, the threshold voltage at which the trigger circuits fire varies slightly from cycle to cycle, and a certain amount of phase jitter is inevitable. Reducing the VCO center frequency does not eliminate the phase jitter, but seems to reduce its effect on the performance of the analogue. Presumably, this is because the overall error in one cycle of the Josephson frequency is due to the sum of many jitter errors, one for each half cycle of the VCO. If these errors are random and unbiased, statistical arguments suggest that the cumulative error at the end of one Josephson cycle would be proportional to $(f_{10})^{\frac{1}{2}}$, where f_{10} is the VCO frequency. (This is based on the assumption that the total jitter error for N jitters is proportional to $N^{\frac{1}{2}}$.) Thus a small reduction in the VCO center frequency can yield a large reduction in the inaccuracy due to phase jitter.

It turns out that for a commercial function generator, reducing the VCO gain center frequency is consistent with reducing the VCO gain constant. For example, lowering the center frequency from 100 kHz requires switching the front panel scale factor, which causes the VCO gain constant to decrease from 10 kHz/volt to 1 kHz/volt, a factor of 10. Although it would be possible to design a home-made circuit in which the VCO center frequency and gain constant are independent, a home-made circuit would lack the quality of design of a commercial unit, particularly with respect

to temperature stability. (It might be noted that the other circuits used in the analogue, such as filters, adders and current sources, are not subject to the noise and temperature problems that are characteristic of oscillators and function generators.)

8.5 LPF Considerations

Reducing the VCO center frequency and gain constant alleviated the problems due to noise pickup and phase jitter, but introduced problems with the design of the low pass filters. In particular, lowering the center frequency makes it much more difficult to design an LPF having a minimal phase shift at low frequency. Additionally, the relative bandwidth for which the LPF must attenuate the signal becomes larger as the VCO center frequency is reduced relative to the Josephson frequency. For example, if the characteristic frequencies of the sine ϕ and cos ϕ signals are 1 kHz, the LPF will need to filter out signals in the range $2f_0 \pm 1\text{kHz}$. As f_0 is reduced, this becomes a more challenging problem.

As a first step towards making the necessary improvements to the LPF, the four pole Butterworth filters used in the original high frequency analogue were replaced by twin-T filters. The twin-T is a notch filter that is noted for having low phase shift away from the notch frequency. In addition, it is quite simple to build, and requires no active circuits or inductors. The twin-T is discussed in more detail in Appendix D, but it is worth noting that its transfer function is given by

$$F(s) = \frac{1 + s + s^2 + s^3}{1 + 5s + 5s^2 + s^3} \quad 8-1$$

where $s = j\omega/\omega_0$ and ω_0 is the notch frequency of the filter.

The equivalent $\cos \phi$ amplitude of the twin-T is found by expanding the transfer function for low frequencies, and equating it to that of a single pole RC type filter (cf. Chapter 3). For a VCO center frequency of 100 kHz, the twin-T will have a null at 200 kHz; relative to a Josephson frequency of 1570 hz (which corresponds to the gap frequency of 1000 hz), the amplitude of the cosine ϕ term is $-.031 \times I_J$ (cf. Chapter 6). A filter with these characteristics was used in an improved RSJ analogue used for some of the experiments described in this and the next chapter.

For the high frequency analogue, the use of a VCO center frequency of 100 kHz was unsatisfactory. Phase jitter and noise pickup caused the device to operate unsatisfactorily at frequencies less than the gap frequency of 1 kHz. (In the case of the RSJ analogue, this problem was circumvented by adjusting the other parameters such that the frequencies of interest in the operation of the analogue were greater than 1 kHz. In the high frequency analogue the gap frequency was fixed, and this option was not available.) The VCO center frequency was lowered to 30 kHz, and a more sophisticated low pass filter was designed. (As pointed out above, reducing the VCO center frequency from 100 kHz to 30 kHz causes a factor of ten reduction in the VCO gain constant, with a corresponding improvement to the problem of noise pickup. Reducing the center frequency by this factor of 3.33 yields approximately a factor of 10 reduction in the effects of phase jitter, as discussed in Section 8.4. From the point of view of designing an LPF, further reduction of the VCO center frequency is undesirable.)

The design details of the improved low pass filter are discussed in Appendix D. However, a few of the details bear mentioning here. First,

the filter was designed to minimize the low frequency phase shift, while maintaining a relatively wide notch at 60 kHz (twice the VCO center frequency). After some mathematical analysis, it was decided to build a filter having the following transfer function:

$$F(s) = \frac{1 + s + s^2 + s^3}{1 + s + 5s^2 + s^3} \quad (8-2)$$

This transfer function retains many of the properties of the twin-T, most notably the notch at $s = 1$. However, the low frequency phase shift of the filter is zero to first order. Realizing a filter having the response given above is complicated by the fact that $|F(s)|$ can be greater than one (which is not true for the twin-T). Consequently, the filter must include some sort of circuit which sums the outputs of filters which model the biquadratic components of $F(s)$. It was decided to use the network topology shown in Figure 8-1, in which three passive circuits are operated in parallel. By using passive components, including inductors, the circuit can be made to operate with a null at 60 kHz, a frequency which is quite high in terms of op amp design. By incorporating the op amps in the manner shown, the individual filters are buffered from each other, and their outputs are summed in such a way that the limited performance of the op amps at 60 kHz does not affect the existence of the null. At low frequencies, the op amps introduce a phase shift similar to that of a single pole RC filter.

An important consequence of this design is that the null frequency and the low frequency phase shift of the improved filter are theoretically independent of each other. The null is determined by the passive

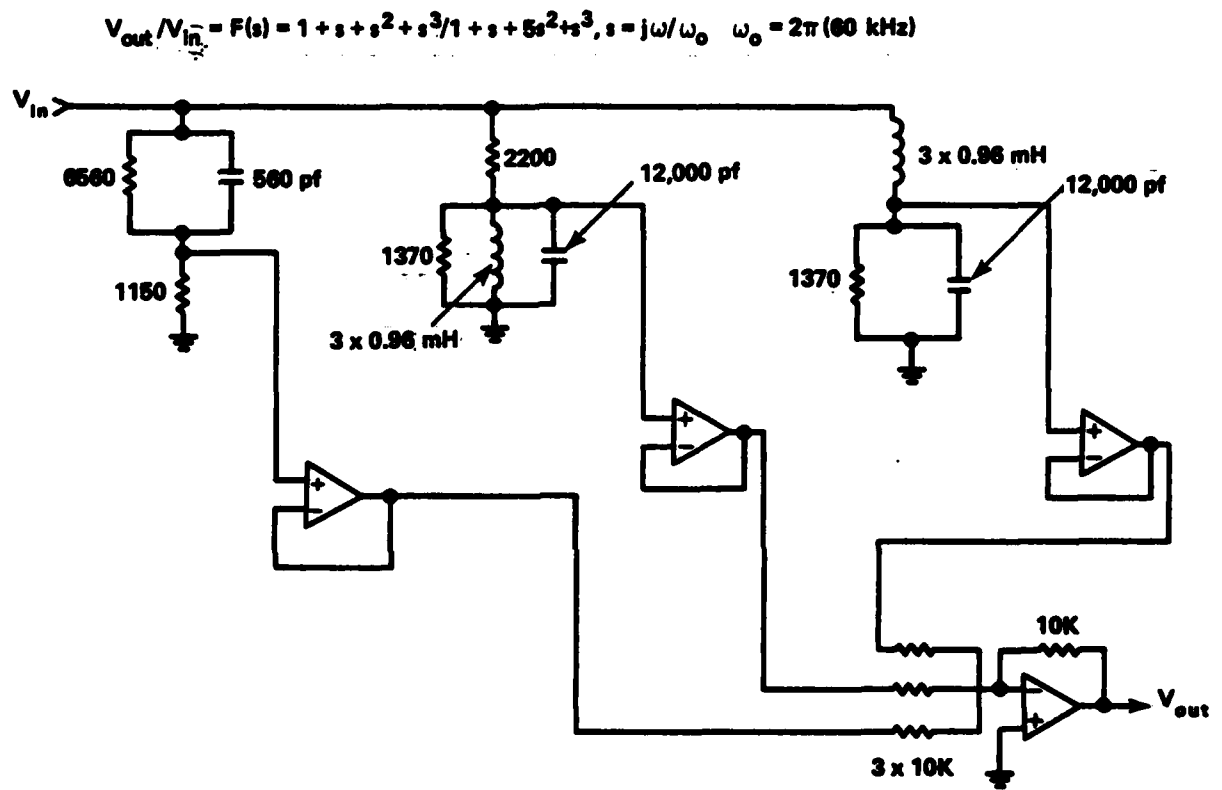


FIGURE 8-1 IMPROVED LOW PASS FILTER

components, and the phase shift by the op amps. Unfortunately, in practice, the phase shift is determined primarily by the accuracy with which the passive components are matched. However, the filter of this type used in the analogue was a substantial improvement over the twin-T, in that the twin-T has a relative $\cos \phi$ amplitude of $-.031$ for a notch frequency of 200 kHz, whereas the improved filter has a measured $\cos \phi$ amplitude of $-.025$ for a notch frequency of 60 kHz. There is little doubt that this can be improved further by taking greater care in the matching of components. In particular, it would make sense to incorporate some adjustable components into the filter, so as to permit final compensation of phase shift errors due not only to LPF component inaccuracy, but to cumulative phase error throughout the remainder of the analogue as well. However, the filter proved quite adequate for using the analogue to obtain the results presented in this and the next chapter. In passing, it is interesting to note that two of the sub-filters in Figure 8-1 have the same resonant frequency. Unfortunately, it was impossible to consolidate the two sections and still realize the particular transfer function required.

The last consideration related to the LPF is the question of high frequency feedthrough near the notch frequency $2f_o$, and at the local oscillator and VCO center frequency f_o . Some of the mixer outputs at $2f_o \pm KV_{in}$ will get through the filter, as will any carrier feedthrough at f_o . This latter signal is of concern because f_o is not only well below the notch frequency, but is in the region where the filter amplifies, instead of attenuates, the signal. Fortunately, the carrier feedthrough of the multiplier is essentially zero, provided that the outputs of the LO and VCO have no DC offset. As most signal generators produce some DC at their

output, trimmer circuits were added to the analogue to compensate for this. With proper adjustment, the feedthrough at f_o was unnoticeable in the sine $\phi/2$ and cosine $\phi/2$ signals at the outputs of the low pass filters.

Feedthrough at the notch frequency of the filters was noticeable, as was expected. However, over the range of operation of the analogue, this unwanted signal had an amplitude less than five percent of that of the desired $\sin\phi/2$ and $\cos \phi/2$ signals. Under current bias conditions, this high frequency feedthrough will be fed back into the VCO in an amount roughly equal to five percent of I_J times R. Mathematically,

$$V = (.05)I_J R_N \sin(4\pi f_o t + k \int V_{in} dt) \quad (8-3)$$

The effect of this unwanted high frequency feedback will be to remodulate the VCO output frequency. If we consider the effects of feeding the unwanted signal back into the VCO only once, we have that the output of the VCO will contain a term proportional to:

$$J_1 \left(\frac{.05 I_J R_N K}{4\pi f_o + K V_{in}} \right) \sin(2\pi f_o t + k \int V_{in} dt) \quad (8-4)$$

where J_1 is the ordinary Bessel function of the first kind.

This will mix with the LO to generate a low frequency error proportional to:

$$I_J \times J_1 \left(\frac{.05 I_J R_N K}{4\pi f_o + k V_{in}} \right) \quad (8-5)$$

Due to the large magnitude of f_o , this error is quite small, and may be neglected. Experimental observations are consistent with this assumption (cf. Figures 8-2 and 8-3; Table 8-1).

The problem of harmonic distortion of the VCO and LO is related to the above discussion. Any harmonics of f_o present in the outputs of the LO or VCO can pass through the low pass filters and be fed back to the input. There is the possibility that the second time through the system, DC components will be generated at the output of the VCO which will affect the current-voltage characteristics of the analogue. Calculations similar to those above, as well as practical experience, indicate that this is not a problem.

8.6 Phase Shift Errors

The next source of error to be considered is the consequence of the sine phi and cosine phi signals not being exactly 90 degrees out of phase. To see the possible effect of this, let the analogue be voltage biased such that:

$$\begin{aligned}\sin \phi/2 &= \sin \omega t \\ \cos \phi/2 &= \cos \omega t\end{aligned}\tag{8-6}$$

where $\omega = kV_{in}$.

Introducing a small phase error δ , we have

$$\begin{aligned}\sin \phi/2 &= \sin \omega t \\ \cos \phi/2 &= \cos(\omega t + \delta) \\ &= \cos \omega t \cos \delta - \sin \omega t \sin \delta \\ \text{for } \delta \ll 1, \cos \phi/2 &\approx \cos \omega t - \delta \sin \omega t\end{aligned}\tag{8-7}$$

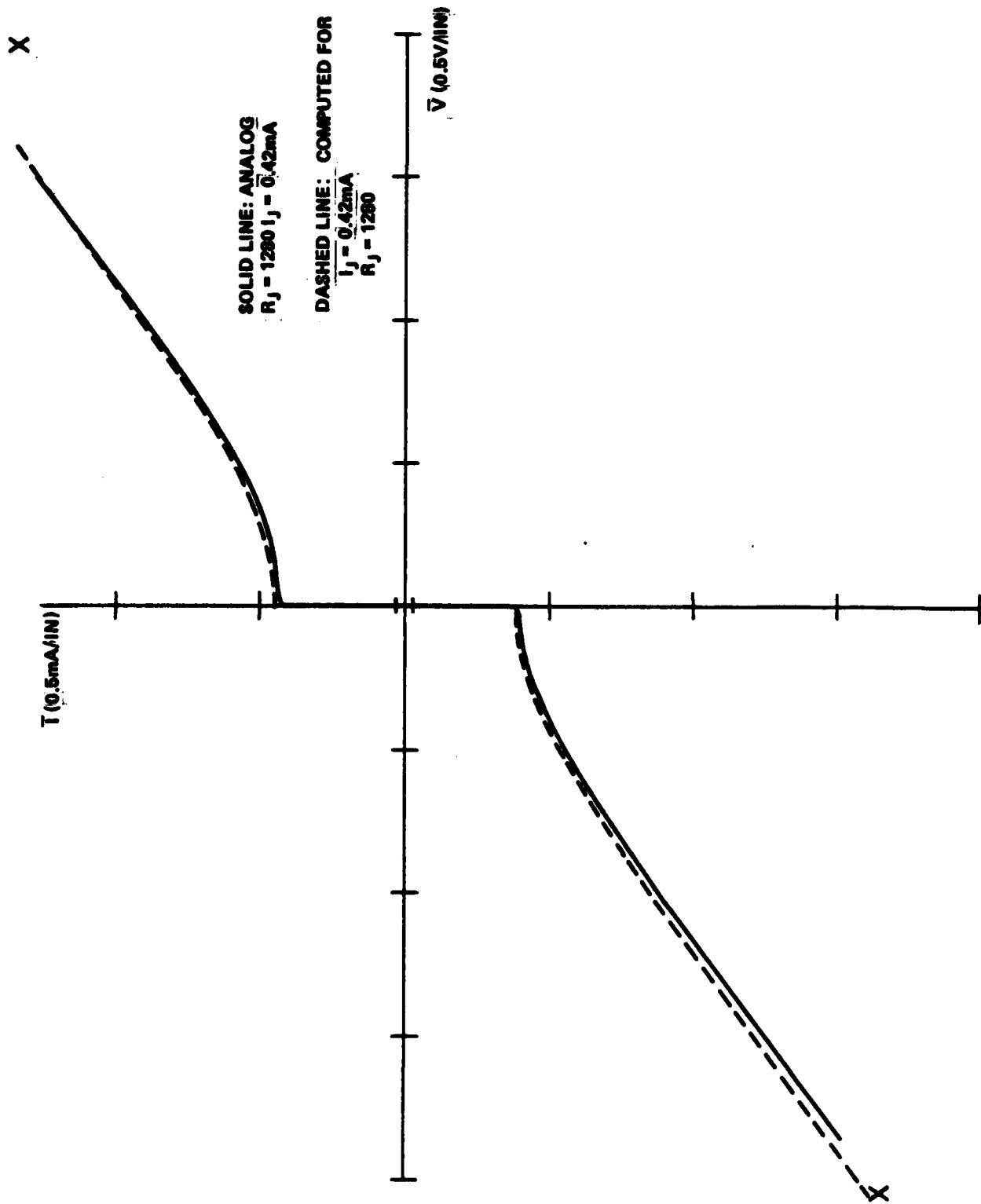


FIGURE 8-2. HIGH-FREQUENCY ANALOGUE IN RSJ MODE: COMPARISON OF MEASURED I-V CURVE WITH THEORETICAL CALCULATION

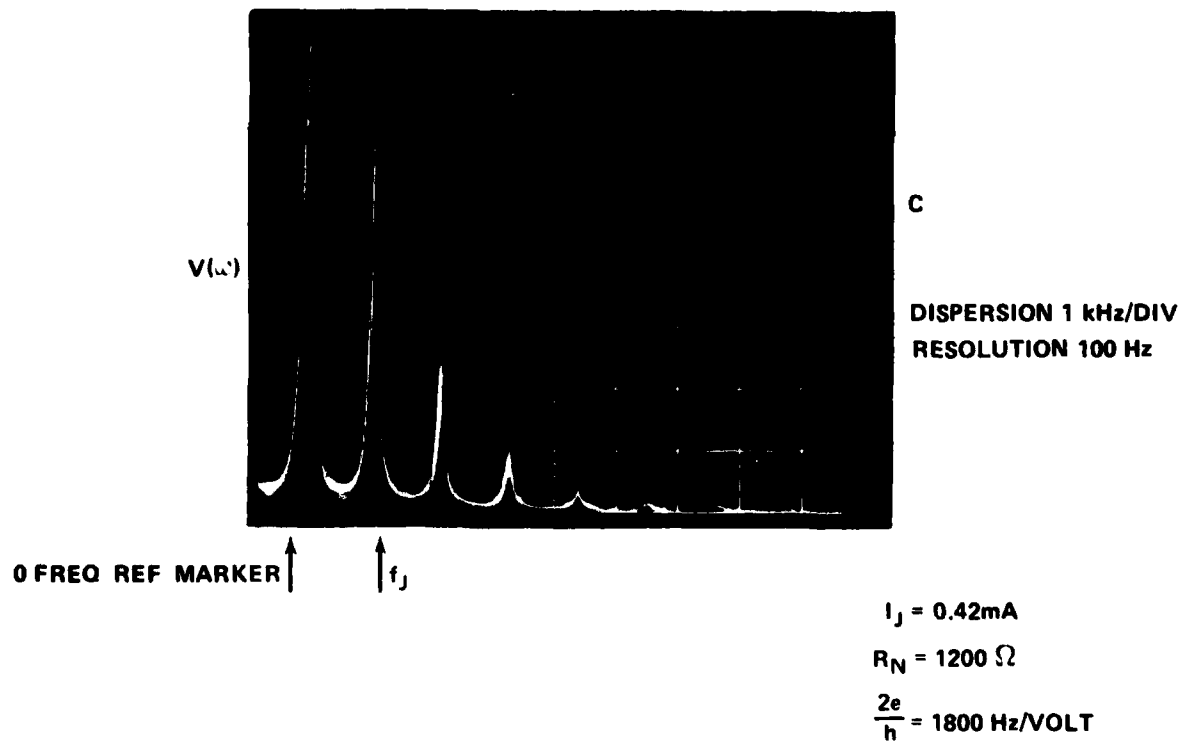
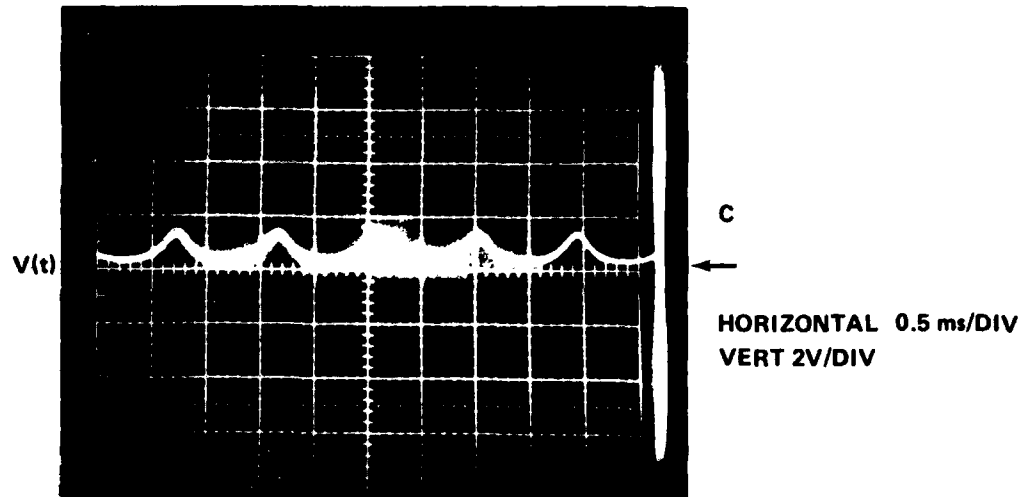


FIGURE 8-3. MEASURED VOLTAGE ACROSS THE HIGH-FREQUENCY ANALOGUE (RSJ LIMIT)

Table 8-1 Numerical Interpretation of Figure 8-3

In the RSJ, current bias limit, the amplitude of the n^{th} harmonic of the junction voltage at a particular I_{DC} is proportional to (cf. sec. 2.4):

$$Y^n = \left(\frac{1 - \sqrt{1 - \gamma^2}}{\gamma} \right)^n \quad (1)$$

where $\gamma = I_J / I_{\text{DC}}$.

The Josephson frequency $f_J = \frac{2e\bar{V}}{h}$ is related to γ by $\frac{\bar{V}}{I_J R_N} = \frac{1}{\gamma^2} - 1$. (2)

From 8-7a, the Josephson frequency is measured to be 857 Hz. Using (2) above, along with the values of I_J , R_N , and $2e/h$ from the figure, γ is found to be $\gamma = .727$.

The relative amplitudes of the various harmonics of $V(t)$ are found from 8-7b to be approximately:

$$f_J \quad 4.7X = Y \quad (3a)$$

$$2f_J \quad 2.1X = Y^2 \quad (3b)$$

$$3f_J \quad .95X = Y^3 \quad (3c)$$

$$4f_J \quad .45X = Y^4 \quad (3d)$$

$$5f_J \quad .15X = Y^5 \quad (3e)$$

where X relates the height of the spectral line in centimeters to its corresponding voltage, and Y is defined in (1) above.

Combining (3a) and (3b), γ is found to be $\gamma = .745$ (compare with $\gamma = .727$ above). Using (3a) again, X is found to be $X = .095$. Using this value of X , the amplitudes of the 3rd, 4th, and 5th harmonics are .0903, .0428, and .0143.

Using $\gamma = .745$, the corresponding values of Y^n are .0893, .0399, and .0178.

The above calculations suggest that the high frequency analogue, when operating in the RSJ limit, is producing results with an accuracy of 95% or more.

Using equation 4-1 for the current through the analogue, we have

$$I(V) = \text{Im}J_1(V) + \text{Re}J_2(V)\sin\phi + \text{Im}J_2(V)\cos\phi \quad (8-8)$$

$$- \delta\text{Im}J_2(V)\sin\phi - \delta(1 - \cos\phi)\text{Re}J_2(V)$$

Note that to a first approximation, the phase shift error does not affect the terms in J_1 . However, it has the effect of mixing the real and imaginary parts of J_2 .

The local oscillator provides two sine waves whose relative phase can be varied continuously. It was found that with careful adjustment using a PSD* and oscilloscope, there were no appreciable discrepancies in the results obtained with the analogue that could be attributed to this source of error.

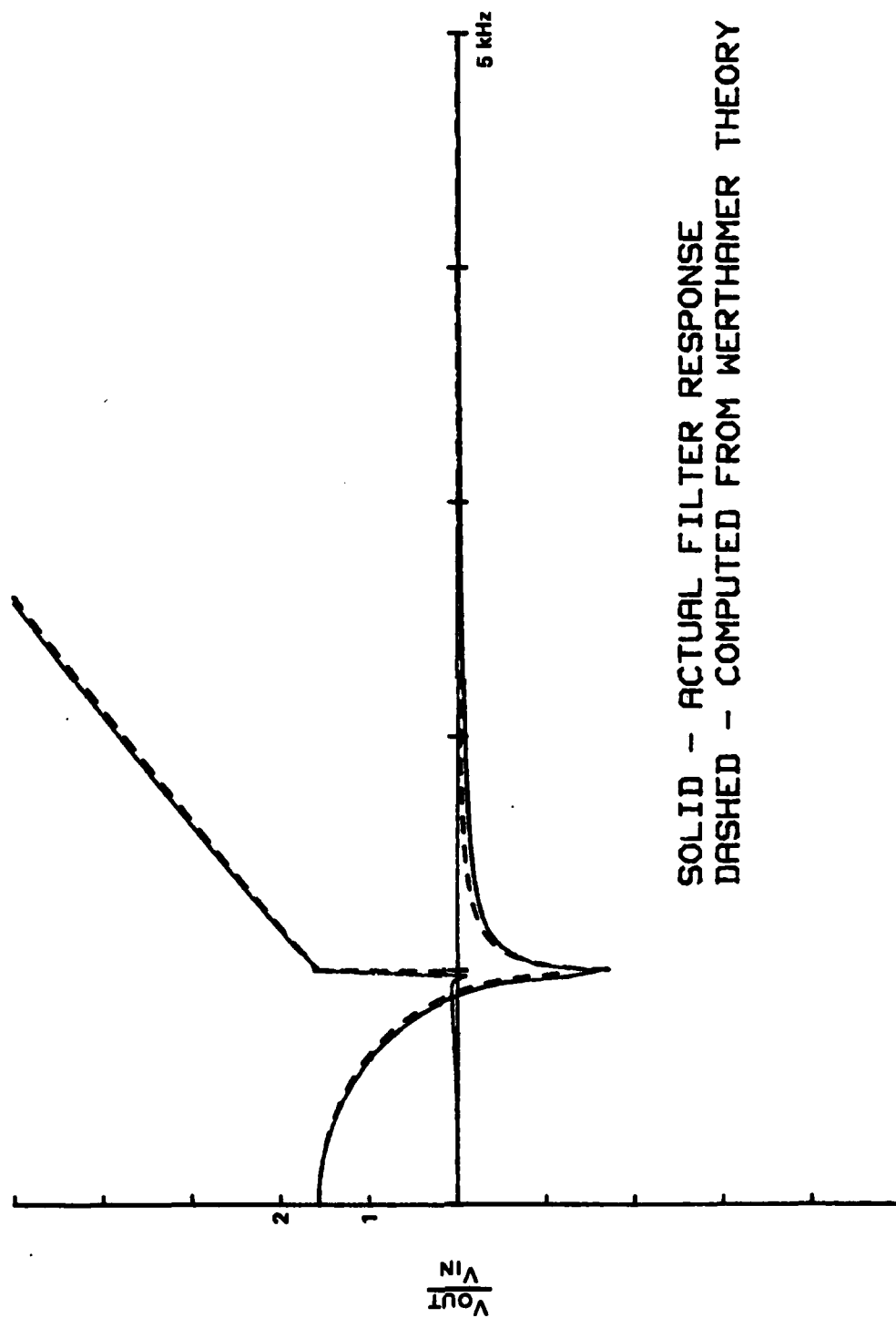
8.7 Accuracy of the J_1 and J_2 Filters

The previous discussion has been concerned with what could be called the "mainframe" of the analogue. The filters for J_1 and J_2 essentially plug into this mainframe, and for most applications can be considered separately. This was done in the previous chapter, but with particular emphasis on the design of filters for $T \neq 0$. In this section we continue the discussion of filter design, but in terms of the $T = 0$ filters, and with emphasis on how the accuracy of these filters affects the performance of the complete analogue. Two problems are addressed. First, it is important to know how well the electronic filters used in the analogue model the response functions in the Werthamer theory. Second, the filters in the analogue occur in duplicate pairs, and one must ask what happens to the operation of the analogue if the actual response functions of a particular pair are not identical.

*PSD: Phase Sensitive Detector

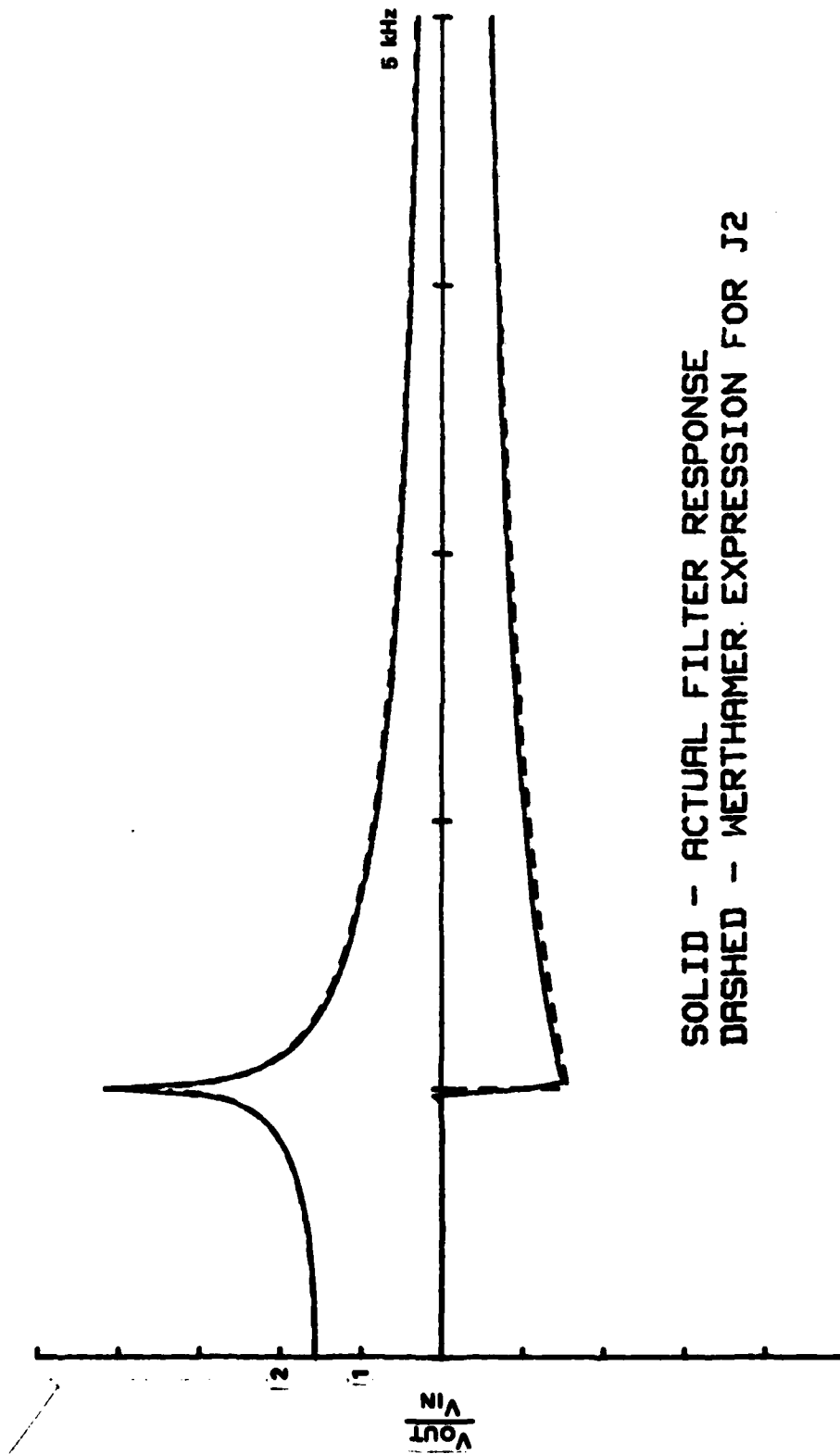
The first of these questions is answered schematically in Figures 8-4 and 8-5, which compare the theoretical expressions for J_1 and J_2 at $T = 0$ (in terms of the original elliptic integrals, and not the Pade approximates) with the measured responses of the J_1 and J_2 filters used in the analogue. (These are rebuilt versions of the filters discussed in Chapter 4.) (A comparison of the measured responses with theory for the filters for $T = .72T_c$ and $T = .9T_c$ is given in Figures 7-5 and 7-6.) In Figures 8-4 and 8-5, the agreement between the measured and calculated response is good except in three respects. First, the Gibbs type overshoot at the gap discontinuity is undesirable, particularly in the case of $\text{Im } J_1$, where it can cause negative resistance problems (cf. Section 4.6). Second there is some error caused by the inability of an electronic filter to model the $1/(\text{abs } f)$ behavior in the real parts of J_1 and J_2 at high frequency. Third, the discontinuity in $\text{Im } J_1$ at the gap frequency should be equal to the amplitude of the critical current. However, it is slightly higher, with the result that photon assisted tunnelling steps will be slightly larger with respect to Josephson steps than they should be. In terms of computing the relative step heights of the Josephson and PAT steps as done in the next chapter, this means that the PAT steps should be normalized to the height of the discontinuity in $\text{Im } J_1$ at the gap edge.

The question of how well one can match two filters for a particular function for a given temperature is partially answered by Figures 8-6 and 8-7, which show a comparison of the measured responses of the identical J_1 and J_2 filters for $T = 0$. The main disagreement occurs at the gap singularity, where high Q filters are used to model the Riedel peak. The high Q biquads are more sensitive to slight errors in component



SOLID - ACTUAL FILTER RESPONSE
DASHED - COMPUTED FROM WERTHAMER THEORY

FIGURE 8-4. COMPARISON OF MEASURED J_1 RESPONSE WITH THEORY



SOLID - ACTUAL FILTER RESPONSE
DASHED - WERTHAMER EXPRESSION FOR J2

FIGURE 8-5. COMPARISON OF MEASURED J_2 FILTER WITH THEORY

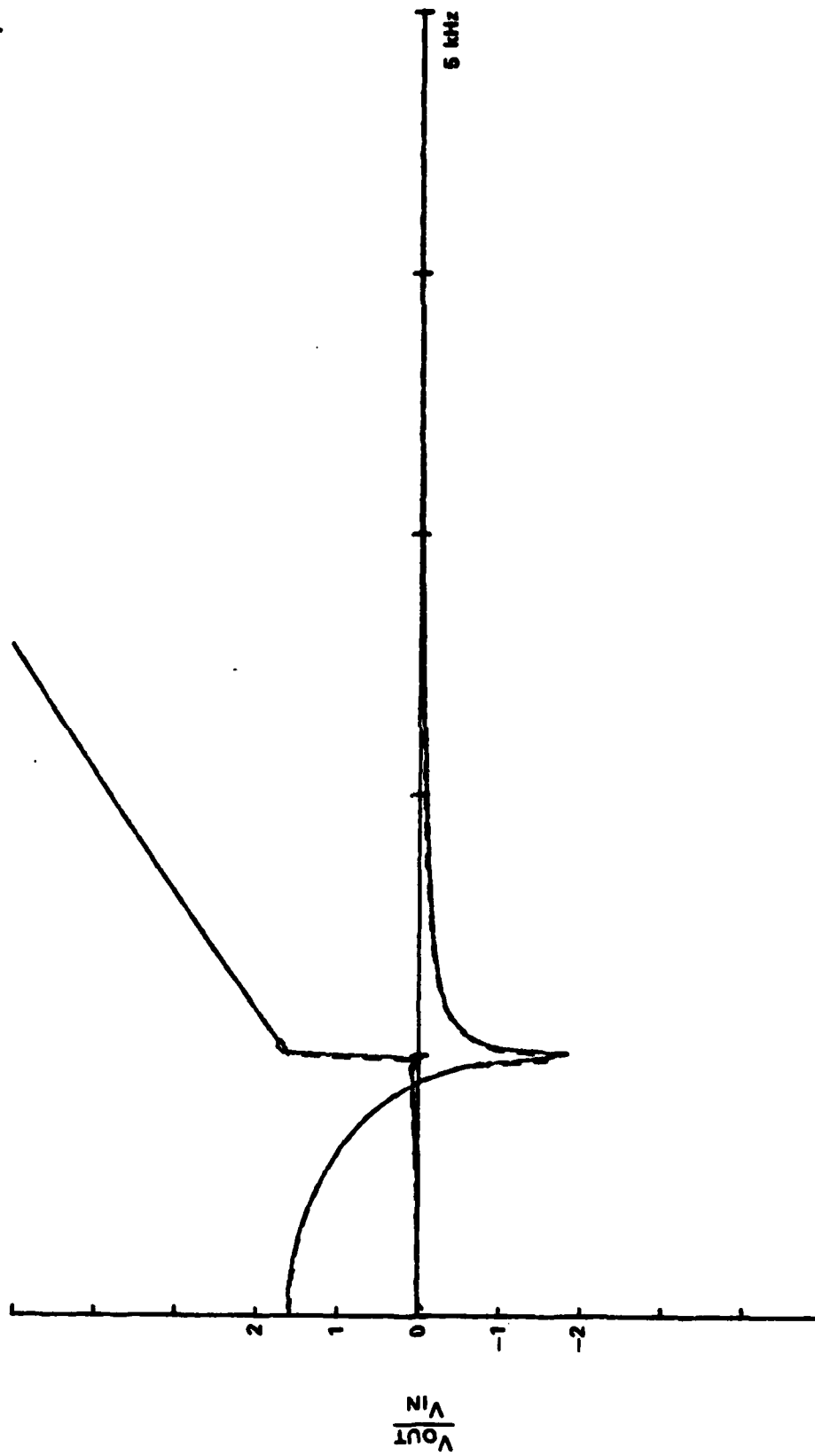


FIGURE 8-6. COMPARISON OF TWO J_1 FILTERS

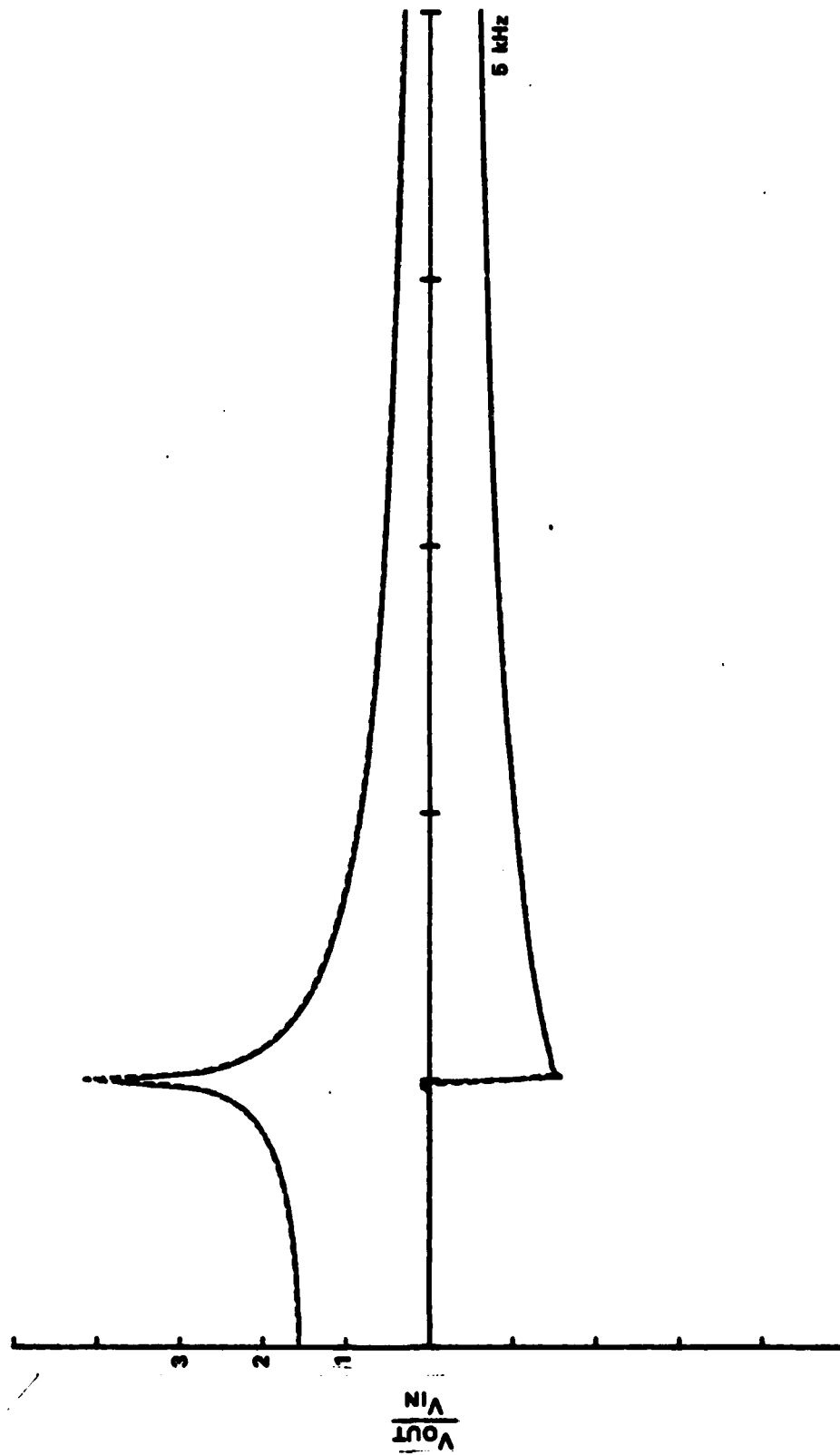


FIGURE 8-7. COMPARISON OF TWO J_2 FILTERS

values than are low Q filters, and it is not surprising that the various filters disagree. It should be noted that this disagreement can be reduced if painstaking care is used to match components for the high Q biquads in each filter. This was not done when these filters were constructed; standard 2% components were used with no special attention given to matching.

To estimate the quantitative effect of mismatch, it is interesting to calculate the effect of discrepancies in the two responses for $\text{Im } J_1$ on the DC I-V characteristic of a voltage biased junction. Rewriting equation 2-1 for the current through a tunnel junction in terms of non-identical J_1 filters, we have:

$$I(t) = \text{Im } J_a + \delta_r \sin 2\omega t - \delta_i \sin^2 \omega t \quad (8-9)$$

where J_a and J_b are the different J_1 filters, and $\delta_r = \text{Re } J_a - \text{Re } J_b$, $\delta_i = \text{Im } J_a - \text{Im } J_b$.

We see that the effect of the mismatch is to average the two J_1 filter responses to get the DC response, and that there is an AC error term that is proportional to the difference between the two curves. Using numerical data from the curves in Figures 8-6 and 8-7, we can calculate the DC average and the error term in the region near the gap. This is shown in Table 8-2. The error is noticeable, but there is little doubt that with additional effort, the filters for J_1 and J_2 can be matched better than they are now. Nevertheless, the results obtained with the analogue have been quite good, and to a first approximation, this source of error can be ignored. In the case of filters for nonzero temperatures, the Riedel peak diminishes significantly, and the electronic filters do not contain

Table 8-2 Effect of a Mismatch Between the Measured Responses
of the J_1 Filters for $T = 0$

The two J_1 filters are designated J_a and J_b . From equation 2-1, we have for the current due to J_1 :

$$I(t) = \cos \frac{d}{2} (\sin \frac{d}{2} * j_a) - \sin \frac{d}{2} (\cos \frac{d}{2} * j_b)$$

In the voltage biased limit, $\phi/2 = \omega t$. Letting $\delta_r = \text{Re } J_a - \text{Re } J_b$ and $\delta_i = \text{Im } J_a - \text{Im } J_b$,

$$I(t) = \text{Im } J_a + \delta_r \sin 2\omega t - \delta_i \sin 2\omega t$$

$$I(t) = \text{Im } J_a - \delta_i/2$$

For the $T = 0$, J_1 filters used in the analogue:

freq	Im J_a	Im J_b	$I(t)_{\text{meas}}$	$I(t)_{\text{theor}}$
941	-.050	-.010	-.03	0
961	-.091	-.006	-.049	0
981	-.214	-.085	-.150	0
1001	1.483	.297	.890	1.57
1021	1.634	1.777	1.704	1.62
1041	1.647	1.714	1.682	1.66

*The appropriate linear term has been added to Im J_a and Im J_b (see section 4.3)

difficult-to-match high-Q biquads. As a result, the duplicate filters for $T \neq 0$ match extremely well.

There is a final point that bears quick mention in this section. It was reported in Chapter 4 that the overshoot in $\text{Im } J_1$ for $T = 0$ at the gap voltage could produce anomalous results, particularly if there was any shunt capacitance across the junction. This overshoot is a direct consequence of the use of a high-Q bandpass filter to model the step discontinuity in $\text{Im } J_1$. Removing the relevant biquad would cure the anomaly, at a cost of decreasing the ability of the analogue to model accurately photon-assisted tunnelling steps. It is likely that some compromise could be reached, but only at a cost of redesigning the entire filter. In the meantime, the $T = 0$ filters were used with careful attention to any possible problems. In any event, adding some leakage current by decreasing the $I_J R_N$ product will provide a quick fix.

8.8 Preliminary Results

At this stage, we present some simple results obtained using the high frequency analogue in the RSJ mode (e.g., with the filters disconnected.) Figure 8-2 shows the time averaged I-V characteristics of the analogue under current bias conditions, plotted against the theoretical solution to the RSJ equation. The agreement is relatively good, although it could probably be improved by giving more attention to the various calibration steps (e.g., adjusting DC offsets and the relative phase of the VCO and LO, etc.). However, the major disagreement between experiment and theory may well be due to scaling and plotting difficulties. The choice of $R_J = 1280$ ohms for the theoretical calculation did not take into account the possibility of non-infinite source impedance, which would lower the

effective R_j of the analogue slightly. Also, the superposition of the two graphs was done in an ad hoc manner using two different plotters, and the zero voltage steps are not precisely aligned.

Figures 8-3a and 8-3b show photographs of the voltage as a function of time for a particular value of current, as well as a photo of a spectrum analyzer display of the voltage. Comparison of several photos taken at different values of I_{DC} indicates that the harmonic content, as well as the variation of the amplitude of the fundamental component with DC current, agree with the theory. Any significant errors would be expected to show up either as amplitude errors, or by the appearance of spurious spectral lines. A numerical analysis of Figure 8-3b is given in Table 8-1.

Figures 8-8 and 8-9 are a retake of the impedance data shown in Chapter 3 for the RSJ analogue. The data presented here was obtained with the simple RSJ analogue (not the high frequency analogue in the RSJ mode). However, the low pass filter consisted of a twin-T with a center frequency of 100 kHz, and an equivalent cosine phi amplitude of -.031.

The data is plotted against the results of the theoretical calculations of Auracher and van Duzer. This was done by digitizing graphs from their original publication, and having a desktop computer plot them on top of the results obtained using the analogue. The level of agreement is roughly the same as that in Figure 8-2 for the DC I-V curves of the high frequency analogue operated in the RSJ mode. The close agreement between the theoretical and simulated curves indicates not only that the junction impedance varies as predicted, but that the measured step heights agree with theory as well. The major disagreement seems to be within the zeroth order step. The effect of the unwanted $\cos \phi$ term immediately comes to mind, but this has yet to be investigated. (As the analogue is being

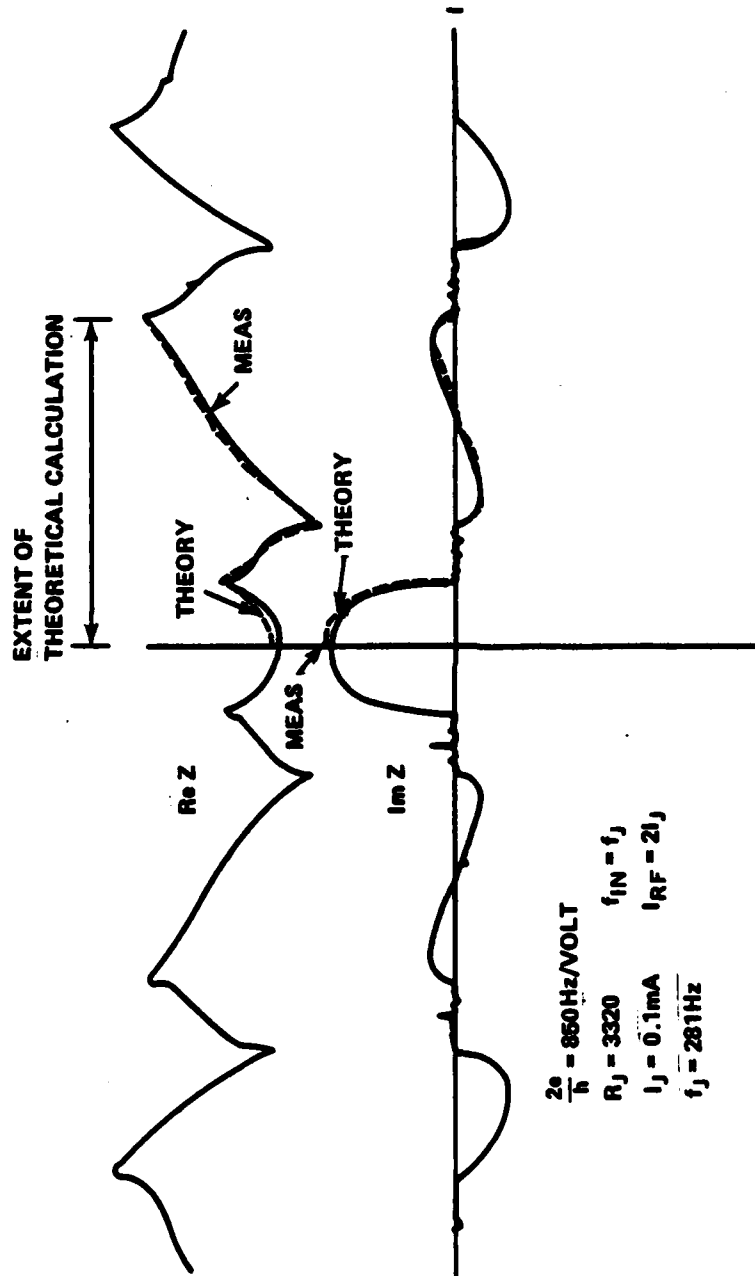


FIGURE 8-3 RF IMPEDANCE OF RSJ ANALOGUE COMPARED WITH CALCULATIONS OF AURACHER AND VAN DUZER³⁴, $f = f_J$

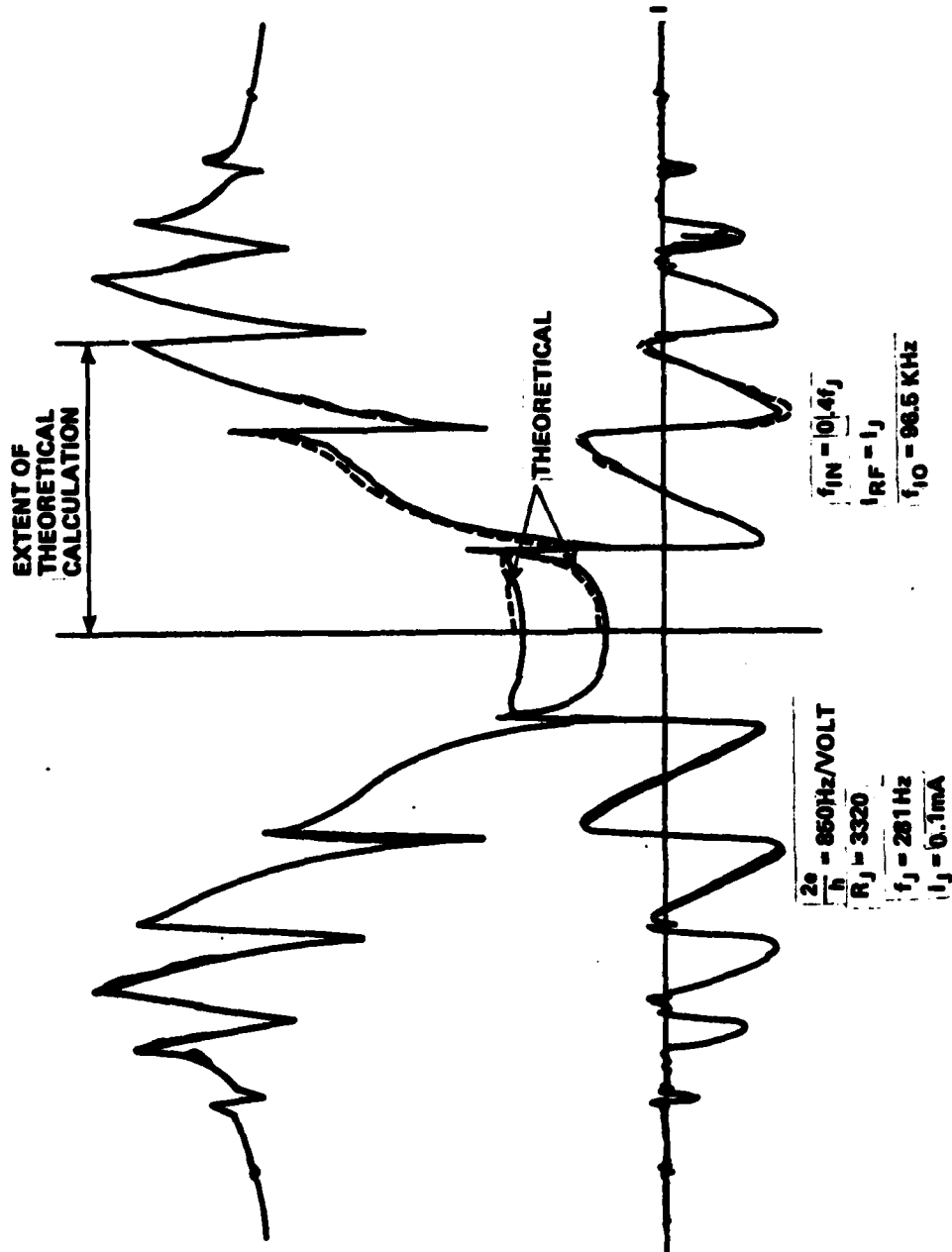


FIGURE 8-9 RF IMPEDANCE OF RSJ ANALOGUE COMPARED WITH CALCULATIONS OF AURACHER AND VAN DUZER³⁴, $f = 10.4f_J$

operated in a high-signal limit, the small-signal theory of Chapters 3 and 6 does not apply.)

In the time since these measurements were made, some improvements have been made to the PSD measuring techniques, and to the analogue itself, and it seems likely that these results could be improved somewhat. Given the constraints of time, this has not been done.

At this stage, the results to be presented begin to fall more into the category of using the analogue, and less into the category of testing it. The discussion will be less in terms of electronics, and more in terms of the physics of the Josephson effects. To emphasize this philosophical transition, the remainder of the results are organized into a separate chapter.

CHAPTER 9

FURTHER RESULTS

9.1 Introduction

With the improvements described in the previous chapter, it became possible to use the analogue to quantitatively model a wide range of experiments. In this chapter, results are presented which illustrate the performance of the analogue in a variety of experimental situations. Where possible, these results are compared with theoretical calculations, and with experimental data obtained from real junctions.

The discussion begins with a presentation of current-voltage characteristics obtained with the analogue using the various filters under different bias conditions. These results illustrate the temperature dependence of the energy gap, Riedel peak, and quasiparticle resistance.

Next is a comparison of analogue data with the step height calculations published by Hamilton.²¹ To the author's knowledge, this is the first time an electronic analogue has been used to measure the properties of photon-assisted tunnelling steps.

This is followed by measurements of the Q of the plasma resonance versus frequency in the RSJ and $T = .72T_c$ limits. The results support the prediction made in chapter 6 that the nonlinearity of $\text{Im } J_1$ can have a major effect on the Q of the plasma oscillations.

Then there is a brief discussion of the effect of series inductance on the dynamics of a voltage biased junction. It was found that the inductance permits parasitic oscillations to occur when the analogue is biased in the region behind the Riedel peak. These oscillations appear to be responsible for the anomalous broadening of the Riedel peak reported in Chapter 4.

Lastly, an explanation is offered to explain the apparently anomalous sub-gap structure observed in some of the measured I-V characteristics of the capacitively shunted analogue.

9.2 Current-Voltage Characteristics at Various Temperatures

Figures 9-1 and 9-2 show the time averaged I-V characteristics of the analogue with the various filters connected. In Figure 9-1, the analogue is voltage biased, and the curves represent $\text{Im } J_1$ as a function of voltage for $T = 0$, $T = .72T_c$, and $T = .9T_c$, as well as for the RSJ limit, where the characteristic is just that of the resistor connected in parallel with the analogue. Except for switching in the various filters, no adjustments were made to the analogue, the drive circuitry, or the plotter between the different measurements. The agreement between Figure 9-1 and the Werthamer theory is quite good. Note how the gap voltage decreases and the leakage current increases as the temperature is reduced. The relationship between gap voltage and temperature is that given by the BCS theory, which is built into the Werthamer theory.⁵

The spikes at zero voltage in Figure 9-1 are caused by the J_2 filters, which were left connected for the experiment. It was found that if the analogue is left very near $V = 0$, the plotter pen will oscillate between $+I_J$ and $-I_J$. This is simply the oscillation of the supercurrent at the Josephson frequency. For large voltages, the Josephson oscillations are rapid enough to be eliminated by the low pass filters used to average V and I . As V approaches zero, the Josephson frequency is small enough to be passed by the filters, and the oscillations are slow enough that the servos in the plotter can trace them out. In Figure 9-1, the voltage

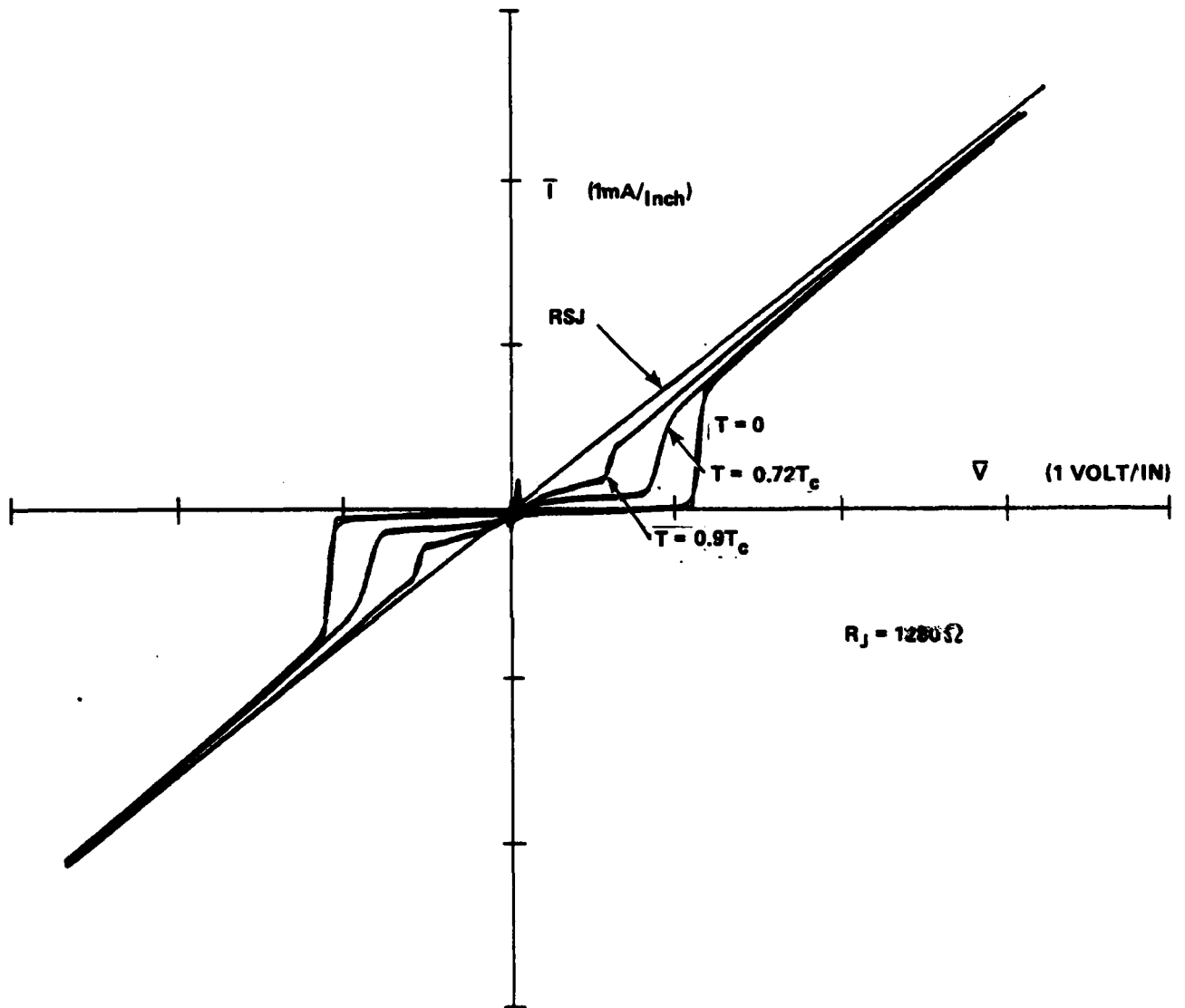


FIGURE 9-1 I-V CHARACTERISTICS OF VOLTAGE BIASED ANALOGUE AT DIFFERENT TEMPERATURES

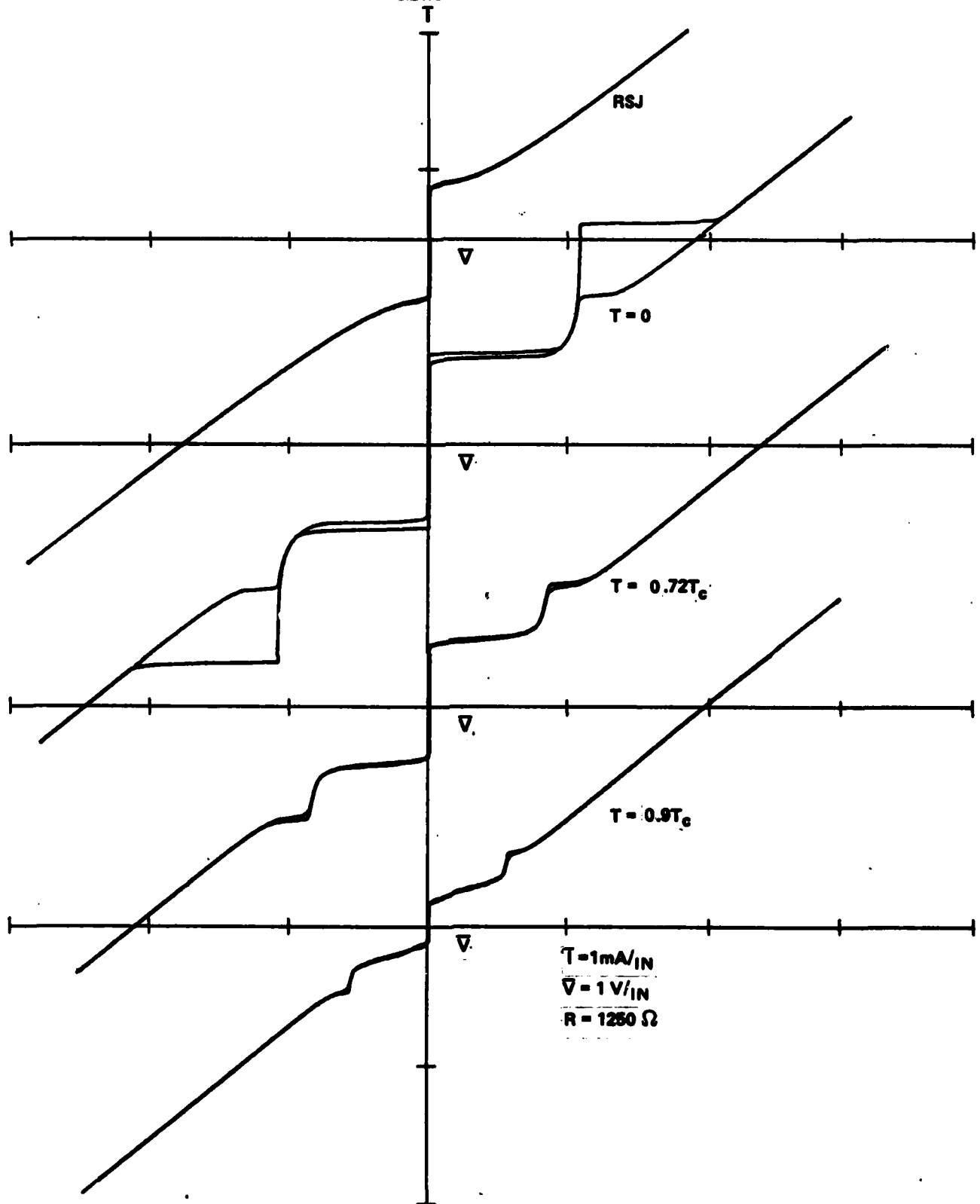


FIGURE 9-2 I-V CHARACTERISTICS OF THE CURRENT BIASED ANALOGUE AT DIFFERENT TEMPERATURES

is swept too rapidly for this to occur to its full extent, but in later experiments, this effect was used to measure the heights of the Josephson steps.

Figure 9-2 illustrates the effect of current bias. No adjustments were made to the analogue or plotter between plotting Figures 9-1 and 9-2. A single switch is used to change the external bias circuitry from a voltage source to a current source. Note how the critical current, as well as the gap voltage and the height of the Riedel peak, decrease with increasing temperature. However, the normal state resistance remains constant.

Figure 9-3 is a prelude to a comparison of analogue results with data published by Hamilton.²¹ The figure shows the effect of "microwaves" at 82.4 Hz on the current and voltage biased characteristics of the analogue with the $T = 0$ filters connected. (82.4 Hz in the analogue is equivalent to 23.4 GHz in a tin tunnel junction.) The current biased characteristic illustrates the hysteresis and smearing effects discussed in chapter 4. Upon switching to voltage bias (the characteristic is reversed in the figure to separate it from the current bias case) the characteristic is much more stable. The Josephson steps appear as spikes centered about $V = 0$, and the photon-assisted tunnelling steps appear as steps centered around the gap voltage. Note that the Josephson steps are spaced twice as closely as the PAT steps, as predicted by theory (cf. Chapter 5).

In switching from current to voltage bias, the RF source went from providing .75mA p-p to providing .75V p-p. If the analogue was in the RSJ limit and the junction resistance was 1000 ohms, then the voltage at the input to the analogue would have approximately the same amplitude (although

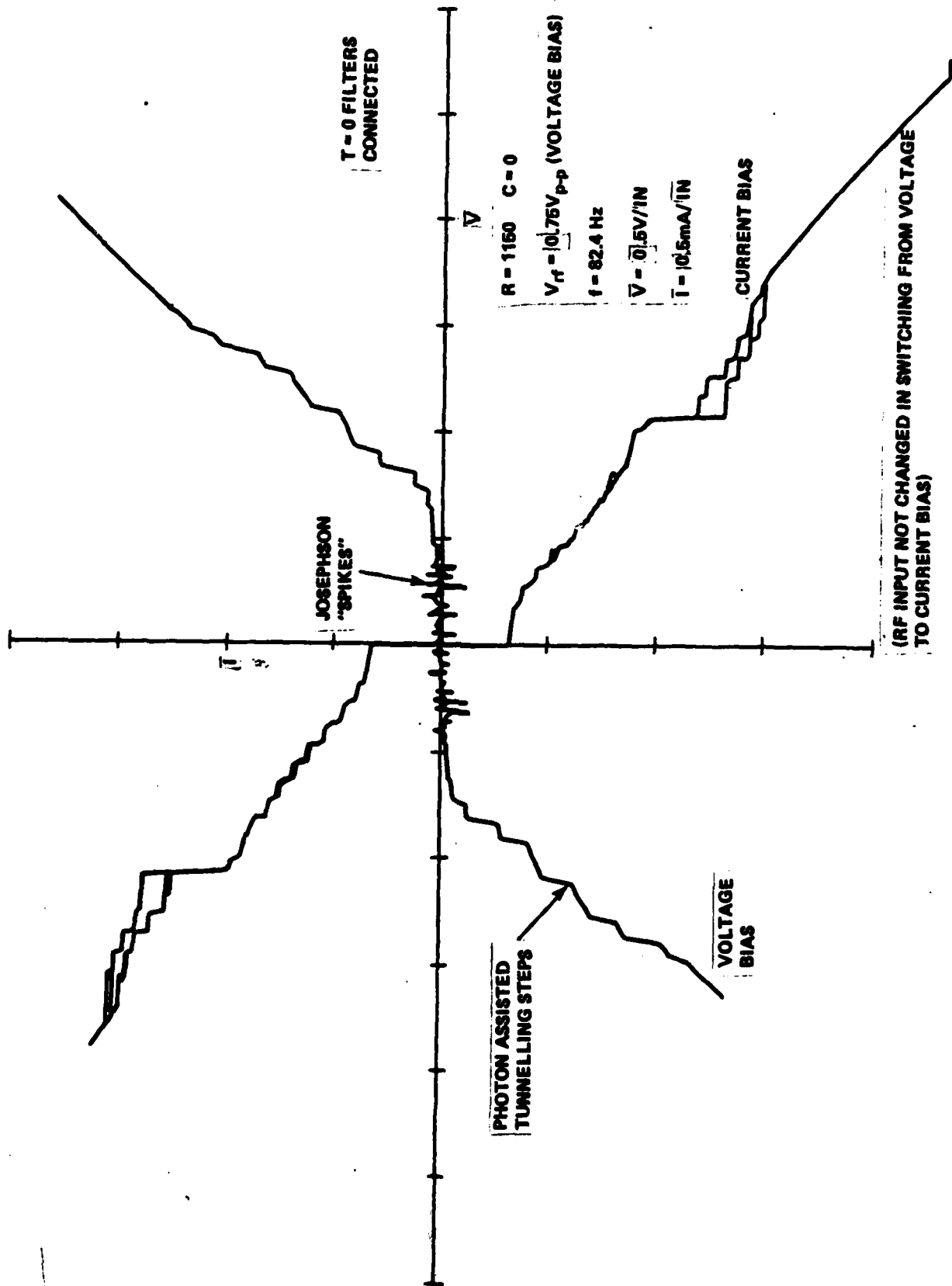


FIGURE 9-3 EFFECT OF RF BIAS ON HIGH FREQUENCY ANALOGUE

different harmonic content) in each case. (In the example shown, the normal state resistance is 1150 ohms.) However, when the $T = 0$ filters are used, the RF resistance at frequencies below the gap frequency will be considerably greater than R_J (cf. eqn. 2-25 and 6-12), and switching from voltage to current bias without adjusting the bias amplitude will cause a big change in the RF voltage at the input to the analogue. Thus, when the analogue is biased at frequencies below the gap frequency $2\Delta/h$, switching from voltage to current bias can be expected to cause a substantial change in the RF impedance and the step heights.

A similar effect occurs if the analogue is current biased at an RF frequency below the gap frequency $2\Delta/h$, and the analogue is switched from the RSJ to the $T = 0$ limit. In this case, the large increase in the quasi-particle resistance below the gap frequency causes a large change in the input voltage, and hence a large change in the RF impedance and step heights.

On the other hand, if the frequency of the RF bias is greater than the gap frequency, switching in the $T = 0$ filters does not cause a dramatic change in the amplitude of the RF voltage for a given level of RF current bias. Thus, if the applied frequency is greater than $2\Delta/h$, switching from the RSJ to the $T = 0$ limits would not be expected to cause as dramatic a change in the RF impedance of the analogue as when the applied frequency is less than $2\Delta/h$.

This helps explain an apparent anomaly in the impedance data presented in chapter 4. The impedance was measured at a particular level of RF current bias with the analogue in the RSJ limit. The $T = 0$ filters were then switched in, but the RF input current was left unchanged. Figure 9-4 shows this for an applied frequency of .4 times the Josephson frequency $2eI_J R_N/h$

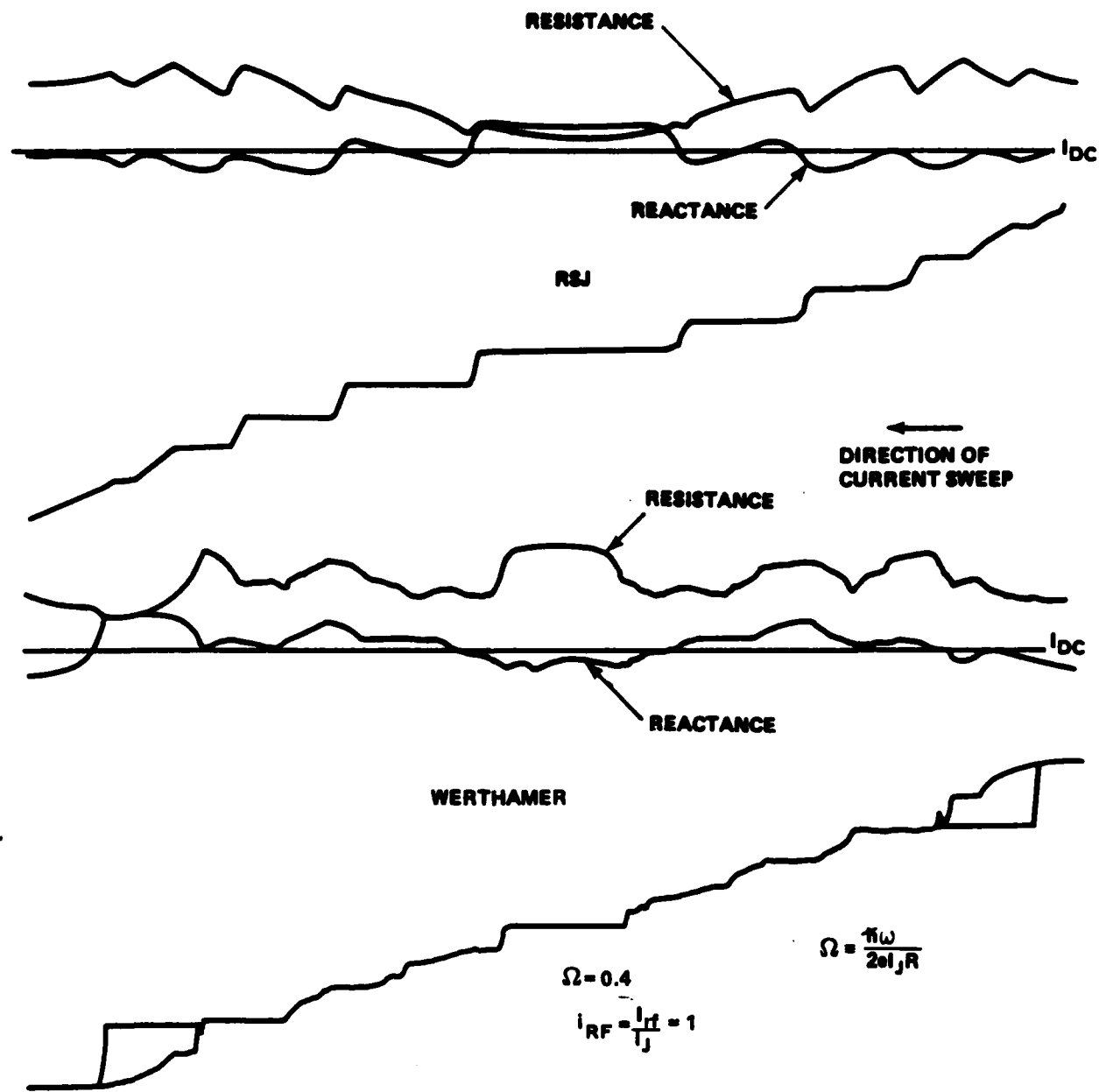


FIGURE 9-4 HIGH FREQUENCY IMPEDANCE I

(cf. Fig. 3-12). The Josephson frequency is $\pi/2$ times the gap frequency, which means that $.4 f_J$ is less than $2\Delta/h$. Note that there is a substantial change in the RF impedance in the two limits.

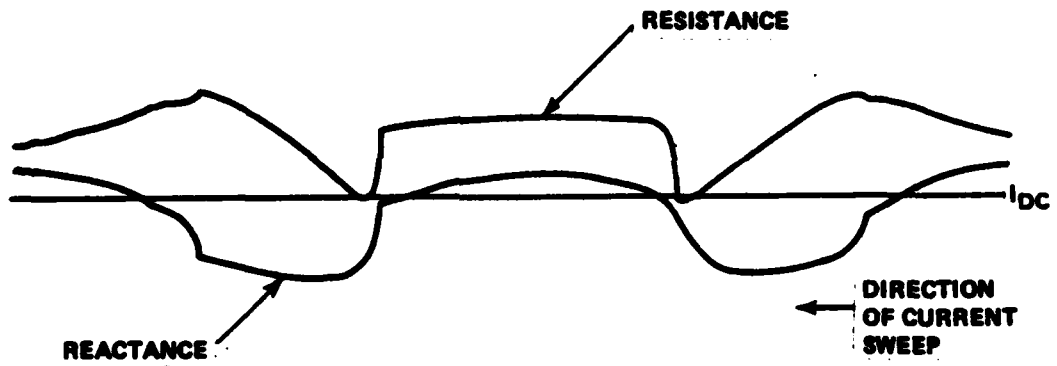
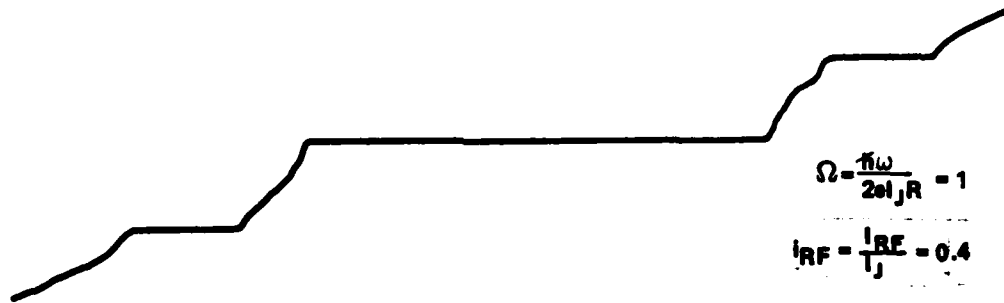
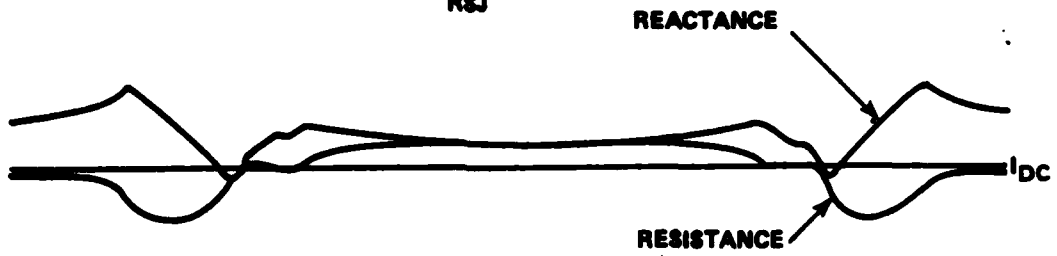
Upon further investigation, it was found that if the RF bias level was scaled downward to compensate for the increase in the quasiparticle resistance, the impedance became similar to the original impedance measured in the RSJ limit (e.g. - inductive instead of capacitive in the zeroth order step). Conversely, it was found that at certain bias levels the impedance in the RSJ limit will be capacitive, instead of inductive, in the zeroth order step; thus, the capacitive reactance shown in Figure 9-4 is not a unique consequence of the Werthamer theory. Furthermore, it was determined that in the high frequency limit, switching off the J_1 filters (e.g. - lowering the RF quasiparticle resistance) had approximately the same effect as reducing the RF current.

Figure 9-5 offers further evidence to support the above argument. In this case, the frequency of the applied RF is equal to the Josephson frequency, and hence greater than the gap frequency. As the analogue is switched between the RSJ and $T = 0$ limits, the change in the RF impedance, particularly in the zeroth order step, is much less drastic than that shown in Figure 9-4.

9.3 Simulation of the Hamilton Experiments

Hamilton has performed a series of experiments directly aimed at verifying certain aspects of the Werthamer theory, most notably the frequency dependence of $\text{Re}J_2$.²¹ Using frequencies in the 25 GHz range, he measured the power and frequency dependences of the Josephson and photon-assisted tunneling steps in tin tunnel junctions. His results, which were compared with

R&J



WERTHAMER

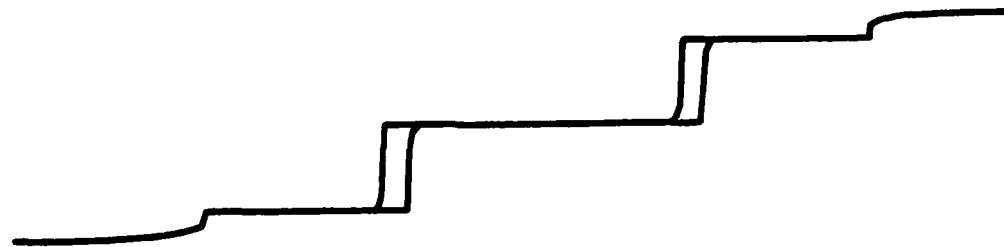


FIGURE 9-5 HIGH FREQUENCY IMPEDANCE II

theoretical calculations, offer strong support for the Werthamer theory.

As 25 GHz is only a small fraction of the gap frequency $2\Delta/h$ of 284 GHz for tin, most of the high frequency corrections to the RSJ model were quite small, and required extremely careful measurement to be observed. For this reason, an electronic simulation of Hamilton's experiments proved to be a challenging test for the electronic analogue. In this section, we describe the results of this test.

Hamilton's data was obtained by measuring the time averaged I-V characteristics of tin tunnel junctions under DC current bias conditions. Although the junctions were small (10^{-6} cm^2), their capacitance was presumed sufficient for the microwave radiation to be treated as a voltage source. This assumption, which was validated by the close agreement between experiment and calculation, greatly simplifies theoretical calculations.

Figure 9-6 shows two I-V characteristics obtained using the analogue with the $T = 0$ filters. The first curve was obtained with the analogue voltage biased with a DC and an RF signal. Both the RF frequency and the RF voltage are scaled to the levels used in Hamilton's experiments. The second curve shows the analogue under current bias conditions, but with a 4 microfarad capacitor across the input. This value was scaled to the estimated capacitance of Hamilton's tin tunnel junctions. Comparison of the step heights in the two cases suggests that Hamilton's assumption that the capacitance causes the junction to look voltage biased at high frequencies is valid. Examination of $V(t)$ on an oscilloscope indicated that harmonics of the applied RF frequency were observable until C was increased to approximately 10 microfarads. However, at $C = 4$ microfarads, the harmonic distortion was only about ten percent. In a real junction, the microwave source impedance

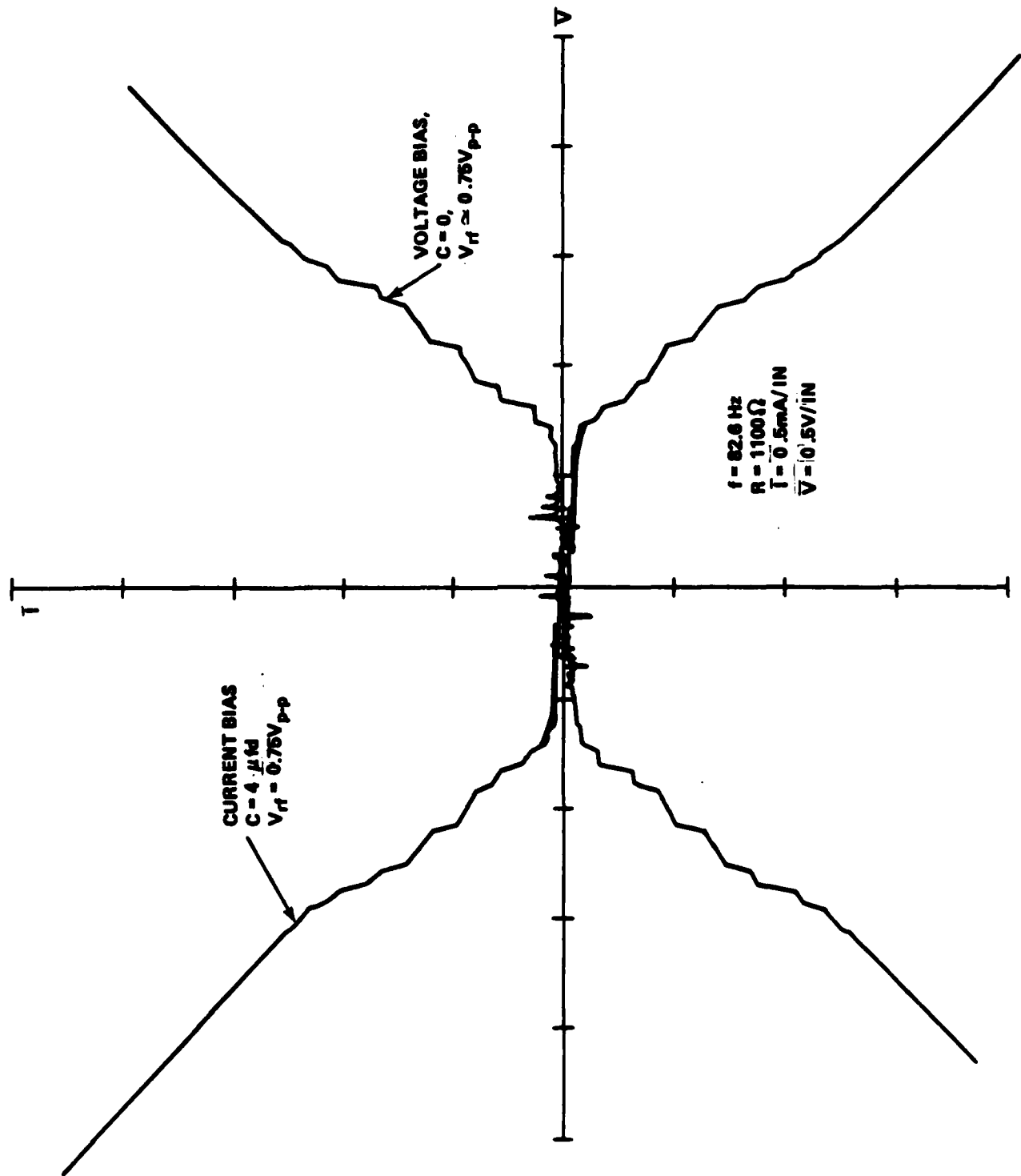


FIGURE 9-6 COMPARISON OF CURRENT BIAS WITH A CAPACITOR WITH VOLTAGE BIAS AND NO CAPACITOR

in the absence of a capacitor is unlikely to be as high as the source impedance of the current source in the analogue. Thus, Hamilton's assumption is probably more valid for a real junction than it is for the case described above.

Because of the existence of supercurrents, the relationship between the applied RF current and the RF voltage across the analogue was extremely non-linear at low values of RF current. This made it difficult to accurately adjust the voltage across the analogue by varying the current. In addition, it was found that the I-V characteristics under current bias conditions were often unstable, and exhibited much hysteresis, sub-gap structure, and complicated interactions between photon steps and Josephson steps. Furthermore, when capacitance was added, half harmonic steps began to appear. (The appearance of half-harmonic structure when there is shunt capacitance is predicted by the RSJ model. It is not surprising to observe it in the high frequency model as well.)⁵⁰ The net result of all this is that the current biased characteristics are quite complicated and difficult to interpret, whereas the voltage biased characteristics behave in a relatively simple and predictable manner. For this reason, it was decided to simulate the Hamilton experiments using the analogue with a voltage source and no capacitance.

In Figure 9-6, the Josephson steps show up as spikes whose heights could be measured by changing the voltage very slowly, and allowing the plotter to sweep out the Josephson oscillations as f_J became very small. To make sure that the spikes were fully traced out, 50 ohms of series resistance was added to the voltage source. This reduced the slope of the load line which traces out the spike, and ensured that the current at a spike didn't change too

rapidly for the servo motors in the plotter to respond. It was verified that the 50 ohm resistance has a negligible effect on the amplitude and harmonic content of the input voltage. It might be noted that the change in the spike shape upon introduction of the additional 50 ohms indicates that the original output impedance of the voltage source is quite small. Some typical current-voltage relationships obtained in this way are shown in Figure 9-7. Note that the supercurrent Josephson spikes, which depend on $\text{Re } J_2$, are quite different from the photon-assisted tunnelling steps, which can be looked upon as images of the discontinuity in $\text{Im } J_1$. Most of the data on step heights was obtained from plots such as those in Figure 9-7.

Before presenting any further results, it is useful to review some aspects of the Werthamer theory that are relevant to the measurement of step heights. Equations 9-1 and 9-2 show the theoretical expressions for the DC current at a step for the cases of pair tunnelling and quasiparticle tunnelling, respectively.²¹ Equation 9-3 shows the expression for the DC current of a Josephson step in the RSJ limit. (There are no PAT steps in the RSJ limit.)

$$I_{dc}(V_{dc}) = \sum_N \left| \sum_n J_n(\alpha) J_{N-n}(\alpha) \text{Re} J_2((2n - N)f) \right| \delta(V_{dc} \pm Nhf/2e) \quad (9-1)$$

$$I_{dc}(V_{dc}) = \sum_n J_n^2(\alpha) \text{Im} J_1(V_{dc} + nhf/e) \quad (9-2)$$

$$I_{dc}(V_{dc}) = \text{Re} J_2(0) \sum_N |J_N(2\alpha)| \delta(V_{dc} \pm Nhf/2e) \quad (9-3)$$

where delta is the Kronecker delta function, and $\alpha = eV_{rf}/hf$.

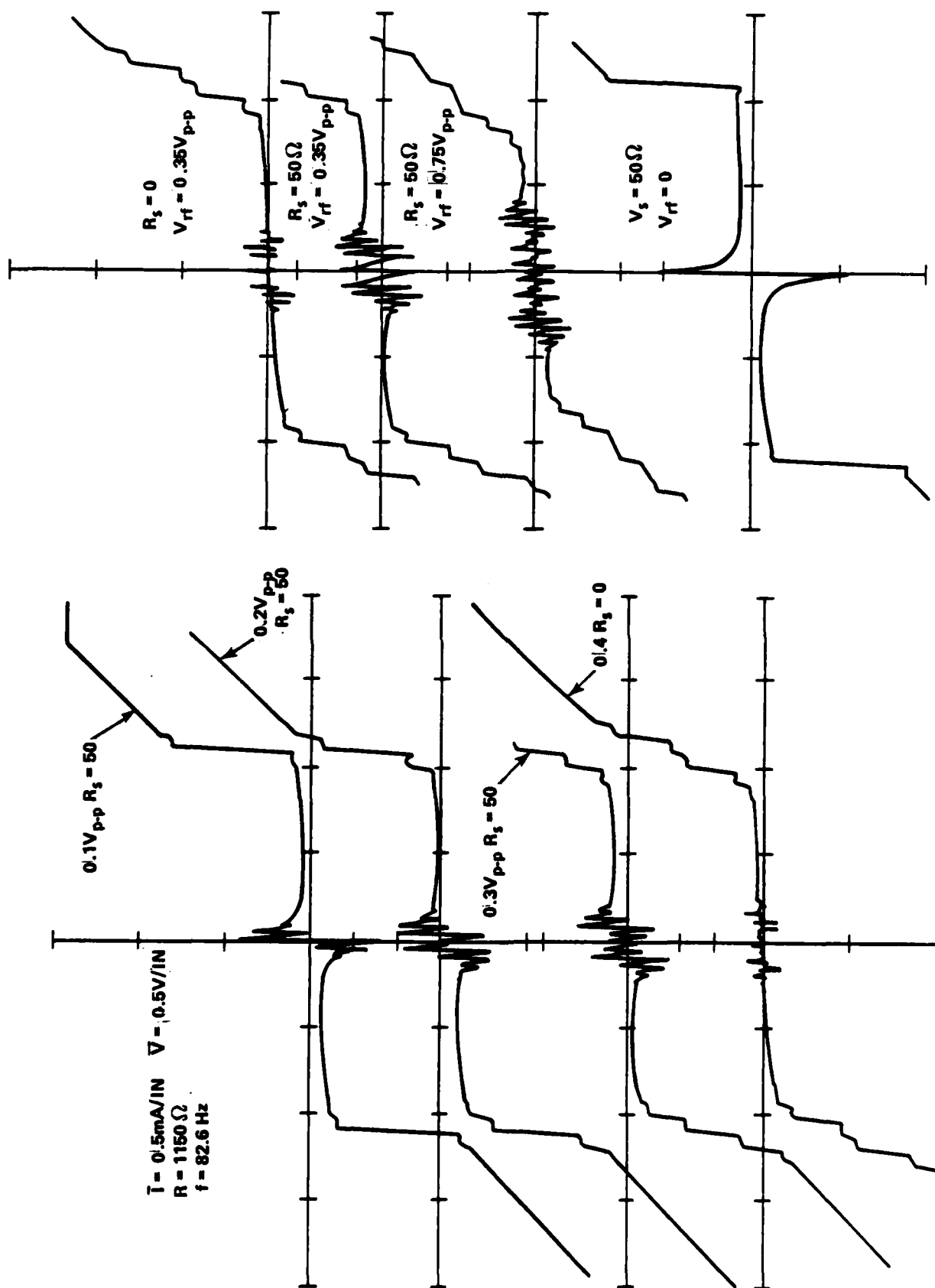


FIGURE 9-7 EFFECT OF 50Ω SOURCE IMPEDANCE ON VOLTAGE BIASED CHARACTERISTICS

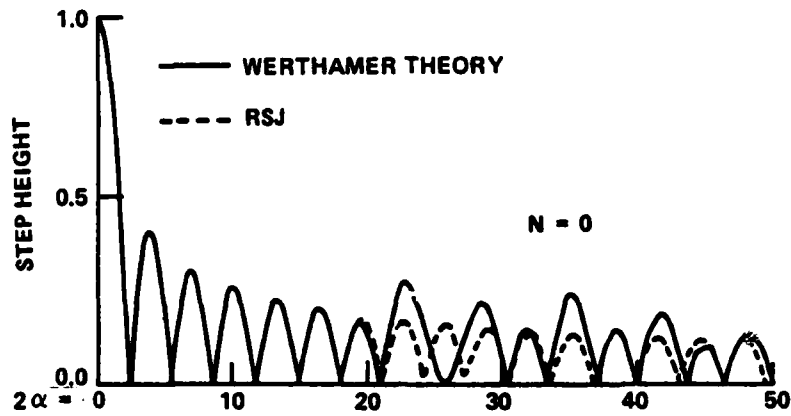
Note that the Josephson steps occur at $V_{dc} = Nh\bar{f}/2e$. The photon-assisted tunnelling steps occur when the argument of $\text{Im } J_1$ is equal to $2\Delta/e$, which is when $V_{dc} = (2\Delta/e \pm nh\bar{f}/e)$.

The above equations are obtained by letting the junction voltage = $V_{dc} + V_{rf} \cos 2\pi f t$ and solving for the current using equations 2-1 and 2-4. Note that the step heights in the high frequency case are proportional to $J_n^2(\alpha)$ as opposed to $J_n(2\alpha)$, as predicted by the RSJ theory.* This results from the use of the quantities $\sin \phi/2$ and $\cos \phi/2$ in the Werthamer theory, instead of $\sin \phi$ and $\cos \phi$ as in the RSJ theory. If the amplitude of $\text{Re } J_2$ and the slope of $\text{Im } J_1$ are treated as being constant, then the summations in 9-1 will converge to that of 9-3. Because there is no discontinuity in $\text{Im } J_1$ in the RSJ limit, the PAT steps disappear.

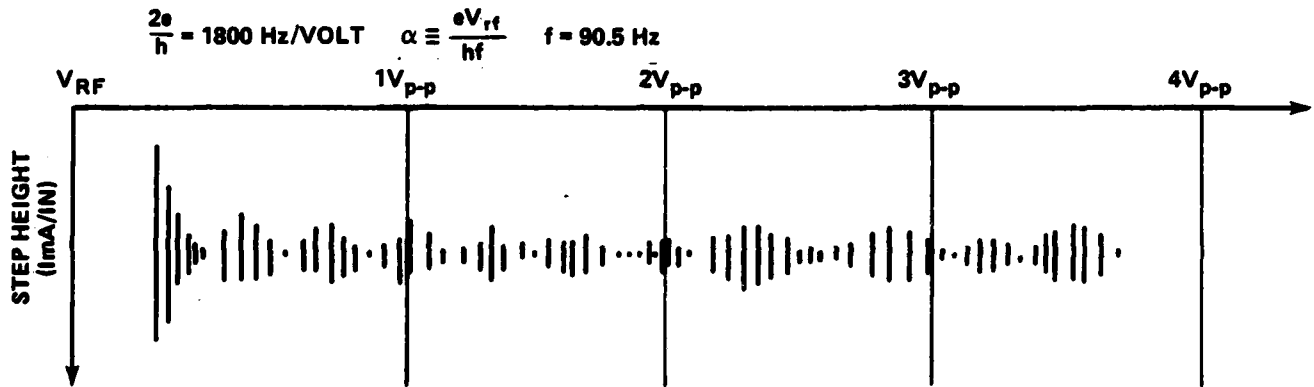
The photon-assisted tunnelling steps are readily apparent in the measured characteristics of the analogue. However, the effect of the Riedel singularity on the heights of the Josephson steps is minimal until large values of α are reached. This is shown in Figure 9-8a, where Hamilton has used equations 9-1 and 9-3 to calculate the variation of the height of the $N = 0$ Josephson step as a function of input power for both the RSJ and Werthamer cases.²¹ Note that no differences are observed until the seventh zero of the step height has occurred.

Figures 9-8b and 9-8c show results obtained with the analogue in both the RSJ and $T = 0$ cases. The horizontal axis corresponds to the RF voltage, as measured with a lock-in amplifier. The vertical lines were obtained by letting the plotter pen oscillate for several seconds as the analogue remained biased in the zeroth order step. The 50 ohm source impedance was deleted, and

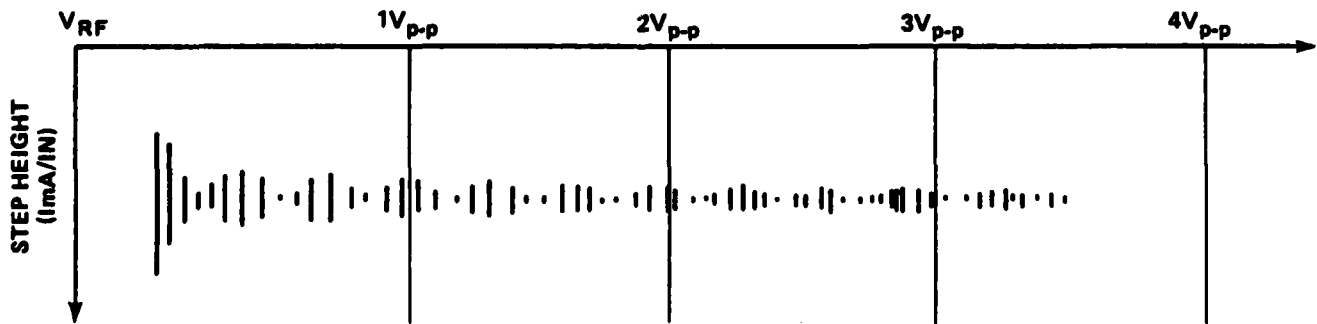
* $\alpha = eV_{rf}/h\bar{f}$



9-8a. THEORETICAL PREDICTION (AFTER HAMILTON⁵⁹)



9-8b. ANALOGUE IN WERTHAMER LIMIT, $T = 0$



9-8c. ANALOGUE IN RSJ LIMIT

FIG. 9-8 VARIATION OF $N = 0$ JOSEPHSON STEP WITH R-F VOLTAGE

the measurement of the step height is relatively inaccurate. However, note the good qualitative agreement between the analogue and calculations based on equations 9-1 and 9-3, particularly in the 2 to 4 volt region.

The VCO gain constant of the analogue was such that e/h was 900 Hz/volt. The dimensionless quantity $\alpha = eV_{rf}/(hf)$ scales quite well between the analogue and Hamilton's calculation. The difference in relative step heights between the $T = 0$ and RSJ limits is a factor of $\pi/2$, which is the DC gain of the J_2 filters used in the analogue. (Removing the J_2 filters for the RSJ case lowers the critical current by this amount.)

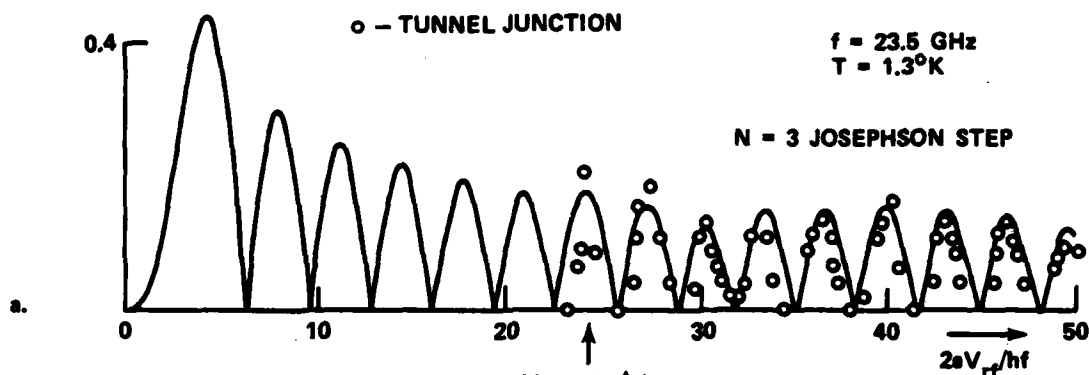
Figure 9-9a shows the height variation of the $N = 3$ Josephson and the $n = 3$ PAT steps, as calculated by Hamilton using equations 9-1 and 9-2. The circles are experimental points obtained by Hamilton using a tin tunnel junction at 1.3K with applied RF at 23.5 GHz. Note that Hamilton was only able to obtain data for large values of α for the $N = 3$ Josephson step, and small values of α for the $n = 3$ PAT step. The former limitation resulted from hysteresis in the current biased characteristic at low power levels, which made some of the Josephson steps inaccessible to measurement. The latter restriction arose from the problem of Josephson steps obscuring the PAT steps at large values of RF power. (As the RF power is increased, Josephson steps begin to appear away from $V_{dc} = 0$, whereas PAT steps begin to appear away from $V_{dc} = 2\Delta/e$. Eventually, the two interfere with each other.)

Neither of the above restrictions applied to the analogue. As the analogue was voltage biased, hysteresis wasn't present. When the Josephson spikes started interfering with the PAT steps, either the J_1 or J_2 filters could be temporarily disconnected. (Note that equations 9-1 and 9-2 are completely independent. In the voltage biased limit, disconnecting one set

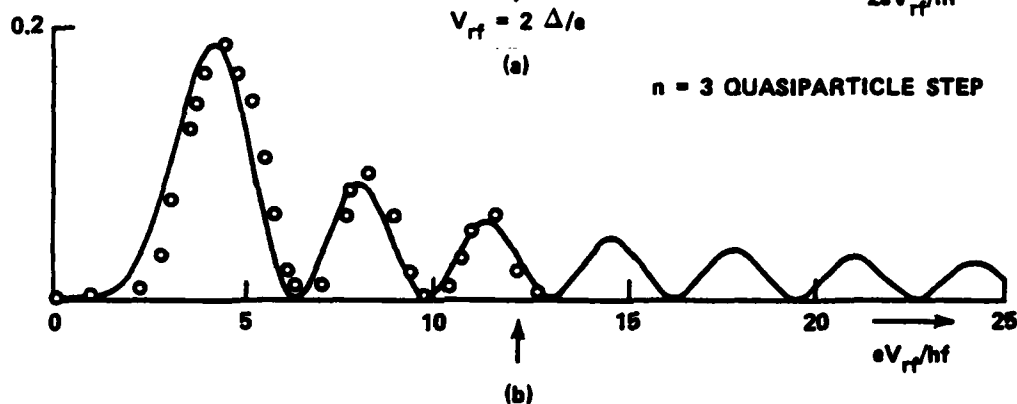
○ - TUNNEL JUNCTION

 $f = 23.5 \text{ GHz}$
 $T = 1.3^\circ \text{K}$

N = 3 JOSEPHSON STEP

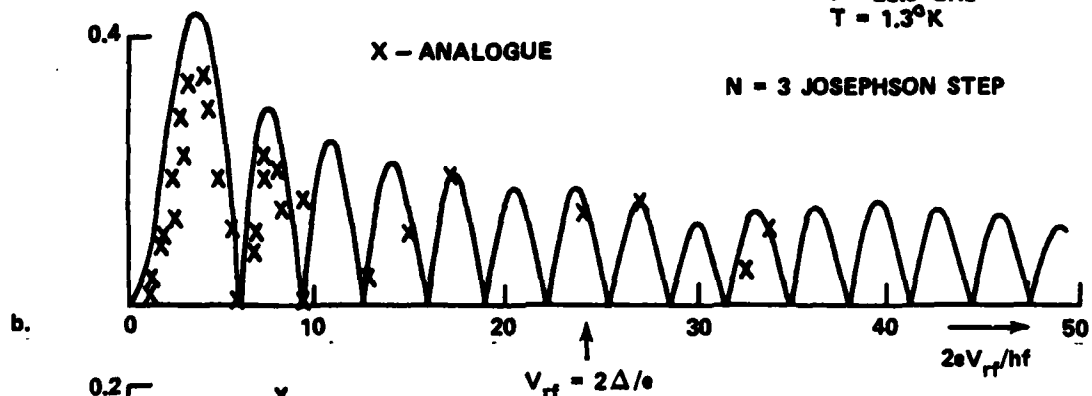


n = 3 QUASIPARTICLE STEP


 $f = 23.5 \text{ GHz}$
 $T = 1.3^\circ \text{K}$

X - ANALOGUE

N = 3 JOSEPHSON STEP



n = 3 QUASIPARTICLE STEP

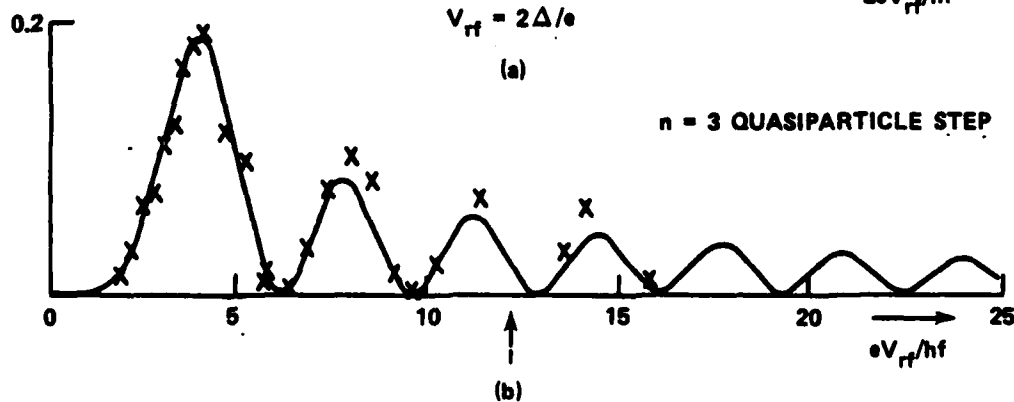


FIGURE 9-9 VARIATION OF N = 3 JOSEPHSON AND n = 3 PAT STEPS WITH R-F POWER
 (AFTER HAMILTON)²¹

of filters will not affect the steps due to the other set of filters.)

Figure 9-9b shows results obtained with the analogue, scaled to and plotted on top of Hamilton's results. As before, the scaling of normalized step height, frequency, and voltage was reasonably accurate. The only correction factor was that the PAT steps were normalized to the measured height of the discontinuity in $\text{Im } J_1$ at the gap, which is slightly higher than its theoretical value of $\text{Re } J_2(0)$ (cf. section 8.7). The Josephson steps were normalized to the measured critical current.

The inaccuracies can be attributed to filter error, any misadjustment of analogue calibration settings, and error in determining V_{rf} . All things considered, the results are reasonable, although they probably could be improved if the measurement were done with less attention to time and more attention to accuracy. The locations of the zeros, which are independent from the filter responses, are in good agreement with theory, which suggests that the VCO and "mainframe" circuitry are functioning well. It should be pointed out that in the voltage bias limit, the $\cos \phi$ term due to $\text{Im } J_1$ does not appear in the equations for the step heights. However, the unwanted phase shift due to the low pass filters will modify slightly the effective amplitudes of $\text{Re } J_2$ and $\text{Im } J_2$, but this effect should be minimal.

The next figure illustrates the frequency dependence of the $N = 0$ Josephson step at a given level of RF bias. Figure 9-10a shows Hamilton's calculations compared with his experimental data for tin as the frequency is varied between 23 and 26 GHz. The dashed line refers to the theoretical prediction of the RSJ theory, namely that the step height in the voltage biased limit is independent of frequency. Figure 9-10b shows the same results, but with data from the analogue superimposed. The analogue data was

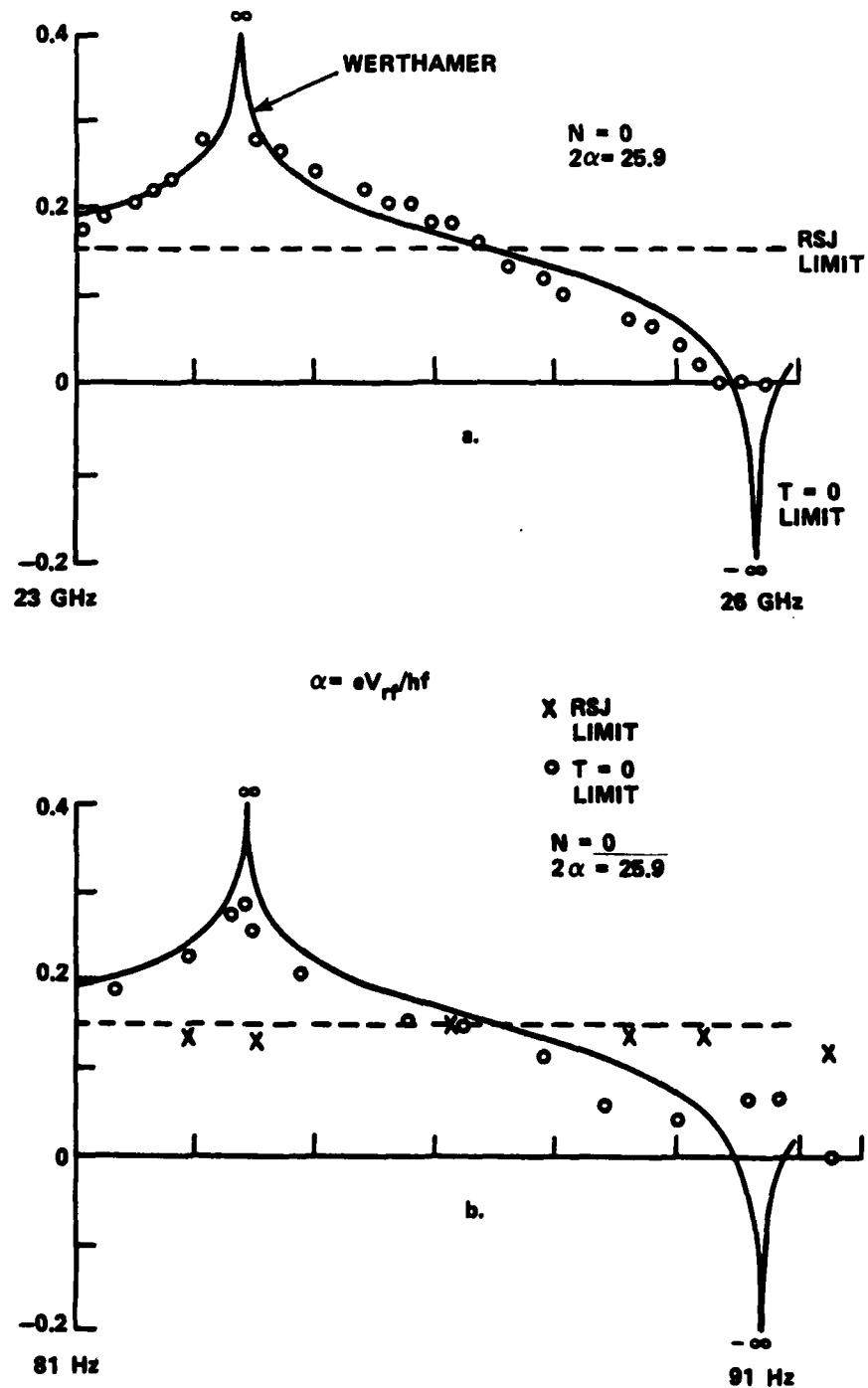


FIGURE 9-10 VARIATION OF $N = 0$ JOSEPHSON STEP WITH FREQUENCY (AFTER HAMILTON)²¹

obtained by varying the frequency from 81 to 91 Hz at a particular level of RF voltage. The measurement is very sensitive to slight variations in V_{rf} , and misadjustment of V_{rf} is probably the prime source of error. (Note that Hamilton's calculations allow for negative step heights; the absolute value should be taken as shown in 9-10b.)

The last figure in this section (Fig. 9-11) is a comparison of an I-V characteristic calculated on a desktop computer with a measurement done using the analogue. The analogue measurement is presented both separately and as an overlay to the digital computation. The J_2 filters were disconnected, and the analogue was voltage biased. Using equation 9-2, it took the Hewlett-Packard 9835 system several hours to calculate the curve. The analogue completed the measurement in less than 15 seconds.

As it stands, the results presented above could almost certainly be improved. However, it was decided not to dote on the measurement of step heights, but to proceed with measurements of the plasma resonance using some of the finite temperature filters.

9.4 The Plasma Resonance

The improvements to the analogue described in the previous chapter, as well as the availability of improved measuring equipment, made it worthwhile to repeat the plasma resonance experiments discussed in Chapter 4 (cf. Fig. 4-32 and 4-33). The experimental setup is relatively simple, and is outlined in Figure 9-12. The analogue is shunted with a capacitor, and current biased within the zeroth order step. At low input levels, the device behaves as a parallel RLC network whose inductance is determined by the equilibrium value of cosine phi, which in turn is determined by the DC current. A frequency response analyzer (FRA) is used to generate the AC current. The voltage at

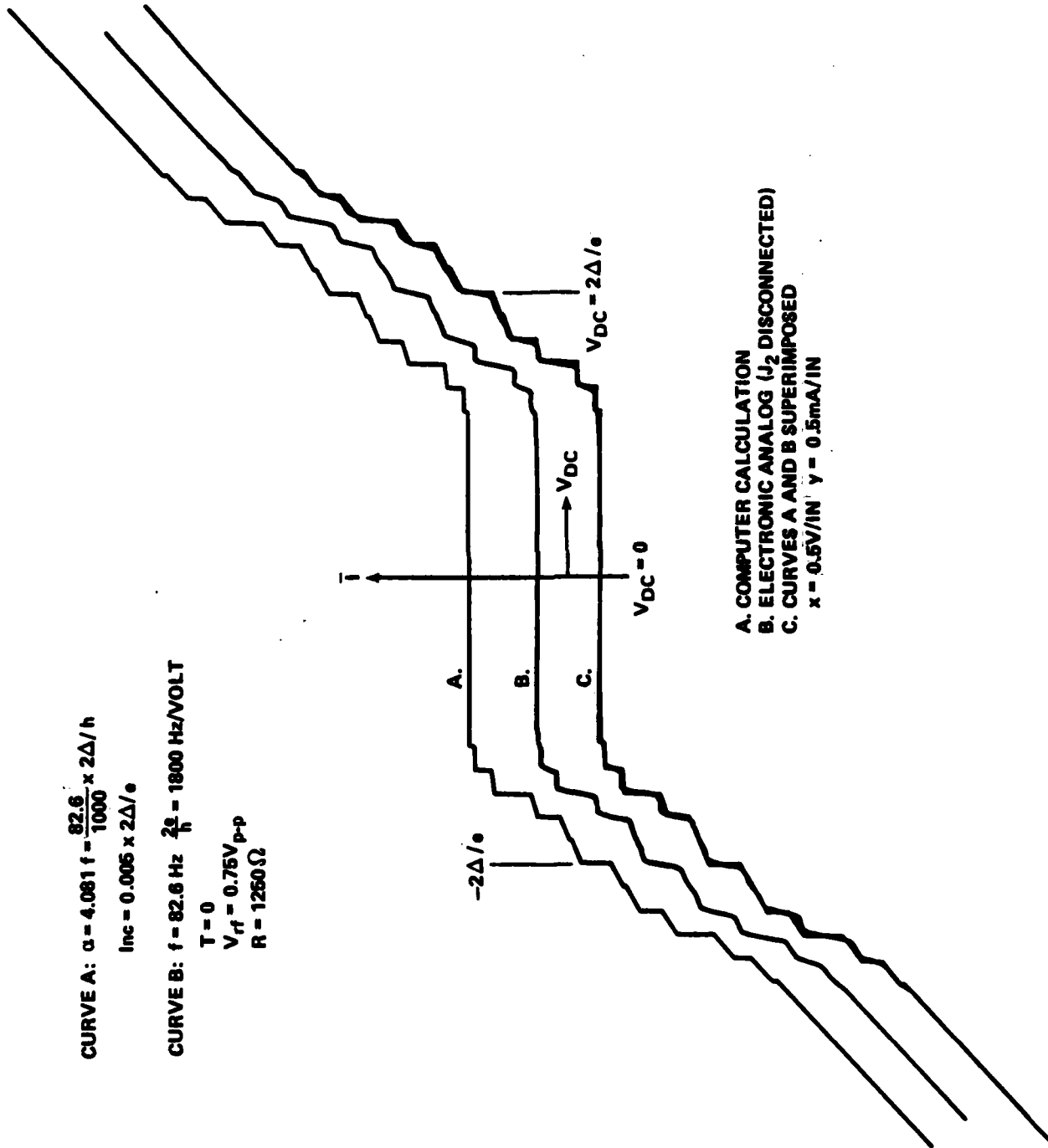
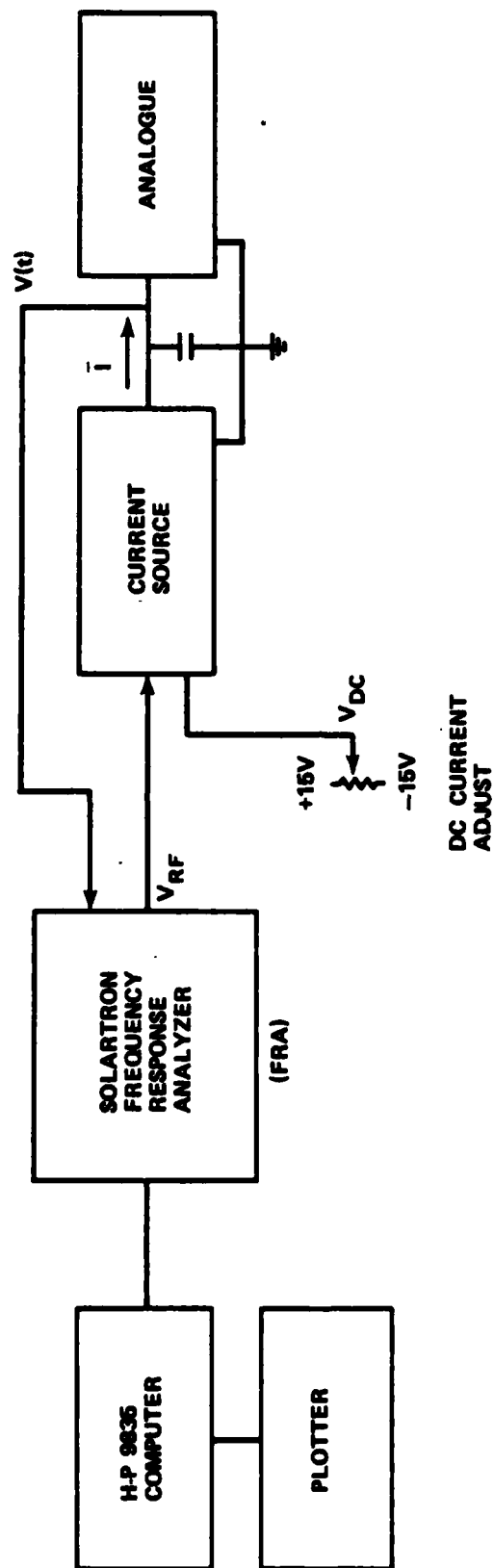


FIGURE 9-11. PHOTON ASSISTED TUNNELLING STEPS: DIGITAL COMPUTER VERSUS THE ELECTRONIC ANALOGUE



FRA GENERATES A SIGNAL $V_{RF} = A \sin \omega t$
 CURRENT SOURCE GENERATES $I = G(V_{DC} + V_{RF})$ $G = 1 \text{ mA/VOLT}$
 FRA AND COMPUTER COMPARE $V(t)$ WITH V_{RF} TO DETERMINE COMPLEX IMPEDANCE AT VARIOUS
 VALUES OF ω , I_{DC}

FIGURE 9-12 SETUP FOR PLASMA RESPONSE EXPERIMENT

the input to the analogue is returned to the FRA, which measures its amplitude and phase relative to the current. This information is stored in a desktop computer, and is processed upon completion of a series of measurements.

The first experiments were done using a simple RSJ analogue containing a twin-T filter. Typical results are shown in Figure 9-13, which shows the impedance as a function of frequency for several values of cosine phi. At resonance, the height of an impedance curve in Figure 9-13 is proportional to the resistance. In the figure, a height of 1 corresponds to $R = R_J$. When the height is greater than 1, as is the case for large values of cos phi, it means that the negative cos phi amplitude is causing the apparent value of the junction resistance to increase. Since $Q = \omega_p RC$, the amplitude of the impedance at resonance is proportional to the Q. The variation of R with cos phi is given by:

$$R = R_J / (1 + \gamma \cos \phi) \quad (9-4)$$

This curve is plotted for $\gamma = -.057$ as the envelope containing the maxima of the curves for the real part of the impedance. This represents a "best fit" to the data. However, the predicted value of gamma was $-.031$. This was verified by independent measurement of the low pass filter response. It turned out that the cumulative phase shift of the remainder of the analogue was responsible for the remaining contribution to gamma.

To emphasize the effect of a negative cos phi amplitude on the impedance of the analogue, the low pass filter was replaced by a filter having a relative cos phi amplitude of $-.83$. The effects of this are illustrated in Figure 9-14. Note that for cosine phi = 1, the junction's resistance is almost six times as great as R_J . An envelope to the impedance maxima based on a value of

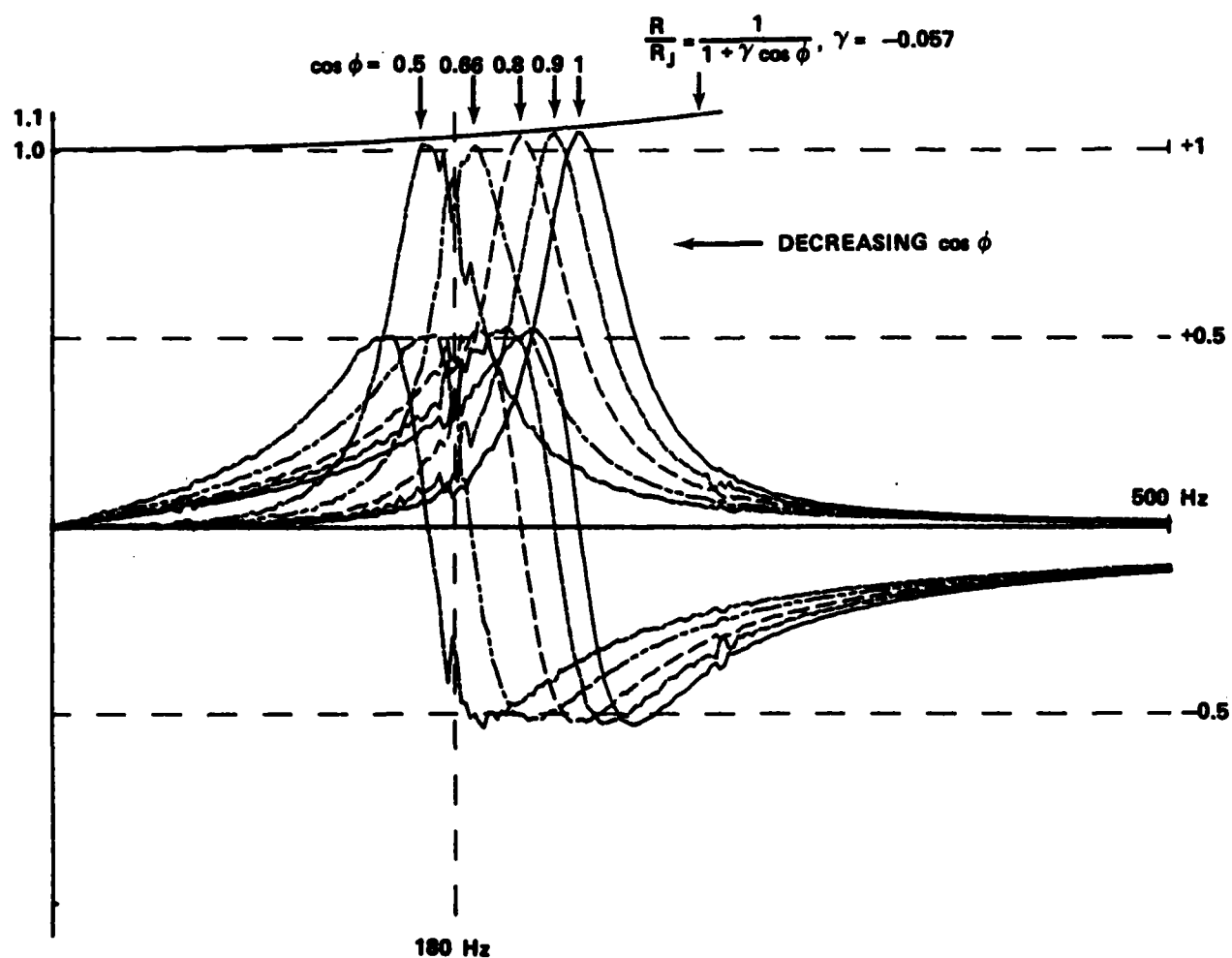


FIGURE 9-13 IMPEDANCE VS FREQ FOR THE RSJ ANALOGUE SHUNTED BY A CAPACITOR (SMALL-SIGNAL LIMIT)

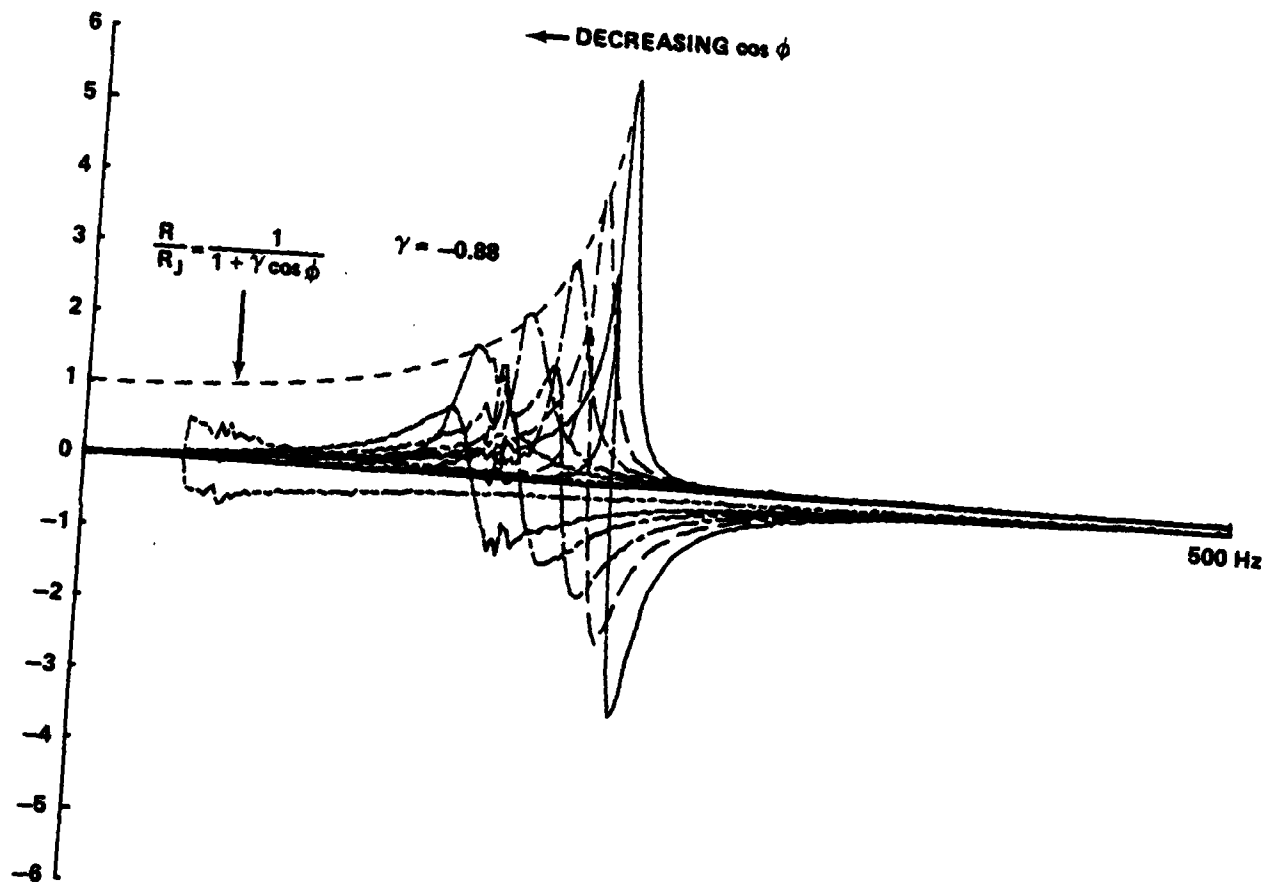


FIGURE 9-14 EFFECT OF LOW PASS FILTER ON Q OF PLASMA RESONANCE

$\gamma = -.88$ is plotted in the figure. Note that as cosine ϕ goes to zero, the junction resistance approaches R_j . The difference between the predicted γ of $-.83$ and the value of $-.88$ can be attributed to a combination of extra phase shift contributions in the circuit, and conservatism in fitting the envelope curve.

Measurements of the Q of the resonance curves from the bandwidth of the impedance curves are consistent with measurement of Q from the resistance of the analogue at resonance. These results are summarized in Table 9-1.

The above measurements were repeated using the high frequency analogue with the $T = .72T_c$ filters at a nominal plasma frequency of 500 Hz. At this frequency, the $\cos \phi$ amplitude is small (approx. $+ .026$), and is expected to have relatively little effect on the apparent resistance of the analogue. The measurements were first made using only the J_2 filters, so that the shunt resistance was constant, independent of frequency. The experiment was then repeated with no changes except to connect the J_1 filters to introduce a frequency dependent value of shunt resistance.

Figure 9-15 shows the I-V characteristics of the analogue in the $T = .72T_c$ mode with both J_1 and J_2 connected, with and without capacitance; and with only the J_2 filter connected, with and without capacitance. The voltage biased limit, with both J_1 and J_2 connected and $C = 0$, is also shown to illustrate the variation of $\text{Im } J_1$ with voltage (and frequency).

Figure 9-16 shows the variation of impedance with cosine ϕ with the J_1 filters disconnected. Note the small variation of the impedance at resonance with $\cos \phi$. This indicates that the effect of the $\text{Im } J_2 \cos \phi$ amplitude is minimal, as expected. In this and the next figure, the vertical axis is scaled in units of 1000 ohms. The amplitudes of the maxima are

TABLE 9-1 F_p AND F_p/Q FOR THE RSJ ANALOGUE FOR TWO
DIFFERENT VALUES OF COS PHI COEFFICIENT

Vin(rms)	cos phi	F_p (meas)	F_p (pred)	F_p/Q (meas)	F_p/Q (pred)
----------	---------	--------------	--------------	----------------	----------------

With only a Twin-T filter:

(F_p/Q (pred) is calculated using $\gamma = -.03$)

.05	1	236	237.7	45	45.3
.015	.9	225	225.5	46	45.4
.025	.9	225	225.5	44	45.4
.05	.8	210	212.6	46	45.6
.05	.66	187	193.1	46	45.8
.025	.5	168	168.1	46	45.0

With the addition of a low pass filter:

(F_p/Q (pred) based on $\gamma = -.83$)

.015	1	230	237.7	8	7.9
.025	1	226	237.7	9	7.9
.015	.9	220	225.5	11	11.8
.015	.8	208	212.6	15	15.7
.015	.66	190	193.1	24	21.1
.015	.5	168	168.1	24	27.3

(Note, the measurement of F_p/Q with the LPF connected is suspect, as some of the curves were showing non-Lorentzian behavior, and it was not always obvious what value should be used for the half power bandwidth.)

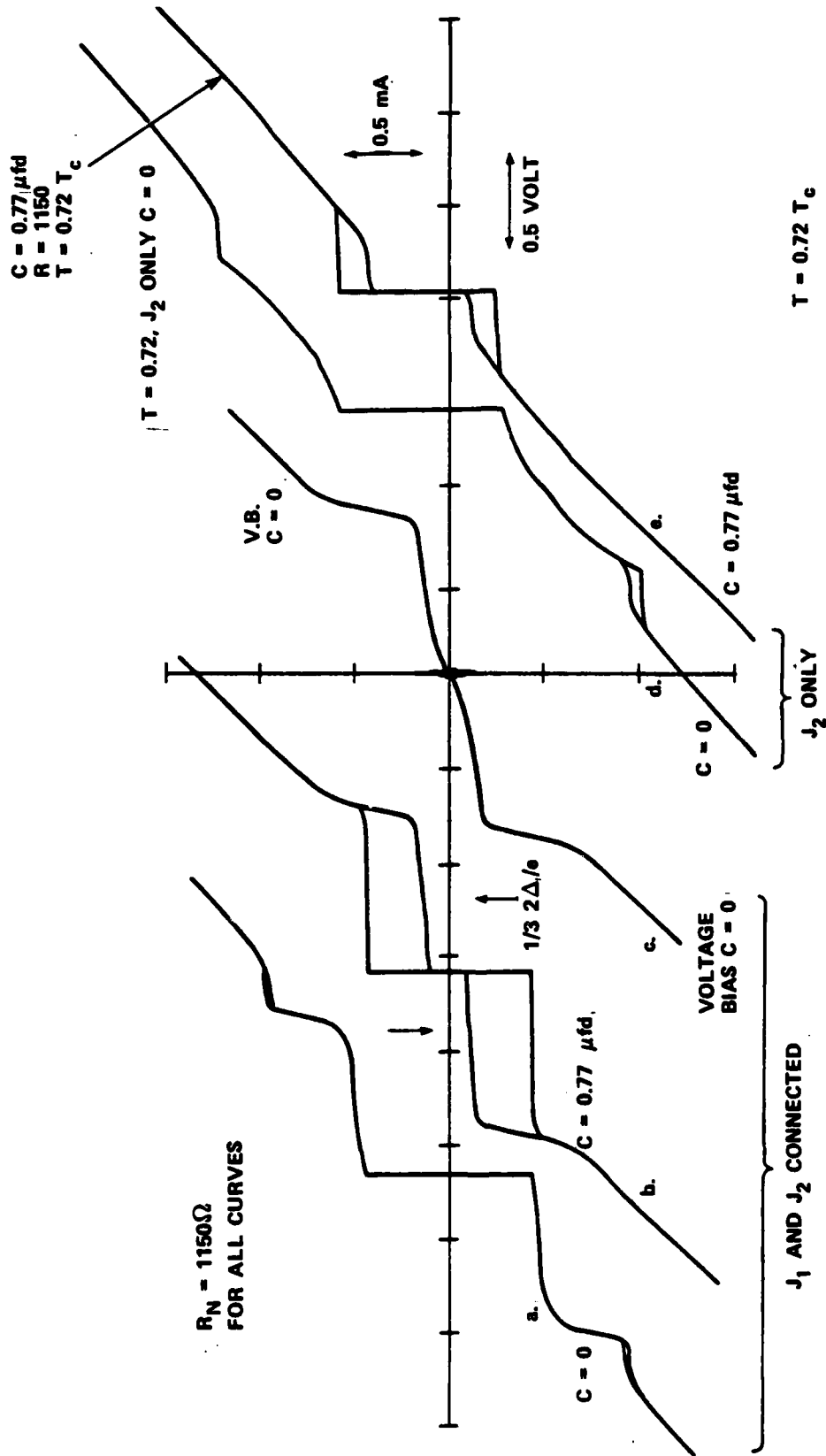


FIGURE 9-15 I-V CHARACTERISTICS FOR T = 0.72 T_c

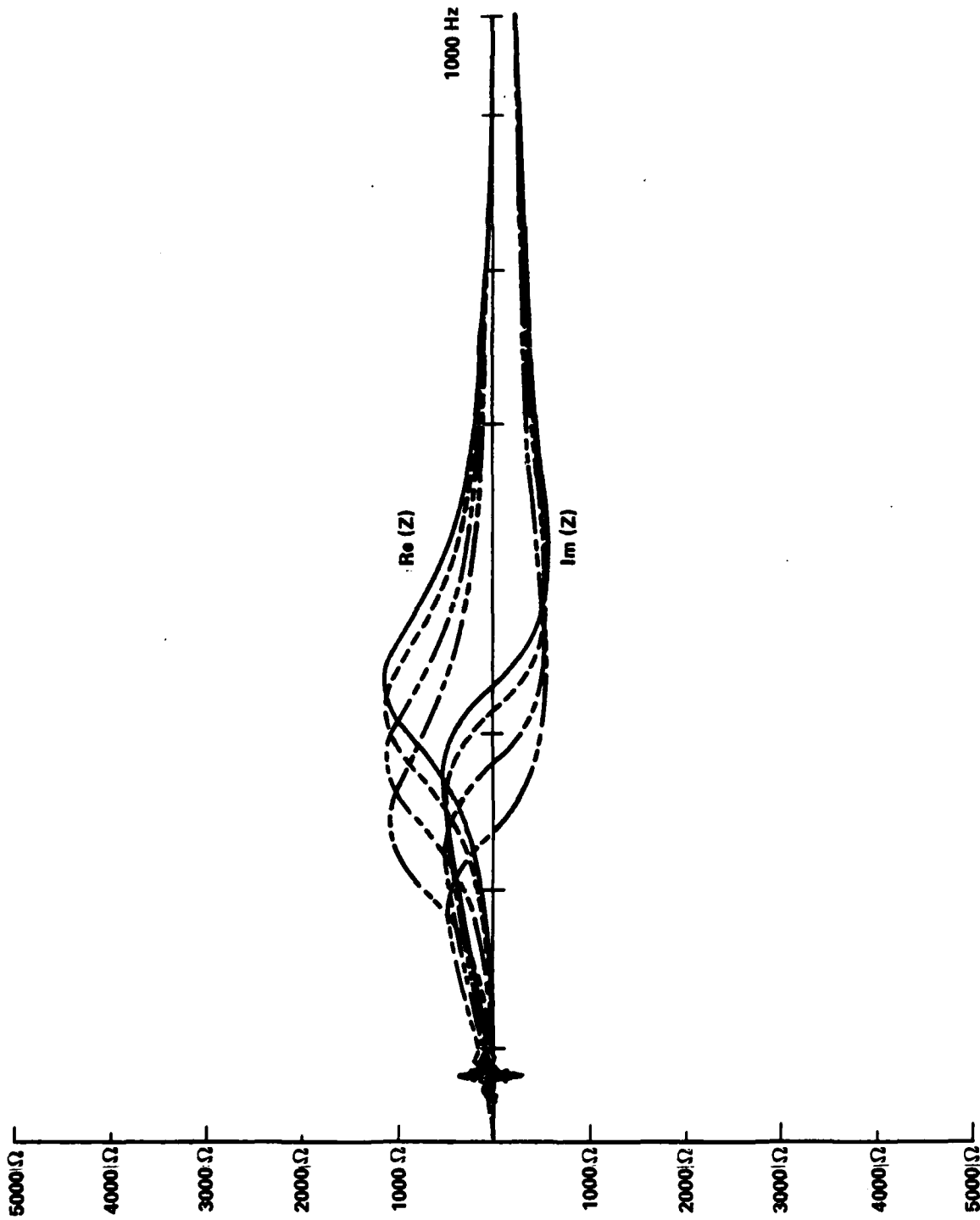


FIGURE 9-16 PLASMA RESONANCE J_1 DISCONNECTED $T = 0.72T_c$

consistent with the value of shunt resistance of 1150 ohms.

Figure 9-17 shows the same measurement, but with the J_1 filters connected. Note the large increase in the apparent resistance of the analogue, as well as the strong frequency (as opposed to cosine ϕ) dependence of the amplitude and bandwidth of the resonance. (The interference at 60 Hz and its multiples is mains pickup.) The discussion in section 6.4 explains this dependence, and its similarity to the effect of a negative $\cos \phi$ amplitude, in terms of the frequency dependence of $\text{Im } J_1$. A quantitative analysis of the data in Figures 9-16 and 9-17 is shown in Table 9-2.

There is good agreement between the above results and the theory described in Chapter 6 for the effect of $\text{Im } J_1$ on the plasma resonance. The particular choice of parameters, in terms of temperature, frequency, junction resistance, and capacitance, represents a situation that should be realizable using real tunnel junctions.

The above experiment, if repeated using tunnel junctions as described in section 6.6, would confirm the relationship between $\text{Im } J_1(V)$, as measured from the current-voltage characteristic of a junction, and $\text{Im } J_1(f)$, which determines the resistance of the junction at microwave frequencies. Additionally, the experimental results could shed considerable light on the still unresolved cosine ϕ controversy.

In other experiments done to measure the relationship between the quasiparticle conductance ($\text{Im } J_1$) and the $\cos \phi$ term ($\text{Im } J_2$), the frequency is generally fixed (cf. Chapter 6). The above experiment, however, would investigate the frequency dependence of these terms, and thus yield information of considerable importance in verifying the accuracy of the Werthamer theory. Furthermore, performing measurements at more than one frequency would aid in

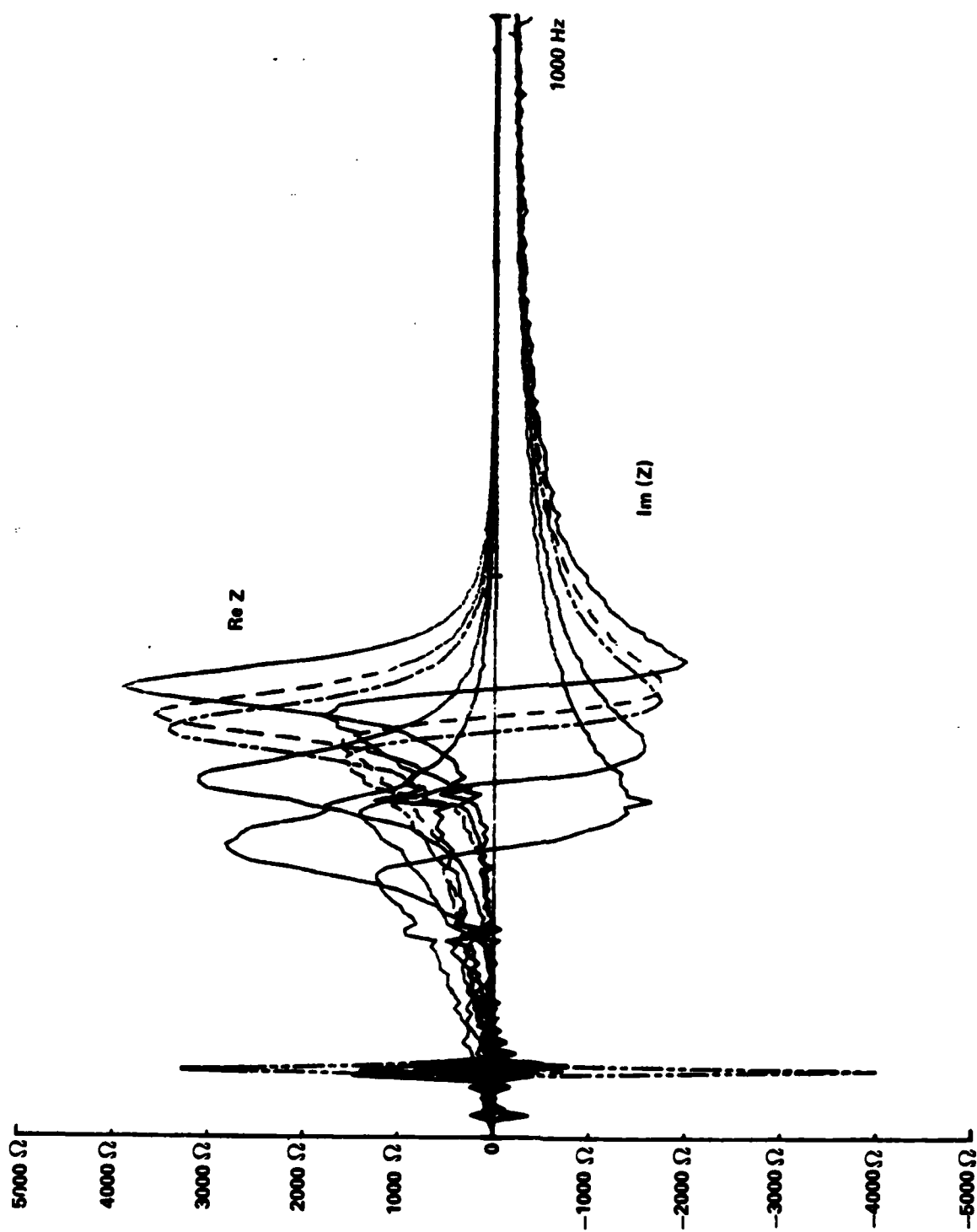


FIGURE 9-17 PLASMA RESONANCE $T = 0.72T_c$

TABLE 9-2 PLASMA RESONANCE, $T = .72 T_C$ a. J_1 FILTERS DISCONNECTED, $I_J = .45$ mA (measured)

$$2e/h = 1800 \text{ Hz/volt} \quad R = 1150\Omega$$

$$C = .81\mu\text{fd (measured)}$$

$\cos \phi_0$	f_p (theor)	f_p (meas)	R (theor)	R (meas)
1	399	405	1150	1153
.914	381	380	1150	1139
.785	353	335	1150	1116
.475	275	275	1150	1086

b. J_1 FILTERS CONNECTED, $I_J = .43$ mA (measured)

$$2e/h = 1800 \text{ Hz/volt} \quad R_n = 1150$$

$$C = .81\mu\text{fd (measured)}$$

$\cos \phi_0$	f_p (theor)	f_p (meas)	R (theor)	R (meas)
1	391	400	3500	3923
.88	367	375	3336	3582
.81	352	360	3306	3421
.63	311	315	3125	3106
.46	265	260	2833	2828

$$4\pi^2 f_p^2 = \frac{2eI_J}{\hbar C} \cos \phi$$

OBTAINED FROM A MEASUREMENT OF

$$\text{Im } J_1(V), T = .72 T_C$$

$$\frac{1}{R} = \frac{e}{\hbar f} \text{Im } J_1(f)$$

$$f = eV/\hbar$$

the elimination of spurious data.

9.5 Anomalous Broadening of the Riedel Peak

To conclude this chapter, we discuss further observations of the effect of series inductance on the performance of the analogue in the voltage biased limit. With the $T = 0$ filters, it was found that the shape of the back of the Riedel peak could be observed. (In the current biased limit, this region is inaccessible). However, as the inductance was increased, the Riedel peak became broader and higher than predicted by the shape of $\text{Re } J_2$ (cf. Figures 4-17 and 4-18).

Observation of the junction current and voltage indicated that the negative slope of $\text{Re } J_2$ behind the Riedel peak was causing a complicated series of oscillations. Figure 9-18 shows this anomalous broadening of the Riedel peak, along with the time dependent current and voltage at various bias points.

In qualitative terms, it appears that the negative slope of the I-V characteristic behind the Riedel peak causes the bias point to drift towards the gap singularity when the analogue is biased at DC voltages slightly greater than $2\Delta/e$. A small decrease in voltage causes a slight increase in current, which causes an additional decrease in voltage, and so on.

The analysis of the problem is complicated by the different time scales involved. At any instant, the Josephson oscillations appear to satisfy an instantaneous version of the RSJ equation. That is, the individual oscillations in the photographs in Figure 9-18 look like those predicted by the RSJ model for particular values of I_J and R_N . However, the frequency, amplitude, and DC offset of these oscillations vary in a time frame that is slow relative to an individual Josephson oscillation (e.g., one over the gap frequency), but quite fast relative to the time constants associated with measuring the DC I-V characteristic.

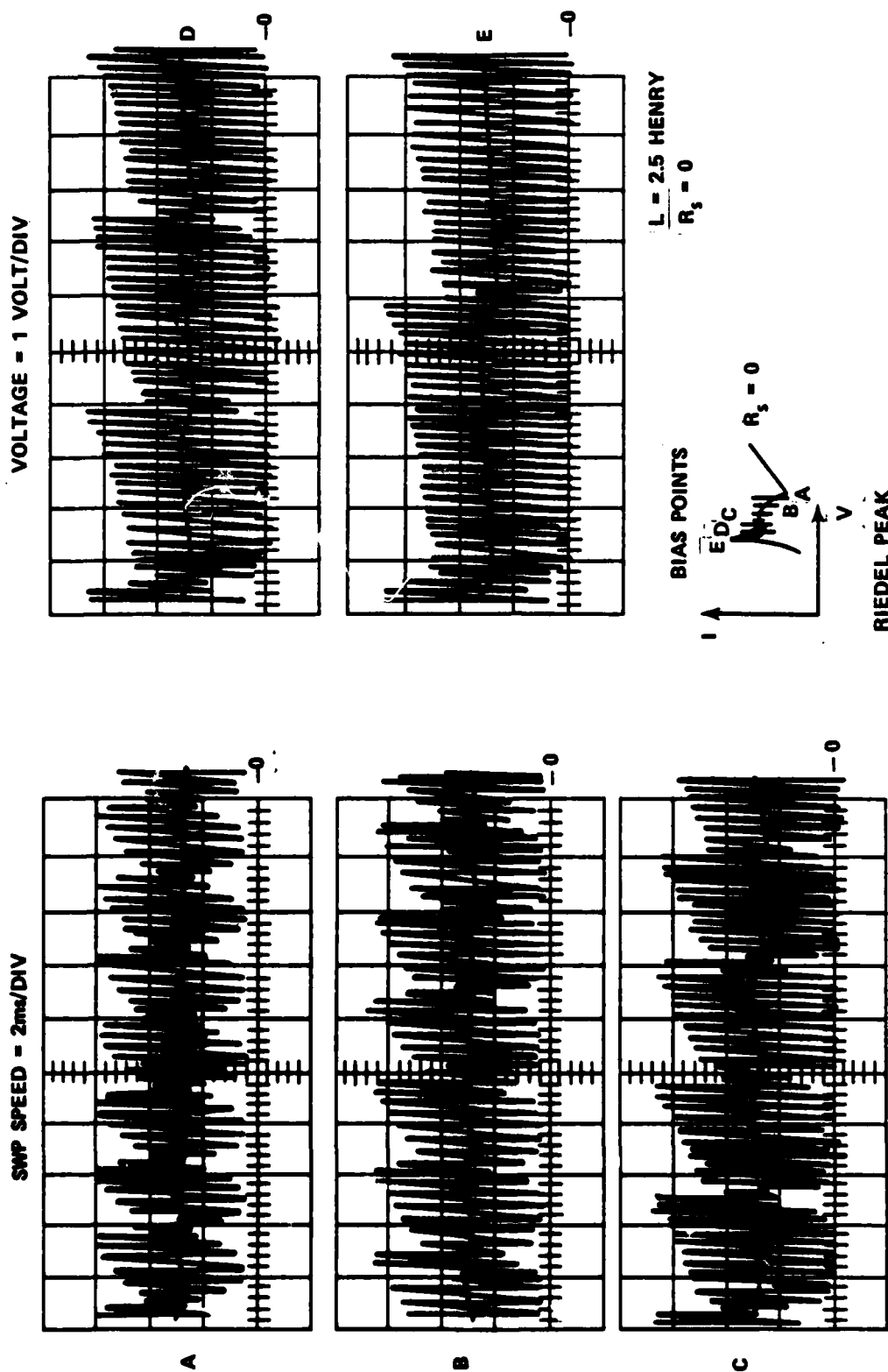


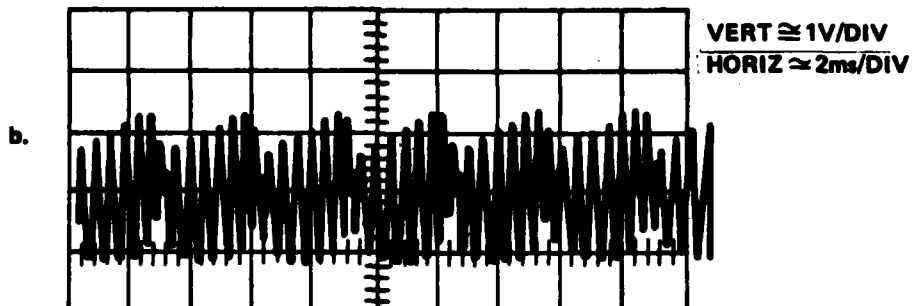
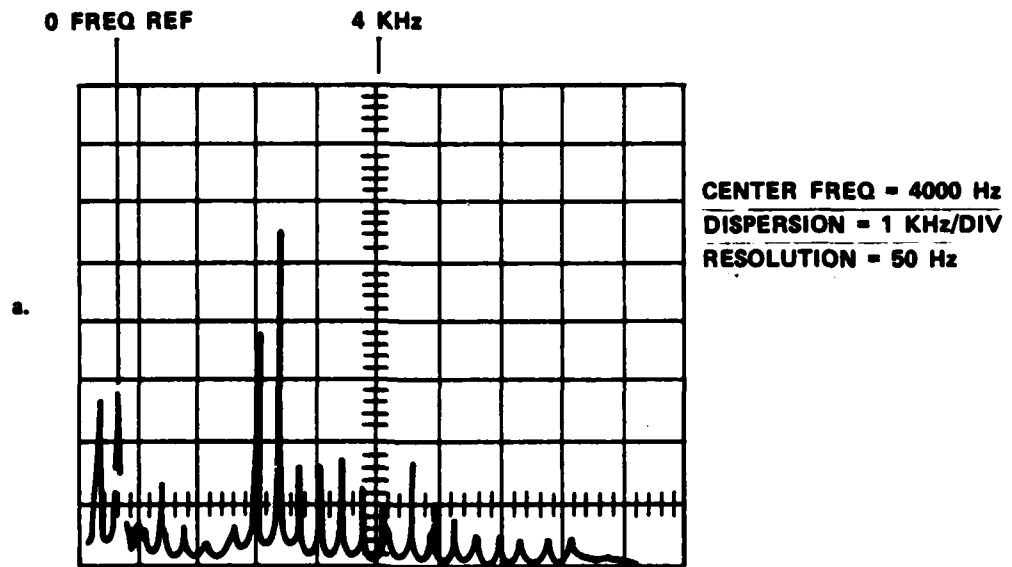
FIGURE 9-18 ANOMALOUS BROADENING OF THE RIEDEL PEAK

Measurement of the Josephson frequencies from Figure 9-18 indicates that the oscillations spend much of the time near the gap frequency of 1 khz. However, the sharp decrease in current seems to be accompanied by a short burst of high frequency oscillations and a momentary rise in the "average" voltage. This suggests that the temporary operating point is jumping to a voltage greater than the applied voltage, and the current is decreasing in accordance with the change in $\text{Re } J_2$ beyond the Riedel peak. The operating point then appears to drift back past the bias voltage to repeat the cycle.

Measurement of the frequency spectrum of the oscillations is consistent with this argument. Figure 9-19a shows the frequency domain representation of the series of oscillations shown in Figure 9-19b. Although the photograph doesn't make it entirely obvious, the spectral response seems to be a collection of the spectra of RSJ-type oscillations at various values of the Josephson frequency (see Figure 8-7). These spectra are offset from each other with a spacing equivalent to the repeat frequency of the envelope of the signal in Figure 9-19b.

The frequency of this cycle increases as the external bias voltage approaches the region where dI/dV in the characteristic is no longer negative. (This corresponds to the bottom of the hysteresis region in the current biased characteristic of the analogue.) As the external bias is increased past this trough the oscillations abruptly cease.

For large values of inductance, the negative resistance oscillations sometimes follow a very complicated pattern, as illustrated in Figure 9-20. The reason for this is not understood.



$R_s = 0$
 $L = 2.5h$
BIAS PT A (SEE FIGURE 9-18)

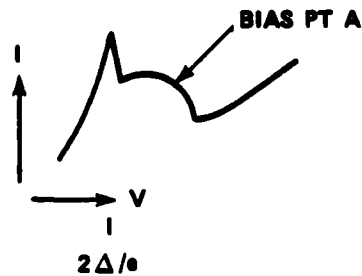


FIGURE 9-19 SPECTRAL ANALYSIS OF THE RIEDEL PEAK OSCILLATIONS

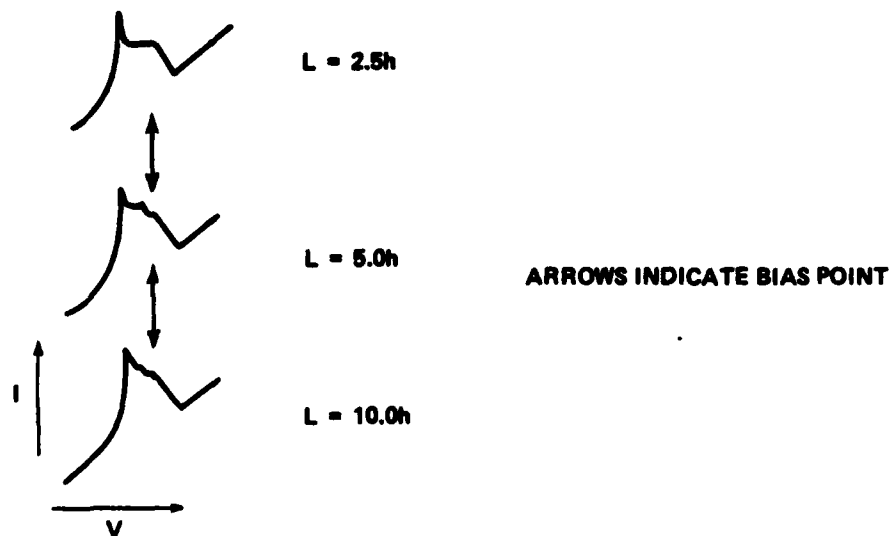
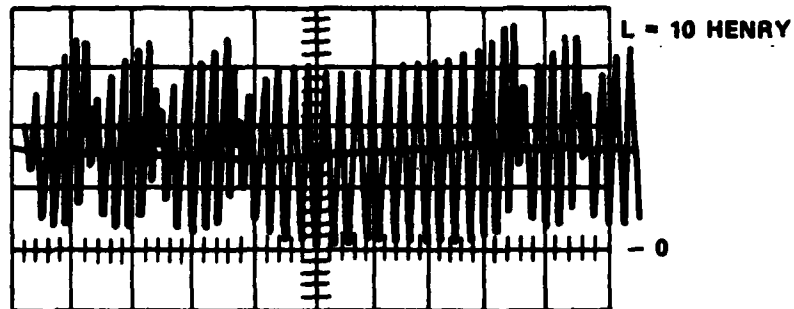
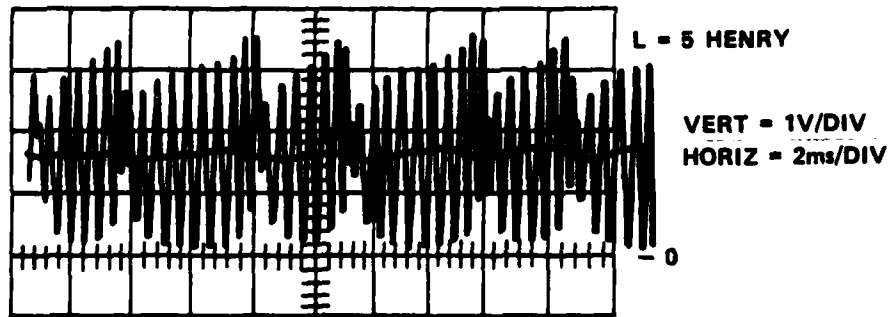


FIGURE 9-20 EFFECT OF CHANGING THE INDUCTANCE

The study of the effects described above has not been pursued very far. The intent of this section has been to identify the nature of the problem, and to verify that the phenomena is not due to a fault with the analogue. It appears that the oscillations are a genuine consequence of the Werthamer theory, although due to the effect of shunt capacitance, it is unlikely that these oscillations could easily be observed in a real junction. (The capacitance will reduce the effective AC source impedance; the oscillations depend on the presence of a high AC source impedance, namely the inductor. If the inductor was removed, the I-V characteristic would be equal to $I_m J_1$ and the Riedel peak and supercurrent effects would not be noticeable.)

9.6 SGS in the Capacitively Shunted Analogue

As a final discussion point, it is interesting to analyze the appearance of apparently anomalous structure in the I-V characteristics of the high frequency analogue when shunted with a capacitor. In Figure 4-22b, repeated here as Figure 9-21a, there is a noticeable discontinuity at $V = 1/3 \times 2\Delta/e$. A similar structure is evident in the I-V characteristic in Figure 9-15b.

Investigation of the latter revealed that the structure occurs precisely at $1/3$ the gap voltage, and is accompanied by an increase in the component of the RF voltage at the third harmonic of the Josephson frequency, which is equal to the gap frequency $2\Delta/h$. As the current is reduced, the voltage decreases to $1/3$ the gap voltage, and then abruptly jumps towards $V = 0$. This suggests that the apparent discontinuity in the current appears at the cusp of a sub-gap structure. Since the analogue is current biased, the opposite side of the structure is not accessible as the current is reduced. Nor is it accessible as the current is increased from $I = 0$, as the zero voltage supercurrent is traced out instead.

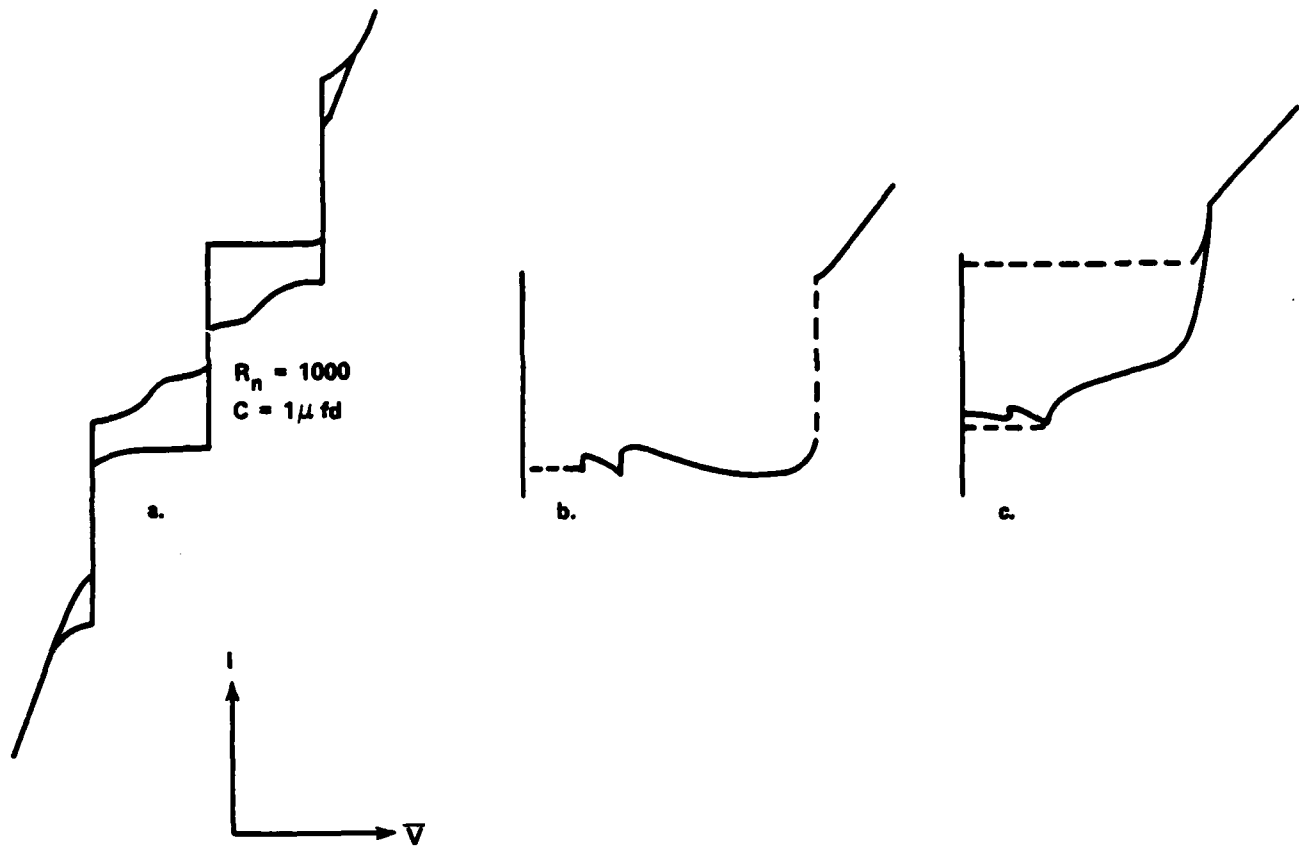


FIGURE 9-21 EFFECT OF CAPACITANCE AND LEAKAGE RESISTANCE ON SUB-GAP STRUCTURE

Figure 9-21b shows calculated results for the I-V characteristic under current bias conditions at $T = 0$ in the presence of a shunt capacitance (after McDonald, et al.²) In a real situation, the negative resistance regions in the characteristic would be inaccessible, and would show up as hysteresis loops in the characteristic.

If an ohmic leakage current were present, the characteristics in Figure 9-21b would slope upward, and a typical characteristic, including hysteresis, might look like Figure 9-21c. In the case of Figure 4-22b, such a leakage current was deliberately introduced into the analogue to prevent any problems due to the overshoot in $\text{Im } J_1$ at the gap frequency in the $T = 0$ filters (see Figure 4-21). In the case of Figure 9-15b, the leakage current is already present by virtue of the nonzero temperature.

CHAPTER 10

SUMMARY AND CONCLUSIONS

10.1 The Electronic Analogue

In the previous chapters, we have demonstrated that electronic circuitry can be used to model Werthamer's formulation of the Josephson effects with good accuracy. Due to the complicated nature of the response functions J_1 and J_2 , this was not obvious at the outset of the project. A technique for designing filters that model these functions was successfully developed, and at the time of writing the electronic analogue is probably the only electronic simulator of the Josephson effects which can model accurately the effects of temperature and the superconducting energy gap.

Using the analogue, it has been possible to confirm and extend many of the calculations done by others using the high frequency theory. The close agreement between results reported by Hamilton, McDonald, and others with results obtained using the analogue indicates that the electronic analogue can be used to obtain both qualitative and quantitative results. In many cases, such as the calculation of the heights of photon-assisted tunnelling steps, the analogue is significantly faster than a digital computer.

The analogue is very useful for modelling the dynamic behavior of a tunnel junction. For example, the analogue exhibits the hysteresis behavior characteristic of a real junction, but which is not evident from a digital computation. Other dynamic effects, such as the plasma oscillations, are quite well modelled by an analogue. Lastly, the analogue has exhibited dynamic behavior that has not been reported before, namely

the complex oscillations that occur at the Riedel peak when the analogue is biased through an inductor.

There is no doubt that improvements can be made to the design and construction of the analogue. However, the results obtained thus far indicate that the analogue, at its current level of performance, is sufficiently accurate and versatile to be an important tool with which to investigate the properties of tunnel junctions. In this regard, it is hoped that many of the results presented in previous chapters will speak for themselves.

10.2 The High Frequency Theory

The predominant concern of this project has been the implementation of Waldram's scheme for modelling the Werthamer theory, as opposed to a justification of the theory. Although Werthamer's basic equation is limited to junctions comprised of weak-coupling superconductors, and no geometrical effects are included, the theory is appropriate for many of the junctions that are currently of interest for both applications and research (e.g. - small tin junctions). However, strong-coupling effects that occur in lead junctions, for instance, can be modelled by the analogue in an ad-hoc manner (e.g. - by adjusting the $I_J R_N$ product, or by modifying the filter responses). Although it would be difficult to include the geometrical effects observed in large junctions, it is fortuitous that most of the practical applications of the Josephson effects require junctions that are small enough to exclude geometrical factors.

In any event, the usefulness of the analogue seems to be diminished only slightly by the shortcomings inherent in the Werthamer theory.

Certainly, when one is concerned with a tunnel junction, the Werthamer theory represents an improvement over the RSJ model.

At this stage, it is worthwhile to summarize the differences between the Werthamer and RSJ formulations:

1. The RSJ model can be derived from the high frequency theory.
2. The main differences between the I-V characteristics of the two models under current bias conditions are the presence of the Riedel peak and sub-gap structure.
3. Under voltage bias conditions, the time averaged I-V characteristic of the RSJ model is linear (i.e., Ohmic). The characteristic of the high frequency theory is very nonlinear, with a sharp reduction in current at voltages less than the gap voltage $2\Delta/e$.
4. A shunt capacitance causes the I-V curves of each theory to be hysteretic. For a given amount of capacitance, the hysteresis in the high frequency case will be much more pronounced, due to the larger effective RC product.
5. In the high frequency calculations, one should replace I_J in the RSJ model with a value obtained using a combination of the DC and high frequency values of $\text{Re } J_2(\omega)$.
6. In the high frequency theory, there is a reactive term that depends on $\left[\text{Re } J_1(\omega) \right] - \text{Re } J_1(0)$, where ω is the frequency of oscillation of the junction voltage. Provided that ω is much less than the gap frequency $2\Delta/h$, this term can be ignored.
7. The quasiparticle resistance in the high frequency theory is both voltage and frequency dependent.

8. The amplitude of the $\cos\phi$ term is comparable, at low frequency, with the amplitude of the quasiparticle conductance. As Harris has pointed out, the effect of this term is negligible much of the time,⁸ but it is significant from the point of view that experimental evidence contradicts the theory. The $\cos\phi$ term can have a noticeable effect on the small signal AC impedance of a junction.

10.3 Circuit Considerations

As with any electronic device, there will always be improvements that can be made to the design of the electronic analogue. However, at its current level of design, there do not seem to be any major problems concerning the accuracy of the analogue. The problems that had previously existed concerning multiplier calibration and an excessively high $\cos\phi$ amplitude have been reduced to the point where for most purposes they can be ignored.

The peculiar negative resistance problem associated with the overshoot in the response of $\text{Im}J_1$ in the nine pole $T = 0$ filter is still a nuisance. However, it appears to be an unavoidable consequence of the sharp discontinuity in $\text{Im}J_1$ at the gap frequency. For the most part, this overshoot does not cause any difficulties. Where necessary, any unwanted effects can be removed by decreasing the $I_J R_N$ product, which corresponds to adding a leakage current at frequencies and voltages below the gap. This problem does not exist when the T is not equal to zero filters are used.

With careful design, the effective cosine ϕ amplitude of the analogue can be reduced further. This would involve rebuilding the existing low pass filters using extremely accurate components. The

main difficulty would be in matching the values of several inductors to within a percent or so. With enough effort, there is no doubt that this can be done, but the necessity for doing this is questionable.

There are undoubtedly other parts of the design which could be improved, but as it stands, the electronics of the analogue are both simple and reliable, and the device is more than adequate for modelling a wide variety of situations easily and with high accuracy.

10.4 Suggestions for Future Work

In addition to the results presented in earlier chapters, there are several areas which deserve further investigation. Some of these are listed below.

1. Investigation of sub-gap structure in the I-V characteristics of the analogue. Qualitatively, the analogue is in good agreement with the predictions of Werthamer, McDonald, Harris, and others. However, no careful observations have been made using the analogue of the shape and amplitude of this structure as a function of source impedance, temperature, etc.

2. Investigation of non-steady-state behavior. The analogue is ideal for studying the dynamic behavior of a Josephson junction. The unexpected negative-resistance oscillation observed when the analogue is voltage-biased through an inductor are an excellent example of this. These oscillations are quite complex, and need to be investigated further. There is a slight chance that this phenomenon may have some practical application.

3. The cosine ϕ problem. As predicted in Chapter 2, and demonstrated in Chapter 9, the response function $\text{Im } J_1(\omega)$ can cause frequency

dependent effects similar to those predicted for a negative $\cos \phi$ term. This is a factor that was neglected in the interpretation of the Pedersen, Langenberg, and Finnegan experiment to measure the $\cos\phi$ amplitude for a lead tunnel junction.⁹ It would be worthwhile for this experiment to be repeated, preferably using much smaller tunnel junctions. Performing and interpreting the experiment from the viewpoint of the Werthamer theory, as opposed to the RSJ model, might lead to a substantially different result concerning the cosine ϕ amplitude.

4. Measurement of the performance of a quasiparticle mixer. The most promising microwave application of a Josephson junction is the QPPAT, or quasi-particle photon assisted tunnelling mixer.⁵¹ This device depends on the frequency dependence of both $\text{Im } J_1(\omega)$ and $\text{Re } J_1(\omega)$ for its operation. To the author's knowledge, the electronic analogue is the only electronic simulator in existence which models properly the frequency dependence of $\text{Re } J_1(\omega)$ and $\text{Im } J_1(\omega)$. Hence, it is a unique and valuable tool for investigating the practicality of QPPAT devices.

5. Noise effects. The influence of noise on junction dynamics is an extremely complicated but important subject which can be studied using the analogue. In particular, the various instabilities inherent to Josephson devices are closely related to noise phenomena and are of much interest.⁴⁹

The above list is by no means comprehensive and is only meant to illustrate area that the author considers to be important and

interesting. There are undoubtedly many other applications of the analogue that have been overlooked.

10.5 Conclusion

This thesis has been concerned primarily with the behavior predicted by the high frequency theory, as opposed to the behavior observed in real tunnel junctions. Until recently, real tunnel junctions have had such a large shunt capacitance that most of the effects which require the high frequency theory for their explanation are masked. However, as the technology of fabricating smaller, less capacitive tunnel junctions improves, these effects will become more and more apparent.

In one of his many excellent papers on the high frequency theory, Harris comments, "The theoretical expression for the current through a small Josephson tunnel junction is quite complicated and seemingly defiant to intuitive physical interpretation."¹⁵ Although the previous chapters have been more concerned with the mathematical expression itself than with its physical interpretation, it is hoped that this thesis has helped to shed some light on the problem.

REFERENCES

1. Sullivan, D. B., "The Role of Superconductivity in the Space Program: An Assessment of Present Capabilities and Future Potential," NBSIR 78-885, May 1978.
2. McDonald, D. G., Johnson, E. G., and Harris, R. E., "Modeling Josephson Junctions," Physical Review B, Vol. 13, No. 3, 1 Feb 1976, p. 1028.
3. Adler, R., "Locking Phenomena in Oscillators," Proceedings of the Institute for Radio Engineers, Vol. 34, 1946, p. 351.
4. Bak, C. K., and Pedersen, N. F., "Josephson Junction Analog and Quasiparticle-Pair Current," Applied Physics Letters, Vol. 22, No. 4, 15 Feb 1973, p. 149.
5. Werthamer, N. R., "Nonlinear Self-Coupling of Josephson Radiation in Superconducting Tunnel Junctions," Physical Review, Vol. 147, No. 1, 8 Jul 1966, p. 255.
6. Waldram, J. R., in "A Theoretical Survey of Josephson Frequency Mixers for Heterodyne Reception in the Submillimetre Wavelength Range," ed. Blaney, National Physical Laboratory, U.K., 1976.
7. Josephson, B. D., "Possible New Effects in Superconductive Tunnelling," Physics Letters, Vol. 1, No. 7, 1 Jul 1962, p. 251.
8. Harris, R. E., "Cosine and Other Terms in the Josephson Tunnelling Current," Physical Review B, Vol. 10, No. 1, 1 Jul 1974, p. 84.
9. Pedersen, N. F., Finnegan, T. F., and Langenberg, D. N., "Magnetic Field Dependence and Q of the Josephson Plasma Resonance," Physical Review B, Vol. 6, No. 11, 1 Dec 1972, p. 4151.
10. Rudner, S., and Claeson, T., "Basic Josephson Tunnel Parameters at Microwave Frequency-Strong Temperature variations," Journal of Applied Physics, Vol. 50, No. 11, Nov 1979, p. 7070.
11. Waldram, J. R., "The Josephson Effects in Weakly-Coupled Superconductors", Reports on Progress in Physics, Vol. 39, 1976, pp. 751-821.
12. Ashcroft, N. W., and Mermin, N. D., Solid State Physics (New York: Holt, Rinehart, and Winston, 1976), pp. 725-256.
13. Matisoo, J., "Superconducting Computers", Scientific American, May 1980.
14. Aslamazov, L. G., and Larkin, A. I., "Josephson Effect in Superconducting Point Contacts," Soviet JETP Letters, Vol. 9, No. 2, 20 Jan 1969, p. 87.
15. Harris, R. E., "Josephson Tunnelling Current in the Presence of a Time-Dependent Voltage," Physical Review B, Vol. 11, No. 9, 1 May 1976, p. 3329.

REFERENCES (Cont.)

16. Harris, R. E. "Intrinsic Response Time of a Josephson Tunnel Junction," Physical Review B, Vol. 13, No. 9, 1 May 1976, p. 3818.
17. Shapiro, S., Smith, P. H., Nicol, J., Miles, J. L., and Strong, P. F., "Superconductivity and Electron Tunnelling," IBM Journal of Research and Development, Jan 1962, p. 34.
18. Schlup, W., "Possible Influence of the Quasiparticle-pair Interference Term on the Current-Voltage Characteristics of Oxide Barrier Josephson Junctions," Solid State Communications, Vol. 12, No. 7, 1973, p. 631.
19. Poulsen, U. K., "Quasiparticle Interference Current in Josephson Junctions," Physics Letters, Vol. 41A, No. 3, 25 Sep 1972, p. 195.
20. Tucker, J. R., "Predicted Conversion Gain in Superconductor-Insulator-Superconductor Quasiparticle Mixers," Applied Physics Letters, Vol. 36, No. 6, 15 Mar 1980, p. 477.
21. Hamilton, C. A., "Frequency Dependence of the Josephson Current," Physical Review B, Vol. 5, No. 3, 1 Feb 1972, p. 912.
22. Thompson, E. D., "Perturbation Theory for a Resistively Shunted Josephson Element," Journal of Applied Physics, Vol. 44, No. 12, Dec 1973, p. 5587.
23. Claassen, J. H., Taur, Y., and Richards, P. L., "Noise in Josephson Point Contacts with and without RF Bias," Applied Physics Letters, Vol. 25, No. 12, 15 Dec 1974, p. 759.
24. Longacre, A., "The Cavity-Coupled Josephson Device," Journal of Applied Physics, Vol. 50, No. 10, Oct 1979, p. 6451.
25. Tuckerman, D. B., "Analog Simulator of a Josephson Quantum Interference Device," Review of Scientific Instruments, Vol. 49, No. 6, Jun 1978, p. 835.
26. Taunton, J. C., and Halse, M. R., "A Josephson Junction Analogue Incorporating the Effects of Thermal Noise and Phase-Dependent Conductivity," Journal of Physics E, Vol. 10, No. 5, May 1977, p. 505.
27. Hamilton, C. A., "Analog Simulation of a Josephson Junction," Review of Scientific Instruments, Vol. 43, No. 3, Mar 1972, p. 445.
28. Magerlein, J. H., "Accurate Josephson Junction Analog," Review of Scientific Instruments, Vol. 49, No. 4, Apr 1978, p. 486.
29. Yagi, A., and Kurosawa, I., "Precision to Analog Simulator for a Josephson Junction," Review of Scientific Instruments, Vol. 5, No. 1, Jan 1980, p. 15.
30. Werthamer, N. R., and Shapiro, S., "Analog-Computer Studies of Josephson Radiation Effects," Physical Review, Vol. 164, No. 2, 10 Dec 1977, p. 523.

REFERENCES (Cont.)

31. Bak, C. K., "An Electronic Equivalent Scheme of a Josephson Junction," Revue de Physique Appliquee, Vol. 9, 1974, p. 15.
32. Prober, D. E., Slusky, S. E. G., Henry, R. W., and Jackel, L. D., "Simulation of I-V Curves of Small Josephson Tunnel Junctions with Finite Capacitors," Journal of Applied Physics, Vol. 56, No. 6, p. 4145, Jun 1981.
33. Waldram, J. R., Pippard, A. B., and Clarke, J., "Theory of the Current-Voltage Characteristics of SNS Junctions and other Superconducting Weak Links," Philosophical Transactions of the Royal Society, No. 268.
34. Auracher, F., and Van Duzer, T., "RF Impedance of Superconducting Weak Links," Journal of Applied Physics, Vol. 44, No. 2, Feb 1973, p. 848.
35. Jablonski, D. G., and Waldram, J. R., "An Electronic Analogue of a High Frequency Theory of the Josephson Effect," SQUID '80, ed. Hahlbohm, H., and Lubbig, H., (New York: Walter de Gruyter & Co., 1980), p. 115.
36. Tow, J., "Active RC Filters -- A State-Space Realization," Proceedings of the I.E.E.E., Vol. 56, No. 6, Jun 1968, p. 1137.
37. Thomas, L. C., "The Biquad: Part I -- Some Practical Design Considerations," I.E.E.E. Transactions of Circuit Theory, Vol. CT-18, No. 3, May 1971, p. 350.
38. Mukhopadhyay, P., "Study of Subharmonic Gap Structure in Both Symmetric and Asymmetric Superconducting Tunnel Junctions Based on Oxidised PbIn Electrodes," Journal of Physics F, Vol. 9 No. 5, 1979, p. 903.
39. Weitz, D. A., Skocpol, W. J., and Tinkham, M., "High-Frequency Behavior of 'Ideal' Superconducting Point Contacts," Physical Review Letters, Vol. 40, No. 4, 23 Jan 1978, p. 253.
40. Harris, R. E., Dynes, R. C., and Ginsberg, D. M., "Strong-coupling Correction to the Jump in the Quasiparticle Current of a Superconducting Tunnel Junction," Physical Review B, Vol. 14, No. 3, 1 Aug 1976, p. 993.
41. Zorin, A. B., Kulik, I.O., Likharev, K. K., and Schrieffer, J. R., "On the Sign of the Quasiparticle-Pair Interference Current in Superconducting Tunnel Junctions," Fiz. Nizk. Temp., Vol. 5, 1979, p. 1138.
42. Solymar, L., Superconductive Tunnelling and Applications (London: Chapman and Hall, 1972).
43. Pedersen, N. F., Soerensen, O. H., and Mygind, J., "Temperature Dependence of the $\cos\phi$ Conductance in Josephson Tunnel Junctions Determined from Plasma Resonance Experiments," Physical Review B, Vol. 18, No. 7, 1 Oct 1978, p. 3220.
44. Feldman, M. J., Rudner, S., and Claeson, T., "Basic Josephson Tunnel Parameters at Microwave Frequency -- A Reassessment," Journal of Applied Physics, Vol. 51, No. 9 Sep 1980, p. 5058.

REFERENCES (Cont.)

45. Stephen, M. J., "The Pair-Quasiparticle Interference Current in Superconducting Junctions," Physics Letters, Vol. 46A, No. 4, 31 Dec 1973, p. 289.
46. Deaver, B. S. Jr., Boone, B. G., and Rifkin, R., "Nonequilibrium Effects in Superconducting Weak Links," Physics Letters, Vol. 57A, No. 2, 31 May 1976, p. 186.
47. Giaever, I., and Zeller, H. R., "Subharmonic Structure in Superconducting Tunnel Junctions," Physics, Vol. 55, 1971, p. 455.
48. Rickayzen, G., Theory of Superconductivity (New York: John Wiley and Sons, 1965).
49. Chaio, R. Y., Feldman, M. J., Peterson, D. W., Tucker, B. A., and Levinsen, M., in Proceedings of Future Trends in Superconducting Devices (American Institute of Physics, 1978).
50. Hamilton, C. A., and Johnson, E. G. Jr., "Analog Computer Studies of Subharmonic Steps in Superconduction Weak Links," Physics Letters, Vol. 41A, No. 4, 9 Oct 1972, p. 393.
51. Richards, P. L., Shen, J. M., Harris, R. E., and Lloyd, F. L., "Superconductor-Insulator-Superconductor Quasiparticle Junctions as Microwave Photon Detectors," Applied Physics Letters, Vol. 36, No. 6, 15 Mar 1980, p. 480.
52. Young, M., Ph.D. Thesis, Cambridge University, 1979 (unpublished).

APPENDIX A

REPRINT OF "AN ELECTRONIC ANALOGUE OF A HIGH
FREQUENCY THEORY OF THE JOSEPHSON EFFECT,"

BY D. G. JABLONSKI AND J. R. WALDRAM

(PRESENTED AT IC SQUID, BERLIN 1980)

Note: The sign conventions for $J_1(\omega)$ and $J_2(\omega)$ in this reprint differ from those used throughout the rest of this dissertation. However, the sign convention used in performing the convolution integrals is different as well. All results involving current and voltage are consistent with those in the rest of this dissertation, as well as with results in the general literature.

INTRODUCTION

A prototype electronic analogue has been built which models Josephson tunneling between identical superconductors at $T = 0$ and, with modification, at higher temperatures. Unlike simulators reported in the literature,^{A-1,A-2} this device includes high frequency and gap effects, the Riedel peak, and non-linear quasiparticle tunneling. It is based on the high frequency form of Josephson's theory^{A-3} as developed by Wethamer^{A-4} and later extended by Harris^{A-5,A-6,A-7} and McDonald, Johnson, and Harris.^{A-8} The principle on which this analogue was based was first described by one of us in 1978.^{A-9} The circuit uses a phase-locked loop of the type described by Bak^{A-1} in a new way.

We begin this paper with a brief review of the high frequency theory. This is followed by a description of the design and construction of the device. Simple results are presented to show the limitations and overall accuracy of the analogue. A comparison is made with previously published results obtained numerically. Finally, there is a discussion of how the analogue can be

improved, and what part the analogue might play in the continuing development of Josephson technology.

THEORY

The current in a Josephson junction can be written as^{A-7,A-10}

$$I(t) = I_m \exp(-i\frac{\phi}{2}(t)) \int_0^t \exp(i\frac{\phi}{2}(t')) j_1(t - t') dt' \quad (A-1)$$

$$+ \exp(i\frac{\phi}{2}(t)) \int_{-\infty}^t \exp(i\frac{\phi}{2}(t')) j_2(t - t') dt'$$

where $\frac{d\phi}{dt} = \frac{2eV}{\hbar}$, and $j_1(t)$ and $j_2(t)$ are real response functions determined

by the gap parameter, density of states, Fermi factors, etc.

If the voltage V is held constant, we may write $\frac{1}{2}\phi(t) = \omega t$, where $\hbar\omega = eV$, and ω is one half the usual Josephson frequency. Equation (A-1) becomes

$$I(V) = I_m J_1(\omega) - \sin \phi \operatorname{Re} J_2(\omega) + \cos \phi \operatorname{Im} J_2(\omega) \quad (A-2)$$

where $J_1(\omega)$ and $J_2(\omega)$ are the Fourier transforms of $j_1(t)$ and $j_2(t)$.

The following points should be noted:

1. There is a direct correspondence between ω and V when V is constant.
2. $J_2(\omega)$ describes the excess currents first described by Josephson.^{A-3} $-\operatorname{Re} J_2(\omega)$ is the critical supercurrent, and $\operatorname{Im} J_2(\omega)$ is the coefficient of the $\cos \phi$ term.
3. $\operatorname{Im} J_1(\omega)$ describes the ordinary tunnel current. If $\operatorname{Im} J_1(\omega) = \omega$, then this term is equivalent to an ohmic resistance where $I = V$.
4. $\operatorname{Re} J_1(\omega)$ does not affect the current if V is constant.

The widely-used resistively-shunted junction (RSJ) model is obtained from equation (A-2) if we set $\operatorname{Im} J_1(\omega) = \omega$, $\operatorname{Re} J_2(\omega) = \text{constant}$, and Im

$J_2(\omega) = 0$. It is important to realize that there is no limit in which the RSJ model is correct. The RSJ model always ignores the $\cos\phi$ term and the large nonlinearities in the quasiparticle current.

Equation (A-1), on the other hand, not only includes all quasi-particle tunnelling and the $\cos\phi$ term, but is also valid at all frequencies and for all forms of $V(t)$.

The analogue is based on the follows idea. Equation (A-1) can be written

$$I(t) = \cos\frac{\phi}{2}(\sin\frac{\phi}{2} * j_1) - \sin\frac{\phi}{2}(\cos\frac{\phi}{2} * j_1) + \sin\frac{\phi}{2}(\cos\frac{\phi}{2} * j_2) + \cos\frac{\phi}{2}(\sin\frac{\phi}{2} * j_2) \quad (A-3)$$

where the terms in the brackets represent convolution integrals of the form

$$(\sin\frac{\phi}{2} * j_1) = \int_{-\infty}^t \sin\frac{\phi(t')}{2} j_1(t - t') dt' \quad (A-4)$$

If the voltage signals representing $\sin\frac{\phi}{2}$ and $\cos\frac{\phi}{2}$ are available, these integrals may be simulated by applying the voltages to electronic filters whose pulse responses have the form $j_1(t)$ or $j_2(t)$ as appropriate. The filter output then represents the integral. Note that this part of the simulator is entirely linear in operation. $j_1(t)$ and $j_2(t)$ are real, and may be regarded as being zero for negative argument. Thus filters with pulse responses $j_1(t)$ and $j_2(t)$ can, in principle, be constructed. (It is worth noting that $\text{Re } J_1(\omega)$ and $\text{Im } J_1(\omega)$, the Fourier transforms of $j_1(t)$, are Kramers-Kronig conjugates, as are $\text{Re } J_2(\omega)$ and $\text{Im } J_2(\omega)$.)

The complete simulation of equation (A-3), including the generation of the $\sin\frac{\phi}{2}$ and $\cos\frac{\phi}{2}$ voltages, is done using an elaboration of the phase-locked loop

loop circuit described by Bak,^{A-1} as shown in Figure A-1. With no input voltage, the voltage controlled oscillator (VCO) in Figure A-1 oscillates at frequency ω_0 . With a voltage present at the input, the output of the VCO has the form

$$V_1 = A \sin(\omega_0 t + k \int V_{in} dt) \quad (A-5)$$

where A , ω_0 , and k are constants determined by the circuit designer. The local oscillator produces a signal

$$V_{LO} = B \sin(\omega_0 t) \quad (A-6)$$

This is phase shifted to produce an additional signal

$$V_2 = B \cos(\omega_0 t) \quad (A-7)$$

(The gain and phase of the phase shifter are frequency dependent. The phase shifter is calibrated to produce a unity-gain, 90° phase shift at frequency ω_0 .) These two signals are each multiplied by the VCO output, each producing signals at the sum and difference frequencies of the LO and VCO. Low pass filters remove the sum frequencies, leaving signals proportional to $\sin \frac{\phi}{2}$ and $\cos \frac{\phi}{2}$, where $\frac{d\phi}{dt} = 2kV_{in}$.

These signals are then filtered, multiplied, and added according to equation (A-3). The resulting voltage is converted to a current by the voltage controlled current source (VCCS), which is connected back to the input. Current from the input flows into the VCCS and shunt resistor, but not into the VCO, which is a high input impedance device.

The remaining problem is to synthesize filters whose pulse response functions have the form $j_1(t)$ and $j_2(t)$. Even using very simple filters of the type shown in Figure A-2, $j_1(t)$ and $j_2(t)$ can be approximated surprisingly well. The dashed lines in Figure A-3 show Werthamer's results^{A-4} for $J_1(\omega)$ and $J_2(\omega)$ at $T = 0$ for identical superconductors. The solid

lines in Figure A-3 show the corresponding response curves for the filters actually used in the analogue. The difference between the theoretical $J_1(\omega)$ and the corresponding response function is deliberate. It will be noted that a

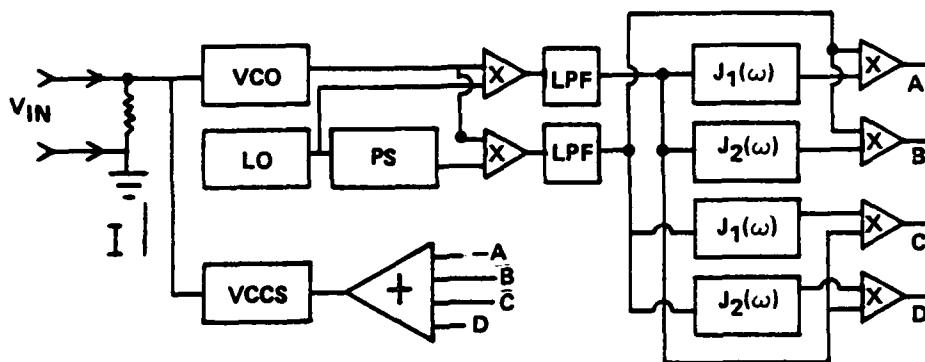


FIGURE A-1. BLOCK DIAGRAM OF THE ANALOGUE

VCO	VOLTAGE CONTROLLED OSCILLATOR
LO	LOCAL OSCILLATOR
PS	PHASE SHIFTER
VCCS	VOLTAGE CONTROLLED CURRENT SOURCE
LPF	LOW PASS FILTER

resistor has been placed in parallel with the input to the analogue (cf. Figure A-1). This resistor is equivalent to a linear term in $\text{Im } J_1(\omega)$, which would have been inconvenient to model as a filter response. When this linear term is added to the response of the $J_1(\omega)$ filter one gets a reasonable approximation to the theoretical curve. A linear term in $\text{Im } J_1(\omega)$ adds a constant to $\text{Re } J_1(\omega)$, as can be seen from the

Kramers-Kronig relations. However, we see from Equation A-1 that an arbitrary constant in $\text{Re } J_1(\omega)$ has no effect on the observed tunnel current. For comparison purposes, the theoretical expression for $\text{Im } J_1(\omega)$ minus its linear component, is plotted as a dotted line in Figure A-3b.

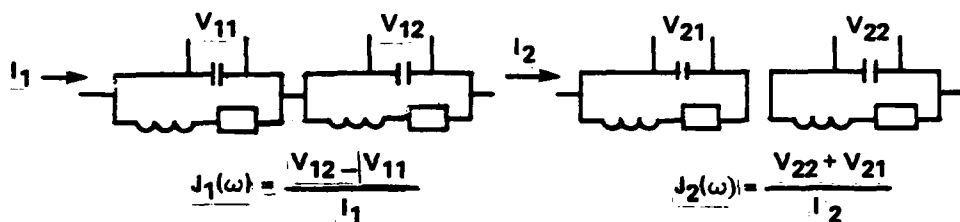


FIGURE A-2. RLC MODELS FOR $J_1(\omega)$ AND $J_2(\omega)$

At this stage, it is worthwhile to emphasize certain points about the synthesis of $j_1(t)$ and $j_2(t)$.

1. Analytic expressions for $J_1(\omega)$ and $J_2(\omega)$ exist only at $T = 0$. Harris^{A-5, A-6} and Shapiro^{A-11} have calculated these functions numerically for nonzero temperatures. Figure A-4 shows $J_1(\omega)$ and $J_2(\omega)$ for identical superconductors at $T \approx .7T_c$.

2. The divergence at $\hbar\omega = 2\Delta$ (the Riedel peak) is related to the singularity in the density of states at the gap edge in the superconductors. This is a weak, integrable singularity.

3. There is a problem concerning the high frequency behavior of $J_1(\omega)$ and $J_2(\omega)$. For example, expansion in powers of $\frac{1}{\omega}$ shows that (at $T = 0$, at least) $\text{Re } J_2(\omega)$, which is an even function, falls off as $\frac{1}{\omega^2}$ at high frequencies. This behavior cannot be modeled by a filter containing a finite number of elements. It arises in Werthamer's theory through the use of the

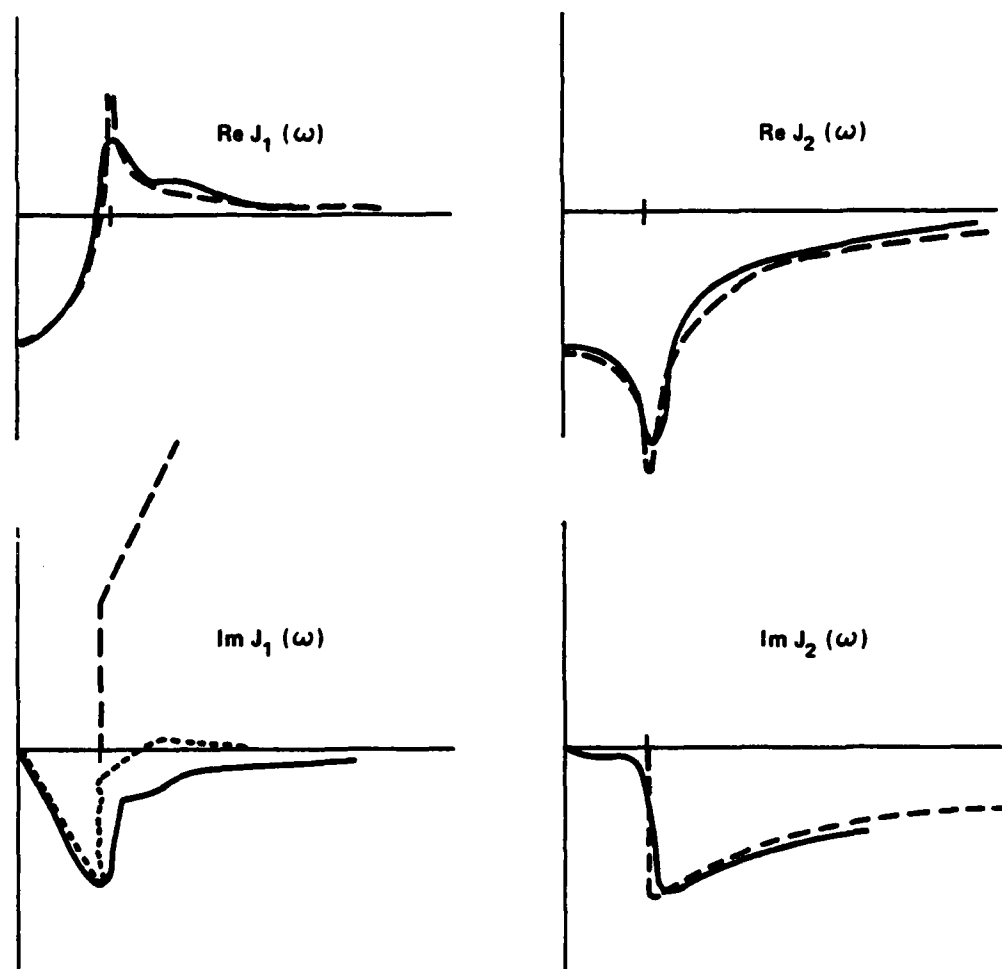


FIGURE A-3. THEORETICAL FUNCTIONS $J_1(\omega)$ AND $J_2(\omega)$ COMPARED WITH RESPONSE OF THE CORRESPONDING FILTERS

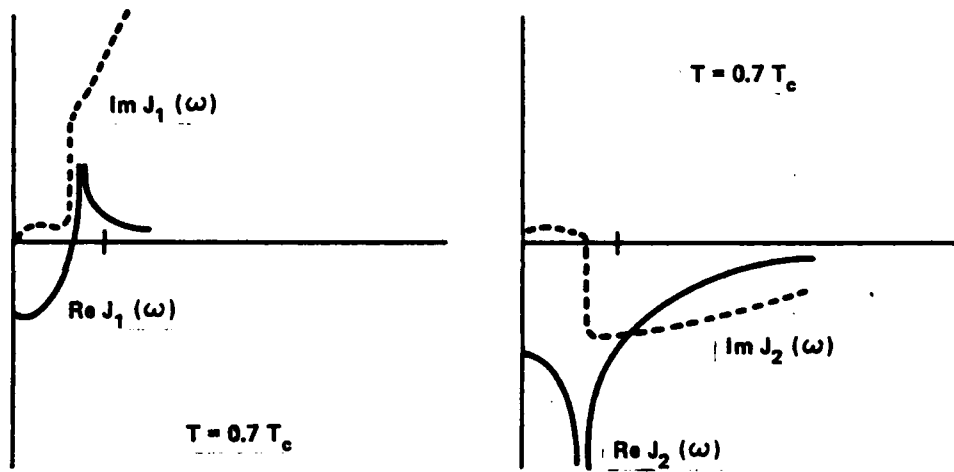


FIGURE A-4. THEORETICAL RESPONSE FUNCTIONS FOR $T = 0.7 T_c$.

weak-coupling approximation in which one treats the gap parameter Δ_k as a constant and ignores the fact that Δ_k is modified at excitation energies of the order of the phonon frequency. In the spirit of the weak-coupling approximation, it seems best to use filters which are as accurate as possible at frequencies comparable with the Riedel peak frequency, but whose frequency response at the highest frequencies is inaccurate.

4. An ideal way to synthesize the filters would be to find continued fraction expansions of the expressions for $J_1(\omega)$ and $J_2(\omega)$. This would yield the poles and zeros of the filter responses, and standard synthesis techniques would be applicable. However, no exact continued fraction expansions of the analytic expression at $T = 0$ seem to exist, and we have used more empirical methods to obtain suitable filters.

5. By designing filters with response functions $\{J_1 - J_2\}$ and $\{J_1 + J_2\}$, it would be possible to reduce the number of complete filters in the analogue from four to two. However, this would prevent separate measurement and control of the pair and quasiparticle currents, which is a useful feature of the analogue.

CIRCUIT CONSIDERATIONS

The prototype analogue was built using conventional integrated circuit technology (op amps, integrated circuit multipliers, and function generator chips). Table A-1 shows the operating parameters of the analogue compared with their counterparts in a typical tunnel junction.^{A-12} The gap frequency of the analogue is 1000 Hz. The analogue is designed to operate at input frequencies up to five times this with reasonable accuracy. The local oscillator frequency

is about 100 kHz. These frequencies are arbitrary, but reflect various tradeoffs in circuit design. The predominant consideration was to keep the frequencies in a range where simple op amp design and breadboarding techniques work well. However, there are several other considerations which affect the

TABLE A-1 PARAMETERS OF ANALOGUE COMPARED WITH THOSE OF A TYPICAL TUNNEL JUNCTION

	I_j	$V_{gap} = \frac{2\Delta}{e}$	R_n	$\frac{2e}{h}$	$f_{gap} = \frac{2\Delta}{h}$
Typical Junction ¹²	1 ma	3 mV	100 Ω	483 $\frac{MHz}{\mu V}$	725 GHz
Analogue	1 ma	.6 m	560 Ω	3125 $\frac{Hz}{V}$	1000 GHz

accuracy and stability of the device. These are straightforward, and are encountered in any phase-locked loop design. They will not be discussed here.

The filter circuits warrant special discussion. Figure A-2 shows the RLC models for $J_1(\omega)$ and $J_2(\omega)$ at $T = 0$. Figure A-5 shows the circuit actually used in the analogue for $J_1(\omega)$. Instead of the six components shown in Figure A-2, the circuit in Figure A-5 has almost 30 components. But it is actually the simpler of the two circuits to build and incorporate into the analogue. It requires no additional interface circuitry, whereas the RLC equivalent would require a current source to drive it, and another circuit for subtracting the output voltages. The circuit in Figure A-5 contains no inductors. At the low frequencies involved, the necessary inductors would be very large and prohibitively expensive. The circuit in Figure A-5 is both inexpensive and easy to design. This circuit consists of two "biquad" filters.^{A-13,A-14} The biquad gets its name from its transfer function, which is the ratio of two quadratics. It is an extremely flexible circuit, and with appropriate resistor values can be used to model almost any RLC network.

The versatility of the biquad opens up many possibilities for the electronic analogue. The accuracy of the analogue depends largely on how good the filters are. Extremely accurate filters will be very complicated, and may require ten or more biquads per filter. But the technology now exists to make custom designed biquads in small quantities for as little as \$2 each.^{A-15}

To adjust the "temperature" of the analogue, it is necessary to modify the filter functions (cf. Figure A-4). This can easily be accomplished using variable resistors in the biquads. The most practical approach, however, seems to be to design specific filters for each of a limited number of temperatures. A general purpose set of variable filters would provide greater flexibility, but would be difficult to calibrate.

SIGNS

A brief word about signs is in order. The literature is full of discrepancies concerning the sign conventions for $J_1(\omega)$ and $J_2(\omega)$. Harris has discussed this in detail.^{A-6} In the analogue, the signs largely take care of themselves. The real filters in the analogue will always satisfy causality requirements, and the signs adjust themselves accordingly. It is not possible for the designer to influence the sign relation between the real and imaginary parts of $J_1(\omega)$ and $J_2(\omega)$. What signs one uses in describing these functions depends largely on convention. However, the designer can add an overall sign change to either or both $J_1(\omega)$ and $J_2(\omega)$. This will affect both the real and imaginary parts of each function. Changing the sign of $J_1(\omega)$ will make the quasiparticle resistance look negative instead of positive, an obviously unphysical situation. The overall sign of $J_2(\omega)$, however, has no effect on the input/output characteristics of the analogue. It does affect whether the VCO phase-locks at 0° or 180° with respect to the LO when the analogue is biased within the zeroth order step.

As for the sign of the $\cos\phi$ term, the real issue is whether the $\cos\phi$ term increases or decreases the dissipation of energy within the junction. If the $\cos\phi$ term serves to increase the Q of the plasma resonance, its sign is considered to be negative.^{A-16} However, it should be remembered that the coefficient of the $\cos\phi$ term is a function of frequency, voltage, and temperature. While the overall effect of this term can often be neglected, one must still be careful about treating the coefficient as a constant.

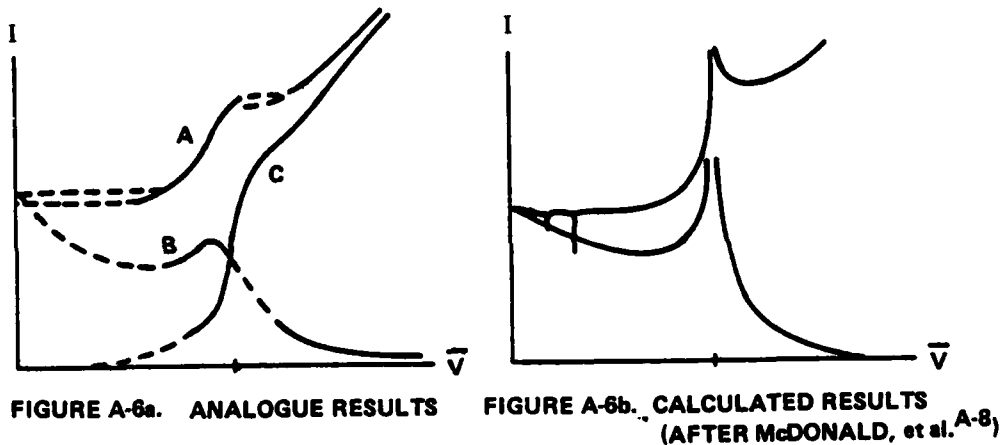


FIGURE A-6. EXPERIMENTAL AND CALCULATED I-V CHARACTERISTICS

RESULTS

Figure A-6a shows the an I-V characteristic of the current biased analogue. Curve a shows the total DC current, and curve b the DC Josephson currents. Hysteresis is present in the characteristic in the regions where the

slope of curve a (the total current) is negative. Under current bias conditions, regions of negative differential resistance are inaccessible. However, in regions where the total differential resistance (i.e., the slope of curve a) is positive, negative differential resistance regions of curve b (the Josephson current) are accessible. The fine structure and divergence shown in Figure A-6b are not present in the curves of Figure A-6a as a consequence of the crudeness of the prototype filters used in the analogue. Curve c in Figure A-6A shows the effect of shunt capacitance on the total current. The capacitor serves to short out the higher harmonics of the AC voltages across the junction. At the same time, it provides a return path for AC currents through the junction, which otherwise could not flow. In other words, the capacitor serves to reduce the source impedance, moving the junction from current bias towards the condition of voltage bias. In the voltage biased limit, a plot of average current versus average voltage is identical with $\text{Im } J_1(\omega)$, the quasiparticle current. The strong nonlinearity of this current is apparent in the figure.

FUTURE WORK

Work is currently underway to improve the existing filters for $T = 0$, and to design filters for nonzero temperature. This is being done using empirical techniques of curve-fitting. But more sophisticated numerical techniques (i.e., use of Pade approximates) may be attempted in the future. Some preliminary work has been done to model various experiments. Briefly, these include:

1. Observation of the plasma resonance. This is simple if done qualitatively, but accurate measurements will require care. These measurements may provide some insight into the ambiguity of the results of experiments done to measure the sign of the $\cos\phi$ term. Unlike experiments involving real junctions,

A-16

geometrical considerations may be ignored, greatly simplifying the experiment. If need be, the non-linear quasiparticle resistance can be made linear as well.

2. Investigation of quasiparticle mixing. Recent work^{A-17} indicates that use of the nonlinear quasiparticle resistance for microwave mixing will result in an extremely low-noise device. The analogue will be ideal for modeling the performance of this and other microwave devices.

3. Investigation of computer switches. Josephson junctions can be used as extremely fast switching devices.^{A-18,A-19} These devices require a hysteretic junction with a highly nonlinear quasiparticle resistance. The analogue can be used to model a computer switch with the addition of a circuit for controlling the amplitude of the $J_2(\omega)$ filter response. Varying this amplitude is analogous to applying a magnetic field to the junction. A suitable nonlinear network could be added to model the $\frac{\sin\phi}{\phi}$ dependence of critical current on magnetic field. An additional filter added to this network could model the propagation delays associated with a superconducting stripline in a real device. Simple switching action has already been observed using the analogue, and it is hoped that quantitative results will be available in the near future.

ACKNOWLEDGMENTS

The authors would like to acknowledge helpful discussions with R. E. Harris, C. Hamilton, D. G. McDonald, and their colleagues at the National Bureau of Standards, Boulder, Colorado. Mr. P. Sinclair assisted with the design and testing of the prototype filters. We would also like to acknowledge the financial support of the Hirst Research Centre of the General Electric Co. Ltd., of England for one of the authors, D. G. Jablonski.

REFERENCES

- A-1. Bak, C. K., Rev. de Phys. Appl. 9, 15 (1974).
- A-2. Hamilton, C.A., Rev. Sci. Inst. 43, 445 (1972).
- A-3. Josephson, B. D., Phys. Lett. 1, 251 (1962).
- A-4. Werthamer, N. R., Phys. Rev. B. 147, 255 (1966).
- A-5. Harris, R. E., Phys. Rev. B 10, 84 (1974).
- A-6. Harris, R. E., Phys. Rev B 11, 3329 (1975).
- A-7. Harris, R. E., Phys. Rev. B 13, 3818 (1976).
- A-8. McDonald, D. G., Johnson, E. G., Harris, R. E., Phys. Rev. B 13, 1028 (1976).
- A-9. Waldram, J. R., A Theoretical Survey of Josephson Frequency Mixers for Heterodyne Reception in the Submillimetre Wavelength Range, ed. Blaney, National Physical Laboratory, U.K. 1976.
- A-10. Waldram, J. R., Rep. Prog. Phys. 39, 751 (1976).
- A-11. Shapiro, S., Smith, P. H., Nicol, J., Miles, J. L., Strong, P. F., IBM J. Res. Dev. 6, 34 (1962).
- A-12. Waldram, J. R., Pippard, A. B., and Clarke, J., Phil. Trans. Roy. Soc. A268, 265 (1970).
- A-13. Tow, J., Proc. IEEE (Lett.) 56, 1137 (1968).
- A-14. Thomas, L., IEEE Trans. CT-18, 350 (1971).
- A-15. Thomas, L., Bell Labs., Holmdel, N. J., personal communication.
- A-16. Pedersen, N. F., Finnegan, T. F., Langenberg, D. N., Phys, Rev. B 6, 4151 (1972).
- A-17. Richards, P. L., Shen, T. M., Harris, R. E., Lloyd, F. L., Appl. Phys. Lett. 34, 345 (1979).
- A-18. Matisoo, J., Sci. Amer., May 1980.
- A-19. Anacker, W., IBM J. Res. Dev., Mar 1980.

APPENDIX B

HIGH FREQUENCY APPLICATIONS OF JOSEPHSON DEVICES

The research described in this thesis was originally intended to be investigation of parametric effects in Josephson junctions. As the work progressed, it became apparent that Josephson parametric devices were not going to be as practical or useful as had been anticipated. This, combined with the difficulties involved in setting up even a simple parametric amplifier experiment (i.e., fabricating junctions, procuring equipment, etc.), led to the conclusion that another line of research would be more profitable. However, it is worth summarizing a few aspects of the behavior of parametric amplifiers and other high frequency devices.

First, the motivation for using Josephson junctions for high frequency applications is that they are highly nonlinear, very fast, and hopefully low noise devices. Unfortunately, dependable Josephson junctions are difficult to fabricate. They have low dynamic range, and their unusual properties often result in poor noise performance despite their cryogenic operation. The only major high frequency application where a Josephson device seems practical is that of a submillimeter wavelength low noise mixer for radio astronomy applications. High dynamic range is not essential, and the noise performance and frequency response may prove to be better than those of competing semiconductor devices.^{B-1}

Amplifiers based on Josephson junctions have, however, been a disappointment, as they are much noisier than first expected.^{B-2} Much of this problem can be attributed to nonthermal noise mechanisms which are difficult to understand. And the effect of thermal noise is abnormal, in that the noise

temperature of the amplifier depends on the nature of the input signal. As a result, the original expectations of a high bandwidth, low noise, high frequency paramp have never been realized.^{B-1}

Two kinds of Josephson junction mixer and the Josephson junction parametric amplifier are discussed below.

The conventional Josephson junction mixer takes advantage of microwave induced steps in the current biased I-V characteristic of the junction. The junction is usually DC current biased between the zeroth and first order steps. The relative heights of these steps depends on the power level of an applied local oscillator signal. A signal of substantially less power, but approximately the same frequency as the local oscillator is applied. This causes the DC characteristic to be modulated at the difference between the LO and signal frequencies. This IF signal can be detected using a low frequency circuit. Provided that suitable matching conditions exist, the mixer can theoretically exhibit gain. But achieving these conditions is quite difficult. This type of mixer has been extensively studied by Blaney and others.^{B-3}

A second type of high frequency mixer utilizes the nonlinearity of the quasiparticle conductance in a tunnel junction. The Josephson, or pair tunnelling, is usually suppressed using a magnetic field. This device is similar to a nonlinear diode in many respects, but because of the reactance associated with $\text{Re } J_1(\omega)$, it can exhibit gain. Richards, et al. have made measurements on a real device, and Tucker has investigated the theory.^{B-4, B-5}

A lot of work has been done on the unbiased Josephson parametric amplifier.^{B-6, B-2, B-7} This amplifier usually takes the form of an array of tunnel junctions or microbridges in a superconducting thin film stripline. By using an array, the problem of matching is less severe, and the dynamic range is

increased. The junctions are unbiased in the sense that the DC voltage and current are zero. The amplifier is operated as a reflection type, doubly-degenerate negative resistance paramp. That is, the signal, pump, and idler frequencies are related by

$$2f_p \approx f_s + f_i$$

$$f_p \approx f_s \approx f_i$$

A circulator is required to separate the input and output signals. Unless cooled to cryogenic temperatures, this circulator can be a major source of thermal noise.

There are several problems with this type of Josephson junction paramp. First, it is difficult to manufacture reliable arrays of Josephson junctions. Second, the gain of the device is critically dependent on pump power. Third, the device is extremely noisy. The mixing efficiency is such that even small quantities of wideband thermal noise at the input will saturate the amplifier.^{B-2} There are also several nonthermal mechanisms by which noise is generated. These are difficult to understand, but are apparently a result of instabilities inherent in the $\sin\phi$ nonlinearity of the Josephson effect.^{B-8} All things considered, this amplifier does not look very promising.

There have been attempts to use other modes of amplification (i.e., singly degenerate and nongenerate). These have not been investigated as much as the doubly degenerate case, but it is unlikely that they will be significantly better. For a more complete review of these and other Josephson junction devices, the reader is referred to the review article by

4/4

NL

END

Fly Me!

1

1116



REFERENCES

- B-1. Sullivan, D. B., The Role of Superconductivity in the Space Program: An Assessment of Present Capabilities and Future Potential, National Bureau of Standards NBSIR 78-885 (May 1978).
- B-2. Feldman, M. J., J. Appl. Phys. 48, 1301 (1977).
- B-3. Waldram, J. R., A Theoretical Survey of Josephson Frequency Mixers for Heterodyne Reception in the Submillimetre Wavelength Range, ed. Blaney, National Physcial Laboratory, U. K. (1976).
- B-4. Tucker, J. R., Appl. Phys. Lett. 36, 477 (Mar 1980).
- B-5. Richards, P. L., Shen, J. M., Harris, R. E., and Lloyd, F. L., Appl. Phys. Lett. 36, 480 (1980).
- B-6. Rudner, S. and Claeson, T., J. Appl. Phys. 50,7070 (1979).
- B-7. Walhsten, S., Rudner, S., and Claeson, T., Appl. Phys. Lett. 30, 298 (1977).
- B-8. Chiao, R. Y., Feldman, M. J., Peterson, D. W., Tucker, B. A., and Levinsen, M., Proc. Future Trends in Supercond. Devices, Charlottesville, AIP (1978).

APPENDIX C

FABRICATION OF SUPERCONDUCTING TUNNEL JUNCTIONS

In connection with the study of parametric effects described in Appendix B, a preliminary investigation was made into methods of fabricating tunnel junctions. In addition to experiments done using conventional thin film techniques, a novel technique was investigated for fabricating tunnel junctions on anodically oxidized bulk tantalum. This technique involved the development of various processes which may be of use to future researchers. The processes include the construction of a simple photolithography facility, techniques of electropolishing, and the use of anodic oxide films. This appendix is a brief description of the tantalum tunnel junctions, followed by a review of these techniques.

TANTALUM TUNNEL JUNCTIONS

The motivation behind the use of the bulk tantalum for tunnel junctions was the need for a simple-method of making temperature recyclable tunnel junctions. The major difficulty in fabricating tunnel junctions using thin film techniques is in maintaining reproducible conditions for the evaporation and oxidation of the junction electrodes. And even when successful junctions are made, they often fail to work after one or more recyclings to helium temperature.

Valve metals such as niobium, tantalum, and aluminum, are noted for their robust oxides. Of these metals, only aluminum can be evaporated easily. But its transition temperature is too low for it to be used easily in a standard helium 4 system. Niobium and tantalum have transition temperatures above 4.2k, but must be RF sputtered or evaporated using an E-beam.

It is quite easy to put thin oxide layers onto either tantalum or niobium using anodic techniques. The thickness can be controlled precisely without the need for expensive equipment. This suggests the use of anodic oxide films for tunnelling barriers in Josephson junctions. Since no RF sputtering or E-beam equipment was readily available, it was necessary to use bulk material. From a metallurgical point of view, this was more satisfactory than the use of thin films anyway. Thin films don't always superconduct at low temperatures, and an electropolished surface can be better than that obtained by sputtering or evaporation.^{C-1} The main disadvantage of using bulk material is the difficulty in making a small area junction without resorting to point contact techniques. A way around this problem was found, but the resulting junctions had an inherently high shunt capacitance. The use of the substrate as one of the electrodes of the junction limits the technique considerably in terms of multiple junction applications. However, the method may prove useful for some applications, and the preliminary results are described below. In the experiments, tantalum was used. It was readily available, and there is a wealth of information about its anodic oxidation.^{C-2}

The procedure for making a tantalum tunnel junction starts with preparation of the tantalum by electropolishing. This serves to smooth the surface, and to remove any oxide or impurities present. The sample is then anodically oxidized to put an insulating layer of Ta_2O_5 approximately 1000 Angstroms thick on the surface. However, part of the surface is shielded by a thin strip of photoresist during this process. The photoresist is removed with acetone afterwards, leaving a canyon in the Ta_2O_5 . The bottom of this canyon is then anodized to an oxide thickness of between 10 and 50 Angstroms. Finally, a

tin or lead counterelectrode is evaporated at right angles to the canyon. Overall, the system looks like a tantalum electrolytic capacitor. But the oxide layer at the bottom of the canyon is sufficiently thin that Josephson tunnelling can occur there.

Figure C-1 shows the I-V characteristics for two representative tantalum-tin junctions, along with a sketch and an enlarged photograph of the junction. In the photograph, the canyon in the oxide is visible as the lighter region of the substrate. The tin counter-electrode is the almost vertical line running through the center of the picture.

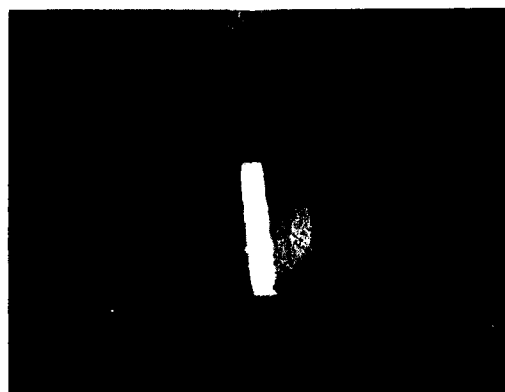
The two I-V characteristics both exhibit a DC supercurrent, but are quite different in other respects. To verify that the Josephson effects are really what are being observed, it would be useful to radiate the junctions with microwaves and look for step behavior. Unfortunately, it was not possible to do this at the time the measurements were made. However, the presence of what appears to be energy gap structure in the second I-V characteristic suggest that tunnelling is indeed occurring.

Other samples were tested, with similar results. However, it wasn't possible to correlate the junction characteristics with the oxide thickness and junction area from the small number of samples that were tested. The development of this technique was discontinued in favor of researching the high frequency analogue.

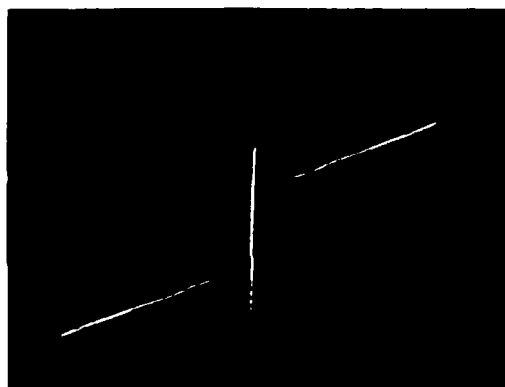
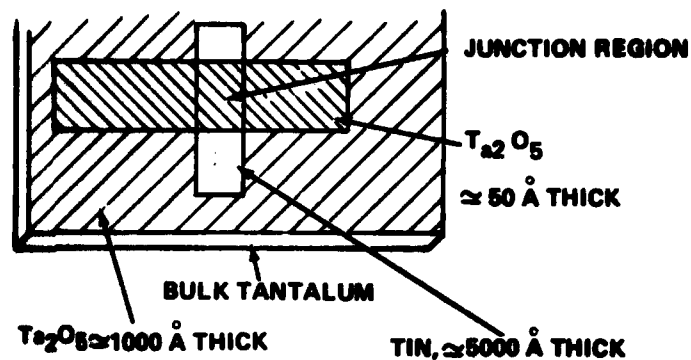
MISCELLANEOUS TECHNIQUES

1. ELECTROPOLISHING OF TANTALUM.

A mixture of nine parts concentrated sulphuric acid and one part 40 percent hydrofluoric acid is used as the polishing solution. Either a platinum or carbon anode can be used, and the tantalum is polished for between 10 and 15



I. A TANTALUM-TIN TUNNEL JUNCTION



II. I-V CHARACTERISTICS OF TWO CURRENT-BIASED JUNCTIONS ($T \approx 2.1 \text{ K}$)

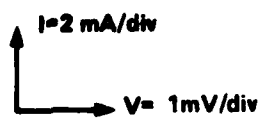
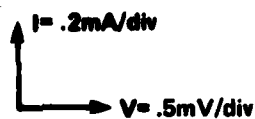


FIGURE C-1 CURRENT-VOLTAGE CHARACTERISTICS OF A TANTALUM-TIN TUNNEL JUNCTION

minutes at a current density of 100 mA/cm.^{C-3} It is important to keep the temperature of the solution at between 35 and 45 degrees centigrade, and stirring of the polishing solution is essential. To accomplish this, the plastic beaker of HF/H₂SO₄ is placed in a crystallizing basin filled with water, which is then placed on a magnetic stirrer. The water is heated with a small immersion heater. (Hot plates are not very good for temperatures this low.) The immersion heater is switched on and off as required.

As polishing progresses, a diffusion layer in the form of a white film will appear on the tantalum. This must be rinsed off promptly after the sample is removed, or it is apt to stick.

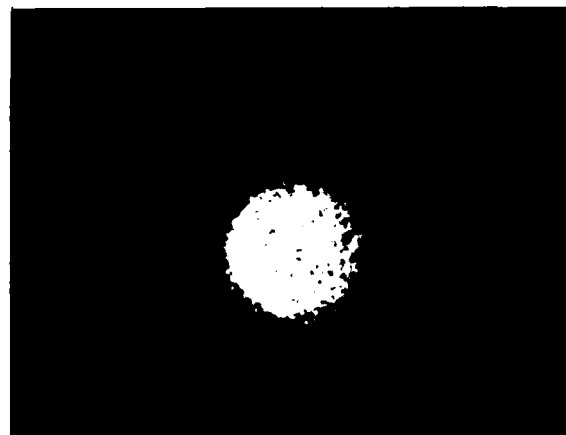
Etching of the tantlum is sometimes preferred to polishing. No electric currents are used, and the tantalum is simply immersed in a combination of 6 parts 40 percent HF, 2 parts 98 percent H₂SO₄, and 1 part 70 percent HNO₃.^{C-3} With a large sample, the resulting chemical reaction is spectacular.

After polishing or etching, the sample should be rinsed thoroughly, and then leached in boiling water for 10 to 30 minutes. This last step removes a leftover residue from the surface of the tantalum. This residue will reduce the adhesion of any oxide layers subsequently placed on the surface.^{C-2}

Figure C-2 shows a photograph of a sample of tantalum after various treatments. The first photograph shows the original surface finish of some tantalum sheet. Horizontal rolling marks are visible. The second photograph shows the effect of etching the sample. The rolling marks disappear, and grain boundaries become apparent. The third photograph shows an electropolished surface. The sample appears quite dull, as there are few imperfections for light to diffuse from. The "orange peel" structure of the surface is typical of electropolished tantalum.^{C-2} The last photograph shows the effect of



ORIGINAL MATERIAL



ETCHED



POLISHED



PITTED

FIGURE C-2. PREPARATION OF BULK TANTALUM

polishing at too high a current density. Large chunks of material are removed at once, resulting in a pitted surface.

When working with hydrofluoric acid, it is essential that adequate safety precautions be observed. This means always using a fume cupboard, being extremely careful not to spill or splash HF or other acids, and wearing gloves that can stand up, at least temporarily, to the acids involved. Many types of gloves are not adequate. Concentrated sulphuric acid will go through almost any type of glove given time. HF will not go through neoprene, but neoprene gloves are prone to tearing. Rubber gloves are quite a bit stronger, but less HF resistant and more prone to pinholes. What type of gloves one should use depends on the particular nature of work. But in any event, gloves must be regarded as short term protection only. Proper first aid supplies should be available (i.e., calcium gluconate gel for HF burns), and one should be familiar with proper first aid treatment. It should be realized that the average medical doctor may not be familiar with the treatment of HF burns, and that it is up to the experimenter to ensure that adequate preparation has been made to cope with an accident. An extremely thorough set of guidelines for the use of HF is available from East Anglia Chemicals, and probably from any other chemical supply company.

2. PHOTOLITHOGRAPHY.

The basic requirements for photolithography are a room shielded from white light, a photoresist spinner, some means of baking the resist, and a bright light for exposing the resist. A sink and some beakers are sufficient for handling the various chemicals and developing solutions. For masks, it is possible to use anything from a commercial mask to a metal frame with an appropriate pattern drilled through it.

For the photolithography work done by the author, no special equipment was purchased. The spinner was made from a sixty pence DC motor run by a variable power supply. Speeds between 100 and 3000 RPM were easily obtained, and the substrate was held in place with double-sided tape. The resist was baked under an infrared heat lamp, and exposed using an overhead projector lamp. A safe light was made by covering fluorescent lamp with a green gel.

The basic chemicals needed are the photoresist, developing solution, and acetone. The first two items, along with instructions for their use, were obtained from Shipley.^{C-4} Depending on the details of the work being done, various etching solutions may be needed, but these are easily obtainable.

To put a photoresist stencil onto tantalum, the following procedure was used. Shipley AZ 1350H photoresist was spun onto the substrate at 1500 RPM for 30 second. The sample was baked for approximately 10 minutes at 40-75 degrees centigrade. Exposure times were adjusted so that the pattern in the resist could be developed in 2 minutes using a 50 percent dilution of Shipley AZ Developer with water. This criterion, suggested by the manufacturer, usually meant an exposure time of 3 to 5 minutes using a 300 watt projector lamp 6 inches from the substrate. Line widths of 25 microns were achieved with no difficulty, and it seems likely that significantly better resolution could be easily obtained. Dust was not a problem, even though no attempts were made to eliminate it. To remove the photoresist after processing, it is sufficient to wash the substrate with acetone. All things considered, the use of photoresist was surprisingly successful.

3. ANODIC OXIDATION OF TANTALUM

This is relatively simple. The tantalum is used as the anode in electrochemical cell. The electrolyte is a .03 percent citric acid solution,

and the cathode is either gold or platinum. For tantalum, it is often assumed that 17 Angstroms of Ta_2O_5 will form for every volt of applied potential. This is an over-simplification, but is a good indication of the potential that one should apply to achieve a given oxide thickness. To determine the oxide thickness, both capacitance and charge measurements were performed. For the latter, the electric current as a function of time is plotted while the sample is being anodized. The thickness of the oxide will be proportional to the net amount of charge passed (i.e., the area under the current vs. time curve.) A complete discussion of the anodic properties of tantalum, niobium, and other metals is in the textbook by Young.^{C-2}

REFERENCES

- C-1. Evans, D., Hirst Research Centre, Wembley, England, private communication.
- C-2. Young, L., Anodic Oxide Films, Academic Press (1961).
- C-3. Tegart, W. J., Electrolytic and Chemical Polishing of Metals, Pergamon (1956).
- C-4. Shipley Chemicals, Ltd. Coventry, England.

APPENDIX D

LOW-PASS FILTER CONSIDERATIONS

Several different low-pass and notch-type filter networks have been used in the various versions of the analogue. The single pole RC and three pole Butterworth filters have been discussed previously (cf. sec. 3.3). The four pole Butterworth is similar to the three pole, except that it has a steeper high-frequency rolloff and larger cosine phi amplitude for a given half-power frequency.

To reduce the cos phi amplitude while maintaining good rejection at the second harmonic of the local oscillator frequency, it was decided to investigate the use of notch filters. The twin-T, which is a well known notch filter, was used in an improved version of the RSJ analogue. Its transfer function is given below, and is plotted in Figure D-1a. A schematic of the filter is shown in Figure D-1b. For the twin-T,

$$F(s) = \frac{1 + s + s^2 + s^3}{1 + 5s + 5s^2 + s^3} \quad (D-1)$$

where $s = j\omega/\omega_0$, and ω_0 is the notch frequency of the filter (as opposed to half-power frequency). Note that $F(s) = 0$ when $s = 1$, and that $|F(s)|$ never exceeds 1. The latter point is essential if the filter is to be realized using only passive components.

The equivalent cos phi amplitude of the twin-T is found by expanding $F(s)$ for $s \ll 1$. We have

$$F(s) \approx 1 - 4s \quad (D-2)$$

From equations 3-13 and 3-14, the equivalent cos phi amplitude will be

$$\gamma = \frac{-4\omega_J}{\omega_0} = \frac{-4f_J}{f_0} \quad (D-3)$$

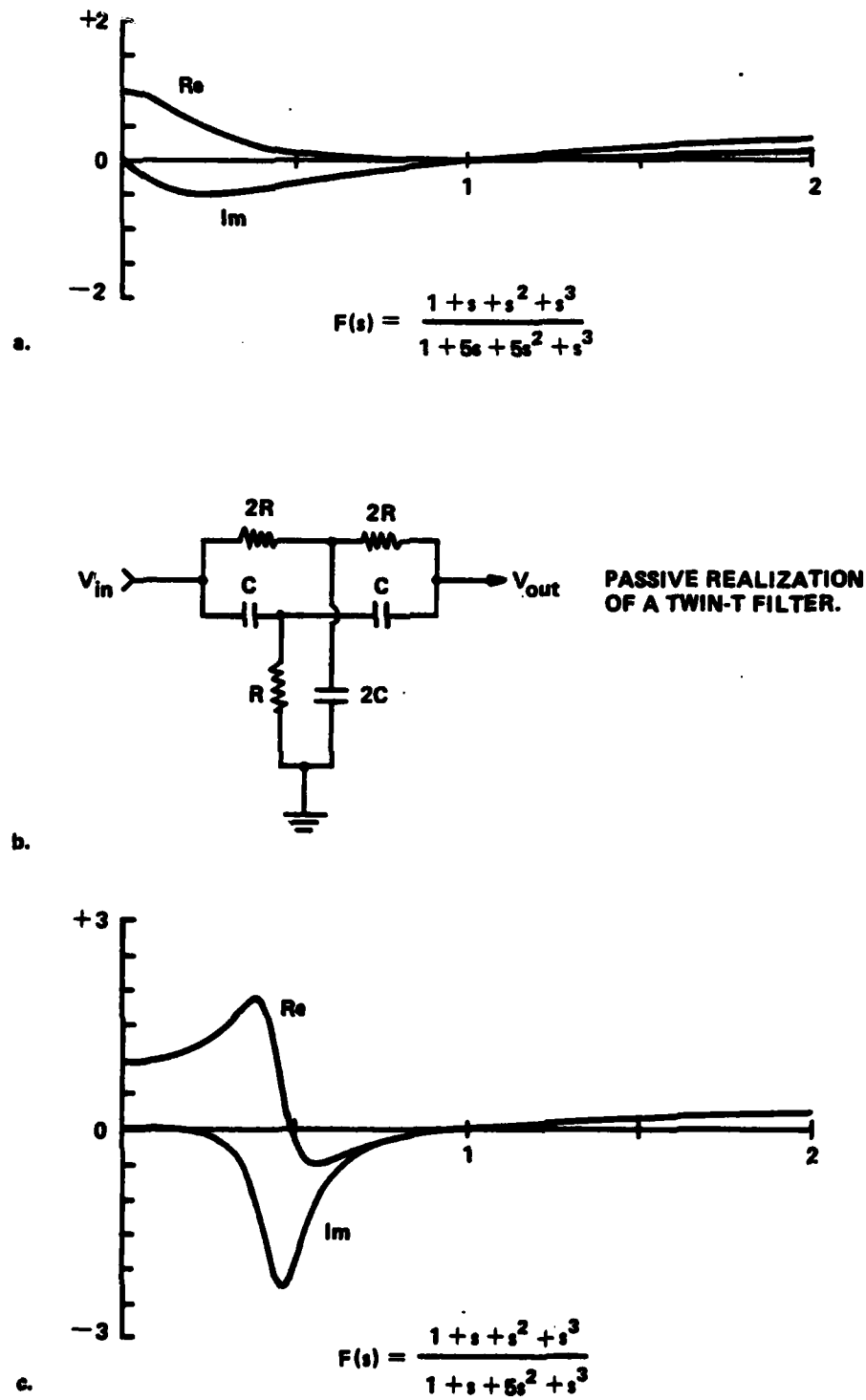


FIGURE D-1. CHARACTERISTICS OF NOTCH FILTERS USED IN THE ANALOGUE

as compared with $\gamma = -\omega_J/\omega_0$ for the RC filter.

f_J is the Josephson frequency $2eI_J R_N/h$, and is typically 1570 Hz ($\pi/2$ times the gap frequency, in the case of the high-frequency analogue). Note that f_0 is the notch frequency of the filter, which is twice the local oscillator frequency. For the RC and other low-pass filters, f_0 corresponds to the half-power frequency, which of necessity is a factor of three to ten below the local oscillator frequency. Thus for the twin-T, the factor of 4 increase in the numerator of (D-3) over the RC case is offset by a comparable increase in f_0 .

As an improvement to the twin-T, a notch filter was designed with

$$F(s) = \frac{1 + s + s^2 + s^3}{1 + s + 5s^2 + s^3} \quad (D-4)$$

Note that the low frequency phase shift is zero to second order. However, the notch at $s = 1$ is degraded somewhat from the twin-T case, and $|F(s)|$ can now exceed 1. This is plotted in Figure D-1c.

As discussed in section 8.5, this new filter requires active components. As the filter must operate at frequencies that are large by op amp standards, careful thought had to be given to the design problem.

By expanding $F(s)$ as a series of partial fractions, the response can be rewritten as the sum of three second order responses, which are implemented using the circuit shown in Figure 8-1. The signals corresponding to the individual response functions are summed using standard op amps. The circuit is intentionally designed so that the limited performance of these op amps affects each filter section in an identical manner. Although the shape of the actual response function is modified by the limitations of the op amps, there is still a notch at

$s = 1$. Mathematically, the overall response of the filter can be written as

$$G(s) = H(s)F(s) \quad (D-5)$$

where $F(s)$ is given by D-4, and $H(s)$ is determined solely by the properties of the op amps. Note that for low frequencies, the op amps will have near-ideal behavior, and $H(s)$ will equal 1. Provided that $H(s)$ at high frequencies doesn't distort grossly the shape and width of the notch, the op amp limitations will not affect the overall performance of the analogue.

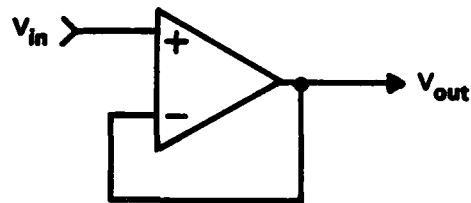
The next step is to investigate the properties of $H(s)$. To minimize noise pickup and prevent instabilities, op amps are frequency compensated with a capacitor. This results in an individual op amp having an open loop response similar to that of a single pole RC filter, with the gain of the op amp given by

$$A(s) = \frac{A_0}{s + B} \quad (D-6)$$

where $s = j\omega$.

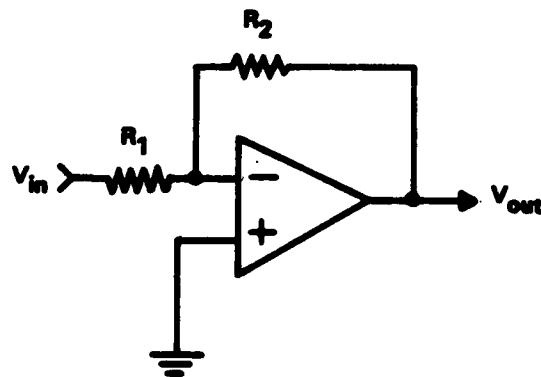
The DC open loop gain of the op amp is A_0/B , and is typically 200,000 for the 741 type op amps used in the analogue. The frequency at which $|A(s)| = 1$ (e.g.- the unity gain bandwidth) is of the order of 1 MHz. Thus $A_0/2\pi = 10^6$, and $B = 2\pi \times 5$. This shows that the open loop half-power bandwidth of a 741 is typically 5 Hz.

The magic ingredient to an op amp circuit is feedback. For example, an op amp voltage follower (cf. Figure D-2a) has a transfer function given by



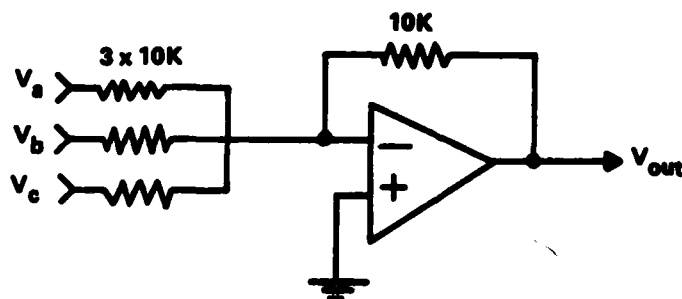
$$V_{out} = V_{in}$$

a. VOLTAGE FOLLOWER



$$V_{out} = -\frac{R_2}{R_1} V_{in}$$

b. INVERTING AMPLIFIER



$$V_{out} = -(V_a + V_b + V_c)$$

c. SUMMING AMPLIFIER

FIGURE D-2. OP AMP CONFIGURATIONS USED IN THE ANALOGUE

$$K(s) = \frac{V_{out}}{V_{in}} = \frac{1}{1 + 1/A(s)} = \frac{A_0}{A_0 + s + B} \quad (D-7a)$$

Since $A_0 \gg B$,

$$K(s) = \frac{A_0}{A_0 + s} \quad (D-7b)$$

Thus the half-power bandwidth of the voltage follower is equivalent to the open-loop unity gain bandwidth of the op amp. In general, the gain-bandwidth product of the op amp remains constant. By using feedback to decrease the gain, the bandwidth is increased. In the case of the voltage follower, the feedback causes a factor of 200,000 decrease in gain, and a corresponding increase in bandwidth.

For the inverting amplifier, shown in Figure D-2b, the transfer function is given by

$$L(s) = \frac{-R_2}{R_1 + (R_1 + R_2)/A(s)} \quad (D-8)$$

This can be generalized to the summing amplifier used in the low-pass filter (cf. Figure D-2c) in the following manner. First, R_1 is set equal to the value of the parallel combination of the multiple input resistors. For a three input summing amplifier having unity gain, this gives

$$L(s) = \frac{3}{1 + 4/A(s)} = \frac{3A_0}{A_0 + 4s} \quad (D-9a)$$

Next, the gain must be renormalized to 1, so that

$$L(s) = \frac{A_0}{A_0 + 4s} \quad (D-9b)$$

This is only an ad hoc technique that has not been fully justified on a theoretical basis. However, it seems to suit the purpose at hand. Continuing, we have for the op amp network in Figure 8-1,

$$H(s) = \frac{A_0}{A_0 + s} \times \frac{A_0}{A_0 + 4s} \quad (D-10)$$

where $s = j\omega$.

To compute the overall response of the low pass filter, it is necessary to normalize s to the notch frequency of the passive network. As an example, consider a low pass filter designed with a notch frequency of 200 kHz. The unity gain bandwidth of the 741 type op amps used in the buffer and summing circuits was measured to be approximately 815 kHz. Renormalizing $H(s)$ such that $s = j\omega/\omega_0$, where ω_0 is the notch frequency of the filter, we have an overall transfer function given by

$$G(s) = \frac{1 + s + s^2 + s^3}{1 + s + 5s^2 + s^3} \times \frac{4.075}{4.075 + s} \times \frac{4.075}{4.075 + 4s} \quad (D-11)$$

This is plotted in Figure D-3, along with the original $F(s)$. Data obtained from an actual filter having the parameters used above is plotted as well. Note that the low-pass effect of the op amps enhances the notch. In addition, equation (D-11) indicates that the low frequency phase shift, and hence the $\cos \phi$ amplitude, is determined primarily by the op amps, whereas the notch frequency is determined by the passive components. Unfortunately, this is not quite the case in practice. Careful measurements

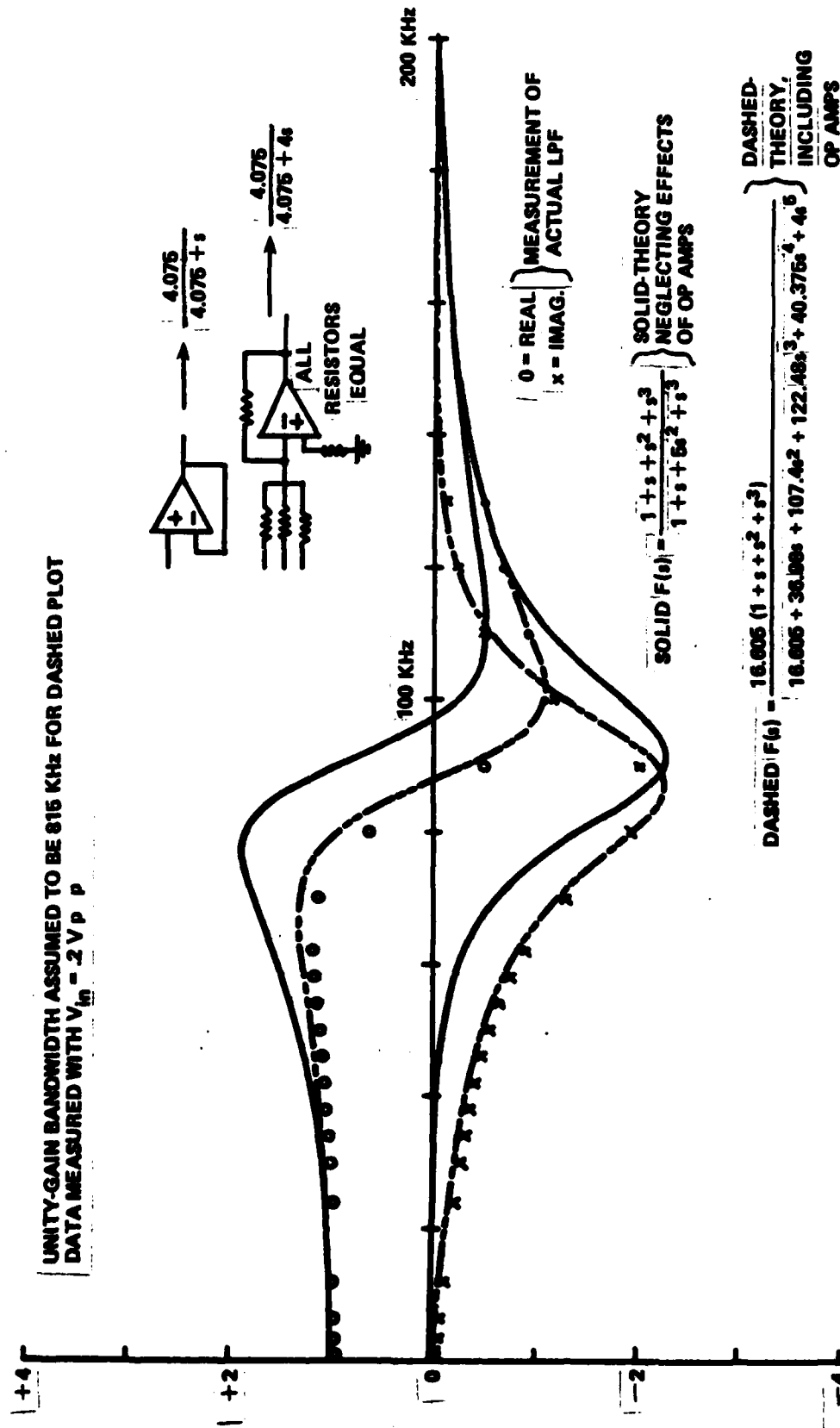


FIGURE D-3. MEASURED RESPONSE OF THE IMPROVED NOTCH FILTER

NSWC MP 81-519

at low frequencies indicate that the primary source of phase shift is due to component inaccuracy in the passive network. Nevertheless, the filter described above represents a significant improvement over previous filters used in the analogue.

DISTRIBUTION

	<u>Copies</u>		<u>Copies</u>
Chief of Naval Research Attn: ONR-414 (E. Edelsack) 800 North Quincy Street Arlington, VA 22217	1	Yale University - Becton Center Department of Engineering and Applied Physics Attn: Dr. D. Prober P.O. Box 2157 Yale Station New Haven, CT 06520	1
Commanding Officer Naval Research Laboratory Attn: Code 6854 (M. Nisenoff) Washington, D.C. 20375	2	Cornell University Department of Physics Attn: M. Roukes Ithaca, NY 14853	1
National Bureau of Standards Cryogenics Division 275.08 Attn: Dr. R. E. Harris Boulder, CO 80302	2	Massachusetts Institute of Technology Attn: Dr. J. Bostock Bldg. 6-204 77 Massachusetts Avenue Cambridge, MA 02139	1
National Bureau of Standards Bldg. 220, Rm. B258 Attn: Dr. B. Taylor Washington, D.C. 20234	2	Massachusetts Institute of Technology Attn: Dr. M. L. A. Macvicar Bldg. 8-201 77 Massachusetts Avenue Cambridge, MA 02139	1
University of California Department of Physics Attn: Dr. P. Richards Berkeley, CA 94720	2	Westinghouse Research Center Attn: Dr. R. Blaughner 1310 Beulah Road Pittsburgh, PA 15235	1
University of California Department of Physics Attn: Dr. J. Clarke Berkeley, CA 94720	1	Defense Technical Information Center Cameron Station Arlington, VA 22314	12
IBM Thomas J. Watson Research Center Attn: Dr. M. Pomerantz P.O. Box 218 Yorktown Heights, NY 10598	1	Library of Congress Attn: Gift and Exchange Division Washington, D.C. 20540	4
IBM Thomas J. Watson Research Center Attn: Dr. H. Zappe P.O. Box 218 Yorktown Heights, NY 10598	1		

DISTRIBUTION (cont'd)

Internal Distribution	<u>Copies</u>
R04 (J. Pastine)	1
R40 (I. Blatstein)	1
R43 (D. Jablonski)	27
X21	9
X22	3
E35	1

END

FILMED